In compliance with the
Canadian Privacy Legislation
some supporting forms
may have been removed from
this dissertation.

While these forms may be included
in the document page count,
their removal does not represent
any loss of content from the dissertation.

Dynamics, State Estimation, and Control of Manipulators with Rigid and Flexible Subsystems

by

Kourosh Parsa

Department of Mechanical Engineering
McGill University, Montreal
Canada

March 2003

A thesis submitted to the Faculty of Graduate Studies and Research
in partial fulfillment of the requirements for the degree of
Doctor of Philosophy

Your file Votre référence
ISBN: 0-612-88549-6
Our file Notre référence
ISBN: 0-612-88549-6

Abstract

Kinematically redundant manipulators composed of a rigid-link, rigid-joint robot and a structurally flexible arm on top of which the former is located constitute a new paradigm of long-reach manipulation systems. In order to have the end-effector of such a system faithfully follow a preplanned path, one should be able to reliably monitor the motions of the flexible submanipulator due to its elastic deformations. To this end, it is proposed that redundant point-acceleration measurements made on the rigid-robot base be used in an extended Kalman filter to estimate the *flexural states* of the flexible submanipulator. More specifically, this is done by processing the above-mentioned acceleration data in a novel pose and twist estimation technique, formulated in this thesis, to obtain those of the tip of the flexible arm; the pose and the twist data are then utilized as the measured outputs for the observer. Of course, the state-output relations should be linearized; the linearization is performed in closed-form.

The mathematical models of the flexible and the rigid submanipulators are derived separately, each through the premultiplication of the transpose of the kinematic-constraint matrix by the assembled set of the link Lagrange equations; this matrix is the *natural* orthogonal complement of the kinematic-constraint wrench. Obviously, the reaction wrench acting between the rigid-robot base and the end-effector of the flexible submanipulator couples the two sets of dynamics equations. This wrench can be determined by substituting the twist-rate of the base, i.e., its angular and translational accelerations, into the dynamics equations of the rigid submanipulator and, subsequently, solving them. Then, considering the wrench as a time-dependent input for the flexible arm, we take the flexible-arm dynamics as the *modelled dynamics* in the observer. The reduced-order dynamics helps dramatically reduce the required floating-point operations within the observer.

Two redundancy-resolution techniques, namely, *rigid-link redundancy resolution* and *flexible-link redundancy resolution*, are discussed. Whereas the former assumes all the links to be rigid, the latter takes the flexibility effects into account. In both approaches, the *self-motion* of the system is computed so as to minimize the forces exciting its lowest "modal coordinates" while imposing a proportional damping on the flexural dynamics.

Résumé

Les manipulateurs cinématiquement redondants, composés d'un robot ayant des liens rigides et des joints rigides montés sur un bras à structure flexible, constituent un nouveau paradigme pour les systèmes de manipulation de longue portée. Afin de permettre à l'effecteur de ce système de suivre une trajectoire prédéterminée, nous devons être capables de surveiller d'une façon fiable les mouvements du sous-manipulateur flexible dus à ses déformations élastiques. À cet effet, des mesures redondantes de l'accélération de points situés sur les liens flexibles seront utilisées comme données dans un filtre de Kalman, de type étendu, dans le but d'estimer les *états flexibles* du sous-manipulateur flexible. Plus précisément, ceci est réalisé en traitant les données d'accélération mentionnées ci-dessus avec une nouvelle technique d'estimation, développée dans le cadre de la présente thèse, dans le but d'obtenir la position et l'orientation du bout du lien flexible; la situation et le torseur cinématique seront ainsi les sorties mesurées pour l'observateur. Bien sûr, nous devons linéariser les relations état-sortie; ceci est effectué sous forme symbolique.

Les modèles mathématiques des sous-manipulateurs rigides et flexibles sont formulés séparément, en multipliant la transposée de la matrice de contraintes cinématiques par l'ensemble des équations Lagrange de chaque lien; la matrice en question constitue le complément orthogonal *naturel* du torseur statique de contraintes cinématiques. Evidenment, le dit torseur de réaction agissant entre la base du robot rigide et l'effecteur du sous-manipulateur flexible effectuera le couplage des deux ensembles des équations dynamiques. En substituant les accélérations, angulaire et punctuelle, de la base, soit la dérivée temporelle du torseur cinématique de la base, le torseur statique est déterminé en résolvant les équations dynamiques du sous-manipulateur rigide. Ensuite en considérant le torseur statique comme une entrée variable dans le temps pour le manipulateur flexible, sa *modélisation dynamique*

sera utilisée dans l'observateur. Le modèle dynamique d'ordre plus petit réduit considérablement les opérations à virgule flottante requises dans l'observateur.

Deux techniques de résolution de redondance, à savoir, la *résolution de redondance des liens rigides* et la *résolution de redondance des liens flexibles* sont discutées. Alors que la première suppose que tous les liens sont rigides, la deuxième tient compte de l'effet de la flexibilité sous-jacente. Dans les deux approches, le *mouvement propre*—*self-motion* en anglais—du système est calculé de façon à minimiser les forces qui excitent les "coordonnées modales" les plus basses, tout en imposant une atténuation proportionnelle sur la dynamique flexible du système.

Acknowledgements

It is a great pleasure to express my deep gratitude and sincere thanks to my research supervisors Professors Jorge Angeles and Arun Misra for their invaluable guidance, encouragement, and support. Without their continuous help and support this thesis could not have been completed. I am also very much indebted to them for the financial support extended to me through the Research Grants OGP0004532 and OGP0000967 of the Natural Sciences and Engineering Research Council of Canada (NSERC), and partly through the STEAR-Quebec COBRA project awarded to Bombardier, Inc.; without it this work could not have even been started. Moreover, I would like to thank them for their scrupulous, critical reading of all the technical documents I have written during the course of my Ph.D. studies at McGill; this manuscript has been no exception. I have learned a lot from all their comments, remarks, and suggestions.

The translation of the thesis abstract into French has been done by Danielle Nasrallah. I would like to thank her for this great help.

I wish to express my wholehearted thanks to Professor Paul Zsombor-Murray and all the colleagues in my group at the Centre for Intelligent Machines (CIM)—particularly to Dr. Svetlana Ostrovskaya, Dr. Alexei Morozov, Chin-Pun (Amy) Teng, Khalid Al-Widyan, and Alessio Salerno—for all the wonderful discussions and the great time we have had over the years. Dr. Ostrovskaya has also helped me by her meticulous review of the thesis, for which I am dearly grateful.

I am also pleased to acknowledge the help and support of Irene Cartier of the Department of Mechanical Engineering, as well as those of the CIM staff Jan Binder, Daniel Chouinard, Cynthia Davidson, and Marlene Gray.

Finally, I would like to express my deepest gratitude to my wife Parisa and my daughter Parmida for their great patience, support, and all the sacrifices they have made. My parents and my brother also deserve sincerest thanks for their encouragements and their unwavering belief in me.

Claim of Originality

The ideas expressed in this thesis, to the best of the author's knowledge, are original[1]. The contributions of this thesis are listed below:

- Novel algebraic definitions for the twist and the Jacobian—in the context of kinematic chains—have been proposed.
- The partial derivative of the angular velocity of a body in a serial kinematic chain—structurally flexible or otherwise—with respect to the chain generalized coordinates has been derived in *closed form*. The relation has then been extended to obtain the linearized kinematic relations of such manipulators.
- The use of *accelerometer arrays* for the estimation of the complete pose and twist of rigid bodies has been proposed. The effect of the accelerometer-array attitude errors on the accuracy of the results has been recognized; to alleviate these errors, two attitude-calibration techniques for accelerometer arrays have been developed.
- An observer structure that is based on the dynamics of the flexible submanipulator alone has been proposed.
- An algorithm for *flexible-link redundancy resolution* has been formulated.
- A novel formulation for the *pose-error vector* has been given.
- The use of proportional-damping properties in a trajectory-tracking control of manipulators with flexible and rigid subsystems has been proposed; with this approach, the control law can conditionally stabilize the flexural motions.

[1]Some of the results reported in this thesis have in part been published in (Parsa *et al.*, 2001; 2002a;b).

Contents

Chapter 1

Introduction

1.1 Background

In many practical applications involving long-reach manipulation it is desirable to have a smaller manipulator located at the end of a larger arm to perform specific tasks. The larger arm, named *macro-manipulator*, does the coarse positioning, whereas the smaller manipulator, called *micro-manipulator*, performs the task requiring fine positioning.

Many potential applications of such kinematically redundant systems, ranging from the Mobile Servicing System (MSS) of the International Space Station to the aircraft industry, and to in-situ robotic brick masonry, have been explored (Robins, 1997). Particularly, in the case of the MSS, shown in Fig. 1.1, the system has been designed to execute a variety of tasks which are not easily performable otherwise, such as cleaning the solar panels. As seen in the figure, the MSS comprises three subsystems: The Mobile Base System; the Space Station Remote Manipulator System (SSRMS), a.k.a. Canadarm2, which acts as the macro-manipulator; and the dual-arm Special Purpose Dexterous Manipulator (SPDM), which is to take on the role of the micro-manipulator.

As an alternative to the *macro-micro* structure, one can use a stationary robotic manipulator. In that case, however, in order to carry out such tasks as shot-peening, painting, stripping, cleaning, and deicing of aircraft, large robots will be required; like

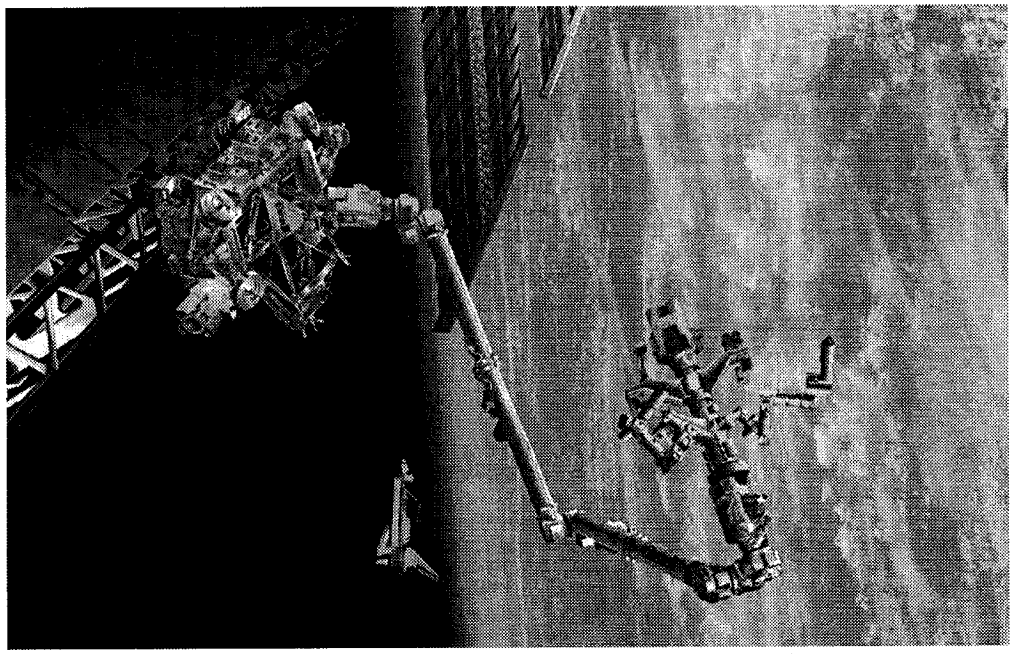

Figure 1.1: The Mobile Servicing System (`http://www.mdrobotics.ca`)

the robotic aircraft-cleaning system shown in Fig. 1.2.

The macro part of the macro-micro setup is often structurally far more flexible than its micro counterpart. This is especially true for space applications because, as Book (1993) put it, "space means long and lean."

For a particular macro-micro system, the great difference in the flexibility of the two subsystems can be ascertained by comparing the lowest of the link natural frequencies of the micro-manipulator with that of the macro-manipulator. If the frequency pertaining to the latter is several orders of magnitude below the one pertaining to the former, then, for all analysis purposes, the micro-manipulator can be assumed to have rigid links—despite the physical impossibility of rigidity (Resnick, 1968). Moreover, the macro-manipulator should be assumed to have flexible links and be modelled accordingly. Otherwise, the flexibility can cause inaccuracies in the Cartesian trajectory of the end-effector, which, if not negligible, may result in serious damage to the workpiece, to the environment, or even to both.

Obviously, the above-mentioned inaccuracies can occur regardless of the size ratio

Figure 1.2: A robotic aircraft-cleaning system (`http://www.putzmeister.de`)

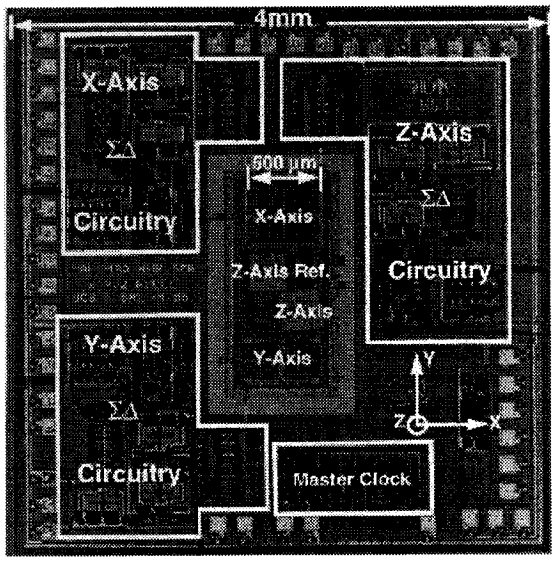

Figure 1.3: A micromachined triaxial accelerometer (`http://www.sandia.gov/micromachine`)

of the two *submanipulators*[1]. Therefore, we henceforth relax the implicit size-ratio condition and, by generalization, call the two subsystems the *flexible submanipulator* and the *rigid submanipulator.*

Effective control of a manipulator having flexible links, in addition to a correct dynamics model, requires accurate information on the states of the system. Apparently, for a flexible-link manipulator, the states must—in some form—include the *flexural generalized coordinates* and the *flexural generalized velocities* of the flexible links. The *flexural generalized coordinates*, or *flexural coordinates* for brevity, are understood here as a set of real variables that can describe the deformed shape of a structurally flexible link or system in a *discretized* sense. These coordinates can be, for example, the nodal displacements in a finite-element mesh, the end-point displacements of the flexible links, or the generalized coordinates used in the assumed-modes method. These generalized coordinates along with their time-rates of change, the *flexural generalized velocities*, constitute the *flexural states.*

[1]In fact, if the micro-manipulator is multiple orders of magnitude smaller than its macro counterpart, as the terms suggest, its motions will clearly have no significant effect on the dynamics of the macro-manipulator.

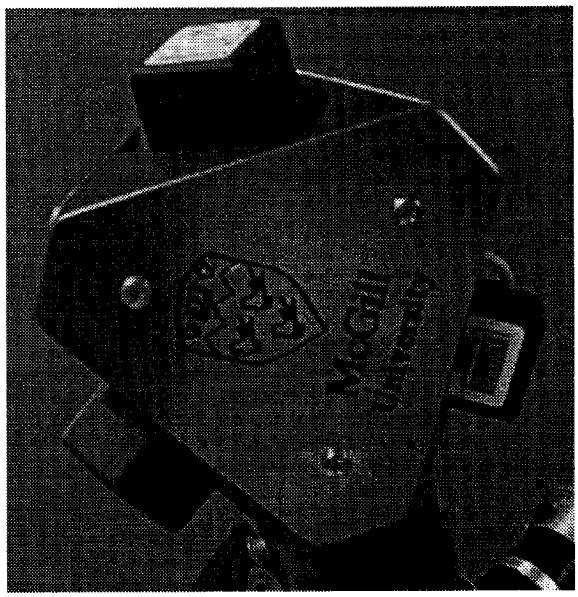

Figure 1.4: An accelerometer array

Most of the times, however, the *flexural states* cannot be measured directly and thus, should unavoidably be inferred from other measurements using a state estimator. In this thesis, we propose a procedure through which these states can be estimated using the position, orientation, velocity, and angular-velocity data of the base of the rigid submanipulator. These data can be inferred from the point-acceleration information acquired from an *accelerometer array*, which is an instrument composed of a kinematically redundant set of triaxial accelerometers; a typical micromachined triaxial accelerometer and a prototype array are shown in Fig. 1.3 and 1.4, respectively.

1.2 Pose and Twist Estimation

The real-time estimation of the pose—position and orientation—and the twist—velocity and angular velocity—of rigid-bodies has been the focus of extensive research for several decades, the principal reason, perhaps, being its application in the guidance and navigation of aircraft, spacecraft, and satellites. However, new applications are being found in the realm of robotics and automation; mobile robots are sometimes equipped with systems that can help determine pose and twist, for example.

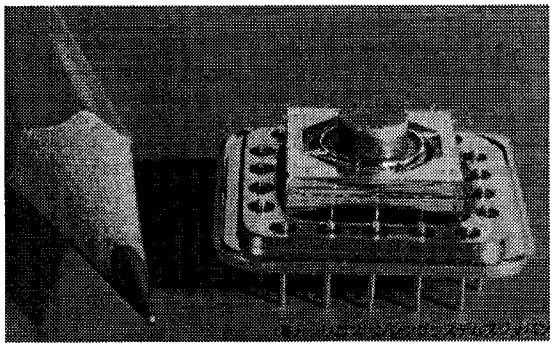

Figure 1.5: A rate-gyro (`http://www.spp.co.jp/sssj/sirikon-e.html`)

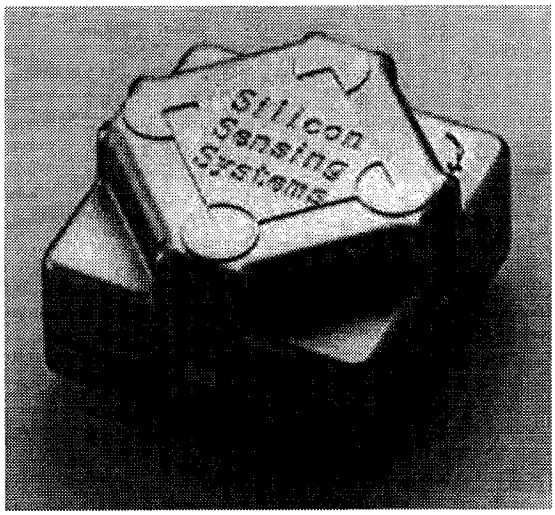

Figure 1.6: A three-axis rate-gyro (`http://www.spp.co.jp/sssj/sirikon-e.html`)

In inertial navigation systems, accelerometers have long been used beside other sensors such as rate-gyros, inclinometers, or combinations thereof to determine the pose and twist of moving bodies. In such a system, the rate-gyro—which may look like one of the sensors shown in Figs. 1.5 and 1.6—is used to measure the absolute angular velocity, upon the numerical integration of which the body attitude is obtained. Then, by reading the accelerometer signals, the navigation system can determine an inertial-frame representation of the absolute acceleration of the body (Grubin, 1973). Next, this acceleration is integrated to infer the full twist and pose of the body. Since different types of sensors are used in these systems, sensor-data fusion becomes an issue; the accelerometer being a part of the sensor system, its readouts are fused with the signals from the other sensors through applicable kinematic relations and noise models. Such an approach has been used in a number of works, some of which are reviewed below.

Vaganay *et al.* (1993) and Vaganay and Aldon (1994) described an attitude-estimation algorithm for mobile robots; in the algorithm, five inertial sensors—two single-axis accelerometers and three rate-gyros—were used in addition to an odometer to estimate the roll, pitch, and yaw angles. The attitude was calculated in two dif-

ferent ways: The first was based on the roll and pitch angles estimated by measuring the components of the gravitational acceleration with the accelerometers[2]; the second, however, was based on obtaining all three angles via integration of the rate-gyro data using a third-order Runge-Kutta method (Grubin, 1973). Finally, the authors fused the two sets of pitch and roll results together through an EKF to obtain better estimates, but, due to the complexity of the dynamics of the underlying system, a rate-gyro noise model was utilized as the system dynamics instead.

Markley *et al.* (1994) reported a spacecraft attitude-estimation algorithm which fused the rate-gyro data with that of one or more sensors of other types such as *star trackers* or *magnetometers.* The measurement system did not include any accelerometer, but the data filtering was still performed based only on kinematic relations and a gyro-drift model, i.e., the spacecraft dynamics was not involved. The approach taken in this reference was deterministic, meaning that the system and the measurement process as well as the errors were assumed to be deterministic while the errors were considered unmeasurable. The algorithm proposed by the authors was H_∞-based, and the resulting filter could thus be seen as an extended H_∞ filter, due to the nonlinearity of the equations. The authors gave a necessary condition for the boundedness of a "generalized estimation error."

In (Baerveldt and Klang, 1997), a low-cost, low-weight attitude-estimation system was proposed for autonomous helicopters. The system comprised a dual-axis inclinometer and a rate-gyro. The sensor signals were conditioned using analog filters that produced independent attitude estimates, and the sensor-data fusion was simply performed by directly summing up the output of the filters.

Roumeliotis *et al.* (1998; 1999a) discussed the problem of attitude estimation for mobile robots in the plane. To determine the yaw angle of the robot, they suggested two separate measurements: The angular velocity of the robot about an axis perpendicular to the plane of motion using a single-axis rate-gyro, which—upon integration—

[2]The authors of the cited references stated that it is impossible to obtain the yaw angle using accelerometers. Obviously, this is so if insufficient acceleration measurements are available.

could produce an online estimate for the body attitude, represented by the angle of rotation; and the absolute orientation of the body measured by another sensor that could give attitude information only intermittently. The authors argued that using a model for gyro bias relieves one from the trouble of the dynamics modelling altogether; consequently, the results obtained would become applicable to any other similar attitude-estimation problems, whether that of mobile robots or otherwise. Through Kalman filtering the rate-gyro signal, Roumeliotis *et al.* integrated the gyro signal to obtain rather accurate estimates for the yaw angle.

The same problem in three dimensions, mostly motivated by the localization problem of Mars rovers, was studied in (Roumeliotis *et al.*, 1998; 1999b), where an instrumentation system composed of three rate-gyros, three single-axis accelerometers, and a sun sensor was proposed. While the gyro signals were integrated forward in time to provide estimates of the attitude of the body as it moved, the accelerometers and the sun sensor were used to obtain more accurate data on the orientation of the robot when it stopped. Then, the accurate data collected were propagated backward until the robot previous stop, to obtain another set of estimates for its attitude over the time-interval. Next, a *smoother* was introduced to reconcile the attitude estimates obtained by both the forward and the backward filters. Finally, the smoothened orientation results were used along with acceleration signals to obtain an estimate of the position vector of the robot.

Rehbinder and Hu (2001) studied the problem of attitude estimation for walking robots, which usually experience periods of abrupt variations in their acceleration, using a triaxial rate-gyro and a triaxial accelerometer. These researchers partitioned the entire manoeuvre time to an alternating sequence of low-acceleration and high-acceleration periods. Over the former periods, they suggested using the accelerometer readouts, which are proportional to the components of the gravitational acceleration, as the output of the dynamic system represented by the kinematic differential relation between the attitude and the angular velocity of the body. The body attitude,

represented by one column of the rotation matrix from a body-attached frame to an inertial frame, was obtained using a "linear" Kalman filter, as opposed to an EKF. Over the latter periods, however, the system became unobservable, and an estimate of the attitude was obtained by numerically integrating the differential kinematic relation, which could be thought of as another Kalman filter with no feedback, the authors assert. In other words, the attitude was calculated through switching back and forth between these two Kalman filters.

In order to time-discretize the system dynamics equations, Rehbinder and Hu integrated the kinematic relation in "closed form," as though the angular velocity remained constant over the sampling period. Then, based on the assumption that the dynamics equations were linear, they showed that, under certain conditions, the system is stochastically observable, the attitude-estimation algorithm thus being convergent. However, the dynamics model was actually a linearized one, and the Kalman filter was indeed an EKF.

Liu and Pang (2001) reported a mobile-robot positioning system in which the signals from a two-axis solid-state accelerometer were integrated twice to estimate the robot position vector. Recognizing the divergence of the integration results from the actual values, the authors suggested, without actual implementation, that the "periodic recalibrations" of the positioning system with the aid of other kinds of sensors which can independently measure the robot position, velocity, and attitude could avert the instability problem. Liu and Pang also proposed Kalman filtering to fuse the sensor data without having to involve the motion dynamics. Some experimental results collected while displacing the positioning system by the end-effector of a Sony SRX-410 robotic arm were reported.

As seen from the references cited above, the problem of dynamics complexity, in this context, has been addressed in the literature. Moreover, although accelerometers have long been employed not only in vibration- and impact-related measurements but also in inertial navigation systems to infer the position and velocity of moving objects,

they had neve been considered to be used alone for real-time, complete pose and twist estimation, until very recently (Parsa *et al.*, 2001).

The determination of the angular-velocity vector of a rigid-body from the velocity data of three noncollinear points of the body was studied by Angeles (1986). Then, in a related work (Angeles, 1987), the same author discussed the determination of the angular-acceleration using the velocity and acceleration information of three noncollinear points of the body; the results were then extended to the redundant-measurement case, for which the compatibility relations were obtained. The methods proposed were linear. Since measurements are more often than not contaminated by noise, Angeles (1990) developed a pose- and twist-estimation algorithm that filtered the noise content of the pose- and the twist-measurement signals through a least-square approach. Later, generalizing the results of (Angeles, 1987) to the situations whereby statistical weighting is desired, Sommer III (1992) proposed a nonlinear algorithm which addresses the problem of determining the angular-acceleration.

Even though the above-mentioned researchers studied the estimation of pose, twist, and angular acceleration of a rigid-body, they both assumed that the data were given in a fixed reference frame, but accelerometers always deliver the acceleration data in their own local frame. Therefore, taking this fact into account, Parsa *et al.* (2001) solved the problem of pose and twist estimation using an *accelerometer array*. However, since they also considered the possibility of accelerometers having installation error in orientation, the authors were able to show that orientation errors as small as 0.1° can cause even the angular-velocity estimate, obtained by integrating the angular acceleration, to rapidly diverge from its actual value, thereby completely undermining the accuracy of the results. To overcome this problem, they suggested fusing the results inferred from acceleration measurements with those from another type of sensor; for this purpose, the authors considered a recently developed pose-measurement fiber-optic sensor, called Shape-Tape (Danisch, 1998; 2000; Danisch *et al.*, 1999). The pose and twist estimation results thus obtained were stable. However, it seems that

an even better solution is to devise attitude-calibration schemes for the accelerometer arrays.

1.3 Estimation of Flexural States and Control of Flexible Manipulators

Since the very early experiments on flexible manipulators, the problem of determining the flexural states has attracted many researchers' attention[3]. Cannon and Schmitz (1984) used an optical sensor comprising a light bulb, a focusing lens, and a photo-detector to determine the end-link displacement of a single-link flexible manipulator. This displacement was then fed back in a full-state, discrete Linear Quadratic Gaussian (LQG) controller to control the end-point motion. Using numerical simulations, the authors showed that the LQG controller suffers from low stability margins. Cannon and Schmitz argued that the stability of the control system can be improved by means of a lower-order compensator. Indeed, Doyle (1978) showed that the LQG controllers can have very poor stability margins. For more on the issue, one can refer to (Maciejowski, 1989).

Kotnik *et al.* (1988) reported on their experiments with a single-link flexible manipulator. The system was equipped with a vision system and an accelerometer located at the end-point of the link. Three different control systems were tested. In the first one, the end-point position, obtained through the vision system, was fed back to a classical control system designed using the root-locus method. The second also used the position data; however, a state estimator and a Linear Quadratic Regulator (LQR) were used to control the system. In the third control system, the end-point acceleration was utilized along with the joint encoder to control the system. The authors asserted that the results of the acceleration feedback were very promising.

A study on the control of a two-link, three-degree-of-freedom flexible manipulator

[3]In this section, the specialized literature on the control of flexible-manipulators is reviewed only as far as it involves the estimation of the flexural states, the exception being a few references regarding *input shaping*, which are cited for sake of completeness.

was conducted by Fukuda and Arakawa (1989), who suggested the use of three-axis force and moment sensors at the the proximal end of each link to estimate the flexural states using an observer. The flexural states considered were the two bending deflections of each link in addition to the link torsion. The estimated states as well as the measured ones were then used in an LQR control system. After presenting some simulation results, the authors discussed the sensitivity of the control system to variations in the physical parameters of the system. From their sensitivity analysis, Fukuda and Arakawa concluded that a "stable domain of the parameter's uncertainty can be found."

Matsuno and Sakawa (1990) used three single-axis accelerometers and "an angular accelerometer of servo type" to estimate the flexural coordinates of a six-degree-of-freedom flexible manipulator. In their case, however, the link masses and inertias were considered negligible compared with those of the end-effector; the authors could thus derive a simple dynamics model by considering equivalent springs representing the arm flexibility. Installing the above-mentioned sensors on the end-effector, Matsuno and Sakawa designed an observer to estimate the flexibility-caused displacement of the end-effector. They also devised a stable control law for the system. At the end, some experimental results were reported.

The end-point control of a single-link flexible arm with a payload which has unknown dynamics was the subject of other research works (Alder and Rock, 1993; 1994). A pendulum of variable length that could be locked at will acted as the payload. The instrumentation system included a CCD camera for measuring the end-point position. The control system comprised a self-tuning regulator that handled the unknown dynamics of the payload; the high-frequency unmodelled dynamics of the flexible arm, on the other hand, was taken care of by a frequency-weighted LQG which had an improved robustness.

In (Chiang *et al.*, 1991), a *macro-mini manipulator* composed of a long, highly flexible link and a short, rigid link was used in fast and accurate pick-and-place oper-

ations by a pneumatic gripper. To accommodate the desired high-speed operations, the manipulator was equipped with an optical measurement system, similar to that used by Cannon and Schmitz (1984), which could determine the position of the tip of the mini-manipulator. The control system comprised two successive loops: The first loop was closed on the wrist tip position, the second trying to control the motion of the flexible link. The authors maintained that the performance achieved was "similar to that obtained ... [using the] LQG control methods." Their results suggested that the performance of the proposed two-loop control system was acceptable.

Qian and Ma (1992) also researched the control of a single-link flexible manipulator, their instrumentation system including four strain gauges along the link and an infrared optical system with the source LED attached to the tip and the position-sensitive device located at the root. The signals from the two middle strain gauges and the one from the optical system were used to directly calculate the three flexural coordinates taken to discretize the link; the flexural generalized velocities and the joint rate were obtained by four independent observers. The tip position was controlled by a sliding-mode controller. The simulation results were compared with those of a simple joint control, which caused long-lasting vibrations in the link. The authors argued that, because of the undershoot in the system step response—which should be due to the system being nonminimum-phase—the control loop must run at a period lower than the time delay between the torque application and the tip displacement in the same direction.

Panzieri and Ulivi (1993) addressed state estimation for a two-link arm in which the second link was flexible. The deformation of the flexible link was measured through optical sensing of the displacements of three different points of the link. The measurements were processed in a steady-state-gain Kalman filter to estimate all the states. Then, a singular-perturbation approach was used to control the tip motion. The control results were compared with those obtained using a PD controller.

The flexible manipulator used by Carusone *et al.* (1993) to perform experiments

on end-effector trajectory tracking was a planar, two-link arm. The deformation of each link was measured by three strain sensors, corresponding to which three flexural coordinates were chosen to describe the link deformation. The flexural coordinates were estimated by applying a curve-fitting technique on the link strain data, which obviated the need to a state estimator, as Carusone *et al.* suggested. The control algorithm used was a gain-scheduled LQR devised by Carusone and D'Eluterio (1993) in which the state-feedback gain at each instant was the steady-state gain computed from the underlying algebraic Riccati equation for the linearized dynamics equations at that instant. Furthermore, to reduce the induced vibrations in the links, the plant dynamics was augmented by sets of two cascaded integrators. In addition to the experimental results of the application of this controller, the authors reported those of a PID joint-motion controller. The former results were considerably better than those of the latter.

To estimate the flexural generalized velocities, Moallem *et al.* (1996) proposed three different observers. In all the three observers, the flexural coordinates were implicitly assumed to be *accurately* obtained from strain measurements on the links. The first observer was a full-flexural-state observer, the second and the third being a reduced-order observer and a sliding-mode observer, respectively. Even though the stability of each of the three observer designs was proven or otherwise concluded, due to the implicit assumption of access to accurate flexural-coordinate data—which is not true in practice—it can be imagined that the observer would actually not remain stable at all times. This is especially crucial because the authors used the assumed-modes method for flexible-link discretization, and there consequently was no exact relation between the measurements made on the link and the link flexural coordinates. The assumption might have been more realistic had the discretization been made using cubic splines; of course, the formulation presented by the authors is symbolic in nature, and can presumably be used for that case too.

The three foregoing observers were implemented on a two-link planar manipulator

whereby the first link was short and rigid, while the second was three-times as long and flexible with a payload at its end. The end-effector trajectory-control strategy used was feedback-linearization-based. As reported in (Moallem *et al.*, 1997), the authors found out that the lower the number of flexural coordinates used the better the results. They also reported some experimental results with regular PD controllers. Not unexpectedly, they found that the results improved when the clamped-free eigenfunctions were replaced by the eigenfunctions of a cantilever beam which has a mass at the end. For the complete details of the observers and the controller, one can see (Moallem *et al.*, 2000).

Konno *et al.* (1997) studied the vibration controllability of flexible manipulators, neglecting all second-order terms of the dynamics equations and the dependence of the mass matrix upon the flexural coordinates. The authors argued that, because the well-known controllability matrix obtained through linearized dynamics equations had no physical interpretation, they projected the equations onto the modal space. Then, the system was called "modal accessible" if all the principal generalized coordinates could be affected by the actuation wrench. A case study on a two-link manipulator kinematically similar to that of Fukuda and Arakawa (1989) was conducted. Konno *et al.*, however, assumed that the link masses were concentrated at the link end-points. In the experimental setup, one strain gauge was attached to the root of each link, by means of which the tip deflection was monitored. Obviously, given the assumptions made in this work, for a general structurally flexible manipulator, their results cannot be directly applied to study the study of the vibration controllability of the system.

Estimation of the elastic displacement of the tip in a single-link manipulator with a mass payload using an optical position-sensing system was revisited by Li and Chen (1998). The laser-emitting diode was installed at the link root, and the position-sensing device was attached at the tip. The estimator proposed by the authors was a fixed gain Kalman filter. The main differences with the work of Cannon and Schmitz (1984), as far as the state estimation is concerned, appear to be in the measurement

system and in the presence of the payload.

Zaki and ElMaraghy (1993) discussed the Model Reference Adaptive Control (MRAC) of an arm kinematically similar to that considered by Fukuda and Arakawa (1989). The MRAC results were compared with those of an LQG controller. The instrumentation system included two single-axis accelerometers attached at the end of each link, from which the authors calculated the second time-derivative of the link deflections using least squares. However, it was not made clear in the paper whether the orientation change of the accelerometers was also accounted for or not.

In a later paper (Zaki and ElMaraghy, 1995), the authors reported the implementation of a full-state sliding observer on the same system; the measurements were the accelerometer signals and the joint variables. The accelerometer signals were filtered and integrated in charge amplifiers to obtain the link end-point velocity, from which it seems that the foregoing orientation change was indeed neglected. A PD controller was used to control the joint variables. Additional experimental results on the system were reported in (Zaki *et al.*, 1998a;b).

Another research work is that of Wilson *et al.* (1998), in which their experiments with two planar, single- and two-link flexible manipulators are reported. Strain gauges were used to infer the flexural coordinates of the links. The generalized velocities of the system were estimated using a linear observer, meaning that the nonlinearity of the system was neglected. The control was achieved using the sliding-mode control.

A large number of other researchers have also reported the use of accelerometers, either alone or along with strain gauges, in the instrumentation system of structurally flexible manipulators, (e.g., Hillsley and Yurkovich, 1991; Sim and Lee, 1993; Tiemin *et al.*, 1996; Tokhi and Azad, 1997). However, they all use the accelerometer signals for feedback, not for estimation of flexural states.

Input shaping is another approach, as reported by some researchers (e.g., Meckl and Seering, 1988; Cleary *et al.*, 1992; Magee and Book, 1995), to reduce the vibration of flexible links. Obviously, such method is only useful for linear systems with

constant coefficients, its effectiveness thus being very limited; a multi-link flexible manipulator with moving joints, for instance, does not fit this description. Indeed, even if the flexible links of this manipulator are linearly elastic, the overall system entails nonlinearities due to the varying geometry of the system.

1.4 Dynamics and Control of Manipulators with Rigid and Flexible Subsystems

There is a vast literature on the dynamics modelling of rigid and flexible multibody systems, of which the two review papers (Schiehlen, 1997; Shabana, 1997) give very detailed accounts for a number of well-known methods; these papers include 197 and 105 references, respectively. Therefore, we will not review the literature available on the subject of dynamics modelling, the reader being referred to these two papers; another paper that can be helpful on the subject of mathematical modelling of multibody systems is (Schwertassek, 1998), where the author also addresses the geometric-stiffening effect (Sadigh and Misra, 1995). Nonetheless, in the next chapters, explanations will be given, and remarks will be made on the specifics of the method used here for the dynamics modelling whenever the need arises.

Regarding the vibrations of the macro-manipulator and its effects on the end-effector trajectory, three different approaches have been pursued: (*i*) Damping the vibrations of the macro using the dynamic forces applied upon its end-effector by the micro base; (*ii*) compensating for the effects of the micro-base motion on the Cartesian trajectory of the end-effector by correcting the trajectory of the micro-manipulator in the joint space on-line; and (*iii*) planning trajectories that, while the end-effector moves to perform a task, excite as little macro flexible motion as possible.

Many researchers have investigated the first approach, for example, (Torres *et al.*, 1996; Lew and Trudnowski, 1996; Sharf, 1996; Lew and Moon, 1999; Book and Loper, 1999); with the exception of Sharf, all of these authors modelled the macro-manipulator as a lumped mass-spring system.

In the control method proposed by Torres *et al.*, the kinetostatic force-torque relation was used to calculate the required joint torques, given the required vibration-dampening force. Lew and Trudnowski (1996) suggested a PD controller for the vibration of a single-link, fixed, flexible-link macro under the action of a single-link rigid arm.

Pursuing the same approach, i.e., approach (i), Sharf (1996) formulated the problem for multiple-link manipulators. Even though the dynamics of the macro-manipulator was considered as well, it was linearized. Moreover, it was implicitly assumed that the macro-joints would not move after redeployment, and that the geometric nonlinearities were small enough, thus neglecting the dependence of the macro-manipulator mass matrix on the flexural coordinates. State-feedback control was used to control the motion of the micro-manipulator joints. The results were then extended to the case whereby the micro-manipulator is kinematically redundant, and the end-effector is to trace a trajectory while trying to minimize its base vibration. However, it is apparent that, to be able to perform both functions simultaneously, the rigid manipulator must have a large degree of redundancy.

Lew and Moon (1999) investigated the problem and tried to solve it using a "simple, robust decoupling method." However, the authors did not substantiate their robustness claim. In this paper, the micro-manipulator base was considered to possess six degrees of freedom. In the control loop, which appears to be feedback-linearization based, the joint accelerations—assumed to be inferred from optical encoders—were used.

Book and Loper (1999) also assumed the macro-manipulator dynamics as linear. Furthermore, the angular motion of the rigid-robot base was neglected. The joint angles were controlled using PI compensators, and some simulation and experimental results were compared, which appeared promising.

Yoshikawa *et al.* (1993), following the second approach, used the self-motion of a redundant micro-manipulator to compensate for the end-effector trajectory errors

caused by the flexural motions of the macro-manipulator. The redundancy of the whole system was resolved by optimizing a performances index called the *compensability measure*, which actually is the inverse of the product of the singular values of a Jacobian matrix that maps the flexural generalized velocities to the required compensatory micro joint rates. (Very recently, Staffetti *et al.* (2002) have argued that such performance indices do not show how well-conditioned a certain configuration is.) Then, two sets of PD controllers were considered for the two submanipulators; the set-point of the micro-manipulator control loop was corrected by the compensatory joint-angle signals. The authors also reported several simulation results.

The foregoing method was generalized by Yoshikawa *et al.* (1996) to be applied for the hybrid control of macro-micro manipulators. Although the dynamics of the system was also taken into account, the dynamics model of the macro was obtained assuming that the mass and the stiffness of the macro links were lumped. Furthermore, the macro links were independently controlled using an LQR controller, presumably a gain-scheduled one, while the hybrid control of the system was realized by hybrid-controlling the micro-manipulator alone.

Torres and Dubowsky (1993) and Torres *et al.* (1994) addressed a trajectory-planning problem, the third approach, in which only two points of the end-effector path were predetermined, the beginning and the end. In other words, no *trajectory tracking* was involved. Assuming that the interaction between the lumped-modelled flexible base and the micro-manipulator dynamics was negligible, these researchers tried to compute joint-space trajectories with minimum elastic potential energy restored in the flexible base. However, such a method could not give the whole picture because its results are totally independent of the manipulator joint-rates. Additionally, not only does the implementation of such a method become complicated as the number of links increases but also its very effectiveness is unclear.

In (Hanson and Tolson, 1995), a locally optimal control of the macro-micro system was proposed to handle the first and the last tasks—base-vibration suppression

and trajectory planning—together. This was achieved using a weighted sum of two control inputs. One input made the micro-manipulator follow a trajectory in the joint space for which, if the base vibration were neglected, the end-effector could follow the desired Cartesian trajectory while causing a minimum dynamic reaction wrench—force and moment—between the base and the rigid robot. The other control input was calculated so as to minimize a pseudo-kinetic energy (Nakamura, 1991) of the rigid submanipulator at the next time step. Hanson and Tolson showed that their second control input could render the pseudo-kinetic energy what, in effect, was a Lyapunov function. However, the authors implicitly assumed that the flexural states were all known exactly. For the simulation results reported, the authors assumed the flexible submanipulator to be actually a rigid-link manipulator with lumped stiffness at the joints; in that case, the flexural states are indeed the joint angles of the macro-manipulator and their time-rates.

A control algorithm designed to achieve all the three goals was proposed by Nenchev *et al.* (1997; 1999). Reportedly, the algorithm was obtained from the marriage of two methods: A control method for flexible-link manipulators and another one for free-flying space robots. The authors assumed that the macro joints were locked after redeployment, i.e., the macro-manipulator was used only for coarse positioning. They further assumed that the self-motion of the micro-manipulator was used to compensate for the errors caused by the macro-manipulator flexibility in a manner that minimized the negative effect on the micro-base vibration. However, the dynamics analysis used by the authors does not appear to be rigorous.

Jiang and Goldenberg (1998) also attempted to combine all three approaches together by defining three state-space performance constraints corresponding to the three approaches, and devising quite a sophisticated control law that forced the macro-micro system to move in the constraint subspace. A major component that this method lacks is an algorithm for resolving kinematic redundancy; therefore, it can only provide end-effector trajectory tracking by controlling the joint angles.

The stability of this control law was proven using a Lyapunov function. It was further shown that the stability was exponential. The dependence of the mass matrix and that of the inertia forces of the system on the state-trajectory of the system, however, were totally neglected in the stability analysis, for which an inaccurately linearized model of the system was used. This practically means that the proof given might not remain valid for the actual dynamics model.

The control of kinematically redundant, flexible manipulators was addressed in (Nguyen *et al.*, 1992). The redundancy resolution and the vibration minimization were done together by obtaining the general expression for the joint accelerations that, if realizable without exciting vibrations in the flexible links, would make the end-effector follow the desired trajectory; then, among the infinitely many possible solutions, the one that would minimize the excitation generalized force in the Euclidean norm was chosen. This planned joint-space trajectory was afterwards put in a computed-torque control loop with a PD compensator to control the robot.

The above method was complemented by Kim and Park (1996; 1998) in the sense that they wrote the driving dynamics of the flexural motions in state space; the authors then tried to use linear-system tools to obtain the lowest-frequency "principal modes" of the vibrations, and to dampen them through a proper choice of the manipulator *self-motions*.

Although many researchers have considered the full-pose trajectory control of the end-effector, the formulations developed do not reflect the *non-vector* nature of the attitude part of the pose. In other words, it has implicitly been assumed that the pose is represented by a six-dimensional vector, and that the pose error can be obtained by an element-by-element subtraction of the current pose form the desired one.

1.5 Thesis Outline

The thesis hinges on a problem of paramount importance in robot control, which, nevertheless, has not been addressed in sufficient detatil in the specialized literature.

Indeed, the effectiveness of any control scheme depends on how accurately the states of the plant are known. By virtue of the unavoidable instrument noise, roundoff error, and unmodellable features, the plant states can be known only approximately, the accuracy of their approximation depending on how accurately these states are estimated. Hence the importance of an effective state estimator, literature on which seems to be scanty. Here is where the main contribution of the thesis lies.

As mentioned in Section 1.1, the pose and twist data of the rigid-robot base, determined through acceleration sensing, are intended for the estimation of the flexural states of the flexible submanipulator in an observer. However, the state-output relations, i.e., the relations between the flexural coordinates and the foregoing data, are nonlinear and, thus, have to be linearized. In Chapter 2, we derive, in closed form, the required partial derivatives in terms of other usually available entities, such as the Jacobian of the flexible submanipulator and the base angular velocity[4]. Both the twist and the Jacobian matrix mentioned above are defined in Section 2.1.

The recursive kinematic relations and the spatial discretization of flexible links are two other subjects discussed in Chapter 2, where some basic relations pertaining to the Euler parameters and their time-derivative are also reviewed.

Chapter 3 is devoted to the estimation of the pose, twist, and twist-rate of a rigid-body from the point-acceleration data delivered by an on-board accelerometer array. To address the attitude-calibration problem mentioned in Section 1.2, two algorithms are proposed, one using gravitational-acceleration measurements and the other employing acceleration data collected over an arbitrary manoeuvre. Our simulation results show that the latter, which is an iterative procedure performed off-line, can be utilized to calibrate an accelerometer array quite accurately. Furthermore, unlike the procedure reported in (Parsa *et al.*, 2001)—where the angular velocity was estimated by numerical integration, the error incurred thus being accumulative—the angular

[4]The partial derivatives at play may, of course, be obtained by symbolic differentiation of the twist relations. However, the drawback of such a method is that the differentiations have to be done for each manipulator separately, and that redundant algebraic manipulations and arithmetic operations are unavoidable.

velocity is determined directly and accurately from the accelerometer data.

The dynamics model of the system is derived in Chapter 4 using the *natural orthogonal complement*. Albeit any manipulator with flexible and rigid *subsystems* can be treated as one manipulator with flexible and rigid *links*, we handle the two submanipulators separately. As explained in Chapter 5, by doing so, the mathematical model of the flexible arm alone—which is obviously of a lower order than that of the entire system—can be used as the *modelled dynamics* in an *extended Kalman filter* acting as the state estimator. The dependence of the mass matrix on the system generalized coordinates is also accounted for in the linearization of the dynamics equations.

The control algorithm we use in this thesis is an extended, more accurate variant of earlier works (Kim and Park, 1996; 1998), which requires less computations; this algorithm is discussed in great detail in Chapter 6. Therein, we try to address the pose-error problem through a mapping that takes the seven-dimensional error in the vector of end-effector generalized coordinates to a six-dimensional vector. At the end of the chapter, some numerical results of the application of the methods developed in the thesis on a planar *RRRR* manipulator are reported.

The thesis ends in Chapter 7 with some concluding remarks and recommendations for further research.

1.6 On Notation

Throughout this thesis, all vectors and cross-product matrices are expressed in their related local frames, unless otherwise specified by use of a left-superscript. For example, while $\mathbf{p}_i$ represents the position vector of the origin of the body-frame $\mathcal{F}_i$ expressed in $\mathcal{F}_i$, ${}^{\mathcal{R}}\mathbf{p}_i$ is the same position vector expressed in the inertial frame $\mathcal{R}$.

Furthermore, two kinds of differentiations with respect to time are used: (*i*) The *element-wise* differentiation of a vector with respect to time, which is denoted by a *dot* on top of a variable; and (*ii*) differentiation with respect to time in an inertial

reference frame, which is specified by d/dt.

Chapter 2

Basic Kinematic Relations

2.1 Rigid-Body Kinematics

This section mainly deals with rigid-body kinematics. At times, however, we will also refer to the case of flexible bodies.

2.1.1 Attitude Representation

The attitude of a rigid body can be expressed using many different three- or four-parameter representations, such as the different sets of Euler angles, Gibbs vectors (Wertz, 1978), natural and linear rotation invariants (Angeles, 2002), Rodrigues vector, Euler parameters, Cayley-Klein parameters, and Pauli's spin operators (Goldstein, 1980). Of course, in any case, only three parameters are independent. Among these different representations, the Euler parameters have proven to be the best regarding the ease of algebraic manipulation, algebraic robustness, and ease of integration into the dynamics models of rigid bodies. In spacecraft applications, particularly, these parameters are desirable because some globally stable control systems have been devised that use Euler parameters as feedback (Reynolds, 1998).

The Euler parameters constitute a set of unit quaternions and can be expressed as a unit-norm, four-dimensional array $\boldsymbol{\eta}$ given by

$$\boldsymbol{\eta} = \begin{bmatrix} \mathbf{u}^T & u_0 \end{bmatrix}^T \triangleq \begin{bmatrix} \mathbf{e}^T \sin\frac{\phi}{2} & \cos\frac{\phi}{2} \end{bmatrix}^T . \tag{2.1}$$

This representation means that the rigid body has arrived at its new attitude, from a

reference orientation, via a rotation through an angle ϕ about an axis parallel to the unit vector $\mathbf{e}$. As shown in (Angeles, 2002), this rotation can also be represented by the rotation matrix $\mathbf{Q}$ given by

$$\mathbf{Q} = e^{\phi\mathbf{E}} \equiv \mathbf{1} + \sin\phi\mathbf{E} + (1 - \cos\phi)\mathbf{E}^2 \tag{2.2}$$

where $\mathbf{E}$ is the cross-product matrix[1] (CPM) of $\mathbf{e}$. In terms of the Euler parameters, $\mathbf{Q}$ can be written as

$$\mathbf{Q} = \mathbf{1} + 2u_0\mathbf{U} + 2\mathbf{U}^2 \tag{2.3}$$

in which $\mathbf{U}$ is the CPM of $\mathbf{u}$, the vector part of the quaternion (Angeles, 2002).

As shown in Appendix A, $\dot{\boldsymbol{\eta}}$, the time-rate of change of $\boldsymbol{\eta}$ in the body-frame, is related to the angular velocity $\boldsymbol{\omega}$ of the body, expressed in the same frame, by

$$\dot{\boldsymbol{\eta}} = \mathbf{H}(\boldsymbol{\eta})\,\boldsymbol{\omega}, \tag{2.4a}$$

$$\mathbf{H} \equiv \mathbf{H}(\boldsymbol{\eta}) \triangleq \frac{1}{2}\begin{bmatrix} u_0\mathbf{1} - \mathbf{U} & -\mathbf{u} \end{bmatrix}^T. \tag{2.4b}$$

Notice that, although the Euler parameters are the same in both the local and the inertial frames, their time rates are different in the two frames.

Furthermore, it can be shown that the inverse relations of eqs. (2.4) are given by

$$\boldsymbol{\omega} = \overline{\mathbf{H}}(\boldsymbol{\eta})\,\dot{\boldsymbol{\eta}}, \tag{2.5a}$$

$$\overline{\mathbf{H}} \equiv \overline{\mathbf{H}}(\boldsymbol{\eta}) \triangleq 4\mathbf{H}^T \equiv 2\begin{bmatrix} u_0\mathbf{1} - \mathbf{U} & -\mathbf{u} \end{bmatrix}. \tag{2.5b}$$

It is thus apparent that the right-hand sides of eqs. (2.4a & 2.5a) are the linear transformations of the Euler parameters into the angular velocity, and vice versa. We now have

Lemma 1. *The relations between the time-derivative of the Euler-parameter array and the angular-velocity vector of a rigid body, eqs. (2.4a & 2.5a), can equivalently be*

[1]The cross-product matrix $\mathbf{V}$ of a vector $\mathbf{v}$, not dependent upon $\mathbf{x}$, is the skew-symmetric matrix given by

$$\mathbf{V} \equiv \mathrm{CPM}(\mathbf{v}) \triangleq \frac{\partial(\mathbf{v}\times\mathbf{x})}{\partial\mathbf{x}}, \quad \forall\mathbf{x}\in\mathbb{R}^3 \qquad \Longrightarrow \qquad \mathbf{V}\mathbf{x} \equiv \mathbf{v}\times\mathbf{x}.$$

expressed as

$$\dot{\boldsymbol{\eta}} = \mathbf{K}(\boldsymbol{\omega})\,\boldsymbol{\eta}, \tag{2.6a}$$

$$\boldsymbol{\omega} = \overline{\mathbf{K}}(\dot{\boldsymbol{\eta}})\,\boldsymbol{\eta}, \tag{2.6b}$$

respectively, where

$$\mathbf{K} \equiv \mathbf{K}(\boldsymbol{\omega}) \triangleq \frac{1}{2}\begin{bmatrix} -\boldsymbol{\Omega} & \boldsymbol{\omega} \\ -\boldsymbol{\omega}^T & 0 \end{bmatrix} \tag{2.6c}$$

$$\overline{\mathbf{K}} \equiv \overline{\mathbf{K}}(\dot{\boldsymbol{\eta}}) \triangleq -\dot{\overline{\mathbf{H}}} \equiv -2\begin{bmatrix} \dot{u}_0\mathbf{1} - \dot{\mathbf{U}} & -\dot{\mathbf{u}} \end{bmatrix} \tag{2.6d}$$

in which $\boldsymbol{\Omega}$ is the cross-product matrix of $\boldsymbol{\omega}$.

Proof: To prove eq. (2.6a), expand eq. (2.4a) using eq. (2.4b):

$$\dot{\boldsymbol{\eta}} = \frac{1}{2}\begin{bmatrix} u_0\mathbf{1} + \mathbf{U} \\ -\mathbf{u}^T \end{bmatrix}\boldsymbol{\omega} = \frac{1}{2}\begin{bmatrix} u_0\boldsymbol{\omega} + \mathbf{U}\boldsymbol{\omega} \\ -\mathbf{u}^T\boldsymbol{\omega} \end{bmatrix} = \frac{1}{2}\begin{bmatrix} u_0\boldsymbol{\omega} - \boldsymbol{\Omega}\mathbf{u} \\ -\boldsymbol{\omega}^T\mathbf{u} \end{bmatrix}$$
$$= \frac{1}{2}\begin{bmatrix} -\boldsymbol{\Omega} & \boldsymbol{\omega} \\ -\boldsymbol{\omega}^T & 0 \end{bmatrix}\begin{bmatrix} \mathbf{u} \\ u_0 \end{bmatrix}$$

which, using the definition given by eq. (2.6c), becomes eq. (2.6a).

To obtain eq. (2.6b), notice that, based on eqs. (2.5a & 2.5b),

$$\boldsymbol{\omega} = 2\begin{bmatrix} u_0\mathbf{1} - \mathbf{U} & -\mathbf{u} \end{bmatrix}\begin{bmatrix} \dot{\mathbf{u}} \\ \dot{u}_0 \end{bmatrix} = 2(u_0\dot{\mathbf{u}} - \mathbf{U}\dot{\mathbf{u}} - \mathbf{u}\dot{u}_0)$$
$$= -2\big[(\dot{u}_0\mathbf{1} - \dot{\mathbf{U}})\mathbf{u} - \dot{\mathbf{u}}u_0\big] = -2\begin{bmatrix} \dot{u}_0\mathbf{1} - \dot{\mathbf{U}} & -\dot{\mathbf{u}} \end{bmatrix}\begin{bmatrix} \mathbf{u} \\ u_0 \end{bmatrix}$$
$$= -\dot{\overline{\mathbf{H}}}\,\boldsymbol{\eta}$$

which basically is eq. (2.6b) with $\overline{\mathbf{K}}(\dot{\boldsymbol{\eta}})$ defined by eq. (2.6d). □

A property of the matrices $\mathbf{H}$ and $\overline{\mathbf{H}}$ which is needed for the derivations reported in Section 2.2 and Appendix B is summarized below:

Lemma 2. *Matrices $\mathbf{H}$ and $\overline{\mathbf{H}}$, defined in eqs. (2.4b & 2.5b), obey*

$$\overline{\mathbf{H}}\,\dot{\mathbf{H}} \equiv \frac{1}{2}\boldsymbol{\Omega} \tag{2.7}$$

where $\boldsymbol{\Omega}$ is the CPM of the angular-velocity vector $\boldsymbol{\omega}$.

Proof. The proof of the counterpart of this property in the fixed frame was given by Nikravesh *et al.* (1985). Nevertheless, because the type of notation used by these authors is very different from the one used in this thesis, an independent proof of eq. (2.7) is produced here.

If the left-hand side of eq. (2.7) is post-multiplied by an arbitrary vector $\mathbf{x}$, and then expanded, we obtain

$$\begin{aligned}\overline{\mathbf{H}}\dot{\overline{\mathbf{H}}}\mathbf{x} &= \begin{bmatrix} u_0\mathbf{1} - \mathbf{U} & -\mathbf{u} \end{bmatrix} \begin{bmatrix} \dot{u}_0\mathbf{1} + \dot{\mathbf{U}} \\ -\dot{\mathbf{u}}^T \end{bmatrix} \mathbf{x} \\ &= (u_0\dot{u}_0\mathbf{1} - \mathbf{U}\dot{\mathbf{U}} + u_0\dot{\mathbf{U}} - \dot{u}_0\mathbf{U} + \mathbf{u}\dot{\mathbf{u}}^T)\mathbf{x}. \end{aligned} \tag{2.8}$$

From the triple-vector-product relation (Arfken, 1985), however, it follows that, for the cross-product matrices $\mathbf{A}$ and $\mathbf{B}$ of any two arbitrary vectors $\mathbf{a}$ and $\mathbf{b}$, respectively, the matrix product $\mathbf{AB}$ can be calculated as

$$\mathbf{AB} \equiv -(\mathbf{a}^T\mathbf{b})\mathbf{1} + \mathbf{b}\mathbf{a}^T \tag{2.9}$$

in which $\mathbf{1}$ is the 3×3 identity matrix. Applying this relation to $\mathbf{U}\dot{\mathbf{U}}$ in eq. (2.8) results in

$$\overline{\mathbf{H}}\dot{\overline{\mathbf{H}}}\mathbf{x} = \left[(u_0\dot{u}_0 + \mathbf{u}^T\dot{\mathbf{u}})\mathbf{1} - \dot{\mathbf{u}}\mathbf{u}^T + u_0\dot{\mathbf{U}} - \dot{u}_0\mathbf{U} + \mathbf{u}\dot{\mathbf{u}}^T\right]\mathbf{x}$$

which, by taking into account that $\boldsymbol{\eta}$ is a unit vector—and thus $\mathbf{u}^T\mathbf{u}+u_0^2$ is constant—becomes

$$\overline{\mathbf{H}}\dot{\overline{\mathbf{H}}}\mathbf{x} = (-\mathbf{u}^T\mathbf{x}\mathbf{1} + \mathbf{u}\mathbf{x}^T)\dot{\mathbf{u}} - u_0\mathbf{X}\dot{\mathbf{u}} + \dot{u}_0\mathbf{X}\mathbf{u}$$

where $\mathbf{X}$ is the cross-product matrix of $\mathbf{x}$.

Now, applying eq. (2.9) to the first two terms on the right-hand side and recalling eqs. (2.5), we can write the above relation as

$$\overline{\mathbf{H}}\dot{\overline{\mathbf{H}}}\mathbf{x} = \mathbf{X}[\mathbf{U}\dot{\mathbf{u}} - u_0\dot{\mathbf{u}} + \dot{u}_0\mathbf{u}] = -\frac{1}{2}\mathbf{X}\boldsymbol{\omega} = \frac{1}{2}\boldsymbol{\Omega}\mathbf{x}. \tag{2.10}$$

Since this relation is valid for any arbitrary vector $\mathbf{x}$, one obtains eq. (2.7). □

Another useful relation for the angular-velocity matrix $\boldsymbol{\Omega}$ is the one that expresses this matrix in terms of the body rotation matrix and its time rate as

$$\boldsymbol{\Omega} \equiv \mathbf{Q}^T \dot{\mathbf{Q}}. \tag{2.11}$$

This relation was proven in (Parsa *et al.*, 2001) using the approach taken in (Angeles, 2002) for its fixed-frame counterpart, namely,

$$^{\mathcal{R}}\boldsymbol{\Omega} \equiv \dot{\mathbf{Q}}\,\mathbf{Q}^T. \tag{2.12}$$

2.1.2 The Twist Vector and Its Time-Rate of Change

The twist vector of a body is defined here as a set of scalar variables that comprise the necessary and sufficient amount of information to determine the velocity field in the body[2]. For a rigid body, these variables can be the three components of the velocity vector of a landmark point and those of the angular-velocity vector of the body. Both vectors are expressed in the same coordinate frame, whether inertial or not, for the concept of twist is purely kinematical. If the body is flexible, the twist is augmented by a set of generalized velocities representing the body deformation rate.

The twist is usually defined as an array comprising the components of the absolute velocities, both translational and angular, expressed in the local frame. An alternative twist vector that includes the element-wise time derivative of the position vector in the local frame facilitates the partial differentiations needed for the linearization of the kinematic relations in Section 2.2. Corresponding to these two definitions, two different—but kinematically equivalent—twist vectors are defined herein. The one corresponding to the alternative twist is denoted by $\mathbf{t}$ and called briefly the *twist*, while the other twist vector is represented by $\bar{\mathbf{t}}$ and termed the *Cartesian twist*, for it

[2]In screw theory, the *twist*—or as originally defined by Ball (1900) the *velocity twist*—is defined as a screw, which is a geometrical object represented by two three-dimensional vectors (Hunt, 2000). This is conceptually different from our definition. Based on our definition, the elements of the twist can serve as generalized velocities, which is not true for the screw twist. Furthermore, if the rigid-body twist is defined as a screw, the generalization of the twist concept to flexible bodies does not seem possible.

contains the Cartesian velocities—angular and translational—of the body, i.e.,

$$\mathbf{t} \triangleq \begin{bmatrix} \dot{\mathbf{p}} \\ \boldsymbol{\omega} \end{bmatrix}, \qquad \bar{\mathbf{t}} \triangleq \begin{bmatrix} \mathbf{v} \\ \boldsymbol{\omega} \end{bmatrix}, \tag{2.13}$$

where $\mathbf{p}$ and $\mathbf{v}$ are the position vector of the local-frame origin and its absolute velocity, respectively, both expressed in the local frame.

From elementary kinematics, one has

$$\bar{\mathbf{t}} = \begin{bmatrix} \dot{\mathbf{p}} + \boldsymbol{\omega} \times \mathbf{p} \\ \boldsymbol{\omega} \end{bmatrix} = \mathbf{R}\,\mathbf{t} \tag{2.14}$$

$$\mathbf{R} \triangleq \begin{bmatrix} \mathbf{1} & -\mathbf{P} \\ \mathbf{O} & \mathbf{1} \end{bmatrix} \tag{2.15}$$

in which $\mathbf{P} \triangleq \mathrm{CPM}(\mathbf{p})$, and $\mathbf{1}$ and $\mathbf{O}$ are the 3×3 identity and zero matrices, respectively.

The translational and angular accelerations $\mathbf{a}$ and $\boldsymbol{\alpha}$ can readily be seen to be related to the time-derivative of the twist vector, called the *twist-rate*, as given below:

$$\mathbf{s} \triangleq \begin{bmatrix} \mathbf{a} \\ \boldsymbol{\alpha} \end{bmatrix} = \dot{\bar{\mathbf{t}}} + \mathbf{W}\,\bar{\mathbf{t}} \tag{2.16}$$

$$\mathbf{W} \triangleq \begin{bmatrix} \boldsymbol{\Omega} & \mathbf{O} \\ \mathbf{O} & \mathbf{O} \end{bmatrix} \tag{2.17}$$

with $\boldsymbol{\Omega}$ defined already as the cross-product matrix of $\boldsymbol{\omega}$.

2.1.3 The Jacobian Matrix

In robot kinematics, the Jacobian $\mathbf{J}$ can be defined as the partial derivative of the twist vector with respect to the vector of generalized velocities, i.e.,

$$\mathbf{J} \triangleq \frac{\partial \mathbf{t}}{\partial \dot{\mathbf{q}}} \tag{2.18}$$

where $\mathbf{q}$ represents the vector of generalized coordinates, $\dot{\mathbf{q}}$ being the vector of generalized velocities. Since the relation between $\mathbf{t}$ and $\dot{\mathbf{q}}$ is linear, the Jacobian is independent of the generalized velocities, and the relation between $\mathbf{t}$ and $\dot{\mathbf{q}}$ can thus be written as

$$\mathbf{t} = \mathbf{J}\dot{\mathbf{q}} + \mathbf{t}_t, \tag{2.19}$$

with $\mathbf{t}_t$ accounting for the motion of the robot base when it undergoes a prescribed motion, or when the base motion is a controlled motion. In general, both $\mathbf{J}$ and $\mathbf{t}_t$ are functions of $\mathbf{q}$ and t, i.e., $\mathbf{J} \equiv \mathbf{J}(\mathbf{q}, t)$, and $\mathbf{t}_t \equiv \mathbf{t}_t(\mathbf{q}, t)$. Moreover, since all the above arguments are valid for the twist vector of any link, rigid or flexible, in a kinematic chain, henceforth, the word *twist* can refer to the twist vector of any link.

Given the way in which the twist vector has been defined, one can partition the Jacobian matrix into two blocks, corresponding to the two parts of the twist vector:

$$\mathbf{J} = \begin{bmatrix} \mathbf{J}_{\dot{p}} \\ \mathbf{J}_{\omega} \end{bmatrix}$$

in which

$$\mathbf{J}_{\dot{p}} \triangleq \frac{\partial \dot{\mathbf{p}}}{\partial \dot{\mathbf{q}}} \quad \text{and} \quad \mathbf{J}_{\omega} \triangleq \frac{\partial \boldsymbol{\omega}}{\partial \dot{\mathbf{q}}}. \tag{2.20}$$

2.2 Linearized Kinematics

The main goal of this section being the linearization, in closed form, of the link twist and its time rate of change, we start with the linearized relations:

$$\delta \bar{\mathbf{t}} = \frac{\partial \bar{\mathbf{t}}}{\partial \mathbf{q}} \delta \mathbf{q} + \frac{\partial \bar{\mathbf{t}}}{\partial \dot{\mathbf{q}}} \delta \dot{\mathbf{q}} \tag{2.21a}$$

$$\delta \mathbf{s} = \frac{\partial \mathbf{s}}{\partial \mathbf{q}} \delta \mathbf{q} + \frac{\partial \mathbf{s}}{\partial \dot{\mathbf{q}}} \delta \dot{\mathbf{q}} + \frac{\partial \mathbf{s}}{\partial \ddot{\mathbf{q}}} \delta \ddot{\mathbf{q}}. \tag{2.21b}$$

The *Cartesian twist* $\bar{\mathbf{t}}$ of a body and its time rate $\dot{\bar{\mathbf{t}}}$, defined in Subsection 2.1.2, are the output variables. This section is based on the results reported by Parsa *et al.* (2002b).

2.2.1 Partial Derivative of the Angular Velocity

A result needed for deriving closed-form expressions for the partial derivatives of the twist and the twist-rate is given below:

Theorem 1. *The partial derivative of the angular velocity $\boldsymbol{\omega}$ of a rigid body in a serial kinematic chain with respect to the chain generalized-coordinate vector $\mathbf{q}$ can be*

expressed in terms of the Jacobian $\mathbf{J}_\omega$*, its time rate, and the cross-product matrix* $\boldsymbol{\Omega}$ *of the angular velocity as*

$$\frac{\partial \boldsymbol{\omega}}{\partial \mathbf{q}} = \dot{\mathbf{J}}_\omega + \boldsymbol{\Omega}\,\mathbf{J}_\omega \tag{2.22}$$

Proof: We first recall eq. (2.5a), whereby the angular velocity of a body is expressed as a function of the Euler parameters and their time derivatives, i.e., as $\boldsymbol{\omega} \equiv \boldsymbol{\omega}(\boldsymbol{\eta}, \dot{\boldsymbol{\eta}})$. Having this functional relation, one can resort to the chain rule to write the partial derivative of $\boldsymbol{\omega}$ with respect to $\mathbf{q}$ as

$$\frac{\partial \boldsymbol{\omega}}{\partial \mathbf{q}} = \frac{\partial \boldsymbol{\omega}}{\partial \boldsymbol{\eta}} \frac{\partial \boldsymbol{\eta}}{\partial \mathbf{q}} + \frac{\partial \boldsymbol{\omega}}{\partial \dot{\boldsymbol{\eta}}} \frac{\partial \dot{\boldsymbol{\eta}}}{\partial \mathbf{q}} \tag{2.23}$$

Then, given that the orientation of a body is, in general, a function of the generalized coordinates as well as time, one can write the first matrix product on the right-hand side of the above relation as

$$\mathbf{T}_1 \triangleq \frac{\partial \boldsymbol{\omega}}{\partial \boldsymbol{\eta}} \frac{\partial \boldsymbol{\eta}}{\partial \mathbf{q}} = \frac{\partial \boldsymbol{\omega}}{\partial \boldsymbol{\eta}} \frac{\partial \dot{\boldsymbol{\eta}}}{\partial \dot{\mathbf{q}}} = \frac{\partial \boldsymbol{\omega}}{\partial \boldsymbol{\eta}} \frac{\partial \dot{\boldsymbol{\eta}}}{\partial \boldsymbol{\omega}} \frac{\partial \boldsymbol{\omega}}{\partial \dot{\mathbf{q}}}$$

which, in light of eqs. (2.4a, 2.6b, 2.6d, & 2.20), becomes

$$\mathbf{T}_1 = \overline{\mathbf{K}}\,\mathbf{H}\,\mathbf{J}_\omega = -\dot{\overline{\mathbf{H}}}\,\mathbf{H}\,\mathbf{J}_\omega.$$

However, since $\overline{\mathbf{H}}\,\mathbf{H} = \mathbf{1}$, upon differentiation with respect to time, we obtain $-\dot{\overline{\mathbf{H}}}\,\mathbf{H} = \overline{\mathbf{H}}\,\dot{\mathbf{H}}$. Thus, according to Lemma 2,

$$\mathbf{T}_1 = \frac{1}{2}\boldsymbol{\Omega}\,\mathbf{J}_\omega. \tag{2.24}$$

The second matrix product on the right-hand side of eq. (2.23), in turn, can be computed as follows:

$$\begin{aligned}\mathbf{T}_2 \triangleq \frac{\partial \boldsymbol{\omega}}{\partial \dot{\boldsymbol{\eta}}} \frac{\partial \dot{\boldsymbol{\eta}}}{\partial \mathbf{q}} &= \frac{\partial \boldsymbol{\omega}}{\partial \dot{\boldsymbol{\eta}}} \frac{\partial}{\partial \mathbf{q}}\Big(\frac{\partial \boldsymbol{\eta}}{\partial \mathbf{q}}\dot{\mathbf{q}} + \frac{\partial \boldsymbol{\eta}}{\partial t}\Big) = \frac{\partial \boldsymbol{\omega}}{\partial \dot{\boldsymbol{\eta}}}\Big[\frac{\partial}{\partial \mathbf{q}}\Big(\frac{\partial \boldsymbol{\eta}}{\partial \mathbf{q}}\dot{\mathbf{q}}\Big) + \frac{\partial}{\partial t}\Big(\frac{\partial \boldsymbol{\eta}}{\partial \mathbf{q}}\Big)\Big] \\ &= \frac{\partial \boldsymbol{\omega}}{\partial \dot{\boldsymbol{\eta}}} \frac{d}{dt}\Big(\frac{\partial \boldsymbol{\eta}}{\partial \mathbf{q}}\Big) = \frac{\partial \boldsymbol{\omega}}{\partial \dot{\boldsymbol{\eta}}} \frac{d}{dt}\Big(\frac{\partial \dot{\boldsymbol{\eta}}}{\partial \dot{\mathbf{q}}}\Big)\end{aligned}$$

Upon noticing that $\dot{\boldsymbol{\eta}} \equiv \dot{\boldsymbol{\eta}}(\boldsymbol{\eta}, \boldsymbol{\omega})$ and applying the chain rule again, the above expression becomes

$$\begin{aligned}\mathbf{T}_2 &= \frac{\partial \boldsymbol{\omega}}{\partial \dot{\boldsymbol{\eta}}} \frac{d}{dt}\Big(\frac{\partial \dot{\boldsymbol{\eta}}}{\partial \boldsymbol{\omega}} \frac{\partial \boldsymbol{\omega}}{\partial \dot{\mathbf{q}}}\Big) = \frac{\partial \boldsymbol{\omega}}{\partial \dot{\boldsymbol{\eta}}}\left[\frac{\partial \dot{\boldsymbol{\eta}}}{\partial \boldsymbol{\omega}} \frac{d}{dt}\Big(\frac{\partial \boldsymbol{\omega}}{\partial \dot{\mathbf{q}}}\Big) + \frac{d}{dt}\Big(\frac{\partial \dot{\boldsymbol{\eta}}}{\partial \boldsymbol{\omega}}\Big) \frac{\partial \boldsymbol{\omega}}{\partial \dot{\mathbf{q}}}\right] \\ &= \frac{d}{dt}\Big(\frac{\partial \boldsymbol{\omega}}{\partial \dot{\mathbf{q}}}\Big) + \frac{\partial \boldsymbol{\omega}}{\partial \dot{\boldsymbol{\eta}}} \frac{d}{dt}\Big(\frac{\partial \dot{\boldsymbol{\eta}}}{\partial \boldsymbol{\omega}}\Big) \frac{\partial \boldsymbol{\omega}}{\partial \dot{\mathbf{q}}}\end{aligned}$$

Using eq. (2.4a), Lemma 2, and eqs. (2.5a & 2.20), one can rewrite this relation in the simpler form given below:

$$\mathbf{T}_2 = \dot{\mathbf{J}}_\omega + \frac{1}{2}\boldsymbol{\Omega}\,\mathbf{J}_\omega \tag{2.25}$$

Finally, adding up eqs. (2.24 & 2.25) yields

$$\frac{\partial \boldsymbol{\omega}}{\partial \mathbf{q}} = \dot{\mathbf{J}}_\omega + \boldsymbol{\Omega}\,\mathbf{J}_\omega.$$

□

Example. To illustrate the foregoing theorem, assume that, for a certain rigid body, its Euler angles (ϕ, θ, ψ) are taken as the generalized coordinates. We will demonstrate that eq. (2.22) holds. To this end, notice that the angular velocity of a rigid body in terms of the Euler angles and their time rates are given by

$$\boldsymbol{\omega} = \begin{bmatrix}\dot{\phi}\sin\theta\sin\psi + \dot{\theta}\cos\psi & \dot{\phi}\sin\theta\cos\psi - \dot{\theta}\sin\psi & \dot{\phi}\cos\theta + \dot{\psi}\end{bmatrix}^T$$

Setting $\mathbf{q} \triangleq \begin{bmatrix}\phi & \theta & \psi\end{bmatrix}^T$, $\mathbf{J}_\omega$ and its time rate can then be found as

$$\mathbf{J}_\omega \equiv \frac{\partial \boldsymbol{\omega}}{\partial \dot{\mathbf{q}}} = \begin{bmatrix}\sin\theta\sin\psi & \cos\psi & 0 \\ \sin\theta\cos\psi & -\sin\psi & 0 \\ \cos\theta & 0 & 1\end{bmatrix}$$

$$\dot{\mathbf{J}}_\omega = \begin{bmatrix}\dot{\theta}\cos\theta\sin\psi + \dot{\psi}\sin\theta\cos\psi & -\dot{\psi}\sin\psi & 0 \\ \dot{\theta}\cos\theta\cos\psi - \dot{\psi}\sin\theta\sin\psi & -\dot{\psi}\cos\psi & 0 \\ -\dot{\theta}\sin\theta & 0 & 0\end{bmatrix}$$

Substituting $\boldsymbol{\omega}$, $\mathbf{J}_\omega$, and $\dot{\mathbf{J}}_\omega$ in the right-hand side of eq. (2.22), after some algebraic manipulations, one obtains

$$\dot{\mathbf{J}}_\omega + \boldsymbol{\Omega}\mathbf{J}_\omega = \begin{bmatrix}0 & \dot{\phi}\cos\theta\sin\psi & \dot{\phi}\sin\theta\cos\psi - \dot{\theta}\sin\psi \\ 0 & \dot{\phi}\cos\theta\cos\psi & -\dot{\phi}\sin\theta\sin\psi - \dot{\theta}\cos\psi \\ 0 & -\dot{\phi}\sin\theta & 0\end{bmatrix}$$

which apparently is the partial derivative of $\boldsymbol{\omega}$ with respect to $\mathbf{q}$, thereby confirming the validity of eq. (2.22). □

Using the above theorem, one can readily show that, in the inertial frame, a similar relation holds, the only difference being the sign between the two right-hand-side terms of eq. (2.22).

Corollary 1. *The partial derivative of the angular velocity* ${}^{\mathcal{R}}\boldsymbol{\omega}$*, where* $\mathcal{R}$ *represents the inertial frame, of a rigid body in a serial kinematic chain with respect to the chain generalized-coordinate vector* $\mathbf{q}$ *can be expressed in terms of the Jacobian* ${}^{\mathcal{R}}\mathbf{J}_{\omega}$*, its time-rate, and the cross-product matrix* ${}^{\mathcal{R}}\boldsymbol{\Omega}$ *of the angular velocity as*

$$\frac{\partial\, {}^{\mathcal{R}}\boldsymbol{\omega}}{\partial \mathbf{q}} = {}^{\mathcal{R}}\dot{\mathbf{J}}_{\omega} - {}^{\mathcal{R}}\boldsymbol{\Omega}\, {}^{\mathcal{R}}\mathbf{J}_{\omega}. \tag{2.26}$$

2.2.2 Partial Derivatives of the Twist

To derive closed-form expressions for the twist and the twist-rate partial derivatives, yet another result is needed, namely,

Lemma 3. *Let* $\mathbf{f} \equiv \mathbf{f}(\mathbf{q}, \dot{\mathbf{q}}, t)$ *be any vector function which is at least twice continuously differentiable, with* $\mathbf{q} \equiv \mathbf{q}(t)$ *a vector function of time, and* $\dot{\mathbf{q}}$ *its element-wise time derivative. The partial derivatives of the element-wise time-derivative of* $\mathbf{f}$ *with respect to* $\mathbf{q}$ *and* $\dot{\mathbf{q}}$ *are given by*

$$\frac{\partial \dot{\mathbf{f}}}{\partial \mathbf{q}} = \frac{d}{dt}\Big(\frac{\partial \mathbf{f}}{\partial \mathbf{q}}\Big) \tag{2.27a}$$

$$\frac{\partial \dot{\mathbf{f}}}{\partial \dot{\mathbf{q}}} = \frac{d}{dt}\Big(\frac{\partial \mathbf{f}}{\partial \dot{\mathbf{q}}}\Big) + \frac{\partial \mathbf{f}}{\partial \mathbf{q}} \tag{2.27b}$$

Proof: To prove eq. (2.27a), consider the (i, j) entry of $\partial \dot{\mathbf{f}}/\partial \mathbf{q}$. Using index notation for the sake of compactness, and according to the chain rule, one can write

$$\begin{aligned}
\frac{\partial \dot{f}_i}{\partial q_j} &= \frac{\partial}{\partial q_j}\Big(\frac{\partial f_i}{\partial q_k}\dot{q}_k + \frac{\partial f_i}{\partial \dot{q}_k}\ddot{q}_k + \frac{\partial f_i}{\partial t}\Big) \\
&= \frac{\partial}{\partial q_k}\Big(\frac{\partial f_i}{\partial q_j}\Big)\dot{q}_k + \frac{\partial}{\partial \dot{q}_k}\Big(\frac{\partial f_i}{\partial q_j}\Big)\ddot{q}_k + \frac{\partial}{\partial t}\Big(\frac{\partial f_i}{\partial q_j}\Big) \\
&= \frac{d}{dt}\Big(\frac{\partial f_i}{\partial q_j}\Big)
\end{aligned}$$

which implies eq. (2.27a).

Equation (2.27b) can be proven likewise: The (i,j) entry of $\partial\dot{\mathbf{f}}/\partial\dot{\mathbf{q}}$ is calculated by

$$\begin{aligned}\frac{\partial \dot{f}_i}{\partial \dot{q}_j} &= \frac{\partial}{\partial \dot{q}_j}\Big(\frac{\partial f_i}{\partial q_k}\dot{q}_k + \frac{\partial f_i}{\partial \dot{q}_k}\ddot{q}_k + \frac{\partial f_i}{\partial t}\Big) \\ &= \frac{\partial}{\partial q_k}\Big(\frac{\partial f_i}{\partial \dot{q}_j}\Big)\dot{q}_k + \frac{\partial f_i}{\partial q_k}\frac{\partial \dot{q}_k}{\partial \dot{q}_j} + \frac{\partial}{\partial \dot{q}_k}\Big(\frac{\partial f_i}{\partial \dot{q}_j}\Big)\ddot{q}_k + \frac{\partial}{\partial t}\Big(\frac{\partial f_i}{\partial \dot{q}_j}\Big) \\ &= \frac{d}{dt}\Big(\frac{\partial f_i}{\partial \dot{q}_j}\Big) + \frac{\partial f_i}{\partial q_k}\delta_{kj}\end{aligned}$$

where δ_{kj} is the Kronecker delta; one therefore obtains

$$\frac{\partial \dot{f}_i}{\partial \dot{q}_j} = \frac{d}{dt}\Big(\frac{\partial f_i}{\partial \dot{q}_j}\Big) + \frac{\partial f_i}{\partial q_j}$$

which completes the proof. □

Relations similar to these appear quite frequently in the derivation of the Lagrange equations of multibody systems. The main difference with analytical dynamics is that, in the latter, one deals mostly with scalar functions.

By means of Theorem 2.2.1, recalling the definition of the twist $\mathbf{t}$, and applying the first result of Lemma 3 on $\dot{\mathbf{p}}$, one can conclude that

$$\frac{\partial \mathbf{t}}{\partial \mathbf{q}} = \begin{bmatrix} \dfrac{\partial \dot{\mathbf{p}}}{\partial \mathbf{q}} \\ \dfrac{\partial \boldsymbol{\omega}}{\partial \mathbf{q}} \end{bmatrix} = \frac{d}{dt}\begin{bmatrix} \dfrac{\partial \dot{\mathbf{p}}}{\partial \dot{\mathbf{q}}} \\ \dfrac{\partial \boldsymbol{\omega}}{\partial \dot{\mathbf{q}}} \end{bmatrix} + \begin{bmatrix} \mathbf{O} \\ \boldsymbol{\Omega}\dfrac{\partial \boldsymbol{\omega}}{\partial \dot{\mathbf{q}}} \end{bmatrix} = \dot{\mathbf{J}} + \overline{\mathbf{W}}\,\mathbf{J} \tag{2.28}$$

where $\overline{\mathbf{W}}$ is given by

$$\overline{\mathbf{W}} \triangleq \begin{bmatrix} \mathbf{O} & \mathbf{O} \\ \mathbf{O} & \boldsymbol{\Omega} \end{bmatrix}. \tag{2.29}$$

Then, from the definition of the Cartesian twist, one obtains the relation between the derivatives of $\mathbf{t}$ and $\bar{\mathbf{t}}$ with respect to $\mathbf{q}$:

$$\begin{aligned}\frac{\partial \bar{\mathbf{t}}}{\partial \mathbf{q}} &= \mathbf{R}\frac{\partial \mathbf{t}}{\partial \mathbf{q}} + \frac{\partial}{\partial \mathbf{q}}\begin{bmatrix} -\mathbf{P}\,\mathbf{c} \\ \mathbf{0}_3 \end{bmatrix}\Bigg|_{\mathbf{c}=\dot{\mathbf{p}}} \\ &= \mathbf{R}\frac{\partial \mathbf{t}}{\partial \mathbf{q}} + \mathbf{W}\,\mathbf{J}\end{aligned} \tag{2.30}$$

which, using eq. (2.28), can be written as

$$\frac{\partial \bar{\mathbf{t}}}{\partial \mathbf{q}} = \mathbf{R}\,\dot{\mathbf{J}} + \overline{\mathbf{R}}\,\mathbf{J} \tag{2.31}$$

$$\overline{\mathbf{R}} \triangleq \mathbf{R}\,\overline{\mathbf{W}} + \mathbf{W} = \begin{bmatrix} \boldsymbol{\Omega} & -\mathbf{P}\,\boldsymbol{\Omega} \\ \mathbf{O} & \boldsymbol{\Omega} \end{bmatrix}, \tag{2.32}$$

where matrices $\mathbf{R}$ and $\mathbf{W}$ were defined in eqs. (2.15 & 2.17). Furthermore, from eqs. (2.13–2.15 & 2.18), we can readily see that

$$\frac{\partial \bar{\mathbf{t}}}{\partial \dot{\mathbf{q}}} = \mathbf{R}\,\mathbf{J}, \tag{2.33}$$

the partial derivatives sought thus having been calculated.

We now turn our attention to the twist-rate.

2.2.3 Partial Derivatives of the Twist-Rate

If eq. (2.27a) is applied to the twist-rate, using eq. (2.28), we arrive at

$$\frac{\partial \dot{\mathbf{t}}}{\partial \mathbf{q}} = \ddot{\mathbf{J}} + \overline{\mathbf{W}}\,\dot{\mathbf{J}} + \dot{\overline{\mathbf{W}}}\,\mathbf{J} \tag{2.34}$$

As pertaining to the time-rate of the Cartesian twist, $\dot{\bar{\mathbf{t}}}$, the same relation leads to

$$\frac{\partial \dot{\bar{\mathbf{t}}}}{\partial \mathbf{q}} = \mathbf{R}\,\ddot{\mathbf{J}} + \left(\dot{\mathbf{R}} + \overline{\mathbf{R}}\right)\dot{\mathbf{J}} + \dot{\overline{\mathbf{R}}}\,\mathbf{J} \tag{2.35}$$

On the other hand, exploiting eq. (2.27b) will provide the second set as

$$\frac{\partial \dot{\mathbf{t}}}{\partial \dot{\mathbf{q}}} = 2\,\dot{\mathbf{J}} + \overline{\overline{\mathbf{W}}}\,\mathbf{J} \tag{2.36}$$

$$\frac{\partial \dot{\bar{\mathbf{t}}}}{\partial \dot{\mathbf{q}}} = 2\,\mathbf{R}\,\dot{\mathbf{J}} + \left(\dot{\mathbf{R}} + \overline{\mathbf{R}}\right)\mathbf{J} \tag{2.37}$$

The last relations reported here are those of the partial derivatives of the vector $\mathbf{s}$, defined in eq. (2.16), with respect to $\mathbf{q}$ and $\dot{\mathbf{q}}$. It can be shown that

$$\frac{\partial \mathbf{s}}{\partial \mathbf{q}} = \mathbf{R}\,\ddot{\mathbf{J}} + \left[\dot{\mathbf{R}} + \overline{\mathbf{R}} + (\mathbf{W} - \mathbf{Y})\mathbf{R}\right]\dot{\mathbf{J}} + \left[\dot{\overline{\mathbf{R}}} + (\mathbf{W} - \mathbf{Y})\mathbf{R}\right]\mathbf{J} \tag{2.38}$$

$$\frac{\partial \mathbf{s}}{\partial \dot{\mathbf{q}}} = 2\mathbf{R}\,\dot{\mathbf{J}} + \left[\dot{\mathbf{R}} + \overline{\mathbf{R}} + (\mathbf{W} - \mathbf{Y})\mathbf{R}\right]\mathbf{J} \tag{2.39}$$

$$\frac{\partial \mathbf{s}}{\partial \ddot{\mathbf{q}}} = \mathbf{R}\,\mathbf{J} \tag{2.40}$$

where $\mathbf{Y}$ is given by

$$\mathbf{Y} \triangleq \begin{bmatrix} \mathbf{O} & \mathbf{V} \\ \mathbf{O} & \mathbf{O} \end{bmatrix} \tag{2.41}$$

in which $\mathbf{V}$ is the cross-product matrix of the velocity $\mathbf{v}$.

2.3 Recursive Kinematic Relations

The manipulator recursive kinematic relations are needed for the derivation of both the Jacobian matrix and the Natural Orthogonal Complement (NOC), explained in Chapter 4, pertaining to the manipulator. These matrices are, in turn, needed for the kinematics and kinetics analyses of the manipulator.

To derive the recursive relations, we begin with assigning a reference frame to each link, posed in accordance with the Denavit-Hartenberg convention proposed by Craig (1989); for a flexible link, this is done on the undeformed link. To obtain the relations for a rigid link, one can simply drop the terms pertaining to the flexural motions. Furthermore, we make a simplifying assumption here: The deformational rotation at the distal end of the link is small.

2.3.1 Rotational Motion

Rotation Matrix

Let us define $\mathbf{Q}_i$ and $\mathbf{R}_i$ as the rotation matrices that take $\mathcal{F}_i$ to $\mathcal{R}$ and $\mathcal{F}_{i-1}$, respectively. From Fig. 2.1, one can obtain the rotation matrix $\mathbf{R}_i$ as

$$\begin{aligned} \mathbf{R}_i = & \begin{bmatrix} 1 & 0 & 0 \\ 0 & \mathrm{c}(\delta_x^{i-1}) & -\mathrm{s}(\delta_x^{i-1}) \\ 0 & \mathrm{s}(\delta_x^{i-1}) & \mathrm{c}(\delta_x^{i-1}) \end{bmatrix} \begin{bmatrix} \mathrm{c}(\delta_y^{i-1}) & 0 & \mathrm{s}(\delta_y^{i-1}) \\ 0 & 1 & 0 \\ -\mathrm{s}(\delta_y^{i-1}) & 0 & \mathrm{c}(\delta_y^{i-1}) \end{bmatrix} \begin{bmatrix} \mathrm{c}(\delta_z^{i-1}) & -\mathrm{s}(\delta_z^{i-1}) & 0 \\ \mathrm{s}(\delta_z^{i-1}) & \mathrm{c}(\delta_z^{i-1}) & 0 \\ 0 & 0 & 1 \end{bmatrix} \\ & \begin{bmatrix} 1 & 0 & 0 \\ 0 & \mathrm{c}(\alpha_{i-1}) & -\mathrm{s}(\alpha_{i-1}) \\ 0 & \mathrm{s}(\alpha_{i-1}) & \mathrm{c}(\alpha_{i-1}) \end{bmatrix} \begin{bmatrix} \mathrm{c}(\theta_i) & -\mathrm{s}(\theta_i) & 0 \\ \mathrm{s}(\theta_i) & \mathrm{c}(\theta_i) & 0 \\ 0 & 0 & 1 \end{bmatrix} \\ \cong & \begin{bmatrix} 1 & -\delta_z^{i-1} & \delta_y^{i-1} \\ \delta_z^{i-1} & 1 & -\delta_x^{i-1} \\ -\delta_y^{i-1} & \delta_x^{i-1} & 1 \end{bmatrix} \begin{bmatrix} 1 & 0 & 0 \\ 0 & \mathrm{c}(\alpha_{i-1}) & -\mathrm{s}(\alpha_{i-1}) \\ 0 & \mathrm{s}(\alpha_{i-1}) & \mathrm{c}(\alpha_{i-1}) \end{bmatrix} \begin{bmatrix} \mathrm{c}(\theta_i) & -\mathrm{s}(\theta_i) & 0 \\ \mathrm{s}(\theta_i) & \mathrm{c}(\theta_i) & 0 \\ 0 & 0 & 1 \end{bmatrix}, \end{aligned} \tag{2.42}$$

where θ_i and α_{i-1} are the ith-joint variable and the $(i-1)$th-joint twist angle, respectively, and $\mathrm{s}(\cdot)$ and $\mathrm{c}(\cdot)$ denote the *sine* and the *cosine* of $(\cdot)$, respectively. Here, δ_x^{i-1}

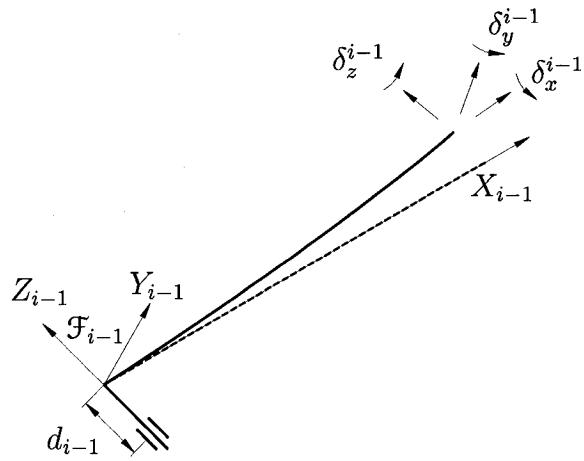

Figure 2.1: The rotations due to bending, at the link endpoint

represents the torsional deformation while δ_y^{i-1} and δ_z^{i-1} represent the rotations due to the bending of the link; all three are assumed to be small.

Moreover, it is clear that the rotation matrix $\mathbf{Q}_i$ can be calculated from

$$\mathbf{Q}_i = \prod_{j=1}^{i} \mathbf{R}_j \triangleq \mathbf{R}_1 \mathbf{R}_2 \cdots \mathbf{R}_{i-1} \mathbf{R}_i, \tag{2.43}$$

in which the product operator is defined such that the order of the matrix multiplications is conserved.

Angular Velocity

The angular velocities of any two consecutive frames are related to one another through

$$\boldsymbol{\omega}_i = \boldsymbol{\omega}_{i-1} + \dot{\boldsymbol{\delta}}_{i-1} + \dot{\theta}_i \mathbf{z}_i \tag{2.44}$$

where the angular velocities $\boldsymbol{\omega}_{i-1}$ and $\boldsymbol{\omega}_i$ pertain to the coordinate frames $\mathcal{F}_{i-1}$ and $\mathcal{F}_i$, respectively, and small angular-deformation vector $\boldsymbol{\delta}_{i-1}$ is given by

$$\boldsymbol{\delta}_{i-1} \triangleq \begin{bmatrix} \delta_x^{i-1} & \delta_y^{i-1} & \delta_z^{i-1} \end{bmatrix}^T. \tag{2.45}$$

The vectors in eq. (2.44) are considered as abstract quantities, on which the algebraic operations can be performed without any need to a common reference frame. In

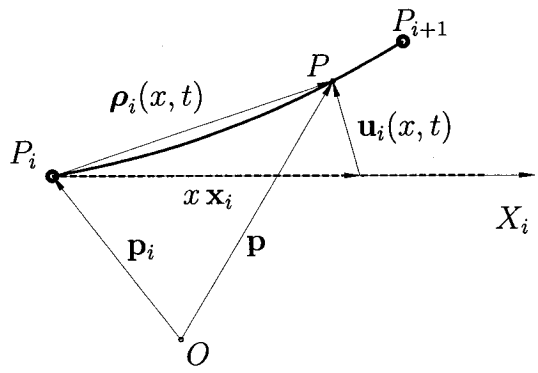

Figure 2.2: A flexible link

component form, the recursive relation becomes

$$\boldsymbol{\omega}_i = \mathbf{R}_i^T(\boldsymbol{\omega}_{i-1} + \dot{\boldsymbol{\delta}}_{i-1}) + \dot{\theta}_i \mathbf{z}_i. \tag{2.46}$$

Using the above relation, the relative angular velocity ${}^i\boldsymbol{\omega}_i^r$ of $\mathcal{F}_i$ with respect to $\mathcal{F}_{i-1}$ can be obtained as

$${}^i\boldsymbol{\omega}_i^r \triangleq \boldsymbol{\omega}_i - \mathbf{R}_i^T\boldsymbol{\omega}_{i-1} = \mathbf{R}_i^T\dot{\boldsymbol{\delta}}_{i-1} + \dot{\theta}_i\mathbf{z}_i \tag{2.47}$$

in which, as per our convention, the left-superscript of ${}^i\boldsymbol{\omega}_i^r$ shows that the vector is expressed in $\mathcal{F}_i$. The cross-product matrix of ${}^i\boldsymbol{\omega}_i^r$ can then be obtained as

$${}^i\boldsymbol{\Omega}_i^r \triangleq \mathrm{CPM}\big({}^i\boldsymbol{\omega}_i^r\big) = \mathrm{CPM}\big(\mathbf{R}_i^T\dot{\boldsymbol{\delta}}_{i-1} + \dot{\theta}_i\mathbf{z}_i\big). \tag{2.48}$$

Moreover, it can readily be seen that

$${}^{i-1}\boldsymbol{\Omega}_i^r \triangleq \mathrm{CPM}\big({}^{i-1}\boldsymbol{\omega}_i^r\big) = \mathrm{CPM}\big(\dot{\boldsymbol{\delta}}_{i-1} + \dot{\theta}_i\mathbf{R}_i\mathbf{z}_i\big). \tag{2.49}$$

2.3.2 Translational Motion

Position Vector

Using the assumptions set forth at the beginning of this section, it is seen from Fig. 2.2 that the deformed position of point P on the neutral axis of the ith link at distance x from its proximal end, in abstract form, is given by the position vector

$$\mathbf{p} = \mathbf{p}_i + \boldsymbol{\rho}_i(x,t) \tag{2.50}$$

in which $\boldsymbol{\rho}_i(x,t)$ is the position vector of the point P with respect to the origin of $\mathcal{F}_i$, and given by

$$\boldsymbol{\rho}_i(x,t) = x\mathbf{x}_i + \mathbf{u}_i(x,t) \tag{2.51}$$

where $\mathbf{u}_i(x,t)$ denotes the three-dimensional displacement vector of the link at P.

Hence, in abstract form, we can write

$$\mathbf{p}_i = \mathbf{p}_{i-1} + \boldsymbol{\rho}_{i-1}(l_{i-1},t) + d_i\mathbf{z}_i, \tag{2.52}$$

the scalars d_i and l_{i-1} representing the ith link offset and the length of the $(i-1)$th link, respectively. Therefore, the foregoing equation can be rewritten as

$$\mathbf{p}_i = \mathbf{p}_{i-1} + l_{i-1}\mathbf{x}_{i-1} + \mathbf{u}_{i-1}(l_{i-1},t) + d_i\mathbf{z}_i. \tag{2.53}$$

To be able to calculate the components of the position vectors, however, one must take the rotation matrix between the two frames $\mathcal{F}_i$ and $\mathcal{F}_{i-1}$ into account, i.e.,

$$\mathbf{p}_i = \mathbf{R}_i^T\big(\mathbf{p}_{i-1} + l_{i-1}\mathbf{x}_{i-1} + \mathbf{u}_{i-1}(l_{i-1},t)\big) + d_i\mathbf{z}_i. \tag{2.54}$$

Translational Velocity

Differentiating the position-vector relation (2.54) *element-wise*, one can readily find the kinematic relation between the time-rate of the position vectors of two adjacent-frame origins as

$$\dot{\mathbf{p}}_i = \mathbf{R}_i^T\big(\dot{\mathbf{p}}_{i-1} + \dot{\mathbf{u}}_{i-1}(l_{i-1},t)\big) + \dot{\mathbf{R}}_i^T\big(\mathbf{p}_{i-1} + l_{i-1}\mathbf{x}_{i-1} + \mathbf{u}_{i-1}(l_{i-1},t)\big). \tag{2.55}$$

In order to simplify this relation, one needs to derive an expression for the time-derivative of the rotation matrix. To this end, we utilize eq. (2.12) to obtain

$${}^{i-1}\boldsymbol{\Omega}_i^r = \dot{\mathbf{R}}_i\,\mathbf{R}_i^T, \tag{2.56}$$

from which the time derivative of the rotation matrix is obtained as

$$\dot{\mathbf{R}}_i = {}^{i-1}\boldsymbol{\Omega}_i^r\;\mathbf{R}_i \tag{2.57}$$

Substituting the above equation into eq. (2.55), we have

$$\dot{\mathbf{p}}_i = \mathbf{R}_i^T\big(\dot{\mathbf{p}}_{i-1} + \dot{\mathbf{u}}_{i-1}(l_{i-1},t)\big) - \mathbf{R}_i^T\,{}^{i-1}\boldsymbol{\Omega}_i^r\,\big(\mathbf{p}_{i-1} + l_{i-1}\mathbf{x}_{i-1} + \mathbf{u}_{i-1}(l_{i-1},t)\big), \quad (2.58)$$

in which the skew-symmetric property of cross-product matrices has been used. Upon substituting ${}^{i-1}\boldsymbol{\Omega}_i^r$, given by eq. (2.49), into eq. (2.58), we obtain

$$\begin{aligned}\dot{\mathbf{p}}_i = \mathbf{R}_i^T\Big[&\dot{\mathbf{p}}_{i-1} + \dot{\mathbf{u}}_{i-1}(l_{i-1},t) - \dot{\boldsymbol{\delta}}_{i-1}\times\big(\mathbf{p}_{i-1} + l_{i-1}\mathbf{x}_{i-1} + \mathbf{u}_{i-1}(l_{i-1},t)\big)\\ &- \dot{\theta}_i(\mathbf{R}_i\mathbf{z}_i)\times\big(\mathbf{p}_{i-1} + l_{i-1}\mathbf{x}_{i-1} + \mathbf{u}_{i-1}(l_{i-1},t)\big)\Big].\end{aligned} \quad (2.59)$$

Hence, the recursive relation for $\dot{\mathbf{p}}_i$ takes on the final form below:

$$\dot{\mathbf{p}}_i = \mathbf{R}_i^T\Big[\dot{\mathbf{p}}_{i-1} + \dot{\mathbf{u}}_{i-1}(l_{i-1},t) + \boldsymbol{\Upsilon}_{i-1}\dot{\boldsymbol{\delta}}_{i-1} + \boldsymbol{\Upsilon}_{i-1}\dot{\theta}_i\mathbf{R}_i\mathbf{z}_i\Big] \quad (2.60)$$

where $\boldsymbol{\Upsilon}_{i-1}$ is defined as

$$\boldsymbol{\Upsilon}_{i-1} \triangleq \mathrm{CPM}\big(\mathbf{p}_{i-1} + l_{i-1}\mathbf{x}_{i-1} + \mathbf{u}_{i-1}(l_{i-1},t)\big). \quad (2.61)$$

2.4 The Flexible-Link Spatial Discretization

The dynamics of a flexible body, in general, is expressed by a partial differential equation, for which a closed-form solution does not usually exist. Consequently, to analyze the dynamics of flexible manipulators—which are usually composed of multiple flexible and rigid elements—it is customary to spatially discretize the partial differential equations in play. By doing so, the flexible links, which have infinite degrees of freedom, are—in effect—approximated by elements with finite degrees of freedom, the partial differential equations thus being replaced by ordinary differential equations. These finite degrees of freedom are described by flexural generalized coordinates.

For the dynamics analysis of flexible manipulators, different methods of spatial discretizations have been reported and utilized in the literature; among others, the assumed-modes (Cyril, 1988), finite-elements (Fattah, 1995), and cubic-splines (Cho, 1995) techniques can be named. The derivations reported in this thesis are independent of the particular discretization technique, the exceptions being the derivations

of the mass and stiffness matrices, given in Appendix C and Section 4.3.1, respectively, and the derivation of the NOC, presented in Appendix D. Since, for these derivations, we will adopt the assumed-modes method, which is closely related to the Rayleigh-Ritz method (Meirovitch, 1997), a few words on this technique are deemed in order.

It is assumed here that each of the flexible links can be considered as an Euler-Bernoulli beam[3]. This means that (*i*) the link material is linearly elastic, and its Young's modulus is the same in both extension and contraction; (*ii*) the bending and torsional deformations are small; (*iii*) the link does not undergo length change; (*iv*) the shear deformation is negligible; (*v*) the geometric shortening is negligible; (*vi*) the slenderness ratio, i.e., the ratio of the link length to the radius of gyration of its cross section, is greater than 10; (*vii*) the cross sections of the link remain planar after deformation; and (*viii*) the variations in the angular momentum due to the link vibration can be neglected.

Using the assumed-modes method, we discretize the link flexural displacement in the form

$$\mathbf{u}_i(x,t) = \mathbf{B}_i(x)\boldsymbol{\xi}_i(t) \tag{2.62}$$

in which the elements of $\boldsymbol{\xi}_i(t)$ are the generalized coordinates describing bending deformation of the link, and the shape-function matrix $\mathbf{B}_i(x)$ is given by

$$\mathbf{B}_i(x) \triangleq \begin{bmatrix} \mathbf{0}^T & \mathbf{0}^T \\ \boldsymbol{\varphi}_i^T(x) & \mathbf{0}^T \\ \mathbf{0}^T & \boldsymbol{\varphi}_i^T(x) \end{bmatrix} \tag{2.63}$$

where $\boldsymbol{\varphi}_i(x)$ is a vector of the shape-functions, or the so-called "modes," representing the bending deformation of the ith link in one direction; the entries of this vector can be the admissible or the quasi-comparison functions for a clamped-free beam (Meirovitch, 1997). The n_{fi}^b-dimensional vector $\boldsymbol{\xi}_i(t)$ can be decomposed into two

[3]For a more general treatment of the problem of rotating flexible beam, one can refer to (Kane *et al.*, 1987).

parts as follows:

$$\boldsymbol{\xi}_i(t) = \left[\boldsymbol{\xi}_{yi}^T(t) \quad \boldsymbol{\xi}_{zi}^T(t)\right]^T. \tag{2.64}$$

Obviously, the two parts represent the bending deformations due to moments exerted on the link about Y_i and Z_i axes. It is worth mentioning that, as argued by Hughes (1987), the "modes should be selected on dynamical grounds other than frequency only."

The torsion angle $\gamma_i(x,t)$ of the link at a distance x from the proximal end of the link is discretized using

$$\gamma_i(x,t) = \mathbf{h}_i^T(x)\boldsymbol{\mu}_i(t) \tag{2.65}$$

where $\mathbf{h}_i(x)$ is the n_{fi}^t-dimensional vector of shape-functions used to discretize the torsional deformation of the ith link.

Moreover, using the assumption of small angular deformation at the link end-point, vector $\boldsymbol{\delta}_i$ is calculated from

$$\boldsymbol{\delta}_i(t) \equiv \begin{bmatrix} \delta_x^i(t) \\ \delta_y^i(t) \\ \delta_z^i(t) \end{bmatrix} = \mathbf{C}_i(l_i)\,\boldsymbol{\mu}_i(t) + \mathbf{D}_i(l_i)\,\boldsymbol{\xi}_i(t) \tag{2.66}$$

where l_i is the link length, and

$$\mathbf{C}_i(x) \triangleq \begin{bmatrix} \mathbf{h}_i^T(x) \\ \mathbf{0}^T \\ \mathbf{0}^T \end{bmatrix}, \quad \mathbf{D}_i(x) \triangleq \begin{bmatrix} \mathbf{0}^T & \mathbf{0}^T \\ \mathbf{0}^T & -\left(\boldsymbol{\varphi}_i'(x)\right)^T \\ \left(\boldsymbol{\varphi}_i'(x)\right)^T & \mathbf{0}^T \end{bmatrix}. \tag{2.67}$$

Chapter 3

Rigid-Body Pose and Twist Estimation

3.1 Introduction

It has been shown (Parsa *et al.*, 2001) that the attitude calibration of an accelerometer array plays a very important role in the accuracy of the results of the pose and twist estimation of rigid-bodies using an accelerometer array. For this reason, in addition to a procedure for pose and twist estimation, we will introduce two calibration schemes in this chapter:

(*i*) A gravitational attitude-calibration scheme, which can be used to calibrate an accelerometer array to a limited extent.

(*ii*) A kinematic calibration scheme, which is capable of identifying accelerometer-attitude errors with high accuracy.

The second scheme is an iterative procedure that can be performed off-line by processing the acceleration readouts recorded over a long-enough, arbitrary motion of the body.

3.2 Gravitational Attitude Calibration

Assume that a triaxial accelerometer is attached at each of the pickup points P_i ($i = 1, 2, \ldots, m$) of the rigid body shown in Fig. 3.1, point C, of position vector

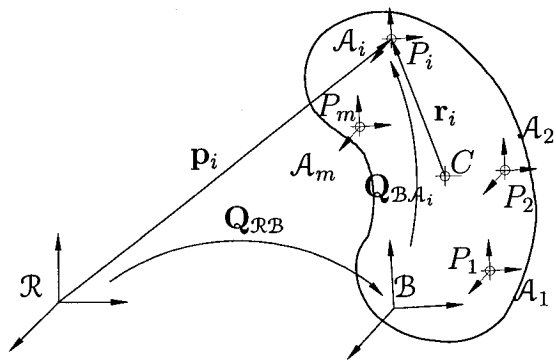

Figure 3.1: A rigid body and its related frames

$\mathbf{c} = (1/m)\sum_{i=1}^{m} \mathbf{p}_i$, being the centroid of $\{P_i\}_i^m$.

Obviously, due to installation errors, not only are the accelerometer axes skew with respect to their nominal installation orientations but also the accelerometers are located at points different from the nominal ones specified by $\mathbf{r}_i$. The effect of the latter is minimized by choosing $\|\mathbf{r}_i\|$ considerably larger than the upper bound of the existing position errors, and by choosing P_i to be the vertices of a Platonic solid (Angeles, 1990). To account for the orientation errors, however, one may use the gravitational attitude-calibration scheme explained in this section. Here, we further assume that the three axes in question are mutually orthogonal.

To identify the attitude error of the accelerometers using gravity, the body is given a redundant number n (more than three) of known orientations. At each instance, while in the given attitude, the accelerometers are used to measure the gravitational acceleration. Then, the data thus obtained are employed to produce estimates $\hat{\mathbf{Q}}_i$ of the rotation matrices $\mathbf{Q}_{\mathcal{B}\mathcal{A}_i}$ that relate the attitudes of the accelerometer frames to that of the body frame. Below is this procedure explained in more detail:

Assuming that the accelerometer gains are known, it is apparent that the gravitational acceleration measured by the accelerometers can be related to the gravitational acceleration in the reference frame $\mathcal{R}$ in the form:

$$(\mathbf{Q}_{\mathcal{R}\mathcal{B}})_j \mathbf{Q}_{\mathcal{B}\mathcal{A}_i}{}^{\mathcal{A}_i}\mathbf{g}_j = {}^{\mathcal{R}}\mathbf{g} \tag{3.1}$$

where $(\mathbf{Q}_{\mathcal{RB}})_j$, the rotation matrix from the body frame $\mathcal{B}$ at the jth measurement to the reference frame, is assumed to be known. Furthermore, ${}^{\mathcal{A}_i}\mathbf{g}_j$ is the gravitational acceleration measured by the ith accelerometer at instance j, and ${}^{\mathcal{R}}\mathbf{g} = \begin{bmatrix} 0 & 0 & -g \end{bmatrix}^T$ since we assume that the third axis of $\mathcal{R}$ is vertical. It is worth mentioning that, as duly noted by Rehbinder and Hu (2001), ${}^{\mathcal{A}_i}\mathbf{g}_j$ is indeed the negative of the acceleration perceived by the accelerometer at rest.

Therefore, for $j = 1, 2, \ldots, n$,

$$\mathbf{Q}_{\mathcal{BA}_i}{}^{\mathcal{A}_i}\mathbf{g}_j = (\mathbf{Q}_{\mathcal{RB}})_j^T {}^{\mathcal{R}}\mathbf{g} = -g(\mathbf{q}_3)_j, \tag{3.2}$$

in which $(\mathbf{q}_3)_j$ is the third column of $(\mathbf{Q}_{\mathcal{RB}})_j^T$. Assembling all the measurements performed by the accelerometer number i, one has

$$\mathbf{Q}_{\mathcal{BA}_i}\left[{}^{\mathcal{A}_i}\mathbf{g}_1 \ \cdots \ {}^{\mathcal{A}_i}\mathbf{g}_n\right] = -g\left[(\mathbf{q}_3)_1 \ \cdots \ (\mathbf{q}_3)_n\right]. \tag{3.3}$$

Let the matrix of measurements on the left-hand side be $\mathbf{G}_i$ and that on the right-hand side be $\mathbf{B}$. Then, eq. (3.2) becomes

$$\mathbf{Q}_{\mathcal{BA}_i}\mathbf{G}_i = -g\mathbf{B}, \quad i = 1, 2, \ldots, m > 3. \tag{3.4}$$

It is known that

$$\mathbf{Q}_{\mathcal{BA}_i} = -g\mathbf{B}\mathbf{G}_i^T(\mathbf{G}_i\mathbf{G}_i^T)^{-1} \tag{3.5}$$

is the least-square solution[1] of the over-determined system of linear equations (3.4), but it should be noted that $\mathbf{G}_i\mathbf{G}_i^T$ is invertible if and only if no less than three of the ${}^{\mathcal{A}_i}\mathbf{g}_j$ measurements are linearly independent. Nevertheless, there is no guarantee that the rotation matrices computed from eq. (3.5) be orthogonal; they must thus be orthogonalized. To this end, the polar-decomposition theorem (Strang, 1988) is used; based on this theorem, any nonsingular, real, square matrix $\mathbf{A}$ can be uniquely decomposed into an orthogonal matrix $\mathbf{U}$ and a positive-definite matrix $\mathbf{P}$ such that

$$\mathbf{A} = \mathbf{U}\mathbf{P}, \quad \mathbf{P} = (\mathbf{A}^T\mathbf{A})^{\frac{1}{2}}, \quad \mathbf{U} = \mathbf{A}(\mathbf{A}^T\mathbf{A})^{-\frac{1}{2}}. \tag{3.6}$$

[1]Solution (3.5) will not be optimal if the measurements are noisy.

It has been proven (Giardina *et al.*, 1975) that the orthogonal matrix described by this theorem minimizes $\|\mathbf{A}-\mathbf{U}\|_2$ over all orthogonal matrices of the same dimensions. Therefore, after calculating $\mathbf{Q}_{\mathcal{BA}_i}$ for $i = 1, \ldots, m$, one can find the best orthogonal matrices approximating them by applying the above theorem, thereby accomplishing a preliminary attitude calibration. These approximate rotation matrices are denoted by $\hat{\mathbf{Q}}_i$.

However, because this type of calibration is indeed imperfect, for the rotation matrix from the body frame to the reference frame cannot be exactly known, we express the actual rotation matrix $\mathbf{Q}_{\mathcal{BA}_i}$ from the ith accelerometer frame to the body frame as

$$\mathbf{Q}_{\mathcal{BA}_i} = \hat{\mathbf{Q}}_i \bar{\mathbf{Q}}_i, \quad i = 1, 2, \ldots, m \tag{3.7}$$

where each calibration error is considered as a rotation matrix $\bar{\mathbf{Q}}_i$, which, according to eq. (2.2), is calculated from

$$\bar{\mathbf{Q}}_i = \mathbf{1} + \sin\phi_i \mathbf{E}_i + (1 - \cos\phi_i)\mathbf{E}_i^2 \tag{3.8}$$

with ϕ_i denoting the angle of the rotation carrying the assumed frame of the accelerometer into its actual attitude; $\mathbf{E}_i$ is the cross-product matrix of the unit vector $\mathbf{e}_i$ of that rotation, and $\mathbf{1}$ is the 3×3 identity matrix. Unfortunately, however, both ϕ_i and $\mathbf{E}_i$ are unknown constants.

Because of the preliminary calibration of the array, all ϕ_i can be assumed small, and hence, the right-hand side of eq. (3.8) can be approximated linearly as

$$\bar{\mathbf{Q}}_i \approx \mathbf{1} + \phi_i \mathbf{E}_i, \quad i = 1, 2, \ldots, m. \tag{3.9}$$

3.3 Accelerometer-Array Kinematics

3.3.1 Angular Acceleration

From rigid-body kinematics, the absolute acceleration of the ith pickup point and that of the centroid C are related by

$$\mathbf{a}_i = \mathbf{a}_C + \boldsymbol{\alpha} \times \mathbf{r}_i + \boldsymbol{\omega} \times (\boldsymbol{\omega} \times \mathbf{r}_i) \tag{3.10}$$

where $\boldsymbol{\omega}$ and $\boldsymbol{\alpha}$ are the angular velocity and angular acceleration of the body, respectively, and $\mathbf{r}_i$, shown in Fig. 3.1, is the position vector of P_i with respect to C. As shown in (Parsa *et al.*, 2001), however, the element-wise time derivative of the angular velocity of a body in its local-frame is exactly equal to its absolute angular acceleration expressed in the same frame, i.e.,

$$\dot{\boldsymbol{\omega}} = \boldsymbol{\alpha}. \tag{3.11}$$

Therefore, using the cross-product matrices $\boldsymbol{\Omega}$ and $\dot{\boldsymbol{\Omega}}$ of $\boldsymbol{\omega}$ and $\dot{\boldsymbol{\omega}}$, respectively, one can rewrite eq. (3.10) in a more suitable form:

$$\mathbf{a}_i - \mathbf{a}_C = (\dot{\boldsymbol{\Omega}} + \boldsymbol{\Omega}^2)\mathbf{r}_i. \tag{3.12}$$

Moreover, using eq. (3.7) and recalling the definition of C, one can calculate the left-hand side of eq. (3.12) as

$$\begin{aligned}
\mathbf{a}_i - \mathbf{a}_C &= \hat{\mathbf{Q}}_i\bar{\mathbf{Q}}_i({}^{\mathcal{A}_i}\mathbf{a}_i + {}^{\mathcal{A}_i}\mathbf{g}) - \frac{1}{m}\sum_{j=1}^{m}\hat{\mathbf{Q}}_j\bar{\mathbf{Q}}_j({}^{\mathcal{A}_j}\mathbf{a}_j + {}^{\mathcal{A}_j}\mathbf{g}) \\
&= \hat{\mathbf{Q}}_i\bar{\mathbf{Q}}_i{}^{\mathcal{A}_i}\mathbf{a}_i - \frac{1}{m}\sum_{j=1}^{m}\hat{\mathbf{Q}}_j\bar{\mathbf{Q}}_j{}^{\mathcal{A}_j}\mathbf{a}_j \\
&= \mathbf{a}_i^{\mathrm{r}} + \mathbf{n}_i^{\mathrm{a}}
\end{aligned} \tag{3.13}$$

in which $\mathbf{a}_i^{\mathrm{r}}$ and $\mathbf{n}_i^{\mathrm{a}}$, after utilizing eq. (3.9), are defined as

$$\mathbf{a}_i^{\mathrm{r}} \triangleq \hat{\mathbf{Q}}_i{}^{\mathcal{A}_i}\mathbf{a}_i - \frac{1}{m}\sum_{j=1}^{m}\hat{\mathbf{Q}}_j{}^{\mathcal{A}_j}\mathbf{a}_j, \tag{3.14}$$

$$\mathbf{n}_i^{\mathrm{a}} \triangleq \phi_i\hat{\mathbf{Q}}_i\mathbf{E}_i{}^{\mathcal{A}_i}\mathbf{a}_i - \frac{1}{m}\sum_{j=1}^{m}\phi_j\hat{\mathbf{Q}}_j\mathbf{E}_j{}^{\mathcal{A}_j}\mathbf{a}_j, \tag{3.15}$$

where ${}^{\mathcal{A}_i}\mathbf{a}_i$ is the acceleration measured by the ith accelerometer. Note that, even though the gravitational acceleration $\mathbf{g}$ must be added to each of the accelerometer measurements in order to obtain the acceleration of the corresponding pickup point, this effect vanishes in $\mathbf{a}_i - \mathbf{a}_C$, no matter how accurate, or inaccurate for that matter, the calibration is. The accuracy of the final results, however, are affected.

Furthermore, let us define the $3 \times m$ matrices $\mathbf{R}$, $\mathbf{A}^{\mathrm{r}}$, and $\mathbf{N}^{\mathrm{a}}$ as

$$\mathbf{R} \triangleq \begin{bmatrix} \mathbf{r}_1 & \mathbf{r}_2 & \dots & \mathbf{r}_m \end{bmatrix}, \tag{3.16}$$

$$\mathbf{A}^{\mathrm{r}} \triangleq \begin{bmatrix} \mathbf{a}_1^{\mathrm{r}} & \mathbf{a}_2^{\mathrm{r}} & \dots & \mathbf{a}_m^{\mathrm{r}} \end{bmatrix}, \tag{3.17}$$

$$\mathbf{N}^{\mathrm{a}} \triangleq \begin{bmatrix} \mathbf{n}_1^{\mathrm{a}} & \mathbf{n}_2^{\mathrm{a}} & \dots & \mathbf{n}_m^{\mathrm{a}} \end{bmatrix}. \tag{3.18}$$

Then, by equating the right-hand sides of eqs. (3.12 & 3.13), assembling all the equations in matrix form, and noticing the definitions given by eqs. (3.14–3.18), one can write

$$\mathbf{W}\mathbf{R} = \mathbf{A}^{\mathrm{r}} + \mathbf{N}^{\mathrm{a}} \tag{3.19}$$

with $\mathbf{W} \triangleq \dot{\mathbf{\Omega}} + \mathbf{\Omega}^2$ known as the *angular-acceleration tensor* (Angeles, 1999). Hence, the least-square solution of eq. (3.19) is

$$\mathbf{W} = (\mathbf{A}^{\mathrm{r}} + \mathbf{N}^{\mathrm{a}})\mathbf{R}^{\dagger}, \qquad \mathbf{R}^{\dagger} \triangleq \mathbf{R}^T(\mathbf{R}\mathbf{R}^T)^{-1}, \tag{3.20}$$

where $\mathbf{R}^{\dagger}$ is the Moore-Penrose generalized inverse (Nobel and Daniel, 1988) of $\mathbf{R}$, which must be calculated only once.

Since $\dot{\mathbf{\Omega}}$ and $\mathbf{\Omega}^2$ are skew-symmetric and symmetric, respectively, one can readily calculate the angular acceleration of the body by taking the axial vector[2] of both sides of eq. (3.20), namely,

$$\dot{\boldsymbol{\omega}} = \mathrm{vect}(\hat{\mathbf{W}}) \tag{3.21}$$

in which $\hat{\mathbf{W}}$ is computed using eq. (3.20) while neglecting $\mathbf{N}^{\mathrm{a}}$.

3.3.2 Angular Velocity

The calculation of the angular velocity from $\mathbf{\Omega}^2$, however, is not as straightforward as that of the angular acceleration when there is a substantial calibration error. The reason is that, in such a case, there are six inconsistent quadratic equations in three unknowns. Therefore, solving them, i.e., calculating the best estimate for the angular-velocity vector, requires an optimum estimation scheme, which can be computationally

[2]The axial vector of a real, 3×3 matrix $\mathbf{V} = [v_{ij}]$ is defined as

$$\mathbf{v} \equiv \mathrm{vect}(\mathbf{V}) \triangleq (1/2) \begin{bmatrix} v_{32} - v_{23} & v_{13} - v_{31} & v_{21} - v_{12} \end{bmatrix}^T.$$

expensive; moreover, the result will not necessarily be consistent with the angular acceleration calculated from eq. (3.21). Our simulations demonstrated that, in the presence of calibration errors, the numerical integration of the angular acceleration alone will provide results suitable enough for the highly accurate calibration method proposed here.

After the installation errors are identified and accounted for, however, the angular velocity can be determined quite accurately from $\mathbf{\Omega}^2$ either using a numerical procedure such as Newton-Raphson's (NR), as done in (Parsa *et al.*, 2002a)[3], or in closed form, as explained below: The system of nonlinear equations to be solved for $\boldsymbol{\omega}$ is given by

$$-\|\boldsymbol{\omega}\|^2\,\mathbf{1} + \boldsymbol{\omega}\boldsymbol{\omega}^T = \hat{\mathbf{W}}^{\mathrm{S}}, \tag{3.22}$$

with

$$\hat{\mathbf{W}}^{\mathrm{S}} \triangleq \frac{1}{2}(\hat{\mathbf{W}} + \hat{\mathbf{W}}^T), \tag{3.23}$$

because the left-hand side of eq. (3.22) is identically equal to $\mathbf{\Omega}^2$ (Angeles, 2002). Upon taking the trace of both sides of the foregoing equation, one obtains

$$\|\boldsymbol{\omega}\|^2 = -\frac{1}{2}\mathrm{tr}(\hat{\mathbf{W}}^{\mathrm{S}}) \tag{3.24}$$

in which $\mathrm{tr}(\cdot)$ represents the trace of $(\cdot)$. As a result, eq. (3.22) can be rewritten as

$$\boldsymbol{\omega}\boldsymbol{\omega}^T = \hat{\mathbf{W}}^{\mathrm{S}} - \frac{1}{2}\mathrm{tr}(\hat{\mathbf{W}}^{\mathrm{S}})\mathbf{1} \tag{3.25}$$

from which, by taking the square root of the diagonal elements, the components of $\boldsymbol{\omega}$ are obtained up to a sign change, which can be fixed by looking at the sign of the components of the approximate value of $\boldsymbol{\omega}$ at $(i+1)$st sampling time obtained using Simpson's rule, namely,

$$\hat{\boldsymbol{\omega}}_{i+1} = \boldsymbol{\omega}_i + \frac{h}{2}(\dot{\boldsymbol{\omega}}_{i+1} + \dot{\boldsymbol{\omega}}_i) \tag{3.26}$$

[3]The procedure reported here in this section is also superior to that of (Parsa *et al.*, 2002a) in that, here, the angular velocity is obtained directly, i.e., no iteration is involved.

where h is the sampling time.

Obviously, the norm of the angular velocity cannot be negative. However, when the angular velocity is at the verge of vanishing, due to round-off or measurement errors, the trace in eq. (3.24) can become positive. In such cases, one has to assume the trace to be zero. The same has to be done when any of the diagonal elements of the right-hand side of eq. (3.25) becomes negative. In other words, the method explained here loses accuracy when the angular-velocity components go through a sign change or when they become zero and remain so.

As seen from eq. (3.21), using the procedure outlined here, one can calculate the angular acceleration of the body without a priori knowledge of the body angular velocity; this brings about a major accuracy improvement when compared with the procedure proposed by Parsa *et al.* (2001), where estimating the angular acceleration of the body required a priori knowledge of the angular velocity. Furthermore, in that paper, the angular velocity was obtained by integrating the angular acceleration, which caused a drift in the estimation of the angular velocity, due to error accumulations. Those results are reproduced here in a more suitable format, as Fig. 3.2, for comparison. The component indices are included in the figures.

3.3.3 Translational Velocity and Position

Using elementary kinematics, it can be shown that

$$\dot{\mathbf{v}}_C = \mathbf{a}_C - \boldsymbol{\Omega}\,\mathbf{v}_C, \tag{3.27}$$

and

$$\dot{\mathbf{c}} = \mathbf{v}_C - \boldsymbol{\Omega}\,\mathbf{c}, \tag{3.28}$$

where $\mathbf{v}_C$ and $\mathbf{c}$ are the absolute velocity and the position vector of the centroid, respectively, expressed in the body-frame. Integrating the two above relations, given the initial conditions, one can obtain $\mathbf{v}_C$ and $\mathbf{c}$.

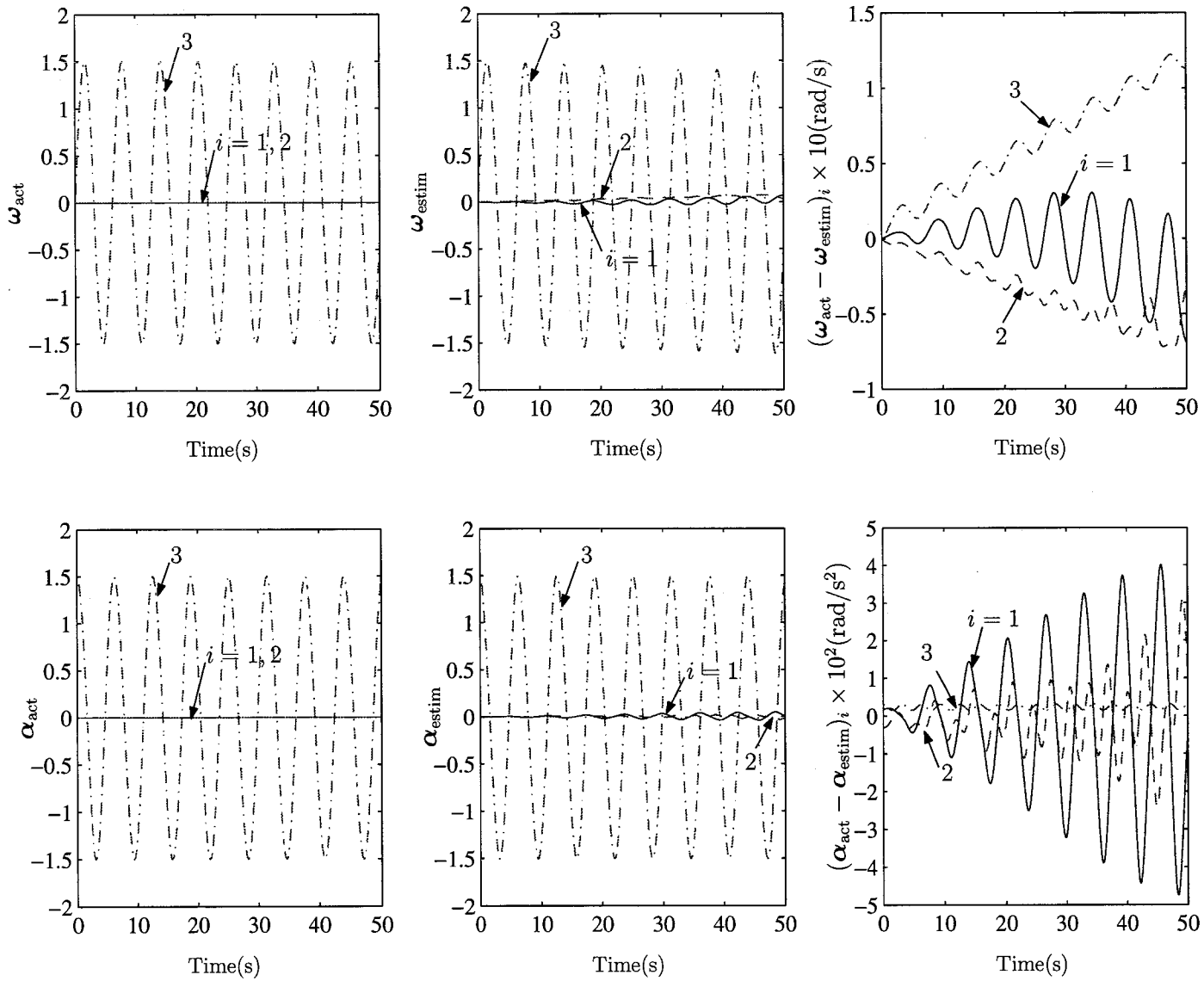

Figure 3.2: Estimation of ω and α, with a 0.1° installation error

3.3.4 The Rigid-Body Attitude

As observed from eqs. (2.6a & 2.6c), recalled here, the time-rate of change of $\boldsymbol{\eta}$ in the body frame, $\dot{\boldsymbol{\eta}}$, is related to the angular velocity $\boldsymbol{\omega}$ of the body, expressed in the same frame, by

$$\dot{\boldsymbol{\eta}} = \mathbf{K}\boldsymbol{\eta}, \qquad \mathbf{K} \triangleq \frac{1}{2}\begin{bmatrix} -\boldsymbol{\Omega} & \boldsymbol{\omega} \\ -\boldsymbol{\omega}^T & 0 \end{bmatrix}. \tag{3.29}$$

This equation can be integrated numerically to compute the orientation of the body[4]. Due to truncation and round-off errors, however, the result of the integration at each time step most likely will not be consistent, i.e, the norm of $\boldsymbol{\eta}$ most likely will fail to be unity.

To overcome this problem, one can find a least-square-error approximation by normalizing the quaternion thus obtained, i.e., by replacing $\boldsymbol{\eta}$ by $\boldsymbol{\eta}/\|\boldsymbol{\eta}\|$ at each time step. The reason, in short, is that the normal projection of any point in the four-dimensional Euclidean space onto the unit hypersphere yields the closest point on the hypersphere.

It has been proven (Giardina *et al.*, 1975) that, if the non-normalized quaternion is used to calculate a corresponding non-orthogonal rotation matrix from eq. (2.3), recalled here,

$$\mathbf{Q} = \mathbf{1} + 2u_0\mathbf{U} + 2\mathbf{U}^2, \tag{3.30}$$

then the orthogonalization of this rotation matrix through the polar-decomposition theorem yields an orthogonal matrix which is exactly the same as the rotation matrix corresponding to the normalized quaternion.

Hence, the system of differential equations to be integrated to estimate the pose and twist of the rigid body is composed of eqs. (3.27–3.29). The important feature of these equations is that, since they are all written in the body-frame, no knowledge of the body attitude is required for the calculation of the twist. Consequently, the error

[4]One may be tempted to find the solution of this differential equation in closed-form as $\boldsymbol{\eta}(t) = \exp\left(\int_0^t \mathbf{K}dt\right)\boldsymbol{\eta}_0$. However, this solution can be correct *only* if the two matrices $\exp\left(\int_0^t \mathbf{K}dt\right)$ and $\mathbf{K}$ commute under multiplication, which is not necessarily the case.

incurred at the pose-estimation level does not propagate back to the twist-estimation level although it causes inaccuracies in the reference-frame representation of the twist.

3.4 Kinematic Attitude Calibration

As shown in Section 3.5, due to gravitational calibration errors, the integration results are not stable even in the presence of small angular errors; in fact, the estimation errors for any of the pose and twist components, as well as the rate at which these errors grow, increase with the calibration errors. Therefore, to remedy the situation and to obtain a better estimate of the actual value of the states, a second calibration scheme, not requiring an accurate knowledge of the accelerometer-array pose, is needed to estimate the calibration-error rotation matrices $\bar{\mathbf{Q}}_i$. One such scheme is proposed in this section.

Firstly, vectors $\bar{\mathbf{e}}_i$ are defined as

$$\bar{\mathbf{e}}_i \triangleq \phi_i \mathbf{e}_i, \quad i = 1, 2, \ldots, m. \tag{3.31}$$

Using these definitions, $\mathbf{n}_i^{\mathrm{a}}$, given by eq. (3.15), can be rewritten as

$$\mathbf{n}_i^{\mathrm{a}} = \hat{\mathbf{Q}}_i \bar{\mathbf{E}}_i^{A_i} \mathbf{a}_i - \frac{1}{m} \sum_{j=1}^{m} \hat{\mathbf{Q}}_j \bar{\mathbf{E}}_j^{A_j} \mathbf{a}_j \tag{3.32}$$

where $\bar{\mathbf{E}}_i \triangleq \mathrm{CPM}(\bar{\mathbf{e}}_i)$. Then, from eq. (3.19), an estimate $\hat{\mathbf{N}}^{\mathrm{a}}$ is evaluated from

$$\hat{\mathbf{N}}^{\mathrm{a}} = \hat{\mathbf{W}}\mathbf{R} - \mathbf{A}^{\mathrm{r}} \tag{3.33}$$

in which $\hat{\mathbf{W}}$ is an estimate of $\mathbf{W}$ and given by eq. (3.23).

Calculating $\hat{\mathbf{N}}^{\mathrm{a}}$, one can obtain an approximate value for $\mathbf{n}_i^{\mathrm{a}}$ by just picking up the ith column of $\hat{\mathbf{N}}^{\mathrm{a}}$. On the other hand, from eq. (3.32), it can be seen that

$$-\frac{m-1}{m} \hat{\mathbf{Q}}_i \mathbf{A}_i \bar{\mathbf{e}}_i + \frac{1}{m} \sum_{\substack{j=1 \\ j \neq i}}^{m} \hat{\mathbf{Q}}_j \mathbf{A}_j \bar{\mathbf{e}}_j = \mathbf{n}_i^{\mathrm{a}} \tag{3.34}$$

where $\mathbf{A}_i \triangleq \mathrm{CPM}({}^{A_i}\mathbf{a}_i)$, and one thus arrives at a set of $3m$ linear equations in $3m$ unknowns, the elements of $\bar{\mathbf{e}}_i$. Assembling all these equations, one obtains

$$\mathbf{\Lambda} \bar{\mathbf{e}} = \mathbf{n}^{\mathrm{a}} \tag{3.35}$$

where the (i,j) block of $\mathbf{\Lambda}$, $\bar{\mathbf{e}}$, and $\mathbf{n}^{\mathrm{a}}$ are defined by

$$\mathbf{\Lambda}_{ij} \triangleq (\frac{1}{m} - \delta_{ij})\hat{\mathbf{Q}}_j \mathbf{A}_j \tag{3.36}$$

$$\bar{\mathbf{e}} \triangleq \begin{bmatrix} \bar{\mathbf{e}}_1^T & \bar{\mathbf{e}}_2^T & \cdots & \bar{\mathbf{e}}_m^T \end{bmatrix}^T, \tag{3.37}$$

$$\mathbf{n}^{\mathrm{a}} \triangleq \begin{bmatrix} \mathbf{n}_1^{\mathrm{a}T} & \mathbf{n}_2^{\mathrm{a}T} & \cdots & \mathbf{n}_m^{\mathrm{a}\,T} \end{bmatrix}^T. \tag{3.38}$$

and δ_{ij} is the Kronecker delta.

However, this system of equations cannot be solved as is because it is not linearly independent, for $\sum_{i=1}^{m}(\frac{1}{m} - \delta_{ij})\hat{\mathbf{Q}}_j \mathbf{A}_j = \mathbf{O}$. Therefore, eq. (3.35) is written for N different measurements during an arbitrary manoeuvre of the body, and all $3mN$ equations thus generated are then assembled:

$$\begin{bmatrix} (\mathbf{\Lambda})_1^T & \cdots & (\mathbf{\Lambda})_N^T \end{bmatrix}^T \bar{\mathbf{e}} = \begin{bmatrix} (\mathbf{n}^{\mathrm{a}})_1^T & \cdots & (\mathbf{n}^{\mathrm{a}})_N^T \end{bmatrix}^T. \tag{3.39}$$

Upon solving this system of equations in the least-square sense, we obtain an approximation of $\bar{\mathbf{e}}$.

Using the vector $\bar{\mathbf{e}}$ thus calculated, one can improve the $\hat{\mathbf{Q}}_i$ estimates by calculating $\bar{\mathbf{Q}}_i$ from eq. (3.8), after computing ϕ_i and $\mathbf{e}_i$ using $\phi_i = \|\bar{\mathbf{e}}_i\|$ and $\mathbf{e}_i = \bar{\mathbf{e}}_i / \|\bar{\mathbf{e}}_i\|$, and then replacing $\hat{\mathbf{Q}}_i$ by $\hat{\mathbf{Q}}_i \bar{\mathbf{Q}}_i$. Notice that eq. (3.8) is used to calculate $\bar{\mathbf{Q}}_i$ even though its linear approximation, eq. (3.9), was originally used to simplify the equations involved; the reason is that $\bar{\mathbf{Q}}_i$ will not turn out to be orthogonal otherwise. This procedure may be implemented iteratively off-line in order to achieve a small enough norm of $\boldsymbol{\phi} \triangleq \begin{bmatrix} \phi_1 & \cdots & \phi_m \end{bmatrix}^T$.

Our simulations show that, using this procedure, angular installation errors as large as 20° can be dealt with.

3.5 Simulation

3.5.1 First Results

The sample rigid-body motion reported in (Parsa *et al.*, 2001) was a harmonic motion about a fixed axis parallel to the vertical direction, so that both angular velocity and

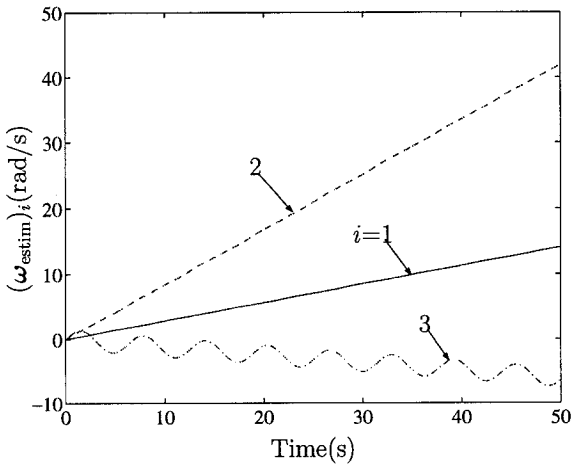

Figure 3.3: The angular-velocity estimate; $\phi_j = 10°$

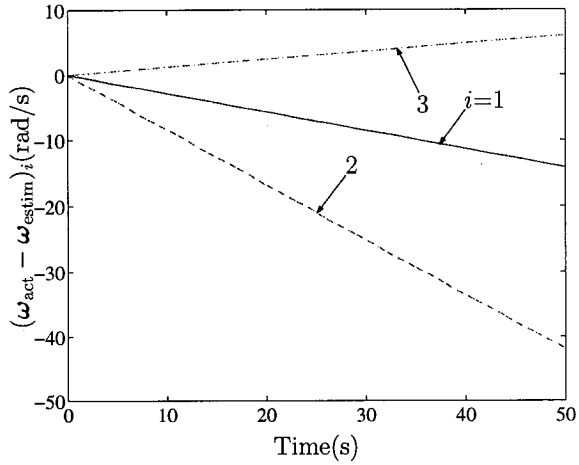

Figure 3.4: Error in the angular-velocity estimate; $\phi_j = 10°$

angular acceleration varied harmonically over time. Figure 3.2 shows the estimated angular velocity and acceleration as well as their errors. The simulation was implemented in Matlab. To integrate the system of differential equations, we used the second-order Runge-Kutta method. Moreover, it was assumed that the accelerometer data, coming from five accelerometers, were read at a rate of 100 Hz, and that the accelerometer calibration errors were 0.1° about arbitrarily chosen axes.

As seen in Fig. 3.2, the results were unstable. Simulations carried out revealed that the estimation errors for any of the pose and twist elements, as well as the pace at which these errors would grow, increased with the calibration errors.

To remedy the above situation and to obtain a better estimate of the actual value of the states, Parsa *et al.* (2001) suggested that one could fuse the integration results with the data coming from a fiber-optic pose sensor called Shape-Tape (Danisch, 1998; 2000; Danisch *et al.*, 1999) at each time-step. To this end, two sets of weighting factors were chosen to be applied on the two sets of data; then, corresponding weighted variables were added up, so that, for each of the pose and twist elements, a corrected value was found.

In the case of angular velocity, for instance, two estimates of $\boldsymbol{\omega}$ were evaluated: One by integrating eq. (3.21), and the other by taking the axial vector of the angular-

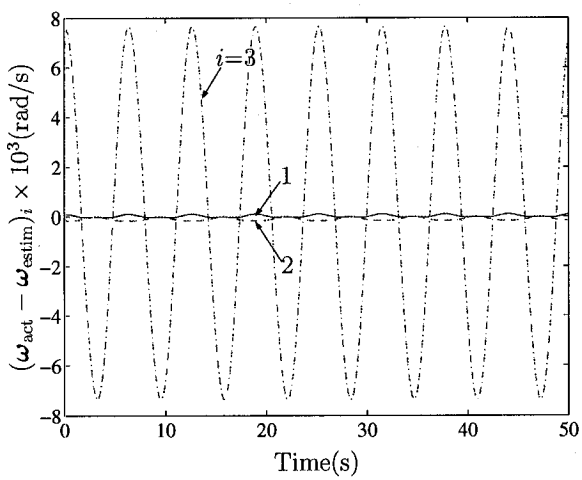

Figure 3.5: Stabilized error in the estimation of body angular velocity; 0.1° calibration error

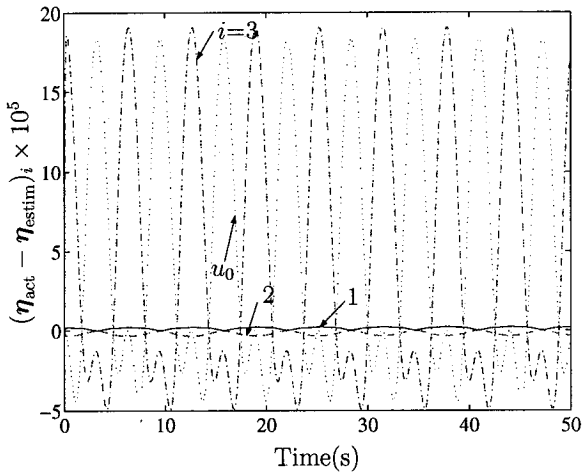

Figure 3.6: Stabilized error in the Euler-parameters estimation; 0.1° calibration error

velocity matrix calculated using eq. (2.11), after the rotation matrix delivered by the Shape-Tape was numerically differentiated. Albeit, theoretically, only three of the nine entries of $\mathbf{\Omega}$ are needed to find the second estimate, we chose to employ this relation to filter the existing errors as far as possible because $\mathbf{\Omega}$ would most likely not be skew-symmetric. Of course, to use this equation, one has to numerically differentiate the rotation matrix $\mathbf{Q}$ calculated using the Shape-Tape software.

Then, simulations were carried out for the same sample motion. The weight given to the integrated data was 0.8; 0.2 was assigned to the Shape-Tape data. By doing so, not only did the maximum errors decrease dramatically but also their growth stopped—see Fig. 3.5, and compare the errors with those shown in Fig. 3.2.

The stabilized estimation error of the angular velocity and that of the attitude are plotted in Figs. 3.5 and 3.6, respectively. In the latter, the numbers refer to the component indices of vector $\mathbf{u}$ of eq. (2.1).

3.5.2 Second Results

The formulation proposed in Sections 3.3 and 3.4 was implemented in MATLAB. To integrate the system of differential equations, the second-order Runge-Kutta method was used. It is assumed that the accelerometer data, coming from an array of five

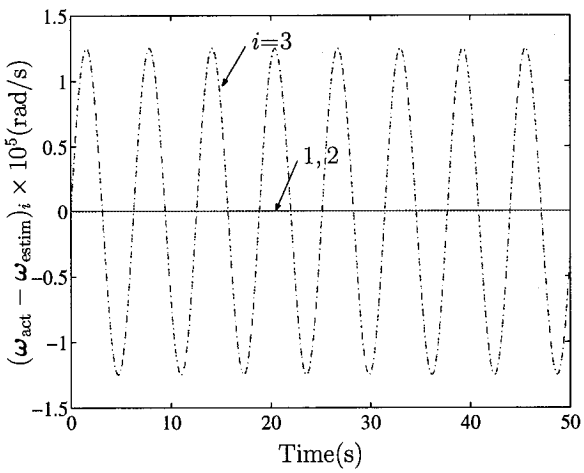

Figure 3.7: Error in the estimation of ω after calibration

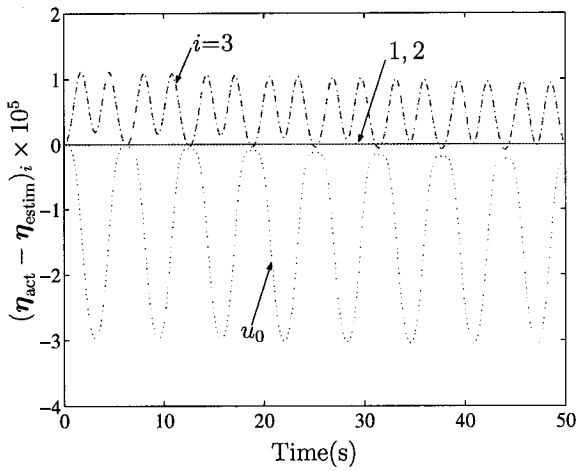

Figure 3.8: The Euler-parameter estimation error after calibration

accelerometers, are read at a 100 Hz rate, and that the accelerometer calibration errors are 10° about arbitrarily chosen axes. The relative poses of the accelerometers with respect to each other, so far as the simulations are concerned, are irrelevant. However, in an actual application, the sensors should be located at the same relative distance and orientation, and as far from one another as possible for the best results.

The first sample rigid-body motion to be observed is the motion considered in the foregoing subsection, namely, a fixed-point harmonic rotation about a vertical axis with an amplitude of 1.5 rad and a circular frequency of 1.0 rad/s. Figures 3.3

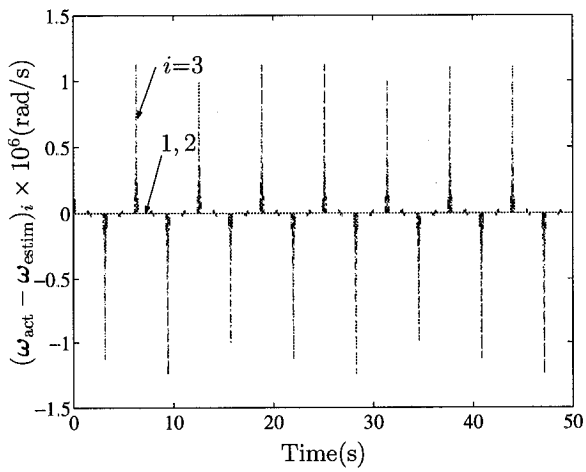

Figure 3.9: Error in the calculation of the skew-symmetric $\sqrt{\Omega^2}$ using NR

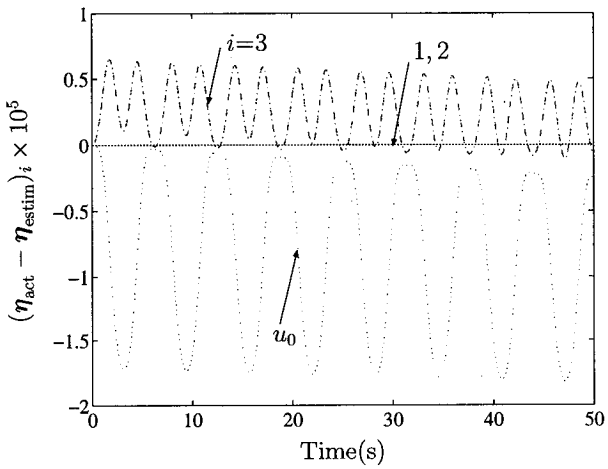

Figure 3.10: The estimation error of the Euler parameters after NR

and 3.4 show the estimated angular velocity and its error, respectively. As seen in Fig. 3.3 and explained in the previous subsection, due to the calibration errors, the angular-velocity estimation results are not stable.

Then, the calibration is applied iteratively six times to decrease the amount of calibration error. At the end of the first iteration, $\boldsymbol{\phi}$ is estimated as $[7.82°, 11.0°, 10.3°, 10.5°, 9.31°]^T$. At the end of the sixth iteration, however, the remaining angular error amounts to $\boldsymbol{\phi} = 10^{-14} \times [1.63°, 1.63°, 4.40°, 2.51°, 1.54°]^T$. The angular-velocity and Euler-parameter error estimates at the end of the sixth iteration are quite small as shown in Figs. 3.7 and 3.8. Similar results were obtained, with the same number of iterations, when the initial orientation errors were set to 20°.

As discussed by Parsa *et al.* (2002a), one can improve the results further by solving eq. (3.22) for $\boldsymbol{\omega}$ using the NR method; the numerical integral of the angular-acceleration vector, i.e., the approximate value given by eq. (3.26), provides the required initial guess. Figures 3.9 and 3.10 show the errors after applying the Newton-Raphson scheme with a relative tolerance of 10^{-7}. One interesting point in Fig. 3.9 is that, as opposed to Fig. 3.7, the highest errors occur when the angular velocity undergoes a sign change, the sole reason being the inherent sign indeterminacy of the square-root problem. As reported in (Parsa *et al.*, 2002a), the angular-velocity results obtained at this stage are three orders of magnitude more accurate than the results presented in (Parsa *et al.*, 2001), where the readings of a fiber-optic pose sensor were used to correct the instability problem incurred due to calibration errors, for the same sample motion, in the presence of 0.1° angular errors. As for the quaternion errors, the results shown in Fig. 3.10 are at least as accurate, without resorting to an additional sensor.

Another motion which is considered here as an example is the motion of a spinning top, shown in Fig. 3.11 as a cone, with the z-y-z Euler angles describing its attitude[5].

[5]Notice that, to calculate the initial attitude and the attitude-estimation error, one should obtain the top attitude in terms of the Euler parameters; this can be done by applying the quaternion-concatenation formula given in (Reynolds, 1998) twice.

We assume that the height of the cone is 0.15 m, and that, at time $t = 0$, $\theta = 30°$, $\psi = 45°$, and $\phi = 60°$. It is further assumed that the precession and the spin motions take place at constant speeds of 0.5 and 1.5 rad/s, respectively, while the nutation angle ψ varies sinusoidally with an amplitude of 22.5° and a circular frequency of 0.2 rad/s.

The plots displayed in Fig. 3.12 show estimation errors for $\boldsymbol{\omega}$ and $\boldsymbol{\alpha}$ under the assumption that each of the accelerometers in the array has a 20° installation error at an arbitrary direction. At this moment, if the kinematic calibration scheme reported in Section 3.4 is applied, after six iterations, the attitude errors can be identified and effectively accounted for. Figure 3.13 shows the results after the installation errors are identified and taken into account in the calculations. At this stage, however, since the angular-velocity vector is still calculated by integrating the body angular acceleration, the amplitude of the error is large. To remedy this problem, the angular velocity of the body is calculated from $\boldsymbol{\Omega}^2$. As a result, the estimation error for the angular velocity, as shown in Fig. 3.14, is dramatically lowered.

If the angular-velocity results are integrated now, the attitude of the top at each instant can be determined. The attitude-estimation errors, in terms of Euler-parameter errors, are given in Fig. 3.15. As seen from this figure, the error is increasing; this was actually expected, for the integration operation is inherently unstable.

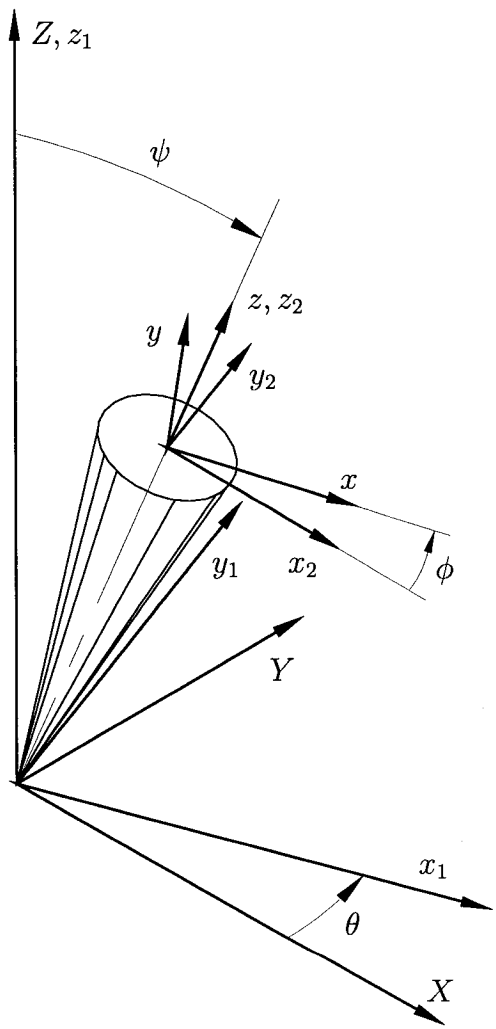

Figure 3.11: A spinning top

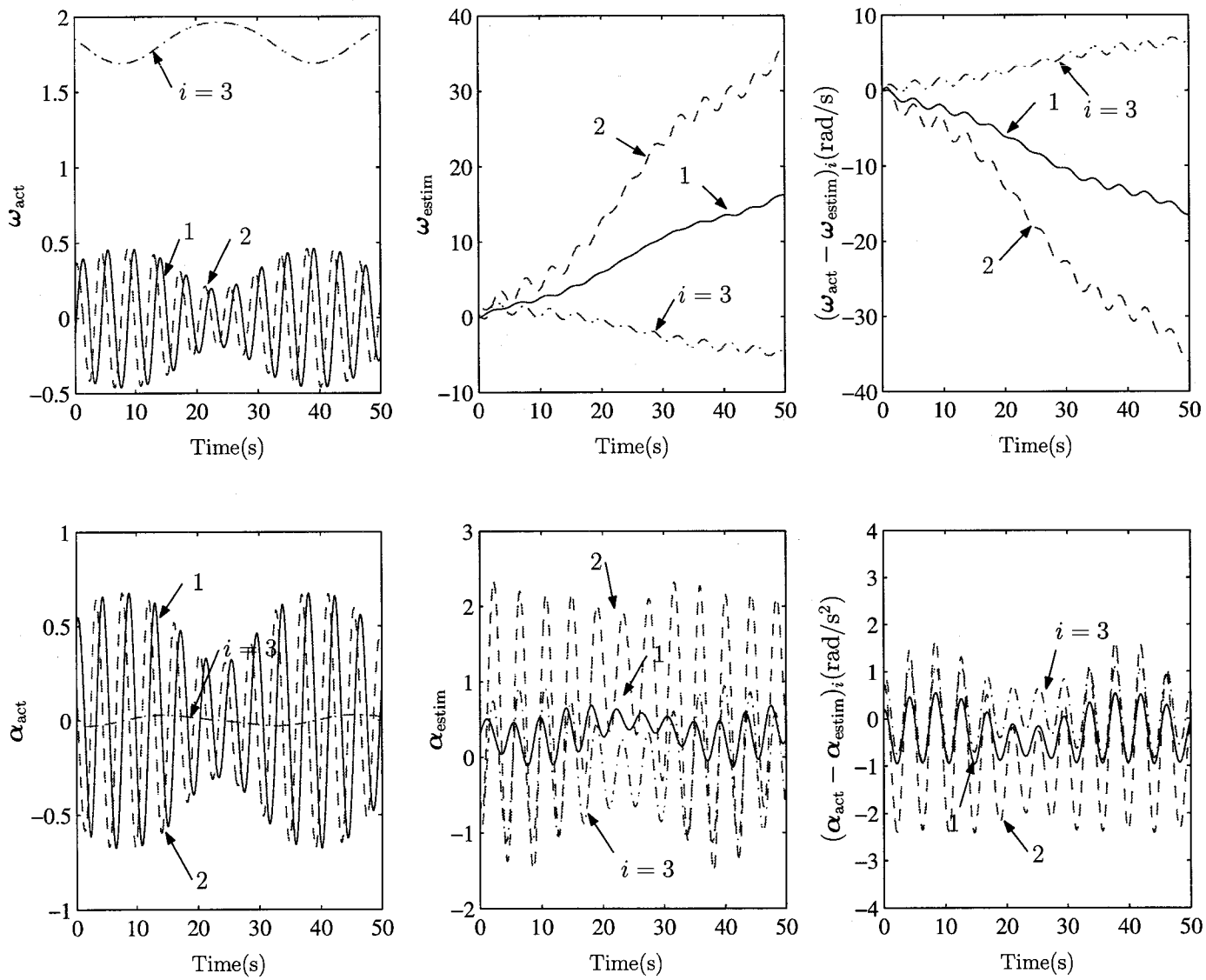

Figure 3.12: Estimation of ω and α for the spinning-top problem before calibration; instalation error 20°

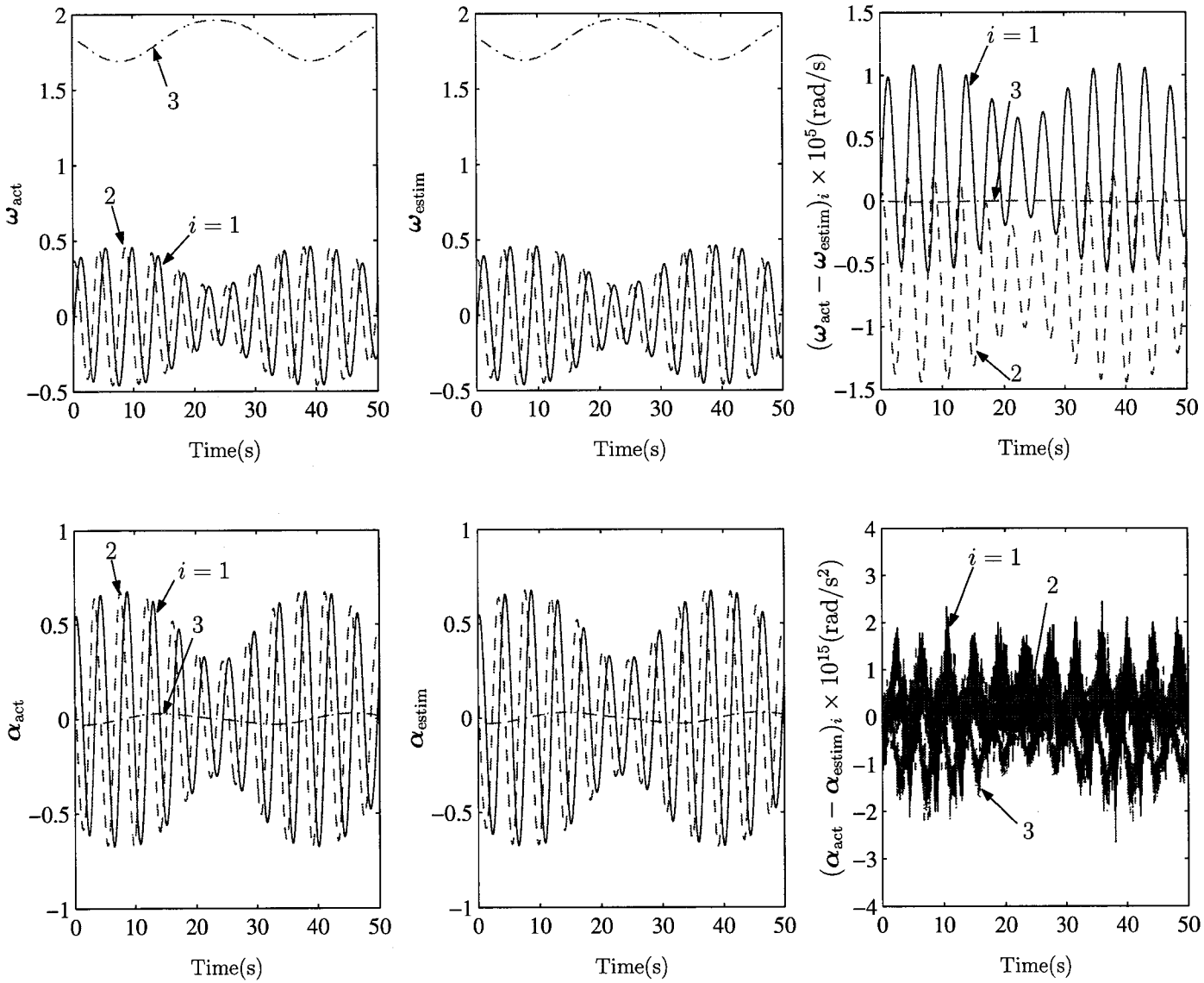

Figure 3.13: Estimation of ω and α for the spinning-top problem after kinematic calibration

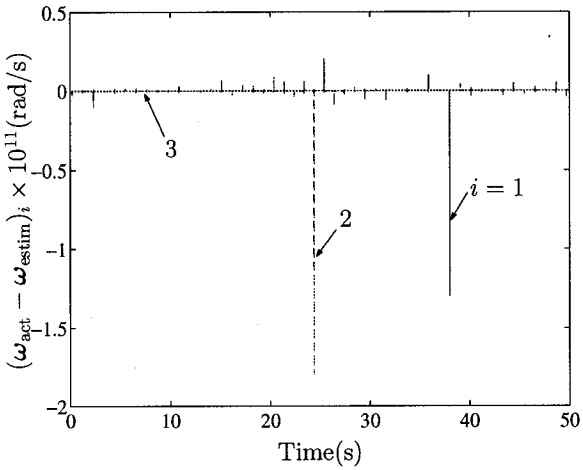

Figure 3.14: Error in calculating ω in closed form for the spinning-top problem, after kinematic calibration

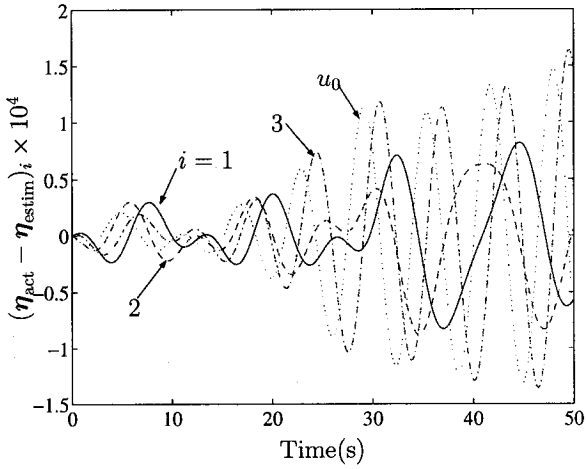

Figure 3.15: The estimation error of the Euler parameters for the spinning-top problem, after kinematic calibration; with closed-form ω

3.6 Real-Time Operation

As explained in (Parsa *et al.*, 2001), in order to render the formulation real-time operational, the authors "translated" the MATLAB m-files into C-code and subsequently compiled the code thus generated using MATLAB's `mcc` translator. Even though special attention was paid to the minimization of the number of calculations in MATLAB, simulations had revealed that the `mcc`-generated C-code was not fast enough. Therefore, an independent estimation program was developed in C. As reported in that paper, the simulations showed a dramatic improvement in computation time: For each 10-ms time step, from 24 ms in MATLAB through 10 ms with MATLAB-generated C-code to less than 0.5 ms with the independent C-code on a 300 MHz SGI machine with a MIPS R12000 Processor and 512 MB of RAM.

Because the estimation procedure explained in (Parsa *et al.*, 2001) is more complicated and thus more time consuming than that of the procedure explained in this chapter, it can safely be assumed that the latter is also real-time operational. Furthermore, with the advent of GHz-processors over the past two years, the clock frequency of common computers have almost quadrupled. Therefore, insofar as the computation

time is concerned, no problem is anticipated in the real-time implementation of the algorithm proposed here.

Chapter 4

Dynamics

4.1 Introduction

To derive the dynamics of the entire system, we separate the manipulator into its two kinematic chains, namely, the flexible submanipulator, and the rigid submanipulator. The dynamics model of each chain is derived by writing the dynamics equations of its links using the Lagrange equations, assembling these equations, and eliminating the additional equations through the application of the Natural Orthogonal Complement (NOC). Then, to obtain the mathematical model of the whole system the two sets of dynamics equations are assembled. This time again the additional equations are eliminated by applying the NOC.

As mentioned in Chapter 1, it is indeed possible to deal with the system as a single chain—without any need to distinguish between the parts of the flexible-manipulator and those of the rigid manipulator—by writing the dynamics equations of all the links, and then assembling the equations thus obtained at once. However, the approach we have taken here turns out to be computationally more efficient for the particular state-estimation technique proposed in this thesis.

The methodology presented in this chapter is used in Appendix E to derive the dynamics equations of a planar *RRR* manipulator comprising a single-link flexible submanipulator and a two-link rigid submanipulator.

4.2 Generalized Coordinates and Generalized Velocities

Even though not all the links of the flexible manipulator have to be flexible, we assume that the generalized coordinates of the flexible-manipulator links, in general, include a set of numbers that, given the discretization method, will provide information on the configuration of the link. In addition, the link-generalized-coordinate *vector*[1] must contain information on the pose of a local frame attached to the link. To satisfy these requirements, we take the vector $\mathbf{q}_{\mathrm{F}i}$ given below as the vector of generalized coordinates of the flexible-manipulator link number i:

$$\mathbf{q}_{\mathrm{F}i} \triangleq \begin{bmatrix} \mathbf{p}_{\mathrm{F}i}^T & \boldsymbol{\eta}_{\mathrm{F}i}^T & \boldsymbol{\zeta}_i^T \end{bmatrix}^T, \qquad \text{for } i = 1, 2, \ldots, n_{\mathrm{F}}, \tag{4.1}$$

with n_{F} being the number of links of the flexible manipulator. Vectors $\mathbf{p}_{\mathrm{F}i}$ and $\boldsymbol{\eta}_{\mathrm{F}i}$ are the position vector and the array of the Euler parameters of the link body-frame $\mathcal{F}_{\mathrm{F}i}$, respectively, expressed in the local frame, with respect to the inertial reference frame $\mathcal{R}$. The vector $\boldsymbol{\zeta}_i$ of the link flexural coordinates has the form

$$\boldsymbol{\zeta}_i = \begin{bmatrix} \boldsymbol{\xi}_i^T & \boldsymbol{\mu}_i^T \end{bmatrix}^T, \tag{4.2}$$

in which $\boldsymbol{\xi}_i$ and $\boldsymbol{\mu}_i$ represent the flexural coordinates pertaining to the bending and torsional deformations, respectively, of the link.

The link generalized coordinates, i.e., the elements of $\mathbf{q}_{\mathrm{F}i}$, however, are not independent, due to the dependence of the Euler parameters; the constraint equation has the form

$$\mathbf{q}_{\mathrm{F}i}^T \boldsymbol{\Sigma}_{\mathrm{F}i} \mathbf{q}_{\mathrm{F}i} = 1, \quad \boldsymbol{\Sigma}_{\mathrm{F}i} \triangleq \mathrm{diag}(\mathbf{O}_{3\times 3}, \mathbf{1}_4, \mathbf{O}_{n_{fi}\times n_{fi}}), \tag{4.3}$$

where $\mathbf{1}_4$ is the 4×4 identity matrix, n_{fi} being the dimension of $\boldsymbol{\zeta}_i$, i.e., the number of flexural coordinates of the ith link.

[1] We use here the term *vector* in the computer-science sense, i.e., to indicate a one-dimensional array, not necessarily in the algebraic sense. For example, the "vector" of generalized coordinates may contain components associated with the attitude of a rigid body; the sum of two such vectors, with regards to its attitude components, has no kinematic meaning.

The vector of link generalized velocities, on the other hand, is defined by the twist $\mathbf{t}_{\mathrm{F}i}$ given below:

$$\mathbf{t}_{\mathrm{F}i} \triangleq \begin{bmatrix} \dot{\mathbf{p}}_{\mathrm{F}i}^T & \boldsymbol{\omega}_{\mathrm{F}i}^T & \dot{\boldsymbol{\zeta}}_i^T \end{bmatrix}^T, \qquad \text{for } i = 1, 2, \ldots, n_{\mathrm{F}} \tag{4.4}$$

where $\boldsymbol{\omega}_{\mathrm{F}i}$ is the angular velocity of the body-frame expressed in the same frame.

For rigid links, whether they belong to the flexible manipulator or to its rigid counterpart, in general, the generalized coordinates and generalized velocities are defined in the same manner, except for the flexural-coordinate part, which will be absent. Therefore, for the rigid link number j, we have

$$\mathbf{q}_j \triangleq \begin{bmatrix} \mathbf{p}_j^T & \boldsymbol{\eta}_j^T \end{bmatrix}^T, \tag{4.5}$$

$$\mathbf{t}_j \triangleq \begin{bmatrix} \dot{\mathbf{p}}_j^T & \boldsymbol{\omega}_j^T \end{bmatrix}^T. \tag{4.6}$$

It is worth mentioning that, because the position vector is expressed in the link body-frame, its element-wise time derivative, which is included in the link array of generalized velocities, will naturally **not** be the absolute velocity of the origin of the frame.

4.3 Dynamics of the Flexible Submanipulator

4.3.1 The Link Kinetic and Potential Energies

Upon spatial discretization of a flexible link, its kinetic and potential energies can be written as

$$T_{\mathrm{F}i} = \frac{1}{2} \mathbf{t}_{\mathrm{F}i}^T \mathbf{M}_{\mathrm{F}i} \mathbf{t}_{\mathrm{F}i}, \tag{4.7}$$

$$V_{\mathrm{F}i} = \frac{1}{2} \boldsymbol{\zeta}_i^T \mathbf{K}_i \boldsymbol{\zeta}_i, \tag{4.8}$$

where $\mathbf{M}_{\mathrm{F}i}$ and $\mathbf{K}_i$ are the positive-definite, symmetric matrices representing the mass and the stiffness of the link, respectively. The structure and the value of the entries of the matrices are dependent on the assumptions made about the flexible links and the type of discretization used to model the flexibility of the link.

Under the assumptions set forth in Section 2.4, the kinetic energy of the link can be expressed as

$$T_{\mathrm{F}i} = \frac{1}{2}\int_0^{l_{\mathrm{F}i}} \rho_i(x)\,\|\mathbf{v}_{\mathrm{F}i}(x,t)\|^2 \mathrm{d}x + \frac{1}{2}\int_0^{l_{\mathrm{F}i}} \rho_i(x)\frac{J_i(x)}{A_i(x)}\left(\frac{\partial\gamma_i(x,t)}{\partial t}\right)^2 \mathrm{d}x \tag{4.9}$$

in which $\rho_i(x,t)$, $J_i(x)$, $A_i(x)$, and $\gamma_i(x,t)$ are the mass per unit length, the polar moment of inertia, the cross-sectional area, and the torsion angle of the link, respectively, while $\mathbf{v}_{\mathrm{F}i}(x,t)$ is the velocity of a typical point of the link neutral axis. If the link also has concentrated masses, they are taken care of by setting $\rho_i(x)$ equal to impulse functions in the space-domain of appropriate magnitude applied at the points where the masses are located.

Kinematic relations can be utilized to express $\mathbf{v}_{\mathrm{F}i}(x,t)$ and $\gamma_i(x,t)$ in terms of the link twist $\mathbf{t}_{\mathrm{F}i}$. Next, these expressions are substituted into eq. (4.9), and the integrals are evaluated. The expression thus obtained for the link kinetic energy is then used to derive the mass matrix. This is done for the special case of uniform links with one concentrated mass at the link distal end in Appendix C.

The potential energy of the link[2], on the other hand, under the same conditions, can be written as

$$\begin{aligned} V_{\mathrm{F}i} = {} & \frac{1}{2}\int_0^{l_{\mathrm{F}i}} EI_y^i(x)\left(\frac{\partial^2 u_z^i(x,t)}{\partial x^2}\right)^2 dx + \frac{1}{2}\int_0^{l_{\mathrm{F}i}} EI_z^i(x)\left(\frac{\partial^2 u_y^i(x,t)}{\partial x^2}\right)^2 dx \\ & + \frac{1}{2}\int_0^{l_{\mathrm{F}i}} GJ_i(x)\left(\frac{\partial\gamma_i(x,t)}{\partial x}\right)^2 dx \end{aligned} \tag{4.10}$$

in which E, G, $I_y^i(x)$, $I_z^i(x)$ are the Young modulus, the shear modulus, the cross-sectional second moment about Y_i axis, and that about Z_i axis, respectively, $u_y^i(x,t)$ and $u_z^i(x,t)$ being the flexural displacements of the link neutral axis along the two axes. If the discretization relations (2.62 & 2.65) are used to simplify the potential-energy expression, the stiffness matrix is then obtained as

$$\mathbf{K}_i \triangleq \mathrm{diag}\left(\int_0^{l_{\mathrm{F}i}} EI_y^i\boldsymbol{\varphi}_i''(\boldsymbol{\varphi}_i'')^T \mathrm{d}x_i, \int_0^{l_{\mathrm{F}i}} EI_z^i\boldsymbol{\varphi}_i''(\boldsymbol{\varphi}_i'')^T \mathrm{d}x_i, \int_0^{l_{\mathrm{F}i}} GJ_i\mathbf{h}_i'(\mathbf{h}_i')^T\right). \tag{4.11}$$

[2]Here, we only consider the elastic potential energy, the effect of gravity being addressed in Section 4.6.

4.3.2 The Link Governing Equations

Using the expressions of the kinetic and potential energies, we can write the link Lagrangian as

$$L_{\mathrm{F}i} = \frac{1}{2}\mathbf{t}_{\mathrm{F}i}^T\mathbf{M}_{\mathrm{F}i}\mathbf{t}_{\mathrm{F}i} - \frac{1}{2}\boldsymbol{\zeta}_i^T\mathbf{K}_i\boldsymbol{\zeta}_i, \tag{4.12}$$

the Lagrange equation of the link being, then,

$$\frac{d}{dt}\Big(\frac{\partial L_{\mathrm{F}i}}{\partial \dot{\mathbf{q}}_{\mathrm{F}i}}\Big) - \frac{\partial L_{\mathrm{F}i}}{\partial \mathbf{q}_{\mathrm{F}i}} = \mathbf{f}_{\mathrm{F}i}^{\mathrm{d}} + \mathbf{f}_{\mathrm{F}i}^{\mathrm{ex}} + \mathbf{f}_{\mathrm{F}i}^{\mathrm{k}} + \mathbf{f}_{\mathrm{F}i}^{\mathrm{a}}, \qquad \text{for } i = 1, \ldots, n_{\mathrm{F}}. \tag{4.13}$$

where $\mathbf{f}_{\mathrm{F}i}^{\mathrm{d}}$, $\mathbf{f}_{\mathrm{F}i}^{\mathrm{ex}}$, $\mathbf{f}_{\mathrm{F}i}^{\mathrm{k}}$, and $\mathbf{f}_{\mathrm{F}i}^{\mathrm{a}}$ are the generalized forces due to the link material damping, the actuation forces, the kinematic-constraint forces, and the algebraic-constraint forces, respectively. Vector $\mathbf{f}_{\mathrm{F}i}^{\mathrm{a}}$ is given by $\mathbf{f}_{\mathrm{F}i}^{\mathrm{a}} \triangleq \lambda_{\mathrm{F}i}\boldsymbol{\Sigma}_{\mathrm{F}i}\mathbf{q}_{\mathrm{F}i}$ in which $\lambda_{\mathrm{F}i}$ is a Lagrange multiplier. It can be shown (Cyril, 1988) that this generalized force lies in the null-space of the matrix $(\partial\dot{\mathbf{q}}_{\mathrm{F}i}/\partial\mathbf{t}_{\mathrm{F}i})^T$. Hence, the premultiplication of eqs. (4.13) by this matrix will eliminate the algebraic-constraint force on the right-hand side:

$$\Big(\frac{\partial\dot{\mathbf{q}}_{\mathrm{F}i}}{\partial\mathbf{t}_{\mathrm{F}i}}\Big)^T\Big[\frac{d}{dt}\Big(\frac{\partial L_{\mathrm{F}i}}{\partial\dot{\mathbf{q}}_{\mathrm{F}i}}\Big) - \frac{\partial L_{\mathrm{F}i}}{\partial\mathbf{q}_{\mathrm{F}i}}\Big] = \Big(\frac{\partial\dot{\mathbf{q}}_{\mathrm{F}i}}{\partial\mathbf{t}_{\mathrm{F}i}}\Big)^T(\mathbf{f}_{\mathrm{F}i}^{\mathrm{d}} + \mathbf{f}_{\mathrm{F}i}^{\mathrm{ex}} + \mathbf{f}_{\mathrm{F}i}^{\mathrm{k}}). \tag{4.14}$$

However, using eq. (4.12), one can readily show that

$$\frac{d}{dt}\Big(\frac{\partial L_{\mathrm{F}i}}{\partial\dot{\mathbf{q}}_{\mathrm{F}i}}\Big) = \frac{d}{dt}\Big(\frac{\partial\mathbf{t}_{\mathrm{F}i}}{\partial\dot{\mathbf{q}}_{\mathrm{F}i}}\Big)^T\mathbf{M}_{\mathrm{F}i}\mathbf{t}_{\mathrm{F}i} + \Big(\frac{\partial\mathbf{t}_{\mathrm{F}i}}{\partial\dot{\mathbf{q}}_{\mathrm{F}i}}\Big)^T\Big(\dot{\mathbf{M}}_{\mathrm{F}i}\mathbf{t}_{\mathrm{F}i} + \mathbf{M}_{\mathrm{F}i}\dot{\mathbf{t}}_{\mathrm{F}i}\Big), \tag{4.15}$$

and

$$\frac{\partial L_{\mathrm{F}i}}{\partial\mathbf{q}_{\mathrm{F}i}} = \Big(\frac{\partial\mathbf{t}_{\mathrm{F}i}}{\partial\mathbf{q}_{\mathrm{F}i}}\Big)^T\mathbf{M}_{\mathrm{F}i}\mathbf{t}_{\mathrm{F}i} + \frac{1}{2}\mathbf{t}_{\mathrm{F}i}^T\frac{\partial\mathbf{M}_{\mathrm{F}i}}{\partial\mathbf{q}_{\mathrm{F}i}}\mathbf{t}_{\mathrm{F}i} - \Big(\frac{\partial\boldsymbol{\zeta}_i}{\partial\mathbf{q}_{\mathrm{F}i}}\Big)^T\mathbf{K}_i\boldsymbol{\zeta}_i \tag{4.16}$$

in which $(\partial\mathbf{M}_{\mathrm{F}i}/\partial\mathbf{q}_{\mathrm{F}i})\mathbf{t}_{\mathrm{F}i}$ is interpreted as

$$\frac{\partial\mathbf{M}_{\mathrm{F}i}}{\partial\mathbf{q}_{\mathrm{F}i}}\mathbf{t}_{\mathrm{F}i} \equiv \frac{\partial(\mathbf{M}_{\mathrm{F}i}\mathbf{a})}{\partial\mathbf{q}_{\mathrm{F}i}}\bigg|_{\mathbf{a}=\mathbf{t}_{\mathrm{F}i}}. \tag{4.17}$$

If relations (4.15 & 4.16) are substituted into eq. (4.14), we can obtain the link dynamics equation as

$$\mathbf{M}_{\mathrm{F}i}\dot{\mathbf{t}}_{\mathrm{F}i} = \mathbf{w}_{\mathrm{F}i}^{\mathrm{s}} + \mathbf{w}_{\mathrm{F}i}^{\mathrm{ex}} + \mathbf{w}_{\mathrm{F}i}^{\mathrm{k}}, \tag{4.18a}$$

$$\mathbf{w}_{\mathrm{F}i}^{\mathrm{ex}} \triangleq \Big(\frac{\partial\dot{\mathbf{q}}_{\mathrm{F}i}}{\partial\mathbf{t}_{\mathrm{F}i}}\Big)^T\mathbf{f}_{\mathrm{F}i}^{\mathrm{ex}}, \tag{4.18b}$$

$$\mathbf{w}_{\mathrm{F}i}^{\mathrm{k}} \triangleq \Big(\frac{\partial\dot{\mathbf{q}}_{\mathrm{F}i}}{\partial\mathbf{t}_{\mathrm{F}i}}\Big)^T\mathbf{f}_{\mathrm{F}i}^{\mathrm{k}}, \tag{4.18c}$$

and

$$\mathbf{w}_{\mathrm{F}i}^{\mathrm{s}} \triangleq -\mathbf{B}_i\Big(\mathbf{C}_i\dot{\boldsymbol{\zeta}}_i - \mathbf{K}_i\boldsymbol{\zeta}_i\Big) - \dot{\mathbf{M}}_{\mathrm{F}i}\mathbf{t}_{\mathrm{F}i} - \overline{\boldsymbol{\Omega}}_{\mathrm{F}i}\mathbf{M}_{\mathrm{F}i}\mathbf{t}_{\mathrm{F}i} + \frac{1}{2}\mathbf{t}_{\mathrm{F}i}^T\frac{\partial\dot{\mathbf{M}}_{\mathrm{F}i}}{\partial\mathbf{t}_{\mathrm{F}i}}\mathbf{t}_{\mathrm{F}i}, \tag{4.18d}$$

with $\mathbf{B}_i$ and $\overline{\boldsymbol{\Omega}}_{\mathrm{F}i}$ defined by

$$\mathbf{B}_i \triangleq \begin{bmatrix}\mathbf{O}_{6\times n_{fi}}\\ \mathbf{1}_{n_{fi}\times n_{fi}}\end{bmatrix}, \quad \overline{\boldsymbol{\Omega}}_{\mathrm{F}i} \triangleq \mathrm{diag}\big(\mathbf{O}_{3\times 3}, \boldsymbol{\Omega}_{\mathrm{F}i}, \mathbf{O}_{n_{fi}\times n_{fi}}\big), \tag{4.19}$$

where $\boldsymbol{\Omega}_{\mathrm{F}i}$ is the cross-product matrix of the link angular velocity. $\mathbf{C}_i$ is the positive-definite, symmetric damping matrix due to the beam material damping; this matrix becomes a multiple of the stiffness matrix $\mathbf{K}_i$ if the Kelvin-Voigt viscoelastic model (Meirovitch, 1997) is used to model the material damping in the system. For the derivation of eqs. (4.18), the identities given below have been used:

$$\frac{\partial\mathbf{t}_{\mathrm{F}i}}{\partial\mathbf{q}_{\mathrm{F}i}} \equiv -\frac{d}{dt}\Big(\frac{\partial\mathbf{t}_{\mathrm{F}i}}{\partial\dot{\mathbf{q}}_{\mathrm{F}i}}\Big), \tag{4.20a}$$

$$\overline{\boldsymbol{\Omega}}_{\mathrm{F}i} \equiv 2\Big(\frac{\partial\dot{\mathbf{q}}_{\mathrm{F}i}}{\partial\mathbf{t}_{\mathrm{F}i}}\Big)^T\frac{d}{dt}\Big(\frac{\partial\mathbf{t}_{\mathrm{F}i}}{\partial\dot{\mathbf{q}}_{\mathrm{F}i}}\Big)^T, \tag{4.20b}$$

$$\mathbf{t}_{\mathrm{F}i}^T\frac{\partial\dot{\mathbf{M}}_{\mathrm{F}i}}{\partial\mathbf{t}_{\mathrm{F}i}}\mathbf{t}_{\mathrm{F}i} \equiv \Big(\frac{\partial\dot{\mathbf{q}}_{\mathrm{F}i}}{\partial\mathbf{t}_{\mathrm{F}i}}\Big)^T\mathbf{t}_{\mathrm{F}i}^T\frac{\partial\mathbf{M}_{\mathrm{F}i}}{\partial\mathbf{q}_{\mathrm{F}i}}\mathbf{t}_{\mathrm{F}i}. \tag{4.20c}$$

The above three identities are proven in Appendix B.

4.3.3 Assembling the Link Equations

To obtain the dynamics equation of the flexible manipulator, the link mass matrices, generalized velocities, and wrenches are assembled:

$$\mathbf{M}_{\mathrm{F}} \triangleq \mathrm{diag}\big(\mathbf{M}_{\mathrm{F}1}, \mathbf{M}_{\mathrm{F}2}, \ldots, \mathbf{M}_{\mathrm{F}n_{\mathrm{F}}}\big), \tag{4.21a}$$

$$\mathbf{v}_{\mathrm{F}} \triangleq \begin{bmatrix}\mathbf{t}_{\mathrm{F}1}^T & \mathbf{t}_{\mathrm{F}2}^T & \cdots & \mathbf{t}_{\mathrm{F}n_{\mathrm{F}}}^T\end{bmatrix}^T, \tag{4.21b}$$

$$\mathbf{w}_{\mathrm{F}}^{\mathrm{ex}} \triangleq \begin{bmatrix}(\mathbf{w}_{\mathrm{F}1}^{\mathrm{ex}})^T & (\mathbf{w}_{\mathrm{F}2}^{\mathrm{ex}})^T & \cdots & (\mathbf{w}_{\mathrm{F}n_{\mathrm{F}}}^{\mathrm{ex}})^T\end{bmatrix}^T, \tag{4.21c}$$

$$\mathbf{w}_{\mathrm{F}}^{\mathrm{k}} \triangleq \begin{bmatrix}(\mathbf{w}_{\mathrm{F}1}^{\mathrm{k}})^T & (\mathbf{w}_{\mathrm{F}2}^{\mathrm{k}})^T & \cdots & (\mathbf{w}_{\mathrm{F}n_{\mathrm{F}}}^{\mathrm{k}})^T\end{bmatrix}^T, \tag{4.21d}$$

$$\mathbf{w}_{\mathrm{F}}^{\mathrm{s}} \triangleq \begin{bmatrix}(\mathbf{w}_{\mathrm{F}1}^{\mathrm{s}})^T & (\mathbf{w}_{\mathrm{F}2}^{\mathrm{s}})^T & \cdots & (\mathbf{w}_{\mathrm{F}n_{\mathrm{F}}}^{\mathrm{s}})^T\end{bmatrix}^T. \tag{4.21e}$$

We can thus write the dynamics of the flexible manipulator as

$$\mathbf{M}_{\mathrm{F}}\dot{\mathbf{v}}_{\mathrm{F}} = \mathbf{w}_{\mathrm{F}}^{\mathrm{ex}} + \mathbf{w}_{\mathrm{F}}^{\mathrm{s}} + \mathbf{w}_{\mathrm{F}}^{\mathrm{k}} \tag{4.22}$$

Because of the kinematic relations among the generalized velocities of the different links, however, the number of equations is greater than the degree of freedom of the flexible manipulator. Thus, to eliminate the extra equations, it is noticed that the total virtual work performed by the kinematic-constraint forces must be zero, i.e.,

$$\delta W_{\mathrm{F}}^{\mathrm{k}} = \sum_{i=1}^{n_{\mathrm{F}}} \left(\mathbf{f}_{\mathrm{F}i}^{\mathrm{k}}\right)^T \delta \mathbf{q}_{\mathrm{F}i} = 0 \tag{4.23}$$

However, the vector $\mathbf{q}_{\mathrm{F}i}$ of the link generalized coordinates is a vector function of the generalized coordinates $\boldsymbol{\psi}_{\mathrm{F}}$ of the flexible manipulator, i.e., $\mathbf{q}_{\mathrm{F}i} \equiv \mathbf{q}_{\mathrm{F}i}(\boldsymbol{\psi}_{\mathrm{F}})$. Furthermore, let us arrange $\boldsymbol{\psi}_{\mathrm{F}}$ as

$$\boldsymbol{\psi}_{\mathrm{F}} \triangleq \begin{bmatrix} \boldsymbol{\theta}_{\mathrm{F}}^T & \boldsymbol{\zeta}^T \end{bmatrix}^T, \tag{4.24}$$

$$\boldsymbol{\zeta} \triangleq \begin{bmatrix} \boldsymbol{\zeta}_1^T & \boldsymbol{\zeta}_2^T & \cdots & \boldsymbol{\zeta}_{n_{\mathrm{F}}}^T \end{bmatrix}^T, \tag{4.25}$$

where $\boldsymbol{\theta}_{\mathrm{F}}$ is an array comprising all flexible-manipulator joint variables. These functional relations can be used to relate the virtual changes of the link generalized coordinates to those of the generalized coordinates of the flexible manipulator:

$$\delta \mathbf{q}_{\mathrm{F}i} = \frac{\partial \mathbf{q}_{\mathrm{F}i}}{\partial \boldsymbol{\psi}_{\mathrm{F}}} \delta \boldsymbol{\psi}_{\mathrm{F}} = \frac{\partial \dot{\mathbf{q}}_{\mathrm{F}i}}{\partial \dot{\boldsymbol{\psi}}_{\mathrm{F}}} \delta \boldsymbol{\psi}_{\mathrm{F}} = \frac{\partial \dot{\mathbf{q}}_{\mathrm{F}i}}{\partial \mathbf{t}_{\mathrm{F}i}} \frac{\partial \mathbf{t}_{\mathrm{F}i}}{\partial \dot{\boldsymbol{\psi}}_{\mathrm{F}}} \delta \boldsymbol{\psi}_{\mathrm{F}} \tag{4.26}$$

Hence, upon substitution of $\delta \mathbf{q}_{\mathrm{F}i}$ into eq. (4.23), the expression for the total virtual work becomes

$$\begin{aligned} \delta W_{\mathrm{F}}^{\mathrm{k}} &= \sum_{i=1}^{n_{\mathrm{F}}} \left[\left(\frac{\partial \mathbf{t}_{\mathrm{F}i}}{\partial \dot{\boldsymbol{\psi}}_{\mathrm{F}}} \right)^T \left(\frac{\partial \dot{\mathbf{q}}_{\mathrm{F}i}}{\partial \mathbf{t}_{\mathrm{F}i}} \right)^T \mathbf{f}_{\mathrm{F}i}^{\mathrm{k}} \right]^T \delta \boldsymbol{\psi}_{\mathrm{F}} = \sum_{i=1}^{n_{\mathrm{F}}} \left[\left(\frac{\partial \mathbf{t}_{\mathrm{F}i}}{\partial \dot{\boldsymbol{\psi}}_{\mathrm{F}}} \right)^T \mathbf{w}_{\mathrm{F}i}^{\mathrm{k}} \right]^T \delta \boldsymbol{\psi}_{\mathrm{F}} \\ &= \left[\left(\frac{\partial \mathbf{v}_{\mathrm{F}}}{\partial \dot{\boldsymbol{\psi}}_{\mathrm{F}}} \right)^T \mathbf{w}_{\mathrm{F}i}^{\mathrm{k}} \right]^T \delta \boldsymbol{\psi}_{\mathrm{F}} = 0 \end{aligned}$$

which shows that, since the entries of $\delta \boldsymbol{\psi}_{\mathrm{F}}$ are independent, the vector $\mathbf{w}_{\mathrm{F}}^{\mathrm{k}}$ of the kinematic-constraint wrench lies in the null-space of the transpose of

$$\mathbf{N}_{\mathrm{F}} \triangleq \frac{\partial \mathbf{v}_{\mathrm{F}}}{\partial \dot{\boldsymbol{\psi}}_{\mathrm{F}}}. \tag{4.27}$$

For this reason, matrix $\mathbf{N}_{\mathrm{F}}$ is called the *Natural Orthogonal Complement* of the system. This property can be used to eliminate $\mathbf{w}_{\mathrm{F}}^{\mathrm{k}}$ from the right-hand side of the dynamics equation (4.22):

$$\mathbf{N}_{\mathrm{F}}^T \mathbf{M}_{\mathrm{F}} \dot{\mathbf{v}}_{\mathrm{F}} = \mathbf{N}_{\mathrm{F}}^T \left(\mathbf{w}_{\mathrm{F}}^{\mathrm{ex}} + \mathbf{w}_{\mathrm{F}}^{\mathrm{s}} \right). \tag{4.28}$$

However, we know that the relation between $\mathbf{v}_\mathrm{F}$ and $\dot{\boldsymbol{\psi}}_\mathrm{F}$ is linear and can thus be written in the form

$$\mathbf{v}_\mathrm{F} = \mathbf{N}_\mathrm{F}\dot{\boldsymbol{\psi}}_\mathrm{F}, \tag{4.29}$$

which, upon differentiation with respect to time, yields

$$\dot{\mathbf{v}}_\mathrm{F} = \dot{\mathbf{N}}_\mathrm{F}\dot{\boldsymbol{\psi}}_\mathrm{F} + \mathbf{N}_\mathrm{F}\ddot{\boldsymbol{\psi}}_\mathrm{F}. \tag{4.30}$$

Substituting for $\dot{\mathbf{v}}_\mathrm{F}$ into eq. (4.28) from eq. (4.30), we obtain the flexible-manipulator dynamics equations as

$$\mathbf{I}_\mathrm{F}\ddot{\boldsymbol{\psi}}_\mathrm{F} = \hat{\mathbf{w}}_\mathrm{F}^\mathrm{ex} + \hat{\mathbf{w}}_\mathrm{F}^\mathrm{s}, \tag{4.31a}$$

$$\mathbf{I}_\mathrm{F} \triangleq \mathbf{N}_\mathrm{F}^T\mathbf{M}_\mathrm{F}\mathbf{N}_\mathrm{F}, \tag{4.31b}$$

$$\hat{\mathbf{w}}_\mathrm{F}^\mathrm{ex} \triangleq \mathbf{N}_\mathrm{F}^T\mathbf{w}_\mathrm{F}^\mathrm{ex}, \tag{4.31c}$$

$$\hat{\mathbf{w}}_\mathrm{F}^\mathrm{s} \triangleq \mathbf{N}_\mathrm{F}^T(\mathbf{w}_\mathrm{F}^\mathrm{s} - \mathbf{M}_\mathrm{F}\dot{\mathbf{N}}_\mathrm{F}\dot{\boldsymbol{\psi}}_\mathrm{F}). \tag{4.31d}$$

The vector $\hat{\mathbf{w}}_\mathrm{F}^\mathrm{s}$ is called the *system wrench* (Cyril, 1988) of the flexible manipulator.

Now, the elements of $\hat{\mathbf{w}}_\mathrm{F}^\mathrm{ex}$ are calculated using the definition of generalized forces as the coefficients of virtual displacements in the expression of the virtual work done by external forces when the virtual displacements are independent. To this end, the virtual work done by external forces is first calculated as

$$\delta W_\mathrm{F}^\mathrm{ex} = \sum_{i=1}^{n_\mathrm{F}} (\mathbf{f}_{\mathrm{F}i}^\mathrm{ex})^T \delta\mathbf{q}_{\mathrm{F}i} = \sum_{i=1}^{n_\mathrm{F}} \tau_{\mathrm{F}i}\delta\theta_{\mathrm{F}i} - (\mathbf{f}_\mathrm{R0}^\mathrm{ex})^T\,\delta\mathbf{q}_\mathrm{R0} \tag{4.32}$$

where $\mathbf{f}_\mathrm{R0}^\mathrm{ex}$ and $\mathbf{q}_\mathrm{R0}$ are the generalized force applied on the base of the rigid manipulator by the tip of the flexible-manipulator end-effector and the generalized coordinates of the base of the rigid manipulator, respectively. The latter is, as in the case of any other rigid link, an array composed of the position vector of a landmark point and the attitude of the base.

Substituting $\delta\mathbf{q}_{\mathrm{F}i}$ and $\delta\mathbf{q}_\mathrm{R0}$ in terms of $\delta\boldsymbol{\psi}_\mathrm{F}$ into eq. (4.32) gives

$$\sum_{i=1}^{n_\mathrm{F}} (\mathbf{f}_{\mathrm{F}i}^\mathrm{ex})^T \frac{\partial\mathbf{q}_{\mathrm{F}i}}{\partial\boldsymbol{\psi}_\mathrm{F}}\delta\boldsymbol{\psi}_\mathrm{F} = \sum_{i=1}^{n_\mathrm{F}} \tau_{\mathrm{F}i}\delta\theta_{\mathrm{F}i} - (\mathbf{f}_\mathrm{R0}^\mathrm{ex})^T\frac{\partial\mathbf{q}_\mathrm{R0}}{\partial\boldsymbol{\psi}_\mathrm{F}}\delta\boldsymbol{\psi}_\mathrm{F},$$

or

$$\sum_{i=1}^{n_F}\Big[\Big(\frac{\partial \mathbf{q}_{Fi}}{\partial \boldsymbol{\psi}_F}\Big)^T \mathbf{f}_{Fi}^{ex}\Big]^T \delta\boldsymbol{\psi}_F = \sum_{i=1}^{n_F} \tau_{Fi}\delta\theta_{Fi} - \Big[\Big(\frac{\partial \mathbf{q}_{R0}}{\partial \boldsymbol{\psi}_F}\Big)^T \mathbf{f}_{R0}^{ex}\Big]^T \delta\boldsymbol{\psi}_F. \tag{4.33}$$

However, since $\dot{\mathbf{q}}_{Fi} \equiv \dot{\mathbf{q}}_{Fi}(\mathbf{t}_{Fi}, \mathbf{q}_{Fi})$ and $\dot{\mathbf{q}}_{R0} \equiv \dot{\mathbf{q}}_{R0}(\mathbf{t}_{R0}, \mathbf{q}_{R0})$, we have

$$\frac{\partial \mathbf{q}_{Fi}}{\partial \boldsymbol{\psi}_F} = \frac{\partial \dot{\mathbf{q}}_{Fi}}{\partial \dot{\boldsymbol{\psi}}_F} = \frac{\partial \dot{\mathbf{q}}_{Fi}}{\partial \mathbf{t}_{Fi}}\frac{\partial \mathbf{t}_{Fi}}{\partial \dot{\boldsymbol{\psi}}_F} + \frac{\partial \dot{\mathbf{q}}_{Fi}}{\partial \boldsymbol{\eta}_{Fi}}\frac{\partial \boldsymbol{\eta}_{Fi}}{\partial \dot{\boldsymbol{\psi}}_F} = \frac{\partial \dot{\mathbf{q}}_{Fi}}{\partial \mathbf{t}_{Fi}}\frac{\partial \mathbf{t}_{Fi}}{\partial \dot{\boldsymbol{\psi}}_F}, \tag{4.34}$$

$$\frac{\partial \mathbf{q}_{R0}}{\partial \boldsymbol{\psi}_F} = \frac{\partial \dot{\mathbf{q}}_{R0}}{\partial \dot{\boldsymbol{\psi}}_F} = \frac{\partial \dot{\mathbf{q}}_{R0}}{\partial \mathbf{t}_{R0}}\frac{\partial \mathbf{t}_{R0}}{\partial \dot{\boldsymbol{\psi}}_F} + \frac{\partial \dot{\mathbf{q}}_{R0}}{\partial \boldsymbol{\eta}_{R0}}\frac{\partial \boldsymbol{\eta}_{R0}}{\partial \dot{\boldsymbol{\psi}}_F} = \frac{\partial \dot{\mathbf{q}}_{R0}}{\partial \mathbf{t}_{R0}}\frac{\partial \mathbf{t}_{R0}}{\partial \dot{\boldsymbol{\psi}}_F}. \tag{4.35}$$

Notice that the reason for the cancellation of the second terms of the chain rule in the above relations is that none of the $\boldsymbol{\eta}_{Fi}$ or $\boldsymbol{\eta}_{R0}$ is a function of $\dot{\boldsymbol{\psi}}_F$.

Hence, eq. (4.33) can be rewritten as

$$\sum_{i=1}^{n_F}\Big[\Big(\frac{\partial \mathbf{t}_{Fi}}{\partial \dot{\boldsymbol{\psi}}_F}\Big)^T\Big(\frac{\partial \dot{\mathbf{q}}_{Fi}}{\partial \mathbf{t}_{Fi}}\Big)^T \mathbf{f}_{Fi}^{ex}\Big]^T \delta\boldsymbol{\psi}_F = \boldsymbol{\tau}_F^T\delta\boldsymbol{\theta}_F - \Big[\Big(\frac{\partial \mathbf{t}_{R0}}{\partial \dot{\boldsymbol{\psi}}_F}\Big)^T\Big(\frac{\partial \dot{\mathbf{q}}_{R0}}{\partial \mathbf{t}_{R0}}\Big)^T \mathbf{f}_{R0}^{ex}\Big]^T \delta\boldsymbol{\psi}_F$$

where $\boldsymbol{\tau}_F$ is an array comprising the flexible-manipulator joint torques. The above relation can readily be rewritten as

$$\Big[\Big(\frac{\partial \mathbf{v}_F}{\partial \dot{\boldsymbol{\psi}}_F}\Big)^T \mathbf{w}_F^{ex}\Big]^T \delta\boldsymbol{\psi}_F = \boldsymbol{\tau}_F^T\delta\boldsymbol{\theta}_F - \Big[\Big(\frac{\partial \mathbf{t}_{R0}}{\partial \dot{\boldsymbol{\psi}}_F}\Big)^T \mathbf{w}_{R0}^{ex}\Big]^T \delta\boldsymbol{\psi}_F. \tag{4.36}$$

Hence, since the elements of $\delta\boldsymbol{\psi}_F$ are independent, looking at eq. (4.36), one can realize that

$$\mathbf{N}_F^T\mathbf{w}_F^{ex} \equiv \hat{\mathbf{w}}_F^{ex} = \boldsymbol{\tau}_F^{ac} - \Big(\frac{\partial \mathbf{t}_{R0}}{\partial \dot{\boldsymbol{\psi}}_F}\Big)^T \mathbf{w}_{R0}^{ex} \tag{4.37}$$

where

$$\boldsymbol{\tau}_F^{ac} \triangleq \begin{bmatrix}\boldsymbol{\tau}_F^T & \mathbf{0}_{n_f}^T\end{bmatrix}^T \tag{4.38}$$

in which $\mathbf{0}_{n_f}$ is the zero vector of dimension equal to the total number of flexural coordinates of the flexible manipulator.

4.4 Dynamics of the Rigid Submanipulator

4.4.1 The Link Governing Equations

The Lagrangian of the ith link can be calculated from

$$L_{\mathrm{R}i} = \frac{1}{2}\mathbf{t}_{\mathrm{R}i}^T \mathbf{M}_{\mathrm{R}i}\mathbf{t}_{\mathrm{R}i}, \quad \text{for} \quad i = 0, 1, \ldots, n_{\mathrm{R}} \tag{4.39}$$

where n_{R} is the number of rigid links of the manipulator, and $i = 0$ corresponds to the rigid-manipulator base. Hence, the link Lagrange equation becomes

$$\frac{d}{dt}\left(\frac{\partial L_{\mathrm{R}i}}{\partial \dot{\mathbf{q}}_{\mathrm{R}i}}\right) - \frac{\partial L_{\mathrm{R}i}}{\partial \mathbf{q}_{\mathrm{R}i}} = \mathbf{f}_{\mathrm{R}i}^{\mathrm{ex}} + \mathbf{f}_{\mathrm{R}i}^{\mathrm{k}} + \mathbf{f}_{\mathrm{R}i}^{\mathrm{a}}, \tag{4.40}$$

which, after eliminating the algebraic-constraint generalized force, takes on the form

$$\mathbf{M}_{\mathrm{R}i}\dot{\mathbf{t}}_{\mathrm{R}i} = \mathbf{w}_{\mathrm{R}i}^{\mathrm{ex}} + \mathbf{w}_{\mathrm{R}i}^{\mathrm{s}} + \mathbf{w}_{\mathrm{R}i}^{\mathrm{k}} \tag{4.41a}$$

$$\mathbf{w}_{\mathrm{R}i}^{\mathrm{ex}} \triangleq \left(\frac{\partial \dot{\mathbf{q}}_{\mathrm{R}i}}{\partial \mathbf{t}_{\mathrm{R}i}}\right)^T \mathbf{f}_{\mathrm{R}i}^{\mathrm{ex}} \tag{4.41b}$$

$$\mathbf{w}_{\mathrm{R}i}^{\mathrm{k}} \triangleq \left(\frac{\partial \dot{\mathbf{q}}_{\mathrm{R}i}}{\partial \mathbf{t}_{\mathrm{R}i}}\right)^T \mathbf{f}_{\mathrm{R}i}^{\mathrm{k}} \tag{4.41c}$$

$$\mathbf{w}_{\mathrm{R}i}^{\mathrm{s}} \triangleq -\dot{\mathbf{M}}_{\mathrm{R}i}\mathbf{t}_{\mathrm{R}i} - \overline{\mathbf{\Omega}}_{\mathrm{R}i}\mathbf{M}_{\mathrm{R}i}\mathbf{t}_{\mathrm{R}i} + \frac{1}{2}\mathbf{t}_{\mathrm{R}i}^T \frac{\partial \dot{\mathbf{M}}_{\mathrm{R}i}}{\partial \mathbf{t}_{\mathrm{R}i}}\mathbf{t}_{\mathrm{R}i} \tag{4.41d}$$

with $\overline{\mathbf{\Omega}}_{\mathrm{R}i}$ defined in a manner similar to the definition of $\overline{\mathbf{\Omega}}_{\mathrm{F}i}$ in eq. (4.19).

4.4.2 Assembling the Link Equations

Now again, let us assemble all the dynamics equations of the links of the rigid manipulator:

$$\mathbf{M}_{\mathrm{R}}\dot{\mathbf{v}}_{\mathrm{R}} = \mathbf{w}_{\mathrm{R}}^{\mathrm{ex}} + \mathbf{w}_{\mathrm{R}}^{\mathrm{s}} + \mathbf{w}_{\mathrm{R}}^{\mathrm{k}}, \tag{4.42a}$$

$$\mathbf{M}_{\mathrm{R}} \triangleq \mathrm{diag}\left(\mathbf{M}_{\mathrm{R}0}, \mathbf{M}_{\mathrm{R}1}, \ldots, \mathbf{M}_{\mathrm{R}n_{\mathrm{R}}}\right), \tag{4.42b}$$

$$\mathbf{v}_{\mathrm{R}} \triangleq \begin{bmatrix}\mathbf{t}_{\mathrm{R}0}^T & \mathbf{t}_{\mathrm{R}1}^T & \cdots & \mathbf{t}_{\mathrm{R}n_{\mathrm{R}}}^T\end{bmatrix}^T, \tag{4.42c}$$

$$\mathbf{w}_{\mathrm{R}}^{\mathrm{ex}} \triangleq \begin{bmatrix}(\mathbf{w}_{\mathrm{R}0}^{\mathrm{ex}})^T & (\mathbf{w}_{\mathrm{R}1}^{\mathrm{ex}})^T & \cdots & (\mathbf{w}_{\mathrm{R}n_{\mathrm{R}}}^{\mathrm{ex}})^T\end{bmatrix}^T, \tag{4.42d}$$

$$\mathbf{w}_{\mathrm{R}}^{\mathrm{k}} \triangleq \begin{bmatrix}(\mathbf{w}_{\mathrm{R}0}^{\mathrm{k}})^T & (\mathbf{w}_{\mathrm{R}1}^{\mathrm{k}})^T & \cdots & (\mathbf{w}_{\mathrm{R}n_{\mathrm{R}}}^{\mathrm{k}})^T\end{bmatrix}^T, \tag{4.42e}$$

$$\mathbf{w}_{\mathrm{R}}^{\mathrm{s}} \triangleq \begin{bmatrix}(\mathbf{w}_{\mathrm{R}0}^{\mathrm{s}})^T & (\mathbf{w}_{\mathrm{R}1}^{\mathrm{s}})^T & \cdots & (\mathbf{w}_{\mathrm{R}n_{\mathrm{R}}}^{\mathrm{s}})^T\end{bmatrix}^T. \tag{4.42f}$$

As in the case of the flexible manipulator, these equations are not independent. and therefore, in order to obtain the dynamics equations of the rigid manipulator, we obtain the total virtual work performed by the kinematic-constraint forces of the rigid manipulator:

$$\delta W_{\mathrm{R}}^{\mathrm{k}} = \sum_{i=1}^{n_{\mathrm{R}}} \left(\mathbf{f}_{\mathrm{R}i}^{\mathrm{k}}\right)^T \delta \mathbf{q}_{\mathrm{R}i} = 0. \tag{4.43}$$

Here, as well, we write the functional relation between the generalized coordinates of the rigid-manipulator links with those of the rigid manipulator, denoted by $\boldsymbol{\phi}_{\mathrm{R}}$, as $\mathbf{q}_{\mathrm{R}i} \equiv \mathbf{q}_{\mathrm{R}i}(\boldsymbol{\phi}_{\mathrm{R}})$, with $\boldsymbol{\phi}_{\mathrm{R}}$ defined as

$$\boldsymbol{\phi}_{\mathrm{R}} \triangleq \begin{bmatrix} \mathbf{p}_{\mathrm{R}0}^T & \boldsymbol{\eta}_{\mathrm{R}0}^T & \boldsymbol{\theta}_{\mathrm{R}}^T \end{bmatrix}^T \tag{4.44}$$

in which $\boldsymbol{\theta}_{\mathrm{R}}$ is an array including all the joint variables of the rigid manipulator. Using the above-mentioned functional relations, eq. (4.43) can be rewritten in the form

$$\delta W_{\mathrm{R}}^{\mathrm{k}} = \sum_{i=0}^{n_{\mathrm{R}}} \left(\mathbf{f}_{\mathrm{R}i}^{\mathrm{k}}\right)^T \frac{\partial \mathbf{q}_{\mathrm{R}i}}{\partial \boldsymbol{\phi}_{\mathrm{R}}} \delta \boldsymbol{\phi}_{\mathrm{R}} = 0. \tag{4.45}$$

However, since the elements of $\boldsymbol{\phi}_{\mathrm{R}}$ are not independent, due to the presence of the Euler parameters of the rigid-manipulator base among the generalized coordinates of the rigid manipulator, one cannot conclude that the summation $\sum_{i=0}^{n_{\mathrm{R}}} (\mathbf{f}_{\mathrm{R}i}^{\mathrm{k}})^T (\partial \mathbf{q}_{\mathrm{R}i}/\partial \boldsymbol{\phi}_{\mathrm{R}})$ vanishes.

To remedy this situation, we express the dependence of the elements of $\boldsymbol{\phi}_{\mathrm{R}}$ in the form of

$$\boldsymbol{\phi}_{\mathrm{R}}^T \boldsymbol{\Sigma}_{\mathrm{R}} \boldsymbol{\phi}_{\mathrm{R}} = 1, \quad \boldsymbol{\Sigma}_{\mathrm{R}} \triangleq \mathrm{diag}(\mathbf{O}_{3\times 3}, \mathbf{1}_4, \mathbf{O}_{n_{\mathrm{R}}\times n_{\mathrm{R}}}). \tag{4.46}$$

Then, taking the virtual variation of the constraint equation, we obtain

$$\boldsymbol{\phi}_{\mathrm{R}}^T \boldsymbol{\Sigma}_{\mathrm{R}} \delta \boldsymbol{\phi}_{\mathrm{R}} = 0. \tag{4.47}$$

This relation shows that the virtual change of $\boldsymbol{\phi}_{\mathrm{R}}$ is such that it lies on a hyperplane normal to the vector $\boldsymbol{\Sigma}_{\mathrm{R}} \boldsymbol{\phi}_{\mathrm{R}}$. Thus, from eqs. (4.45 & 4.47), one can conclude that the only nontrivial value for $\sum_{i=0}^{n_{\mathrm{R}}} (\mathbf{f}_{\mathrm{R}i}^{\mathrm{k}})^T (\partial \mathbf{q}_{\mathrm{R}i}/\partial \boldsymbol{\phi}_{\mathrm{R}})$ is given by

$$\sum_{i=0}^{n_{\mathrm{R}}} \left(\frac{\partial \mathbf{q}_{\mathrm{R}i}}{\partial \boldsymbol{\phi}_{\mathrm{R}}}\right)^T \mathbf{f}_{\mathrm{R}i}^{\mathrm{k}} = \lambda_{\mathrm{R}} \boldsymbol{\Sigma}_{\mathrm{R}} \boldsymbol{\phi}_{\mathrm{R}} \tag{4.48}$$

where λ_{R} is a Lagrange multiplier.

On the other hand, differentiating eq. (4.46) with respect to time results in

$$\dot{\boldsymbol{\phi}}_{\mathrm{R}}^{T}\boldsymbol{\Sigma}_{\mathrm{R}}\boldsymbol{\phi}_{\mathrm{R}} = 0. \tag{4.49}$$

However, $\dot{\boldsymbol{\phi}}_{\mathrm{R}}$ can readily be written in terms of $\mathbf{u}_{\mathrm{R}}$, which is given by

$$\mathbf{u}_{\mathrm{R}} \triangleq \begin{bmatrix} \dot{\mathbf{p}}_{\mathrm{R0}}^{T} & \boldsymbol{\omega}_{\mathrm{R0}}^{T} & \dot{\boldsymbol{\theta}}_{\mathrm{R}}^{T} \end{bmatrix}^{T}. \tag{4.50}$$

Therefore, eq. (4.49) can be rewritten as

$$\mathbf{u}_{\mathrm{R}}^{T}\left(\frac{\partial\dot{\boldsymbol{\phi}}_{\mathrm{R}}}{\partial\mathbf{u}_{\mathrm{R}}}\right)^{T}\boldsymbol{\Sigma}_{\mathrm{R}}\boldsymbol{\phi}_{\mathrm{R}} = 0, \tag{4.51}$$

which, due to the independence of the entries of $\mathbf{u}_{\mathrm{R}}$, yields

$$\left(\frac{\partial\dot{\boldsymbol{\phi}}_{\mathrm{R}}}{\partial\mathbf{u}_{\mathrm{R}}}\right)^{T}\boldsymbol{\Sigma}_{\mathrm{R}}\boldsymbol{\phi}_{\mathrm{R}} = \mathbf{0}. \tag{4.52}$$

Thus, premultiplying eq. (4.48) by $\left(\partial\dot{\boldsymbol{\phi}}_{\mathrm{R}}/\partial\mathbf{u}_{\mathrm{R}}\right)^{T}$ will make the right-hand side of that equation vanish, namely,

$$\sum_{i=0}^{n_{\mathrm{R}}}\left(\frac{\partial\dot{\boldsymbol{\phi}}_{\mathrm{R}}}{\partial\mathbf{u}_{\mathrm{R}}}\right)^{T}\left(\frac{\partial\dot{\mathbf{q}}_{\mathrm{R}i}}{\partial\dot{\boldsymbol{\phi}}_{\mathrm{R}}}\right)^{T}\mathbf{f}_{\mathrm{R}i}^{\mathrm{k}} = \mathbf{0},$$

which, using the chain rule and recalling the definition of the kinematic-constraint wrench, becomes

$$\sum_{i=0}^{n_{\mathrm{R}}}\left(\frac{\partial\dot{\boldsymbol{\phi}}_{\mathrm{R}}}{\partial\mathbf{u}_{\mathrm{R}}}\right)^{T}\left(\frac{\partial\mathbf{t}_{\mathrm{R}i}}{\partial\dot{\boldsymbol{\phi}}_{\mathrm{R}}}\right)^{T}\left(\frac{\partial\dot{\mathbf{q}}_{\mathrm{R}i}}{\partial\mathbf{t}_{\mathrm{R}i}}\right)^{T}\mathbf{f}_{\mathrm{R}i}^{\mathrm{k}} = \sum_{i=0}^{n_{\mathrm{R}}}\left(\frac{\partial\mathbf{t}_{\mathrm{R}i}}{\partial\mathbf{u}_{\mathrm{R}}}\right)^{T}\mathbf{w}_{\mathrm{R}i}^{\mathrm{k}} = \mathbf{0}.$$

Therefore,

$$\left(\frac{\partial\mathbf{v}_{\mathrm{R}}}{\partial\mathbf{u}_{\mathrm{R}}}\right)^{T}\mathbf{w}_{\mathrm{R}}^{\mathrm{k}} = \mathbf{0}.$$

In other words, the premultiplication of eq. (4.42a) by the transpose of the rigid-manipulator Natural Orthogonal Complement, defined as

$$\mathbf{N}_{\mathrm{R}} \triangleq \frac{\partial\mathbf{v}_{\mathrm{R}}}{\partial\mathbf{u}_{\mathrm{R}}}, \tag{4.53}$$

cancels the kinematic-constraint wrench, thus deriving the dynamics equations of the rigid manipulator in the form

$$\mathbf{I}_{\mathrm{R}}\dot{\mathbf{u}}_{\mathrm{R}} = \hat{\mathbf{w}}_{\mathrm{R}}^{\mathrm{ex}} + \hat{\mathbf{w}}_{\mathrm{R}}^{\mathrm{s}}, \tag{4.54a}$$

$$\mathbf{I}_{\mathrm{R}} \triangleq \mathbf{N}_{\mathrm{R}}^{T}\mathbf{M}_{\mathrm{R}}\mathbf{N}_{\mathrm{R}}, \tag{4.54b}$$

$$\hat{\mathbf{w}}_{\mathrm{R}}^{\mathrm{ex}} \triangleq \mathbf{N}_{\mathrm{R}}^{T}\mathbf{w}_{\mathrm{R}}^{\mathrm{ex}}, \tag{4.54c}$$

$$\hat{\mathbf{w}}_{\mathrm{R}}^{\mathrm{s}} \triangleq \mathbf{N}_{\mathrm{R}}^{T}\big(\mathbf{w}_{\mathrm{R}}^{\mathrm{s}} - \mathbf{M}_{\mathrm{R}}\dot{\mathbf{N}}_{\mathrm{R}}\mathbf{u}_{\mathrm{R}}\big), \tag{4.54d}$$

where $\hat{\mathbf{w}}_{\mathrm{R}}^{\mathrm{s}}$ is termed the *system wrench* of the rigid manipulator.

Using an approach similar to the one taken for the derivation of eq. (4.37), one can show that $\hat{\mathbf{w}}_{\mathrm{R}}^{\mathrm{ex}}$ is given by

$$\hat{\mathbf{w}}_{\mathrm{R}}^{\mathrm{ex}} = \boldsymbol{\tau}_{\mathrm{R}}^{\mathrm{ac}} + \Big(\frac{\partial \mathbf{t}_{\mathrm{R0}}}{\partial \mathbf{u}_{\mathrm{R}}}\Big)^{T}\mathbf{w}_{\mathrm{R0}}^{\mathrm{ex}} + \Big(\frac{\partial \mathbf{t}_{\mathrm{ee}}}{\partial \mathbf{u}_{\mathrm{R}}}\Big)^{T}\mathbf{w}_{\mathrm{ee}}^{\mathrm{ex}}, \tag{4.55}$$

$$\boldsymbol{\tau}_{\mathrm{R}}^{\mathrm{ac}} \triangleq \big[\mathbf{0}_{6}^{T} \quad \boldsymbol{\tau}_{\mathrm{R}}^{T}\big]^{T}, \tag{4.56}$$

where $\mathbf{t}_{\mathrm{ee}}$ and $\mathbf{w}_{\mathrm{ee}}^{\mathrm{ex}}$ are the end-effector vectors of the generalized velocities and load wrench applied on the end-effector, respectively.

Notice that $\mathbf{w}_{\mathrm{ee}}^{\mathrm{ex}}$ is not a Cartesian wrench, i.e., its elements are not the mere components of actual force and torque. The calculation of this wrench is the subject of the next subsection.

4.4.3 The End-effector External Wrench

Assume that the Cartesian wrench given by

$$\mathbf{w}_{\mathrm{ee}}^{\mathrm{C}} \triangleq \big[\mathbf{f}_{\mathrm{ee}}^{T} \quad \boldsymbol{\tau}_{\mathrm{ee}}^{T}\big]^{T} \tag{4.57}$$

is applied on the end-effector at a point P_{ee} by sources external to the the flexible and rigid subsystems. Further, assume that the generalized coordinates of a local frame $\mathcal{F}_{\mathrm{ee}}$ with origin at P_{ee} are the elements of $\mathbf{q}_{\mathrm{ee}} \triangleq \big[\mathbf{p}_{\mathrm{ee}} \quad \boldsymbol{\eta}_{\mathrm{ee}}\big]^{T}$. Now, if $\mathbf{f}_{\mathrm{ee}}^{\mathrm{ex}}$ is defined as the generalized force corresponding to the Cartesian wrench given by eq. (4.57), then consistent with the definition of the link external wrench, eq. (4.41b), we have

$$\mathbf{w}_{\mathrm{ee}}^{\mathrm{ex}} \triangleq \Big(\frac{\partial \dot{\mathbf{q}}_{\mathrm{ee}}}{\partial \mathbf{t}_{\mathrm{ee}}}\Big)^{T}\mathbf{f}_{\mathrm{ee}}^{\mathrm{ex}}. \tag{4.58}$$

The virtual work performed by the external forces on the end-effector can be calculated from

$$\delta W_{ee}^{ex} = {}^{\mathcal{R}}\mathbf{f}_{ee}^{T}\,\delta^{\mathcal{R}}\mathbf{p}_{ee} + {}^{\mathcal{R}}\boldsymbol{\tau}_{ee}^{T}\,{}^{\mathcal{R}}\delta\boldsymbol{\theta}_{ee} = (\mathbf{f}_{ee}^{ex})^{T}\delta\mathbf{q}_{ee}, \tag{4.59}$$

where, as per our convention, the left superscript $\mathcal{R}$ indicates an expression in the inertial frame. Notice the special case of $\delta\boldsymbol{\theta}_{ee}$, which represents the virtual rotation of the end-effector in the three-dimensional space. In this case, the left superscript is put *before* δ so as to emphasize that it is the virtual rotation which, due to its infinitesimal norm, has vector properties[3].

The inertial-frame representation of $\mathbf{p}_{ee}$ can be expressed as a function of the pose of $\mathcal{F}_{ee}$ as ${}^{\mathcal{R}}\mathbf{p}_{ee} \equiv {}^{\mathcal{R}}\mathbf{p}_{ee}(\mathbf{p}_{ee}, \boldsymbol{\eta}_{ee}) = \mathbf{Q}_{ee}\mathbf{p}_{ee}$, in which $\mathbf{Q}_{ee}$ is the rotation matrix from $\mathcal{F}_{ee}$ to $\mathcal{R}$. Therefore, the virtual change of ${}^{\mathcal{R}}\mathbf{p}_{ee}$ is given by

$$\delta^{\mathcal{R}}\mathbf{p}_{ee} = \mathbf{Q}_{ee}\delta\mathbf{p}_{ee} + \delta\mathbf{Q}_{ee}\mathbf{p}_{ee}. \tag{4.60}$$

The second term on the right-hand side of the above equation can be simplified as

$$\begin{aligned}\delta\mathbf{Q}_{ee}\mathbf{p}_{ee} &= \left.\frac{\partial(\mathbf{Q}_{ee}\mathbf{c})}{\partial\boldsymbol{\eta}_{ee}}\right|_{\mathbf{c}=\mathbf{p}_{ee}}\delta\boldsymbol{\eta}_{ee} = \left.\frac{\partial(\dot{\mathbf{Q}}_{ee}\mathbf{c})}{\partial\dot{\boldsymbol{\eta}}_{ee}}\right|_{\mathbf{c}=\mathbf{p}_{ee}}\delta\boldsymbol{\eta}_{ee} = \left.\frac{\partial(\mathbf{Q}_{ee}\boldsymbol{\Omega}_{ee}\mathbf{c})}{\partial\dot{\boldsymbol{\eta}}_{ee}}\right|_{\mathbf{c}=\mathbf{p}_{ee}}\delta\boldsymbol{\eta}_{ee} \\ &= -\mathbf{Q}_{ee}\mathbf{P}_{ee}\frac{\partial\boldsymbol{\omega}_{ee}}{\partial\dot{\boldsymbol{\eta}}_{ee}}\delta\boldsymbol{\eta}_{ee},\end{aligned} \tag{4.61}$$

where $\mathbf{P}_{ee}$ and $\boldsymbol{\Omega}_{ee}$ are the cross-product matrices of $\mathbf{p}_{ee}$ and $\boldsymbol{\omega}_{ee}$, respectively, and $\mathbf{c}$ is a dummy variable. Thus, introducing eq. (4.61) into eq. (4.60), one has

$$\delta^{\mathcal{R}}\mathbf{p}_{ee} = \mathbf{Q}_{ee}\left[\delta\mathbf{p}_{ee} - \mathbf{P}_{ee}\frac{\partial\boldsymbol{\omega}_{ee}}{\partial\dot{\boldsymbol{\eta}}_{ee}}\delta\boldsymbol{\eta}_{ee}\right]. \tag{4.62}$$

The second virtual displacement needed for eq. (4.59) is $\delta\boldsymbol{\theta}_{ee}$. To obtain it, we notice that, for any given $\delta\boldsymbol{\theta}_{ee}$, one can find a relative position vector $\mathbf{r}$ on the body such that it would lie in a plane perpendicular to $\delta\boldsymbol{\theta}_{ee}$. Now, when the body undergoes the virtual displacement $\delta\boldsymbol{\theta}_{ee}$, the vector $\mathbf{r}$ changes according to

$$\delta\mathbf{r} = \delta\boldsymbol{\theta}_{ee} \times \mathbf{r}. \tag{4.63}$$

[3] As a matter of fact, $\boldsymbol{\theta}_{ee}$ is not even defined here.

On the other hand, applying eq. (4.62) to the case of vector $\mathbf{r}$, one can readily realize that

$$\delta^{\mathcal{R}}\mathbf{r} = -\mathbf{Q}_{ee}\mathbf{R}\frac{\partial \boldsymbol{\omega}_{ee}}{\partial \dot{\boldsymbol{\eta}}_{ee}}\delta\boldsymbol{\eta}_{ee} = -{}^{\mathcal{R}}\mathbf{R}\,{}^{\mathcal{R}}\left(\frac{\partial \boldsymbol{\omega}_{ee}}{\partial \dot{\boldsymbol{\eta}}_{ee}}\delta\boldsymbol{\eta}_{ee}\right). \tag{4.64}$$

Hence, from eqs. (4.63 & 4.63), we have

$$\delta^{\mathcal{R}}\mathbf{r} = -{}^{\mathcal{R}}\mathbf{r} \times {}^{\mathcal{R}}\delta\boldsymbol{\theta}_{ee} = -{}^{\mathcal{R}}\mathbf{r} \times {}^{\mathcal{R}}\left(\frac{\partial \boldsymbol{\omega}_{ee}}{\partial \dot{\boldsymbol{\eta}}_{ee}}\delta\boldsymbol{\eta}_{ee}\right). \tag{4.65}$$

Since the above relation holds for any vector $\mathbf{r}$ perpendicular to $\delta\boldsymbol{\theta}_{ee}$, and that the only vectors dependent on $\mathbf{r}$ are $\mathbf{r}$ itself and $\delta\mathbf{r}$, we can conclude that

$${}^{\mathcal{R}}\delta\boldsymbol{\theta}_{ee} = \mathbf{Q}_{ee}\frac{\partial \boldsymbol{\omega}_{ee}}{\partial \dot{\boldsymbol{\eta}}_{ee}}\delta\boldsymbol{\eta}_{ee}. \tag{4.66}$$

Substituting for $\delta^{\mathcal{R}}\mathbf{p}$ and ${}^{\mathcal{R}}\delta\boldsymbol{\theta}_{ee}$ from eqs. (4.62 & 4.66) into eq. (4.59) results in

$$\begin{aligned}(\mathbf{f}_{ee}^{ex})^T\delta\mathbf{q}_{ee} &= {}^{\mathcal{R}}\mathbf{f}_{ee}^T\,\mathbf{Q}_{ee}\left[\delta\mathbf{p}_{ee} - \mathbf{P}_{ee}\frac{\partial \boldsymbol{\omega}_{ee}}{\partial \dot{\boldsymbol{\eta}}_{ee}}\delta\boldsymbol{\eta}_{ee}\right] + \boldsymbol{\tau}_{ee}^T\frac{\partial \boldsymbol{\omega}_{ee}}{\partial \dot{\boldsymbol{\eta}}}\delta\boldsymbol{\eta}_{ee} \\ &= \mathbf{f}_{ee}^T\delta\mathbf{p}_{ee} + (\boldsymbol{\tau}_{ee} + \mathbf{p}_{ee} \times \mathbf{f}_{ee})^T\frac{\partial \boldsymbol{\omega}_{ee}}{\partial \dot{\boldsymbol{\eta}}_{ee}}\delta\boldsymbol{\eta}_{ee}.\end{aligned} \tag{4.67}$$

Hence,

$$(\mathbf{f}_{ee}^{ex})^T\delta\mathbf{q}_{ee} = \begin{bmatrix}\mathbf{f}_{ee} \\ (\partial\boldsymbol{\omega}_{ee}/\partial\dot{\boldsymbol{\eta}}_{ee})^T(\boldsymbol{\tau}_{ee} + \mathbf{p}_{ee} \times \mathbf{f}_{ee})\end{bmatrix}^T \delta\mathbf{q}_{ee},$$

from which, by taking into account the norm constraint on $\boldsymbol{\eta}_{ee}$, and by using eq. (4.58), we obtain

$$\mathbf{w}_{ee}^{ex} = \begin{bmatrix}\mathbf{f}_{ee} \\ \boldsymbol{\tau}_{ee} + \mathbf{p}_{ee} \times \mathbf{f}_{ee}\end{bmatrix}. \tag{4.68}$$

4.5 Dynamics of the Entire System

To derive the dynamics equations of the entire system, we start by assembling the dynamics equations of the flexible manipulator, given by eqs. (4.31), and those of its

rigid counterpart , given by eqs. (4.54), namely,

$$\mathbf{I}\,\dot{\mathbf{u}} = \boldsymbol{\tau}^{\mathrm{ac}} + \hat{\mathbf{w}}^{\mathrm{s}} + \hat{\mathbf{w}}^{\mathrm{ex}}_{\mathrm{ee}} + \hat{\mathbf{w}}^{\mathrm{k}}, \tag{4.69a}$$

$$\mathbf{I} \triangleq \mathrm{diag}(\mathbf{I}_{\mathrm{F}}, \mathbf{I}_{\mathrm{R}}), \tag{4.69b}$$

$$\mathbf{u} \triangleq \begin{bmatrix} \dot{\boldsymbol{\psi}}_{\mathrm{F}}^T & \mathbf{u}_{\mathrm{R}}^T \end{bmatrix}^T. \tag{4.69c}$$

$$\boldsymbol{\tau}^{\mathrm{ac}} \triangleq \begin{bmatrix} (\boldsymbol{\tau}^{\mathrm{ac}}_{\mathrm{F}})^T & (\boldsymbol{\tau}^{\mathrm{ac}}_{\mathrm{R}})^T \end{bmatrix}^T, \tag{4.69d}$$

$$\hat{\mathbf{w}}^{\mathrm{s}} \triangleq \begin{bmatrix} (\hat{\mathbf{w}}^{\mathrm{s}}_{\mathrm{F}})^T & (\hat{\mathbf{w}}^{\mathrm{s}}_{\mathrm{R}})^T \end{bmatrix}^T, \tag{4.69e}$$

$$\hat{\mathbf{w}}^{\mathrm{ex}}_{\mathrm{ee}} \triangleq \begin{bmatrix} \mathbf{0}^T_{(n_{\mathrm{F}}+n_f)} & (\mathbf{w}^{\mathrm{ex}}_{\mathrm{ee}})^T(\partial \mathbf{t}_{\mathrm{ee}}/\partial \mathbf{u}_{\mathrm{R}}) \end{bmatrix}^T, \tag{4.69f}$$

$$\hat{\mathbf{w}}^{\mathrm{k}} \triangleq \begin{bmatrix} -(\mathbf{w}^{\mathrm{ex}}_{\mathrm{R0}})^T(\partial \mathbf{t}_{\mathrm{R0}}/\partial \dot{\boldsymbol{\psi}}_{\mathrm{F}}) & (\mathbf{w}^{\mathrm{ex}}_{\mathrm{R0}})^T(\partial \mathbf{t}_{\mathrm{R0}}/\partial \mathbf{u}_{\mathrm{R}}) \end{bmatrix}^T. \tag{4.69g}$$

Now, let us define the vector $\boldsymbol{\psi}$ of the system generalized coordinates as

$$\boldsymbol{\psi} \triangleq \begin{bmatrix} \boldsymbol{\theta}_{\mathrm{F}}^T & \boldsymbol{\theta}_{\mathrm{R}}^T & \boldsymbol{\zeta}^T \end{bmatrix}^T. \tag{4.70}$$

Apparently, $\mathbf{u}$ is a linear function of $\dot{\boldsymbol{\psi}}$; this relation can be given in the form

$$\mathbf{u} \equiv \begin{bmatrix} \dot{\boldsymbol{\psi}}_{\mathrm{F}} \\ \mathbf{u}_{\mathrm{R}} \end{bmatrix} = \mathbf{N}\dot{\boldsymbol{\psi}}, \tag{4.71}$$

with $\mathbf{N}$ given by

$$\mathbf{N} \triangleq \frac{\partial \mathbf{u}}{\partial \dot{\boldsymbol{\psi}}}. \tag{4.72}$$

However,

$$\mathbf{N} \equiv \frac{\partial \mathbf{u}}{\partial \dot{\boldsymbol{\psi}}} = \begin{bmatrix} \frac{\partial \dot{\boldsymbol{\psi}}_{\mathrm{F}}}{\partial \boldsymbol{\theta}_{\mathrm{F}}} & \frac{\partial \dot{\boldsymbol{\psi}}_{\mathrm{F}}}{\partial \boldsymbol{\theta}_{\mathrm{R}}} & \frac{\partial \dot{\boldsymbol{\psi}}_{\mathrm{F}}}{\partial \boldsymbol{\zeta}} \\ \frac{\partial \mathbf{u}_{\mathrm{R}}}{\partial \boldsymbol{\theta}_{\mathrm{F}}} & \frac{\partial \mathbf{u}_{\mathrm{R}}}{\partial \boldsymbol{\theta}_{\mathrm{R}}} & \frac{\partial \mathbf{u}_{\mathrm{R}}}{\partial \boldsymbol{\zeta}} \end{bmatrix} = \begin{bmatrix} \mathbf{1}_{n_{\mathrm{F}}} & \mathbf{O}_{n_{\mathrm{F}}\times n_{\mathrm{R}}} & \mathbf{O}_{n_{\mathrm{F}}\times n_f} \\ \mathbf{O}_{n_f\times n_{\mathrm{F}}} & \mathbf{O}_{n_f\times n_{\mathrm{R}}} & \mathbf{1}_{n_f} \\ \frac{\partial \mathbf{t}_{\mathrm{R0}}}{\partial \boldsymbol{\theta}_{\mathrm{F}}} & \mathbf{O}_{6\times n_{\mathrm{R}}} & \frac{\partial \mathbf{t}_{\mathrm{R0}}}{\partial \boldsymbol{\zeta}} \\ \mathbf{O}_{n_{\mathrm{R}}\times n_{\mathrm{F}}} & \mathbf{1}_{n_{\mathrm{R}}} & \mathbf{O}_{n_{\mathrm{R}}\times n_f} \end{bmatrix}. \tag{4.73}$$

Hence, premultiplying both sides of eq. (4.69a) by $\mathbf{N}^T$, we obtain

$$\mathbf{N}^T\mathbf{I}\,\mathbf{N}\ddot{\boldsymbol{\psi}} = \mathbf{N}^T\boldsymbol{\tau}^{\mathrm{ac}} + \mathbf{N}^T\big(\hat{\mathbf{w}}^{\mathrm{s}} - \mathbf{I}\,\dot{\mathbf{N}}\dot{\boldsymbol{\psi}}\big) + \mathbf{N}^T\hat{\mathbf{w}}^{\mathrm{ex}}_{\mathrm{ee}} + \mathbf{N}^T\hat{\mathbf{w}}^{\mathrm{k}}. \tag{4.74}$$

To simplify this equation, notice that

$$\mathbf{N}^T\boldsymbol{\tau}^{\mathrm{ac}} = \boldsymbol{\tau},$$

$$\mathbf{N}^T\hat{\mathbf{w}}^{\mathrm{ex}}_{\mathrm{ee}} = \Big(\frac{\partial \mathbf{t}_{\mathrm{ee}}}{\partial \dot{\boldsymbol{\psi}}}\Big)^T\mathbf{w}^{\mathrm{ex}}_{\mathrm{ee}},$$

$$\mathbf{N}^T\hat{\mathbf{w}}^{\mathrm{k}} = \mathbf{0}_{(n_{\mathrm{F}}+n_{\mathrm{R}}+n_f)},$$

in which

$$\boldsymbol{\tau} \triangleq \begin{bmatrix} \boldsymbol{\tau}_{\mathrm{F}}^T & \boldsymbol{\tau}_{\mathrm{R}}^T & \mathbf{0}_{n_f}^T \end{bmatrix}^T.$$

Thus, eq. (4.74) takes on the form

$$\mathbf{M}\ddot{\boldsymbol{\psi}} = \boldsymbol{\tau} + \mathbf{w}^{\mathrm{s}} + \left(\frac{\partial \mathbf{t}_{\mathrm{ee}}}{\partial \boldsymbol{\psi}}\right)^T \mathbf{w}_{\mathrm{ee}}^{\mathrm{ex}}, \tag{4.75a}$$

$$\mathbf{M} \triangleq \mathbf{N}^T \mathbf{I}\, \mathbf{N}, \tag{4.75b}$$

$$\mathbf{w}^{\mathrm{s}} \triangleq \mathbf{N}^T \left(\hat{\mathbf{w}}^{\mathrm{s}} - \mathbf{I}\dot{\mathbf{N}}\dot{\boldsymbol{\psi}}\right). \tag{4.75c}$$

Furthermore, it can be shown that, if $\mathbf{I}_{\mathrm{F}}$ and $\mathbf{I}_{\mathrm{R}}$ are divided into blocks corresponding to the independent generalized-velocity vectors $\dot{\boldsymbol{\psi}}_{\mathrm{F}}$ and $\mathbf{u}_{\mathrm{R}}$, respectively, as given by

$$\mathbf{I}_{\mathrm{F}} = \begin{bmatrix} \mathbf{M}_{\mathrm{rr}}^{\mathrm{F}} & \mathbf{M}_{\mathrm{rf}}^{\mathrm{F}} \\ (\mathbf{M}_{\mathrm{rf}}^{\mathrm{F}})^T & \mathbf{M}_{\mathrm{ff}}^{\mathrm{F}} \end{bmatrix}, \quad \dot{\boldsymbol{\psi}}_{\mathrm{F}} = \begin{bmatrix} \dot{\boldsymbol{\theta}}_{\mathrm{F}} \\ \dot{\boldsymbol{\zeta}} \end{bmatrix}, \tag{4.76}$$

$$\mathbf{I}_{\mathrm{R}} = \begin{bmatrix} \mathbf{M}_{\mathrm{bb}}^{\mathrm{R}} & \mathbf{M}_{\mathrm{rb}}^{\mathrm{R}} \\ (\mathbf{M}_{\mathrm{rb}}^{\mathrm{R}})^T & \mathbf{M}_{\mathrm{rr}}^{\mathrm{R}} \end{bmatrix}, \quad \mathbf{u}_{\mathrm{R}} = \begin{bmatrix} \mathbf{t}_{\mathrm{R0}} \\ \dot{\boldsymbol{\theta}}_{\mathrm{R}} \end{bmatrix}, \tag{4.77}$$

then matrix $\mathbf{M}$, corresponding to the generalized velocity $\dot{\boldsymbol{\psi}}$, will have the structure

$$\mathbf{M} = \begin{bmatrix} \mathbf{M}_{11} & \mathbf{M}_{12} & \mathbf{M}_{13} \\ \mathbf{M}_{12}^T & \mathbf{M}_{22} & \mathbf{M}_{23} \\ \mathbf{M}_{13}^T & \mathbf{M}_{23}^T & \mathbf{M}_{33} \end{bmatrix}, \quad \dot{\boldsymbol{\psi}} = \begin{bmatrix} \dot{\boldsymbol{\theta}}_{\mathrm{F}} \\ \dot{\boldsymbol{\theta}}_{\mathrm{R}} \\ \dot{\boldsymbol{\zeta}} \end{bmatrix}, \tag{4.78}$$

where

$$\mathbf{M}_{11} \triangleq \mathbf{M}_{\mathrm{rr}}^{\mathrm{F}} + (\frac{\partial \mathbf{t}_{\mathrm{R0}}}{\partial \dot{\boldsymbol{\theta}}_{\mathrm{F}}})^T \mathbf{M}_{\mathrm{bb}}^{\mathrm{R}} (\frac{\partial \mathbf{t}_{\mathrm{R0}}}{\partial \dot{\boldsymbol{\theta}}_{\mathrm{F}}}), \tag{4.79a}$$

$$\mathbf{M}_{12} \triangleq (\frac{\partial \mathbf{t}_{\mathrm{R0}}}{\partial \dot{\boldsymbol{\theta}}_{\mathrm{F}}})^T \mathbf{M}_{\mathrm{br}}^{\mathrm{R}}, \tag{4.79b}$$

$$\mathbf{M}_{13} \triangleq \mathbf{M}_{\mathrm{rf}}^{\mathrm{F}} + (\frac{\partial \mathbf{t}_{\mathrm{R0}}}{\partial \dot{\boldsymbol{\theta}}_{\mathrm{F}}})^T \mathbf{M}_{\mathrm{bb}}^{\mathrm{R}} (\frac{\partial \mathbf{t}_{\mathrm{R0}}}{\partial \dot{\boldsymbol{\zeta}}}), \tag{4.79c}$$

$$\mathbf{M}_{22} \triangleq \mathbf{M}_{\mathrm{rr}}^{\mathrm{R}}, \tag{4.79d}$$

$$\mathbf{M}_{23} \triangleq (\mathbf{M}_{\mathrm{br}}^{\mathrm{R}})^T \left(\frac{\partial \mathbf{t}_{\mathrm{R0}}}{\partial \dot{\boldsymbol{\zeta}}}\right), \tag{4.79e}$$

$$\mathbf{M}_{33} \triangleq \mathbf{M}_{\mathrm{ff}}^{\mathrm{F}} + \left(\frac{\partial \mathbf{t}_{\mathrm{R0}}}{\partial \dot{\boldsymbol{\zeta}}}\right)^T \mathbf{M}_{\mathrm{bb}}^{\mathrm{R}} \left(\frac{\partial \mathbf{t}_{\mathrm{R0}}}{\partial \dot{\boldsymbol{\zeta}}}\right). \tag{4.79f}$$

Subscripts "r," "b," and "f" refer to the revolute degrees of freedom, the degrees of freedom of the rigid-manipulator base, and the flexible-manipulator flexural degrees of freedom, respectively.

4.6 Motion in a Gravitational Field

To account for gravity effects, one can take $\boldsymbol{\psi}_{\mathrm{F}}$ as

$$\boldsymbol{\psi}_{\mathrm{F}} \triangleq \begin{bmatrix} \mathbf{p}_{\mathrm{F0}}^T & \boldsymbol{\theta}_{\mathrm{F}}^T & \boldsymbol{\zeta}_1^T & \cdots & \boldsymbol{\zeta}_{n_{\mathrm{F}}}^T \end{bmatrix}^T. \tag{4.80}$$

Then, letting $\ddot{\mathbf{p}}_{\mathrm{F0}} = -\mathbf{g}$, and $\dot{\mathbf{p}}_{\mathrm{F0}} = \mathbf{p}_{\mathrm{F0}} = \mathbf{0}$, one can ignore the first three dynamics equations—which pertain to the first three generalized coordinates, i.e., the components of $\mathbf{p}_{\mathrm{F0}}$—unless it is desired to compute the supporting forces applied at the base of the flexible manipulator.

Of course, adding $\mathbf{p}_{\mathrm{F0}}$ to the generalized coordinates of the systems requires some modifications to the dynamics equations even though the procedure remains the same.

Chapter 5

Estimation of the Flexural States

5.1 State-Estimator Structure

State estimation using an observer requires two sets of equations: a set of dynamics equations, expressing the *modelled dynamics* of the state evolution, and a set of measurement equations, otherwise known as state-output relations. The latter is an algebraic relation in the states, whereas the former, in continuous-time domain, comprises—usually—ordinary differential equations. Since the dynamics equations of a multilink manipulator are quite complicated, it would seem promising if the manipulator kinematics relations could be used as the modelled dynamics, for the kinematic relations are far less involved algebraically. However, a kinematics-based observer has a major drawback: The kinematic relations, which relate the evolution of the states to the pose, twist, and twist-rate of one or more bodies in the kinematic chain, are of a pure-integrator nature, thus having an inherent instability problem.

The dynamics equations of the entire system, when used as the modelled dynamics for the observer of a manipulator with flexible and rigid submanipulators, is to be integrated online and at each sampling time. This is especially expensive computationally because of the usually twice-as-large dimension of the system of differential equations for the entire system. For this very reason, we suggest using the dynamics equations of the flexible submanipulator alone as the modelled dynamics. This approach is explained in full detail in Section 5.2.

In the next two sections, the modelled-dynamics equations and the state-output relations are derived, linearized, and time-discretized. Then, in Section 5.4, the results thus obtained are used in an extended-Kalman-filter setting to estimate the flexural coordinates of the flexible submanipulator.

5.2 State-Space Dynamics Model

The flexible-manipulator dynamics, given by eqs. (4.31, 4.37, & 4.38), is recalled here in a more compact form:

$$\mathbf{I}_{\mathrm{F}}\,\ddot{\boldsymbol{\psi}}_{\mathrm{F}} = \hat{\mathbf{w}}^{\mathrm{s}}_{\mathrm{F}} + \boldsymbol{\tau}^{\mathrm{ac}}_{\mathrm{F}} - \left(\frac{\partial \mathbf{t}_{\mathrm{R0}}}{\partial \boldsymbol{\psi}_{\mathrm{F}}}\right)^{T} \mathbf{w}^{\mathrm{ex}}_{\mathrm{R0}}. \tag{5.1}$$

In such a case, however, as seen from the above equation, the reaction wrench applied on the end-link of the flexible manipulator by the base of the rigid one is needed. This wrench can be calculated using the measurements delivered by an accelerometer array installed on the rigid-manipulator base, applying the dynamics equations of the rigid manipulator itself. This approach is formulated below.

To calculate the reaction wrench, it is noticed that, using eqs. (4.54a & 4.77), one has

$$\mathbf{M}^{\mathrm{R}}_{\mathrm{bb}}\dot{\mathbf{t}}_{\mathrm{R0}} + \mathbf{M}^{\mathrm{R}}_{\mathrm{br}}\ddot{\boldsymbol{\theta}}_{\mathrm{R}} = \hat{\mathbf{w}}^{\mathrm{s}}_{\mathrm{Rb}} + \left(\frac{\partial \mathbf{t}_{\mathrm{ee}}}{\partial \mathbf{t}_{\mathrm{R0}}}\right)^{T} \mathbf{w}^{\mathrm{ex}}_{\mathrm{ee}} + \mathbf{w}^{\mathrm{ex}}_{\mathrm{R0}}, \tag{5.2a}$$

$$(\mathbf{M}^{\mathrm{R}}_{\mathrm{br}})^{T}\dot{\mathbf{t}}_{\mathrm{R0}} + \mathbf{M}^{\mathrm{R}}_{\mathrm{rr}}\ddot{\boldsymbol{\theta}}_{\mathrm{R}} = \hat{\mathbf{w}}^{\mathrm{s}}_{\mathrm{Rr}} + \left(\frac{\partial \mathbf{t}_{\mathrm{ee}}}{\partial \boldsymbol{\theta}_{\mathrm{R}}}\right)^{T} \mathbf{w}^{\mathrm{ex}}_{\mathrm{ee}} + \boldsymbol{\tau}_{\mathrm{R}}, \tag{5.2b}$$

in which $\mathbf{M}^{\mathrm{R}}_{\mathrm{bb}}$, $\mathbf{M}^{\mathrm{R}}_{\mathrm{br}}$, and $\mathbf{M}^{\mathrm{R}}_{\mathrm{rr}}$ are the blocks of the mass matrix of the rigid manipulator, and $\hat{\mathbf{w}}^{\mathrm{s}}_{\mathrm{mb}}$ and $\hat{\mathbf{w}}^{\mathrm{s}}_{\mathrm{br}}$ are the corresponding subarrays of its system wrench, expressed in

$$\mathbf{I}_{\mathrm{R}} \equiv \begin{bmatrix} \mathbf{M}^{\mathrm{R}}_{\mathrm{bb}} & \mathbf{M}^{\mathrm{R}}_{\mathrm{br}} \\ (\mathbf{M}^{\mathrm{R}}_{\mathrm{br}})^{T} & \mathbf{M}^{\mathrm{R}}_{\mathrm{rr}} \end{bmatrix}, \quad \hat{\mathbf{w}}^{\mathrm{s}}_{\mathrm{R}} \equiv \begin{bmatrix} \hat{\mathbf{w}}^{\mathrm{s}}_{\mathrm{Rb}} \\ \hat{\mathbf{w}}^{\mathrm{s}}_{\mathrm{Rr}} \end{bmatrix}.$$

Subscripts "b" and "r" refer to the base and the revolute degrees of freedom of the rigid manipulator, respectively.

Now, one can solve eq. (5.2b) and eq. (5.2a) for $\mathbf{M}^{\mathrm{R}}_{\mathrm{rr}}\ddot{\boldsymbol{\theta}}_{\mathrm{R}}$ and $\mathbf{w}^{\mathrm{ex}}_{\mathrm{R0}}$, respectively, to

obtain

$$\mathbf{M}^{\mathrm{R}}_{\mathrm{rr}}\ddot{\boldsymbol{\theta}}_{\mathrm{R}} = -(\mathbf{M}^{\mathrm{R}}_{\mathrm{br}})^T\dot{\mathbf{t}}_{\mathrm{R0}} + \hat{\mathbf{w}}^{\mathrm{s}}_{\mathrm{Rr}} + \boldsymbol{\tau}_{\mathrm{R}} + \left(\frac{\partial \mathbf{t}_{\mathrm{ee}}}{\partial \dot{\boldsymbol{\theta}}_{\mathrm{R}}}\right)^T \mathbf{w}^{\mathrm{ex}}_{\mathrm{ee}}, \tag{5.3a}$$

$$\mathbf{w}^{\mathrm{ex}}_{\mathrm{R0}} = \mathbf{M}^{\mathrm{R}}_{\mathrm{bb}}\dot{\mathbf{t}}_{\mathrm{R0}} + \mathbf{M}^{\mathrm{R}}_{\mathrm{br}}\ddot{\boldsymbol{\theta}}_{\mathrm{R}} - \hat{\mathbf{w}}^{\mathrm{s}}_{\mathrm{Rb}} - \left(\frac{\partial \mathbf{t}_{\mathrm{ee}}}{\partial \mathbf{t}_{\mathrm{R0}}}\right)^T \mathbf{w}^{\mathrm{ex}}_{\mathrm{ee}}. \tag{5.3b}$$

Then, having determined the translational and angular accelerations of the micro base as well as its twist using the method reported in Chapter 3, one can readily obtain $\dot{\mathbf{t}}_{\mathrm{R0}}$ and the other information needed for the right-hand sides of eqs. (5.3). Thereafter, solving the above linear equations sequentially is quite simple.

Let us denote the state vector of the flexible manipulator by $\mathbf{x}$, given by

$$\mathbf{x} \triangleq \begin{bmatrix}\mathbf{x}^1\\ \mathbf{x}^2\end{bmatrix}, \qquad \mathbf{x}^1 \triangleq \boldsymbol{\psi}_{\mathrm{F}} \equiv \begin{bmatrix}\boldsymbol{\theta}_{\mathrm{F}}\\ \boldsymbol{\zeta}\end{bmatrix}, \qquad \mathbf{x}^2 \triangleq \dot{\boldsymbol{\psi}}_{\mathrm{F}} \equiv \begin{bmatrix}\dot{\boldsymbol{\theta}}_{\mathrm{F}}\\ \dot{\boldsymbol{\zeta}}\end{bmatrix}. \tag{5.4}$$

Using the above definitions of the states, one can write the mathematical model of the flexible manipulator, eq. (5.1), in a state-space format:

$$\dot{\mathbf{x}}^1 = \mathbf{x}^2, \tag{5.5a}$$

$$\dot{\mathbf{x}}^2 = \mathbf{f}(\mathbf{x}) + \mathbf{B}(\mathbf{x})\,\mathbf{u}(t), \tag{5.5b}$$

with $\mathbf{f}(\mathbf{x})$, $\mathbf{B}(\mathbf{x})$, and $\mathbf{u}(t)$ defined below:

$$\mathbf{f}(\mathbf{x}) \triangleq \mathbf{H}(\mathbf{x}^1)\,\hat{\mathbf{w}}^{\mathrm{s}}_{\mathrm{F}}(\mathbf{x}), \tag{5.6}$$

$$\mathbf{B}(\mathbf{x}) \triangleq \begin{bmatrix}\mathbf{H}_1 & -\mathbf{H}\,\mathbf{J}^T_{\mathrm{F}}\end{bmatrix}, \tag{5.7}$$

$$\mathbf{u}(t) \triangleq \begin{bmatrix}\boldsymbol{\tau}_{\mathrm{F}}\\ \mathbf{w}^{\mathrm{ex}}_{\mathrm{R0}}\end{bmatrix}, \tag{5.8}$$

in which matrix $\mathbf{H}$, defined as the inverse of the mass matrix $\mathbf{I}_{\mathrm{F}}$, is divided into two blocks:

$$\mathbf{H} \equiv \begin{bmatrix}\mathbf{H}_1 & \mathbf{H}_2\end{bmatrix} \triangleq \mathbf{I}^{-1}_{\mathrm{F}}. \tag{5.9}$$

The first block $\mathbf{H}_1$ is an $N_{\mathrm{F}} \times n_{\mathrm{F}}$ matrix, with N_{F} and n_{F} being the degree of freedom of the flexible manipulator and its number of links, respectively.

Hence, the discrete-time linearized form of eqs. (5.5), obtained via Euler's scheme[1] on the linearized equations, can be written as

$$\mathbf{x}_{k+1}^1 = \mathbf{x}_k^1 + h\mathbf{x}_k^2 + \mathbf{m}_k^1 \tag{5.10a}$$

$$\mathbf{x}_{k+1}^2 = \mathbf{x}_k^2 + h\frac{\partial \mathbf{f}}{\partial \mathbf{x}}\bigg|_{\hat{\mathbf{x}}_k} \mathbf{x}_k + \bar{\mathbf{u}}_k + \mathbf{m}_k^2, \tag{5.10b}$$

in which h is the sampling period, $\mathbf{m}_k^1$ and $\mathbf{m}_k^2$ are the subarrays of the vector $\mathbf{m}_k$ of the uncorrelated white-noise processes representing the unmodelled dynamics, and $\bar{\mathbf{u}}_k$ is a redefined input function given by

$$\bar{\mathbf{u}}_k \triangleq h\left[\mathbf{f}(\hat{\mathbf{x}}_k) - \frac{\partial \mathbf{f}}{\partial \mathbf{x}}\bigg|_{\hat{\mathbf{x}}_k} \hat{\mathbf{x}}_k + \mathbf{B}(\hat{\mathbf{x}}_k)\,\mathbf{u}_k\right]. \tag{5.11}$$

Thus, in standard form, we have

$$\mathbf{x}_{k+1} = \mathbf{A}_k\,\mathbf{x}_k + \tilde{\mathbf{u}}_k + \mathbf{m}_k, \tag{5.12}$$

$$\mathbf{A}_k \triangleq \begin{bmatrix} \mathbf{1} & h\mathbf{1} \\ h(\partial \mathbf{f}/\partial \mathbf{x}^1) & \mathbf{1} + h(\partial \mathbf{f}/\partial \mathbf{x}^2) \end{bmatrix}_{\mathbf{x}=\hat{\mathbf{x}}_k}, \tag{5.13}$$

$$\tilde{\mathbf{u}}_k \triangleq \begin{bmatrix} \mathbf{0}_{N_\mathrm{F}}^T & \bar{\mathbf{u}}_k^T \end{bmatrix}^T. \tag{5.14}$$

To complete the derivation of the state-space dynamics model, the partial derivatives of $\mathbf{f}$ with respect to $\mathbf{x}^1$ and $\mathbf{x}^2$ must be found. Between the two, however, it is the partial derivative of $\mathbf{f}$ with respect to $\mathbf{x}^1$ that needs extra attention, because of the dependence of $\mathbf{H}$ on the generalized coordinates. To obtain this partial derivative, we notice that

$$\frac{\partial \mathbf{f}}{\partial \mathbf{x}^1} = \frac{\partial \mathbf{H}}{\partial \mathbf{x}^1}\,\hat{\mathbf{w}}_\mathrm{F}^\mathrm{s} + \mathbf{H}\frac{\partial \hat{\mathbf{w}}_\mathrm{F}^\mathrm{s}}{\partial \mathbf{x}^1}, \tag{5.15}$$

in which, using an interpretation similar to that of eq. (4.17), $(\partial \mathbf{H}/\partial \mathbf{x}^1)\hat{\mathbf{w}}_\mathrm{F}^\mathrm{s}$ can be written as

$$\begin{aligned} \frac{\partial \mathbf{H}}{\partial \mathbf{x}^1}\,\hat{\mathbf{w}}_\mathrm{F}^\mathrm{s} &\equiv \frac{\partial(\mathbf{H}\,\mathbf{a})}{\partial \mathbf{x}^1}\bigg|_{\mathbf{a}=\hat{\mathbf{w}}_\mathrm{F}^\mathrm{s}} = \frac{\partial(\mathbf{H}\,\mathbf{I}_\mathrm{F}\mathbf{H}\,\mathbf{a})}{\partial \mathbf{x}^1}\bigg|_{\mathbf{a}=\hat{\mathbf{w}}_\mathrm{F}^\mathrm{s}} \\ &= 2\frac{\partial \mathbf{H}}{\partial \mathbf{x}^1}\,\hat{\mathbf{w}}_\mathrm{F}^\mathrm{s} + \mathbf{H}\frac{\partial \mathbf{I}_\mathrm{F}}{\partial \mathbf{x}^1}\,\mathbf{H}\,\hat{\mathbf{w}}_\mathrm{F}^\mathrm{s} \end{aligned} \tag{5.16}$$

[1] Euler's discrerization scheme has been chosen for its simplicity and speed.

from which we can readily conclude that

$$\frac{\partial \mathbf{H}}{\partial \mathbf{x}^1}\,\hat{\mathbf{w}}_{\mathrm{F}}^{\mathrm{s}} \equiv -\mathbf{H}\frac{\partial \mathbf{I}_{\mathrm{F}}}{\partial \mathbf{x}^1}\,\mathbf{H}\,\hat{\mathbf{w}}_{\mathrm{F}}^{\mathrm{s}} = -\mathbf{H}\frac{\partial \mathbf{I}_{\mathrm{F}}}{\partial \mathbf{x}^1}\,\mathbf{f}. \tag{5.17}$$

Hence, using eqs. (5.15 & 5.17), one can derive the partial derivative of $\mathbf{f}$ with respect to $\mathbf{x}^1$ as

$$\frac{\partial \mathbf{f}}{\partial \mathbf{x}^1} = \mathbf{H}\left(\frac{\partial \hat{\mathbf{w}}_{\mathrm{F}}^{\mathrm{s}}}{\partial \boldsymbol{\psi}_{\mathrm{F}}} - \frac{\partial \mathbf{I}_{\mathrm{F}}}{\partial \boldsymbol{\psi}_{\mathrm{F}}}\mathbf{f}\right). \tag{5.18a}$$

The partial derivative of $\mathbf{f}$ with respect to $\mathbf{x}^2$ is apparently given by

$$\frac{\partial \mathbf{f}}{\partial \mathbf{x}^2} = \mathbf{H}\,\frac{\partial \hat{\mathbf{w}}_{\mathrm{F}}^{\mathrm{s}}}{\partial \dot{\boldsymbol{\psi}}_{\mathrm{F}}}. \tag{5.18b}$$

5.3 State-Output Relations

To obtain the state-output relations for the system, we denote the output vector by $\mathbf{y}$ and define it as

$$\mathbf{y} \triangleq \begin{bmatrix}\mathbf{y}^1\\ \mathbf{y}^2\end{bmatrix}, \quad \mathbf{y}^1 \triangleq \begin{bmatrix}\boldsymbol{\theta}_{\mathrm{F}}\\ \dot{\boldsymbol{\theta}}_{\mathrm{F}}\end{bmatrix}, \quad \mathbf{y}^2 \triangleq \bar{\mathbf{t}}_{\mathrm{R0}}, \tag{5.19}$$

where $\bar{\mathbf{t}}_{\mathrm{R0}}$ is the Cartesian twist of the rigid-manipulator base.

Whereas the relation of $\mathbf{y}^1$ with the states of the system is evidently linear and readily known, for the entries of $\mathbf{y}^1$ are among the system states themselves, the state-output relations pertaining to $\mathbf{y}^2$ are indeed nonlinear. However, a great number of today's well-known state-estimation techniques, e.g., the ones discussed in (Misawa and Hedrick, 1989; Canudas de Witt and Slotine, 1991; Sanchis and Nijmeijer, 1998; Söffker *et al.*, 1995), among many others, rely on the linearity of the state-output relations. To apply such techniques in the case state-output relations are nonlinear, one may linearize the relations and then try the particular technique using the linearized relations on the system.

To linearize the nonlinear state-output relations, $\mathbf{y}^2$ is expanded using Taylor's series about $\hat{\mathbf{x}}$. Neglecting the higher-order terms, we obtain

$$\mathbf{y}^2(\mathbf{x}) \approx \mathbf{y}^2(\hat{\mathbf{x}}) + \left.\frac{\partial \mathbf{y}^2}{\partial \mathbf{x}}\right|_{\hat{\mathbf{x}}}(\mathbf{x} - \hat{\mathbf{x}}) \tag{5.20}$$

where $\hat{\mathbf{x}}$ represents the estimated state vector, and, apparently,

$$\frac{\partial \mathbf{y}^2}{\partial \mathbf{x}} \equiv \begin{bmatrix} \dfrac{\partial \mathbf{y}^2}{\partial \mathbf{x}^1} & \dfrac{\partial \mathbf{y}^2}{\partial \mathbf{x}^2} \end{bmatrix} = \begin{bmatrix} \dfrac{\partial \bar{\mathbf{t}}_{\mathrm{R0}}}{\partial \boldsymbol{\psi}_{\mathrm{F}}} & \dfrac{\partial \bar{\mathbf{t}}_{\mathrm{R0}}}{\partial \dot{\boldsymbol{\psi}}_{\mathrm{F}}} \end{bmatrix}. \tag{5.21}$$

The partial derivatives of the Cartesian twist of the base of the rigid manipulator can be obtained using eqs. (2.31 & 2.33), namely,

$$\frac{\partial \bar{\mathbf{t}}_{\mathrm{R0}}}{\partial \dot{\boldsymbol{\psi}}_{\mathrm{F}}} = \mathbf{R}\,\mathbf{J}_{\mathrm{F}}, \qquad \mathbf{R} \triangleq \begin{bmatrix} \mathbf{1} & -\mathbf{P}_{\mathrm{R0}} \\ \mathbf{O} & \mathbf{1} \end{bmatrix}, \tag{5.22}$$

$$\frac{\partial \bar{\mathbf{t}}_{\mathrm{R0}}}{\partial \boldsymbol{\psi}_{\mathrm{F}}} = \mathbf{R}\,\dot{\mathbf{J}}_{\mathrm{F}} + \overline{\mathbf{R}}\,\mathbf{J}_{\mathrm{F}}, \qquad \overline{\mathbf{R}} \triangleq \begin{bmatrix} \boldsymbol{\Omega}_{\mathrm{R0}} & -\mathbf{P}_{\mathrm{R0}}\,\boldsymbol{\Omega}_{\mathrm{R0}} \\ \mathbf{O} & \boldsymbol{\Omega}_{\mathrm{R0}} \end{bmatrix}, \tag{5.23}$$

in which

$$\mathbf{J}_{\mathrm{F}} \triangleq \frac{\partial \mathbf{t}_{\mathrm{R0}}}{\partial \dot{\boldsymbol{\psi}}_{\mathrm{F}}}, \qquad \mathbf{P}_{\mathrm{R0}} \triangleq \mathrm{CPM}(\mathbf{p}_{\mathrm{R0}}), \qquad \boldsymbol{\Omega}_{\mathrm{R0}} \triangleq \mathrm{CPM}(\boldsymbol{\omega}_{\mathrm{R0}}). \tag{5.24}$$

In the above definitions, $\mathbf{t}_{\mathrm{R0}}$, $\mathbf{p}_{\mathrm{R0}}$, and $\boldsymbol{\omega}_{\mathrm{R0}}$ are the twist, the position and the angular-velocity vectors of the rigid-manipulator base, respectively.

Consequently, upon redefining the output vector, the state-output relation can be rewritten as

$$\bar{\mathbf{y}} = \mathbf{C}\,\mathbf{x} + \mathbf{n}(t) \tag{5.25}$$

$$\mathbf{C} \equiv \mathbf{C}(\hat{\mathbf{x}}) \triangleq \begin{bmatrix} \mathbf{E}_{n_{\mathrm{F}} \times N_{\mathrm{F}}} & \mathbf{O}_{n_{\mathrm{F}} \times N_{\mathrm{F}}} \\ \mathbf{O}_{n_{\mathrm{F}} \times N_{\mathrm{F}}} & \mathbf{E}_{n_{\mathrm{F}} \times N_{\mathrm{F}}} \\ \mathbf{R}\,\dot{\mathbf{J}}_{\mathrm{F}} + \overline{\mathbf{R}}\,\mathbf{J}_{\mathrm{F}} & \mathbf{R}\,\mathbf{J}_{\mathrm{F}} \end{bmatrix}, \tag{5.26}$$

in which $\mathbf{n}(t)$ is the vector of the uncorrelated, white measurement-noise processes[2], and $\mathbf{E}_{n_{\mathrm{F}} \times N_{\mathrm{F}}}$ is a rectangular array of ones and zeros in which the largest left-hand-side square block is the $n_{\mathrm{F}} \times n_{\mathrm{F}}$ identity matrix. The new output vector, $\bar{\mathbf{y}}$, is defined as

$$\bar{\mathbf{y}} \triangleq \mathbf{y}(\mathbf{x}) - \mathbf{y}(\hat{\mathbf{x}}) + \left.\frac{\partial \mathbf{y}}{\partial \mathbf{x}}\right|_{\hat{\mathbf{x}}} \hat{\mathbf{x}}. \tag{5.27}$$

The time-discretized form of the state-output relations, eq. (5.25), can be readily written as

$$\bar{\mathbf{y}}_k = \mathbf{C}_k\,\mathbf{x}_k + \mathbf{n}_k. \tag{5.28}$$

[2]A more realistic model for noise on the translational-velocity part of the output, which is inferred from the accelerometer-array signals by integration, will perhaps be a Markov process (Åström and Wittenmark, 1997), of course, if the accelerometer noise is assumed to be white.

Notice that, in Section 2.2, we linearized the twist-rate relations as well. However, taking the twist-rate elements as outputs will then require differentiating the dynamics equations of the flexible manipulator, which, in turn, complicates the linearization of the state-space form of the mathematical model further. Therefore, this is avoided. Nevertheless, if, in a particular problem, taking only the twist does not produce reliable results, one can include the twist-rate in the outputs and use the linearized relations derived in Section 2.2.

5.4 The Extended Kalman Filter

With the linearized governing equations available, one can use the extended Kalman filter (EKF) relations to obtain state estimates. These relations are derived in (Chui and Chen, 1991) as

$$\mathbf{P}_{0,0} = \mathrm{Var}(\mathbf{x}_0), \qquad \hat{\mathbf{x}}_0 = \mathrm{E}(\mathbf{x}_0), \tag{5.29a}$$

$$\mathbf{P}_{k,k-1} = \mathbf{A}_{k-1}\mathbf{P}_{k-1,k-1}\mathbf{A}_{k-1}^T + \mathbf{\Gamma}_{k-1}\mathbf{Q}_{k-1}\mathbf{\Gamma}_{k-1}^T, \tag{5.29b}$$

$$\hat{\mathbf{x}}_{k|k-1}^1 = \hat{\mathbf{x}}_{k-1}^1 + h\,\hat{\mathbf{x}}_{k-1}^2, \tag{5.29c}$$

$$\hat{\mathbf{x}}_{k|k-1}^2 = \hat{\mathbf{x}}_{k-1}^2 + h\left[\mathbf{f}(\hat{\mathbf{x}}_{k-1}) + \mathbf{B}(\hat{\mathbf{x}}_{k-1})\,\mathbf{u}_{k-1}\right], \tag{5.29d}$$

$$\mathbf{G}_k = \mathbf{P}_{k,k-1}\mathbf{C}_k^T(\mathbf{C}_k\mathbf{P}_{k,k-1}\mathbf{C}_k^T + \mathbf{R}_k)^{-1}, \tag{5.29e}$$

and

$$\mathbf{P}_{k,k} = (\mathbf{1} - \mathbf{G}_k\mathbf{C}_k)\mathbf{P}_{k,k-1}, \tag{5.29f}$$

$$\hat{\mathbf{x}}_k = \hat{\mathbf{x}}_{k|k-1} + \mathbf{G}_k(\mathbf{y}_k - \hat{\mathbf{y}}_{k|k-1}), \tag{5.29g}$$

where $\mathbf{Q}_{k-1}$ and $\mathbf{R}_k$ are the covariance matrices of the uncorrelated white-noise processes $\mathbf{m}_{k-1}$ and $\mathbf{n}_k$, respectively.

5.5 Observability of the Flexural Motion

A complete analysis of the observability issue for the type of systems treated in this thesis seems quite elusive, due to the nonlinear, highly complex nature of both dyna-

mics equations and state-output relations. Nonetheless, to intuitively see how many flexural generalized coordinates one can estimate using one accelerometer array, consider a cantilever flexible link. If an accelerometer array is installed at the tip of such a link, the three components of the translational acceleration and those of the angular acceleration of the array, totalling six, can be used to estimate six flexural coordinates: Four flexural generalized coordinates describing bendings in two planes plus two flexural coordinates in each plane; one flexural coordinate representing the torsional twist of the link; and the elongation of the link length. Consequently, if, in a particular case, more than two flexural coordinates are needed to effectively describe the bending of a link in one plane, then additional accelerometer arrays must be installed on the link along its length.

By the same token, if a flexible planar manipulator has more than two links or the bending deformation of any of the links is to be discretized with multiple flexural coordinates, then extra accelerometer arrays, in addition to the one located at the tip of the end link, have to be installed on the distal end-point of the links in order to provide the estimator with enough information. Otherwise, what the estimator will correctly estimate will be the translational and rotational motions of the end-point frame. If additional accelerometer arrays are to be used, one can relate the twist of two subsequent link-end frames to simplify the state-output relations; the required kinematic relations can readily be written using the recursive relations developed in Section 2.3.

Chapter 6

Control Law and Numerical Results

6.1 Redundancy Resolution

The mathematical model of the entire system, given by eqs. (4.75), is partitioned below:

$$\mathbf{M}_{\mathrm{rr}}\ddot{\boldsymbol{\theta}} + \mathbf{M}_{\mathrm{rf}}\ddot{\boldsymbol{\zeta}} = \mathbf{w}_{\mathrm{r}} + \boldsymbol{\tau} \tag{6.1a}$$

$$\mathbf{M}_{\mathrm{rf}}^{T}\ddot{\boldsymbol{\theta}} + \mathbf{M}_{\mathrm{ff}}\ddot{\boldsymbol{\zeta}} = \mathbf{w}_{\mathrm{f}} \tag{6.1b}$$

where

$$\boldsymbol{\theta} \triangleq \begin{bmatrix}\boldsymbol{\theta}_{\mathrm{F}} \\ \boldsymbol{\theta}_{\mathrm{R}}\end{bmatrix}, \qquad \mathbf{w} \equiv \begin{bmatrix}\mathbf{w}_{\mathrm{r}} \\ \mathbf{w}_{\mathrm{f}}\end{bmatrix} \triangleq \mathbf{w}^{\mathrm{s}} + \left(\frac{\partial \mathbf{t}_{\mathrm{ee}}}{\partial \dot{\boldsymbol{\psi}}}\right)^{T} \mathbf{w}_{\mathrm{ee}}^{\mathrm{ex}}, \qquad \boldsymbol{\tau} \triangleq \begin{bmatrix}\boldsymbol{\tau}_{\mathrm{F}} \\ \boldsymbol{\tau}_{\mathrm{R}}\end{bmatrix}, \tag{6.2}$$

and

$$\mathbf{M}_{\mathrm{rr}} \triangleq \begin{bmatrix}\mathbf{M}_{11} & \mathbf{M}_{12} \\ \mathbf{M}_{12}^{T} & \mathbf{M}_{22}\end{bmatrix}, \qquad \mathbf{M}_{\mathrm{rf}} \triangleq \begin{bmatrix}\mathbf{M}_{13} \\ \mathbf{M}_{23}\end{bmatrix}, \qquad \mathbf{M}_{\mathrm{ff}} \triangleq \mathbf{M}_{33}, \tag{6.3}$$

in which $\mathbf{M}_{ij}$, for $i, j = 1, 2, 3$, are given by eqs. (4.79).

Solving eq. (6.1b) for $\ddot{\boldsymbol{\zeta}}$, we obtain

$$\ddot{\boldsymbol{\zeta}} = \mathbf{M}_{\mathrm{ff}}^{-1}(\mathbf{w}_{\mathrm{f}} - \mathbf{M}_{\mathrm{rf}}^{T}\ddot{\boldsymbol{\theta}}). \tag{6.4}$$

Substituting the above relation into eq. (6.1a) and then solving for $\boldsymbol{\tau}$ yield

$$\boldsymbol{\tau} = (\mathbf{M}_{\mathrm{rr}} - \mathbf{M}_{\mathrm{rf}}\mathbf{M}_{\mathrm{ff}}^{-1}\mathbf{M}_{\mathrm{rf}}^{T})\ddot{\boldsymbol{\theta}} + \mathbf{M}_{\mathrm{rf}}\mathbf{M}_{\mathrm{ff}}^{-1}\mathbf{w}_{\mathrm{f}} - \mathbf{w}_{\mathrm{r}}. \tag{6.5}$$

This relation will serve as a basis for devising a computed-torque control law (Slotine and Li, 1991) in Section 6.3.

On the other hand, since the whole system has a fixed base, dropping subscript "ee" from $\mathbf{t}_{ee}$ for simplicity, we can conclude from eq. (2.19) that

$$\mathbf{t} = \begin{bmatrix} \mathbf{J}_r & \mathbf{J}_f \end{bmatrix} \begin{bmatrix} \dot{\boldsymbol{\theta}} \\ \dot{\boldsymbol{\zeta}} \end{bmatrix} \tag{6.6}$$

where $\mathbf{J}_r$ and $\mathbf{J}_f$ refer to the blocks of the Jacobian matrix that correspond to the joint-rates and the flexural generalized velocities, respectively. Differentiating this relation with respect to time, substituting for $\ddot{\boldsymbol{\zeta}}$ from eq. (6.4), and then simplifying, the mathematical model in terms of $\boldsymbol{\theta}$ is derived, namely,

$$(\mathbf{J}_r - \mathbf{J}_f \mathbf{M}_{ff}^{-1} \mathbf{M}_{rf}^T) \ddot{\boldsymbol{\theta}} = \dot{\mathbf{t}} - \dot{\mathbf{J}}_r \dot{\boldsymbol{\theta}} - \dot{\mathbf{J}}_f \dot{\boldsymbol{\zeta}} - \mathbf{J}_f \mathbf{M}_{ff}^{-1} \mathbf{w}_f. \tag{6.7}$$

With the definitions

$$\mathbf{Z} \triangleq \mathbf{J}_r - \mathbf{J}_f \mathbf{M}_{ff}^{-1} \mathbf{M}_{rf}^T, \qquad \mathbf{v} \triangleq \dot{\mathbf{J}}_r \dot{\boldsymbol{\theta}} + \dot{\mathbf{J}}_f \dot{\boldsymbol{\zeta}} + \mathbf{J}_f \mathbf{M}_{ff}^{-1} \mathbf{w}_f, \tag{6.8}$$

the above model becomes

$$\mathbf{Z} \ddot{\boldsymbol{\theta}} = \dot{\mathbf{t}} - \mathbf{v}. \tag{6.9}$$

Because the manipulator is kinematically redundant, this linear system of equations in $\ddot{\boldsymbol{\theta}}$ is underdetermined. This means that, given the joint variables and the joint-rates, the joint accelerations required for producing a desired end-effector twist-rate cannot be determined uniquely. However, using the Moore-Penrose generalized inverse[1] $\mathbf{Z}^\dagger$ of matrix $\mathbf{Z}$, the general solution of the system can be written as

$$\ddot{\boldsymbol{\theta}} = \mathbf{Z}^\dagger (\dot{\mathbf{t}} - \mathbf{v}) + (\mathbf{1} - \mathbf{Z}^\dagger \mathbf{Z}) \boldsymbol{\epsilon} \tag{6.10}$$

in which, if $\mathbf{Z}$ is of full rank, $\mathbf{Z}^\dagger$ can be calculated from

$$\mathbf{Z}^\dagger = \mathbf{Z}^T (\mathbf{Z}\mathbf{Z}^T)^{-1}. \tag{6.11}$$

[1]The generalized inverse $\mathbf{Z}^\dagger$ of $\mathbf{Z}$ need not be calculated explicitly, the solution (6.10) being efficiently calculated from eq. (6.9) using an orthogonalization procedure (Nobel and Daniel, 1988).

Using the solution given above, for a given desired twist-rate $\dot{\mathbf{t}}_d$ and an arbitrary vector $\boldsymbol{\epsilon}$, which represents the "self-motion" of the redundant manipulator[2], one can calculate the required joint trajectories.

If at this stage—the redundancy-resolution stage—we assume that all links are rigid, then we will arrive at a simpler solution to the redundancy-resolution problem. However, to render our formulation independent of whether the link flexibilities are considered or not, four new parameters are defined:

$$\mathbf{Z}_r \triangleq \mathbf{J}_r, \qquad \mathbf{v}_r \triangleq \dot{\mathbf{J}}_r\dot{\boldsymbol{\theta}}, \tag{6.12a}$$

$$\mathbf{Z}_f \triangleq \mathbf{J}_r - \mathbf{J}_f\mathbf{M}_{ff}^{-1}\mathbf{M}_{rf}^T, \qquad \mathbf{v}_f \triangleq \dot{\mathbf{J}}_r\dot{\boldsymbol{\theta}} + \dot{\mathbf{J}}_f\dot{\boldsymbol{\zeta}} + \mathbf{J}_f\mathbf{M}_{ff}^{-1}\mathbf{w}_f. \tag{6.12b}$$

When $\mathbf{Z}$ and $\mathbf{v}$ in eq. (6.10) are replaced by $\mathbf{Z}_r$ and $\mathbf{v}_r$, respectively, the redundancy resolution will be called *rigid-link redundancy resolution*; on the other hand, if $\mathbf{Z}$ and $\mathbf{v}$ are taken as $\mathbf{Z}_f$ and $\mathbf{v}_f$, respectively, we will term the redundancy-resolution formulation *flexible-link redundancy resolution.*

The rigid-link redundancy-resolution method, which is apparently less accurate than its flexible-link counterpart, is the one that was used in (Nguyen *et al.*, 1992; Kim and Park, 1996; 1998).

6.2 Tracking Error

For effective tracking, two error vectors are defined: The *pose-error vector*, denoted by $\mathbf{e}_p$, and the *twist-error vector*, represented by $\mathbf{e}_t$. The latter is simply defined as the numerical difference between the end-effector twist and its desired value:

$$\mathbf{e}_t \triangleq \mathbf{t}_d - \mathbf{t}. \tag{6.13}$$

The former, however, cannot directly be defined as the mere numerical difference of two vectors because the attitude of a rigid-body contributes to its pose vector, and no representation of attitude can be added—or subtracted, for that matter—element

[2] A *self-motion* of a kinemtically redundant manipulator is a joint-space motion of the manipulator which does not result in any change in the end-effector pose, twist, or twist-rate.

by element to produce a meaningful result. To handle this problem, assuming that the attitude errors are small enough, we define the pose error as the image of the end-effector generalized-coordinate error $\Delta\mathbf{q}_{\mathrm{ee}}$ under the mapping given below:

$$\mathbf{e}_{\mathrm{p}} \triangleq \begin{bmatrix} \mathbf{1} & \mathbf{O}_{3\times 4} \\ \mathbf{O}_{3\times 3} & \overline{\mathbf{H}} \end{bmatrix} \Delta\mathbf{q}_{\mathrm{ee}} \tag{6.14}$$

where $\mathbf{1}$ is the 3×3 identity matrix, and matrix $\overline{\mathbf{H}}$ is defined by eq. (2.5b).

6.3 Computed-Torque Control

The computed torque required for control is then suggested as

$$\begin{aligned} \boldsymbol{\tau}_{\mathrm{com}} = &(\mathbf{M}_{\mathrm{rr}} - \mathbf{M}_{\mathrm{rf}}\mathbf{M}_{\mathrm{ff}}^{-1}\mathbf{M}_{\mathrm{rf}}^{T})\mathbf{Z}^{\dagger}(\dot{\mathbf{t}}_{\mathrm{d}} + \mathbf{K}_p\mathbf{e}_{\mathrm{p}} + \mathbf{K}_t\mathbf{e}_{\mathrm{t}} - \mathbf{v}) \\ &+ (\mathbf{M}_{\mathrm{rr}} - \mathbf{M}_{\mathrm{rf}}\mathbf{M}_{\mathrm{ff}}^{-1}\mathbf{M}_{\mathrm{rf}}^{T})(\mathbf{1} - \mathbf{Z}^{\dagger}\mathbf{Z})\boldsymbol{\epsilon} + \mathbf{M}_{\mathrm{rf}}\mathbf{M}_{\mathrm{ff}}^{-1}\mathbf{w}_{\mathrm{f}} - \mathbf{w}_{\mathrm{r}} \end{aligned} \tag{6.15}$$

where $\mathbf{e}_{\mathrm{p}}$ and $\mathbf{e}_{\mathrm{t}}$ are given by eqs. (6.14 & 6.13), and $\mathbf{K}_p$ and $\mathbf{K}_t$ are the gains of the proportional and the derivative actions, respectively. In the case steady-state error is an issue, an integral action can be included as well. Upon the application of the foregoing torque at the joints, eq. (6.5) results in

$$\begin{aligned} (\mathbf{M}_{\mathrm{rr}} - \mathbf{M}_{\mathrm{rf}}\mathbf{M}_{\mathrm{ff}}^{-1}\mathbf{M}_{\mathrm{rf}}^{T})\ddot{\boldsymbol{\theta}} = (\mathbf{M}_{\mathrm{rr}} - \mathbf{M}_{\mathrm{rf}}\mathbf{M}_{\mathrm{ff}}^{-1}\mathbf{M}_{\mathrm{rf}}^{T})\Big[&\mathbf{Z}^{\dagger}(\dot{\mathbf{t}}_{\mathrm{d}} + \mathbf{K}_p\mathbf{e}_{\mathrm{p}} + \mathbf{K}_t\mathbf{e}_{\mathrm{t}} - \mathbf{v}) \\ &+ (\mathbf{1} - \mathbf{Z}^{\dagger}\mathbf{Z})\boldsymbol{\epsilon}\Big] \end{aligned} \tag{6.16}$$

which, by virtue of the non-singularity of the mass matrix $\mathbf{M}$ and as a result of the *matrix inversion lemma* (Brogan, 1991), simplifies to

$$\ddot{\boldsymbol{\theta}} = \mathbf{Z}^{\dagger}(\dot{\mathbf{t}}_{\mathrm{d}} + \mathbf{K}_p\mathbf{e}_{\mathrm{p}} + \mathbf{K}_t\mathbf{e}_{\mathrm{t}} - \mathbf{v}) + (\mathbf{1} - \mathbf{Z}^{\dagger}\mathbf{Z})\boldsymbol{\epsilon}. \tag{6.17}$$

If this vector of joint accelerations is substituted into eq. (6.4), we obtain the flexural dynamics of the manipulator as

$$\mathbf{M}_{\mathrm{ff}}\ddot{\boldsymbol{\zeta}} = -\mathbf{M}_{\mathrm{rf}}^{T}\mathbf{Z}^{\dagger}(\dot{\mathbf{t}}_{\mathrm{d}} + \mathbf{K}_p\mathbf{e}_{\mathrm{p}} + \mathbf{K}_t\mathbf{e}_{\mathrm{t}} - \mathbf{v}) - \mathbf{M}_{\mathrm{rf}}^{T}(\mathbf{1} - \mathbf{Z}^{\dagger}\mathbf{Z})\boldsymbol{\epsilon} + \mathbf{w}_{\mathrm{f}}. \tag{6.18}$$

This mathematical model can then be rewritten as

$$\mathbf{M}_{\mathrm{ff}}\ddot{\boldsymbol{\zeta}} + \mathbf{C}_{\mathrm{d}}\dot{\boldsymbol{\zeta}} + \mathbf{K}\boldsymbol{\zeta} = \mathbf{w}_{\zeta} \tag{6.19}$$

where $\mathbf{C}_\mathrm{d}$ is the desired *proportional-damping*[3] matrix, given by

$$\mathbf{C}_\mathrm{d} \triangleq \alpha \mathbf{M}_\mathrm{ff} + \beta \mathbf{K}. \tag{6.20}$$

The scalars α and β are the proportionality constants. Moreover, $\mathbf{w}_\zeta$ and $\mathbf{K}$ are defined as

$$\begin{aligned} \mathbf{w}_\zeta \triangleq & -\mathbf{M}_\mathrm{rf}^T \mathbf{Z}^\dagger (\dot{\mathbf{t}}_\mathrm{d} + \mathbf{K}_p \mathbf{e}_\mathrm{p} + \mathbf{K}_t \mathbf{e}_\mathrm{t} - \mathbf{v}) - \mathbf{M}_\mathrm{rf}^T (\mathbf{1} - \mathbf{Z}^\dagger \mathbf{Z}) \boldsymbol{\epsilon} \\ & + \mathbf{w}_\mathrm{f} + \mathbf{C}_\mathrm{d} \dot{\boldsymbol{\zeta}} + \mathbf{K} \boldsymbol{\zeta} \end{aligned} \tag{6.21}$$

$$\mathbf{K} \triangleq \mathrm{diag}(\mathbf{K}_{\mathrm{F}1}, \mathbf{K}_{\mathrm{F}2}, \ldots, \mathbf{K}_{\mathrm{F}n_\mathrm{F}}), \tag{6.22}$$

$\mathbf{K}_{\mathrm{F}i}$ being the stiffness matrix of the flexible-link number i. The generalized force $\mathbf{w}_\zeta$ is the force that induces vibrations in the flexible links of the system. The only free parameter that we can choose in eq. (6.19) is $\boldsymbol{\epsilon}$, the vector of the manipulator self-motions. Even though eq. (6.19) looks like the mathematical model of a linear, time-invariant, damped system, it is actually not so, for both the mass matrix $\mathbf{M}_\mathrm{ff}$ and the excitation force depend upon the system generalized coordinates, and the latter also depends on the generalized velocities.

Therefore, in general, system (6.19) cannot be treated using the common linear-vibration tools[4]; for example, neither will the positive-definiteness of the damping matrix, in general, guarantee the stability of the system, nor the time-varying modal matrix diagonalizes the dynamics equations (Browder and Alexander, 1988). Hoping that, in case of a minimum-norm right-hand side, the vibrations are damped, and the system behaviour is acceptable, Nguyen *et al.* (1992) suggested calculating $\boldsymbol{\epsilon}$ in such a way that the norm of the excitation force is minimized by means of a least-square solution. However, if we assume that $\mathbf{M}_\mathrm{ff}$ does not vary dramatically, we can apply modal analysis and calculate the projection of the excitation force onto the modal space; then, one can try to minimize the components of the image corresponding to the lowest "natural frequencies."

[3]For a more general form of proportional damping, see (Angeles and Ostrovskaya, 2002).

[4]Properly speaking, the dynamics expressed by eq. (6.19) is both time-varying and configuration-dependent. As a result, none of the results reported for time-varying linear systems by Browder and Alexander (1988), Zhu and Johnson (1990), and Lee and Park (1998) are directly applicable.

This method was originally suggested by Kim and Park (1996; 1998). However, neither Nguyen *et al.* nor Kim and Park gave any clue as to how the damping matrix is chosen. Furthermore, since the damping matrix Kim and Park use had no specific structure, they had to write the equations in state-space form, thus ending up with a dimensionally-twice-as-large system of equations. Assuming a proportional damping matrix, on the contrary, simplifies the solution in this regard and reduces the number of required floating-point operations.

Following a standard procedure for proportionally damped systems and neglecting the configuration dependence of the modal matrix, one can use eqs. (6.19 & 6.20) to rewrite the flexural dynamics in modal form as

$$\ddot{\boldsymbol{\mu}} + (\alpha\mathbf{1} + \beta\boldsymbol{\Lambda})\dot{\boldsymbol{\mu}} + \boldsymbol{\Lambda}\boldsymbol{\mu} = (\mathbf{T}^T\mathbf{M}_{\mathrm{ff}}\mathbf{T})^{-1}\,\mathbf{T}^T\mathbf{w}_\zeta \tag{6.23}$$

whereby matrices $\boldsymbol{\Lambda}$ and $\mathbf{T}$ are obtained by solving the generalized eigenvalue problem (Meirovitch, 1997) given by

$$\mathbf{K}\,\mathbf{x} = \lambda\mathbf{M}_{\mathrm{ff}}\mathbf{x}. \tag{6.24}$$

$\mathbf{T}$ is the modal matrix, with its columns being the eigenvectors arranged in the ascending order of the corresponding eigenvalues[5]. These, in turn, make up the diagonal elements of the diagonal matrix $\boldsymbol{\Lambda}$. Furthermore, the modal-coordinate vector $\boldsymbol{\mu}$ is defined by

$$\boldsymbol{\mu} \triangleq \mathbf{T}^{-1}\boldsymbol{\zeta}. \tag{6.25}$$

Since both $\mathbf{M}_{\mathrm{ff}}$ and $\mathbf{K}$ are positive-definite, the modal matrix is real, and the eigenvalues are strictly positive. This is another advantage over the method reported by Kim and Park.

If ρ denotes the degree of redundancy of the system, we can set the right-hand sides of the first ρ equations of eq. (6.23) to zero. If we denote the submatrix of $\mathbf{T}$ consisting of the first ρ columns of $\mathbf{T}$ by $\mathbf{T}_\rho$, we obtain

$$\mathbf{T}_\rho^T\left[\mathbf{M}_{\mathrm{rf}}^T\mathbf{Z}^\dagger(\dot{\mathbf{t}}_{\mathrm{d}} + \mathbf{K}_p\mathbf{e}_{\mathrm{p}} + \mathbf{K}_t\mathbf{e}_{\mathrm{t}} - \mathbf{v}) + \mathbf{M}_{\mathrm{rf}}^T(\mathbf{1} - \mathbf{Z}^\dagger\mathbf{Z})\boldsymbol{\epsilon} - (\mathbf{w}_{\mathrm{f}} + \mathbf{C}_{\mathrm{d}}\dot{\boldsymbol{\zeta}} + \mathbf{K}\boldsymbol{\zeta})\right] = \mathbf{0}. \tag{6.26}$$

[5]Because both $\mathbf{M}_{\mathrm{ff}}$ and $\mathbf{K}$ are real, symmetric matrices, all the generalized eigenvalues are real.

One should notice that $(\mathbf{T}^T\mathbf{M}_{\mathrm{ff}}\mathbf{T})^{-1}$ on the right-hand side of eq. (6.23) can be ignored here because it is both diagonal and— obviously—invertible, thus having no effect on the vanishing of $\mathbf{T}_\rho^T\mathbf{w}_\zeta$. The reason is that the "modal vectors," the eigenvectors of the generalized eigenvalue problem, are mutually orthogonal with respect to $\mathbf{M}_{\mathrm{ff}}$, for matrix $\mathbf{K}$ is symmetric[6].

Keeping the terms involving the self-motion on the left-hand side and taking the rest to the other side, one obtains the system of equations[7]

$$\mathbf{A}\boldsymbol{\epsilon} = \mathbf{b} \tag{6.27}$$

$$\mathbf{A} \triangleq \mathbf{T}_\rho^T\mathbf{M}_{\mathrm{rf}}^T(\mathbf{1} - \mathbf{Z}^\dagger\mathbf{Z}), \tag{6.28}$$

$$\mathbf{b} \triangleq \mathbf{T}_\rho^T\Big[-\mathbf{M}_{\mathrm{rf}}^T\mathbf{Z}^\dagger(\dot{\mathbf{t}}_{\mathrm{d}} + \mathbf{K}_p\mathbf{e}_{\mathrm{p}} + \mathbf{K}_t\mathbf{e}_{\mathrm{t}} - \mathbf{v}) + \mathbf{w}_{\mathrm{f}} + \mathbf{C}_{\mathrm{d}}\dot{\boldsymbol{\zeta}} + \mathbf{K}\boldsymbol{\zeta}\Big]. \tag{6.29}$$

The least-square solution of eq. (6.27) is given by

$$\boldsymbol{\epsilon} = \mathbf{A}^\dagger\,\mathbf{b} \tag{6.30}$$

in which $\mathbf{A}^\dagger$ is the Moore-Penrose generalized inverse of $\mathbf{A}$.

If the result given by eq. (6.30) is substituted back into eq. (6.21), the "optimum" excitation force and its corresponding control torque are obtained as

$$\mathbf{w}_\zeta = -\mathbf{M}_{\mathrm{rf}}^T\mathbf{Z}^\dagger(\dot{\mathbf{t}}_{\mathrm{d}} + \mathbf{K}_p\mathbf{e}_{\mathrm{p}} + \mathbf{K}_t\mathbf{e}_{\mathrm{t}} - \mathbf{v}) - \mathbf{M}_{\mathrm{rf}}^T\mathbf{A}^\dagger\,\mathbf{b} + \mathbf{w}_{\mathrm{f}} + \mathbf{C}_{\mathrm{d}}\dot{\boldsymbol{\zeta}} + \mathbf{K}\boldsymbol{\zeta} \tag{6.31}$$

$$\begin{aligned}\boldsymbol{\tau}_{\mathrm{com}} = {} & (\mathbf{M}_{\mathrm{rr}} - \mathbf{M}_{\mathrm{rf}}\mathbf{M}_{\mathrm{ff}}^{-1}\mathbf{M}_{\mathrm{rf}}^T)\left[\mathbf{Z}^\dagger(\dot{\mathbf{t}}_{\mathrm{d}} + \mathbf{K}_p\mathbf{e}_{\mathrm{p}} + \mathbf{K}_t\mathbf{e}_{\mathrm{t}} - \mathbf{v}) + \mathbf{A}^\dagger\,\mathbf{b}\right] \\ & + \mathbf{M}_{\mathrm{rf}}\mathbf{M}_{\mathrm{ff}}^{-1}\mathbf{w}_{\mathrm{f}} - \mathbf{w}_{\mathrm{r}}.\end{aligned} \tag{6.32}$$

Notice that $(\mathbf{1} - \mathbf{Z}^\dagger\mathbf{Z})\mathbf{A}^\dagger\,\mathbf{b} = \mathbf{A}^\dagger\,\mathbf{b}$ because, for any *idempotent*, symmetric matrix $\mathbf{I}$ (Maciejewski and Klein, 1985),

$$\mathbf{I}(\mathbf{B}\,\mathbf{I})^\dagger \equiv (\mathbf{B}\,\mathbf{I})^\dagger, \tag{6.33}$$

[6]Similarly, because of the symmetry of $\mathbf{M}_{\mathrm{ff}}$, the eigenvectors are also mutually orthogonal with respect to $\mathbf{K}$, and $\mathbf{T}^T\mathbf{K}\,\mathbf{T}$ is, hence, diagonal as well.

[7]Kim and Park (1996; 1998) also come up with a similar equation; in their case, however, both $\mathbf{A}$ and $\mathbf{b}$ are, as mentioned before, complex in general. To obtain the least-square solution in such a case, the least-square problem must be reformulated accordingly, for the difference in the norm definition, but these authors do not make such a distinction. It can readily be shown that, if $\mathbf{A}$ and $\mathbf{b}$ are complex, the least-square solution is given by $\boldsymbol{\epsilon} = \left[\Re(\mathbf{A}^H\mathbf{A})\right]^\dagger\Re(\mathbf{A}^H\mathbf{b})$ where the superscript H denotes the *Hermitian*, i.e., complex-conjugate transposed, of a matrix, and $\Re(\cdot)$ is the real part of $(\cdot)$.

and $(\mathbf{1} - \mathbf{Z}^{\dagger}\mathbf{Z})$ is one such matrix.

As seen from eqs. (6.23 & 6.26), the choice of $\boldsymbol{\epsilon}$ can affect the ρ "lower-frequency" elements of the projection of the excitation force onto the "modal" space, i.e., the term $(\mathbf{T}^T\mathbf{M}_{\mathrm{ff}}\mathbf{T})^{-1}\,\mathbf{T}_{\rho}^T\mathbf{w}_{\zeta}$, if and only if none of the elements of $\mathbf{T}_{\rho}^T\,\mathbf{M}_{\mathrm{rf}}^T\mathbf{A}^{\dagger}\,\mathbf{b}$ is zero. This means that the "principal modes" are in a sense "controllable" if $\mathbf{A}^{\dagger}\,\mathbf{b}$ is not orthogonal to any of the columns of the matrix product $\mathbf{M}_{\mathrm{rf}}\mathbf{T}_{\rho}$. This "controllability" analysis appears to be in line with the work of Konno *et al.* (1997); the controllability of structurally flexible manipulators has also been addressed by Tonsunoglu *et al.* (1989; 1990; 1992).

6.4 Stability of the Flexural Motion

For a linear, time-invariant second-order system described by the general form

$$\mathbf{M}\ddot{\mathbf{x}} + \mathbf{C}\dot{\mathbf{x}} + \mathbf{K}\mathbf{x} = \mathbf{0}, \tag{6.34}$$

due to the monotonic reduction of the total energy of the system, the simultaneous positive-definiteness of the mass, the damping, and the stiffness matrices brings about the *global asymptotic stability*[8] of the system. However, if any of the three matrices is not constant, whether time-varying or state-dependent, the stability of the system is, in general, unknown and can only be determined via a more thorough treatment of the system, e.g., by Lyapunov's "second method." In other words, not any mere positive-definite choice of the desired damping matrix, $\mathbf{C}_{\mathrm{d}}$ in eq. (6.19), guarantees the stability of the time-varying system.

However, if we assume that the excitation force $\mathbf{w}_{\zeta}$ can be kept zero at all times through self-motions $\boldsymbol{\epsilon}$ of acceptably small norm for any given $\mathbf{C}_{\mathrm{d}}$, then the flexural motion of the system, described by eq. (6.19), can be rendered stable by proper selection of the damping matrix. This is streamlined next:

[8]In this case, the total energy of the system is a Lyapunov function (Caines, 1999; Slotine and Li, 1991) for the system.

The sum of the elastic-potential energy stored in the flexible links and the part of the kinetic energy of the links due to the flexural motions is given by

$$V \triangleq \frac{1}{2}\dot{\boldsymbol{\zeta}}^T \mathbf{M}_{\mathrm{ff}} \dot{\boldsymbol{\zeta}} + \frac{1}{2}\boldsymbol{\zeta}^T \mathbf{K} \boldsymbol{\zeta}. \tag{6.35}$$

Due to the positive-definiteness of both mass and stiffness matrices, the energy function V is also positive-definite, thus being a candidate Lyapunov function. Then, to assess the stability of the system, one can obtain the time derivative of V with respect to time:

$$\dot{V} = \dot{\boldsymbol{\zeta}}^T \left[\mathbf{M}_{\mathrm{ff}} \ddot{\boldsymbol{\zeta}} + \mathbf{K} \boldsymbol{\zeta} \right] + \frac{1}{2}\dot{\boldsymbol{\zeta}}^T \dot{\mathbf{M}}_{\mathrm{ff}} \dot{\boldsymbol{\zeta}} \tag{6.36}$$

which, based on the dynamics model

$$\mathbf{M}_{\mathrm{ff}} \ddot{\boldsymbol{\zeta}} + \mathbf{C}_{\mathrm{d}} \dot{\boldsymbol{\zeta}} + \mathbf{K} \boldsymbol{\zeta} = \mathbf{0}, \tag{6.37}$$

can be rewritten as

$$\dot{V} = -\dot{\boldsymbol{\zeta}}^T \left[\mathbf{C}_{\mathrm{d}} - \frac{1}{2}\dot{\mathbf{M}}_{\mathrm{ff}} \right] \dot{\boldsymbol{\zeta}}. \tag{6.38}$$

It is apparent that, if the damping matrix is chosen such that $(2\mathbf{C}_{\mathrm{d}} - \dot{\mathbf{M}}_{\mathrm{ff}}) > 0$, $\dot{V}$ turns out to be negative-definite, the energy function V thus being a Lyapunov function, the physical system described by eq. (6.37) being thereby stable.

A note of caution, however, is in order: One cannot choose an arbitrarily "large" desired damping matrix because it may not then be possible to find self-motions of acceptably small norms that render $\mathbf{w}_\zeta$ negligibly small. Note that, by "large," we mean a matrix with a large norm, whatever the norm chosen.

Another very important point to mention is that not all possible initial manipulator postures result in a stable control of flexural motion using the method outlined in Section 6.3, as observed from the simulations. This appears as an increasingly larger self-motion which is needed to keep the effect of $\mathbf{w}_\zeta$ negligible. As the degree of redundancy increases, so does the difficulty of choosing the initial conditions.

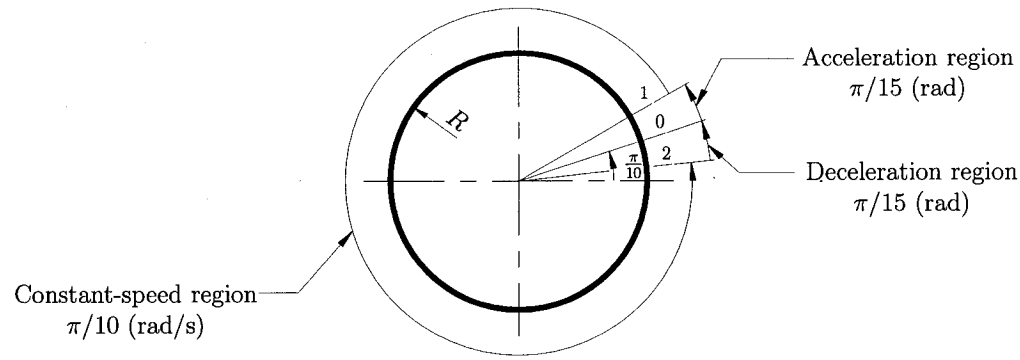

Figure 6.1: The end-effector Cartesian trajectory

6.5 Numerical Results

To demonstrate the ideas expressed here regarding state estimation and control, a planar *RRRR* manipulator is considered. The first two links of this manipulator are flexible and constitute the flexible submanipulator, while the last two are rigid and are assumed to make up the rigid submanipulator. The Cartesian trajectory to be followed by the end-effector is determined by only a prescribed position of the end-effector at any given time, i.e., the orientation of the end-effector is disregarded, and hence, the degree of redundancy is two. All four links are slender, uniform, and of equal length and equal mass, their physical properties being given in Table 6.1.

The desired end-effector trajectory is assumed to be a circle of radius 0.6 m with its centre located at 1.6 m from the origin on the positive x axis. The trajectory, as shown in Fig. 6.1, has three regions: The acceleration region, the constant-speed region, and the deceleration region. The acceleration and the deceleration regions, which are used to reduce the shocks applied to the system, are described by fifth-order polynomials

Subsystem	Link No.	Mass (kg)	Length (m)	EI (Nm^2)
Flexible Submanipulator	1	0.50	1.0	93.266
	2	0.50	1.0	93.266
Rigid Submanipulator	1	0.50	1.0	–
	2	0.50	1.0	–

Table 6.1: The link dimensions of the *RRRR* manipulator

R (m)	θ_1	θ_2	θ_3	θ_4
0.4	40.0°	−124.6°	160.1°	−105.0°
0.5	40.0°	−118.7°	155.1°	−105.0°
0.6	40.0°	−112.9°	149.6°	−105.0°
0.7	40.0°	−107.9°	143.7°	−105.0°
0.8	40.0°	−101.5°	137.4°	−105.0°

Table 6.2: The initial joint angles

and take 1.1 s each; the coefficients of the polynomials are determined based on the assumption that the initial and the final values of the end-effector tangential acceleration for each region are zero. Consequently, given the trajectory parameters specified in Fig. 6.1, the manoeuvre takes 20.9 s to complete. However, the simulations are performed until the 50th second so as to observe the behaviour of the control system when the desired end-effector twist is zero. The initial joint angles are reported in Table 6.2.

As illustrated in Fig. 6.2(c), the joint torques are zero when the manoeuvre finishes. Nevertheless, as seen from Figs. 6.2(a) and 6.3, the joints are still moving thereafter. Our results[9] have shown that, if the control law does not change, albeit the end-effector remains almost fixed, the joints keep rotating indefinitely due to lack of damping. As a consequence, despite the small values of the flexural generalized coordinates and generalized velocities at the time the task is completed, the vibrations of the flexible links continue. To remedy this problem, one can add a light viscous damping to the computed-torque control given by eq. (6.32)[10]. Although this imposed damping solves the problem of indefinite rotation of the joints, its sudden presence has the effect of an impulse function on the system, which causes a jump in the flexural generalized velocities. This behaviour is clearly seen in Fig. 6.5.

The initial and final postures of the manipulator are shown in Fig. 6.4. As seen from this figure and from Fig. 6.2(a), the joint-space trajectory is not cyclic; that is, the posture of the manipulator at the end of a task is different from that at the

[9]These results are not included here as they would unnecessarily increase the bulk of the thesis.
[10]As it turns out, this has also been suggested by Sharf (1996).

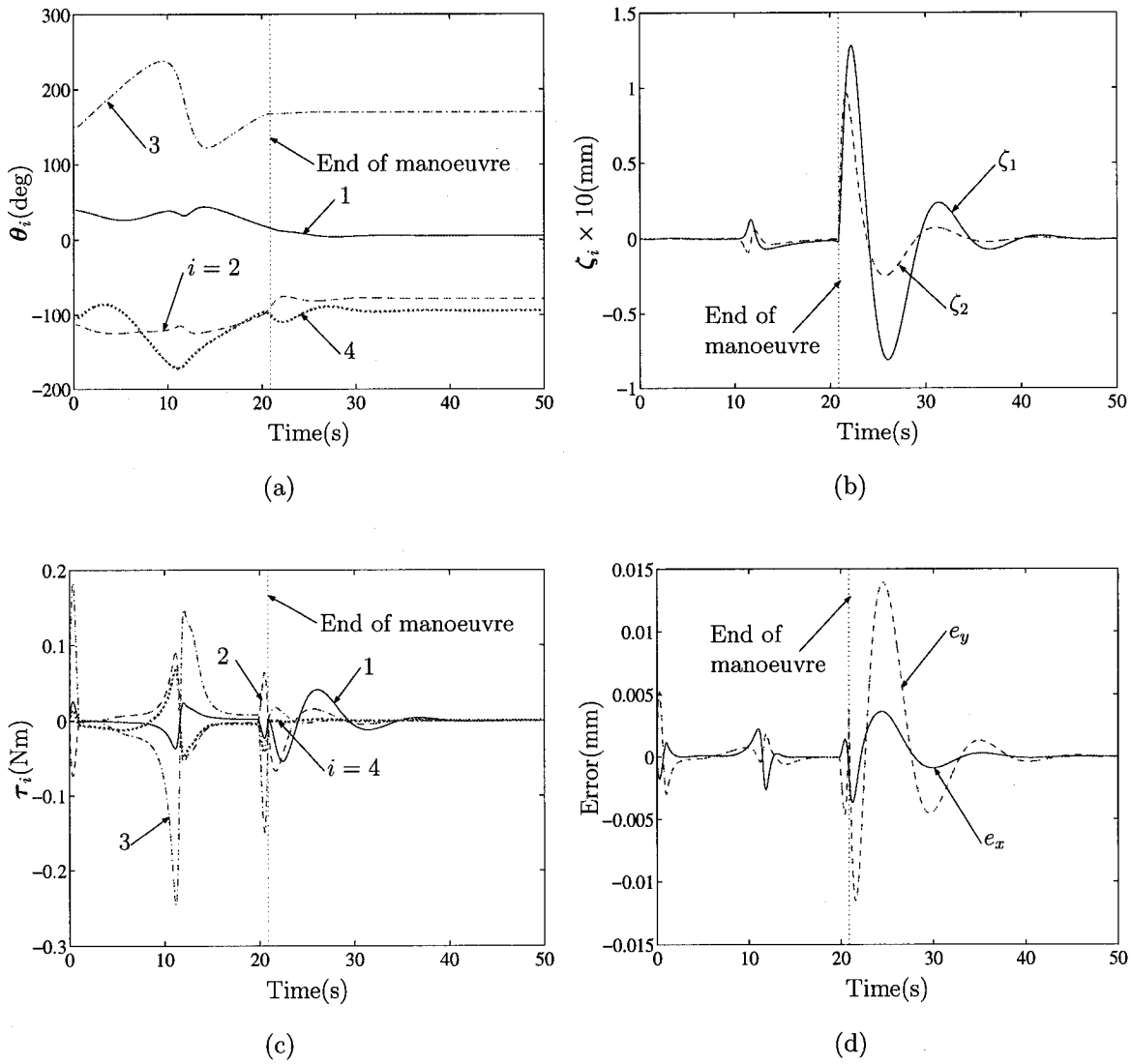

Figure 6.2: Joint angles (a), flexural coordinates (b), actuation torques (c), and end-effector trajectory errors (d) for $R = 0.6$ m; $K_p = 250$ and $K_t = 150$

beginning, even though the Cartesian trajectory of the end-effector is closed, a typical phenomenon in redundant manipulators (Klein and Huang, 1983).

Figure 6.5 demonstrates the time history of the flexural states beside those of their estimated values—which are used in the simulations to determine the control torques—obtained through extended Kalman filtering, as explained in Chapter 5, and the estimation error. As seen from this figure, the estimation errors are quite low for

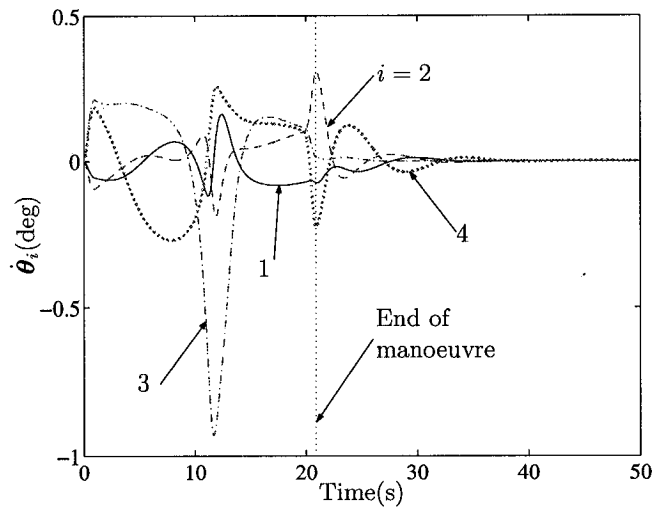

Figure 6.3: The joint speeds for $R = 0.6$ m; $K_p = 250$ and $K_t = 150$

all flexural states.

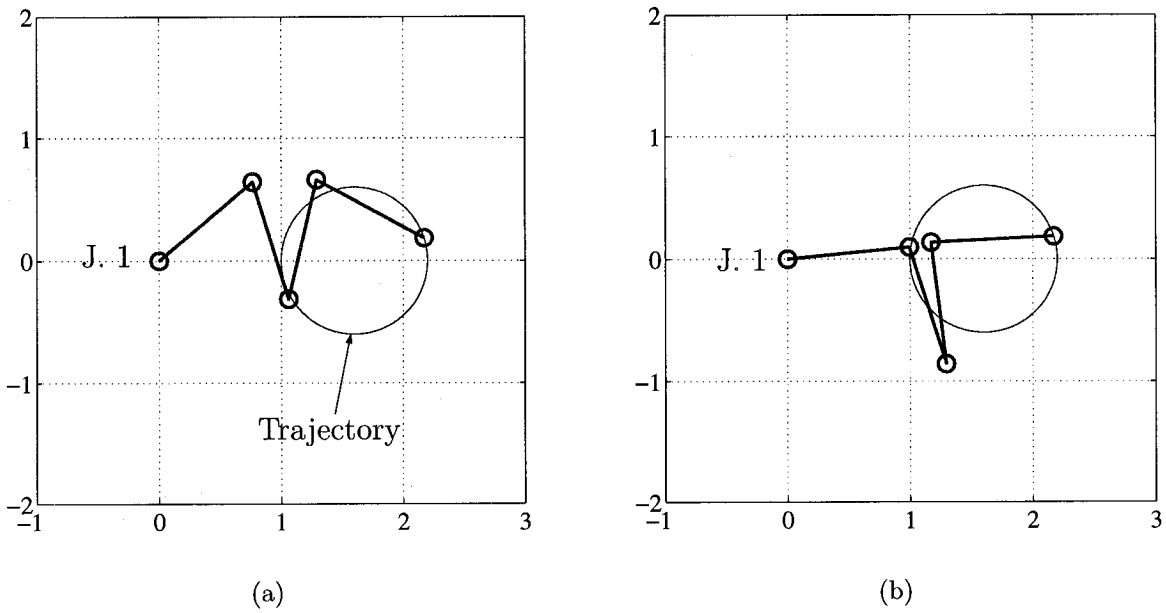

Figure 6.4: Initial (a) and final (b) postures of the manipulator for $R = 0.6$ m; $K_p = 250$ and $K_t = 150$

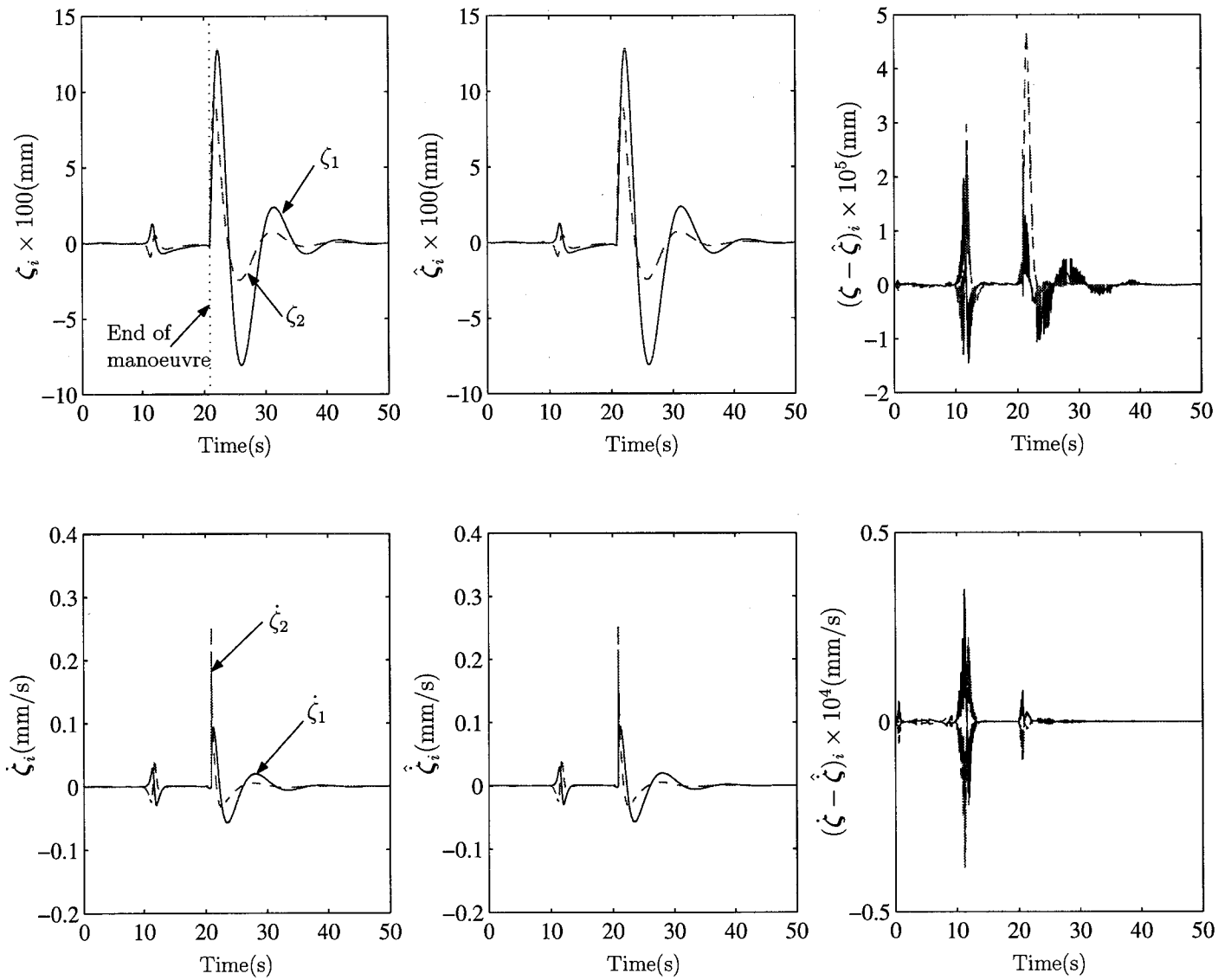

Figure 6.5: The state-estimation results for $R = 0.6$ m

6.5.1 The Effects of Motion Speed and Amplitude

To explore the effects of the speed and amplitude of the desired end-effector motion on the performance of the EKF and that of the control system, simulations have been carried out for circular trajectories 0.4, 0.5, 0.7, and 0.8 m in radius R, while keeping the control gains fixed. Since the angular velocity at the constant-speed region does not change, and neither do the acceleration and the deceleration times (see Fig. 6.1), the manoeuvre time remains unchanged at 20.9 s.

The initial joint variables used in the simulations are given in Table 6.2. They have been chosen so as to put the end-effector on its desired location at the beginning of the manoeuvre; in other words, there is no *initial disturbance.* Furthermore, it is apparent from the values that the first and last joint angles have been kept fixed while the other two are calculated using the initial position of the end-effector; all initial postures belong to the same branch.

The results are plotted in Figs. 6.6–6.17. As seen in these figures, the general behaviour explained for the $R = 0.6$ m case also holds here. However, as shown in Figs. 6.11, 6.8, 6.5, 6.14, and 6.17, the larger the end-effector trajectory the larger the motor torques and the higher the deformation of the flexible links. Naturally, the estimation errors also grow accordingly, but still remain 3–5 orders of magnitude smaller than the flexural states themselves.

6.5.2 The Effects of the Control Gains

The results reported in this subsection illustrate the effects of the control-gain changes on the performance of the control system as far as the tracking error and the deformation of the flexible links are concerned. The state-estimation results are not shown here, as the state estimation is virtually not affected by variations in the control gains.

The control gains $\mathbf{K}_p$ and $\mathbf{K}_t$ are taken to be $K_p\mathbf{1}$ (1/s^2) and $K_t\mathbf{1}$ (1/s), respectively. While K_t is kept fixed at 150, K_p is given values 25, 50, 100, 250, and 300, the results being shown in Figs. 6.18, 6.19, 6.20, 6.21, and 6.22, respectively. The results

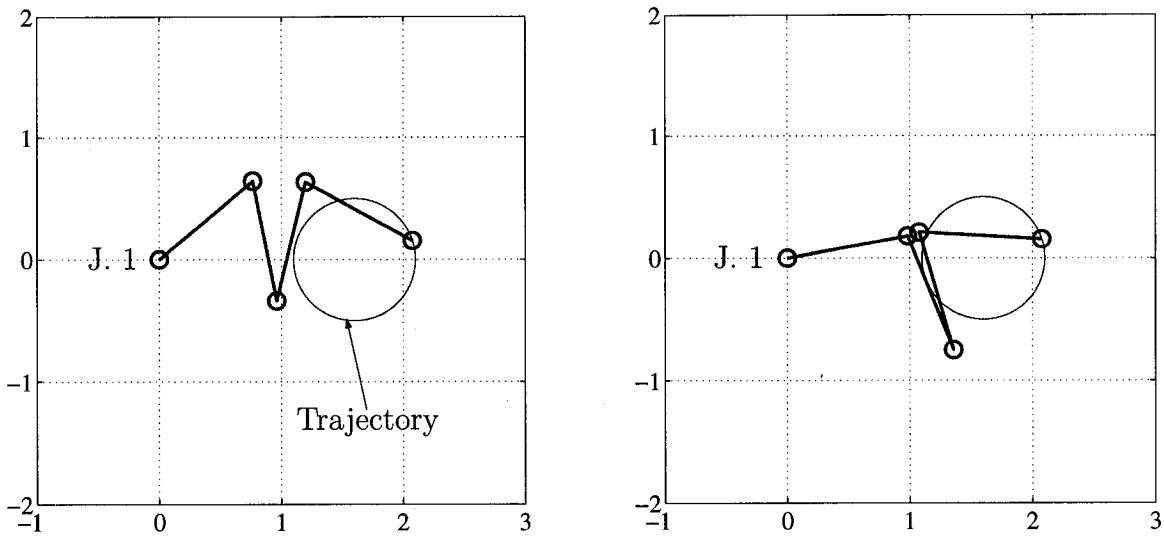

Figure 6.6: Initial (left) and final (right) postures of the manipulator for $R = 0.5$ m

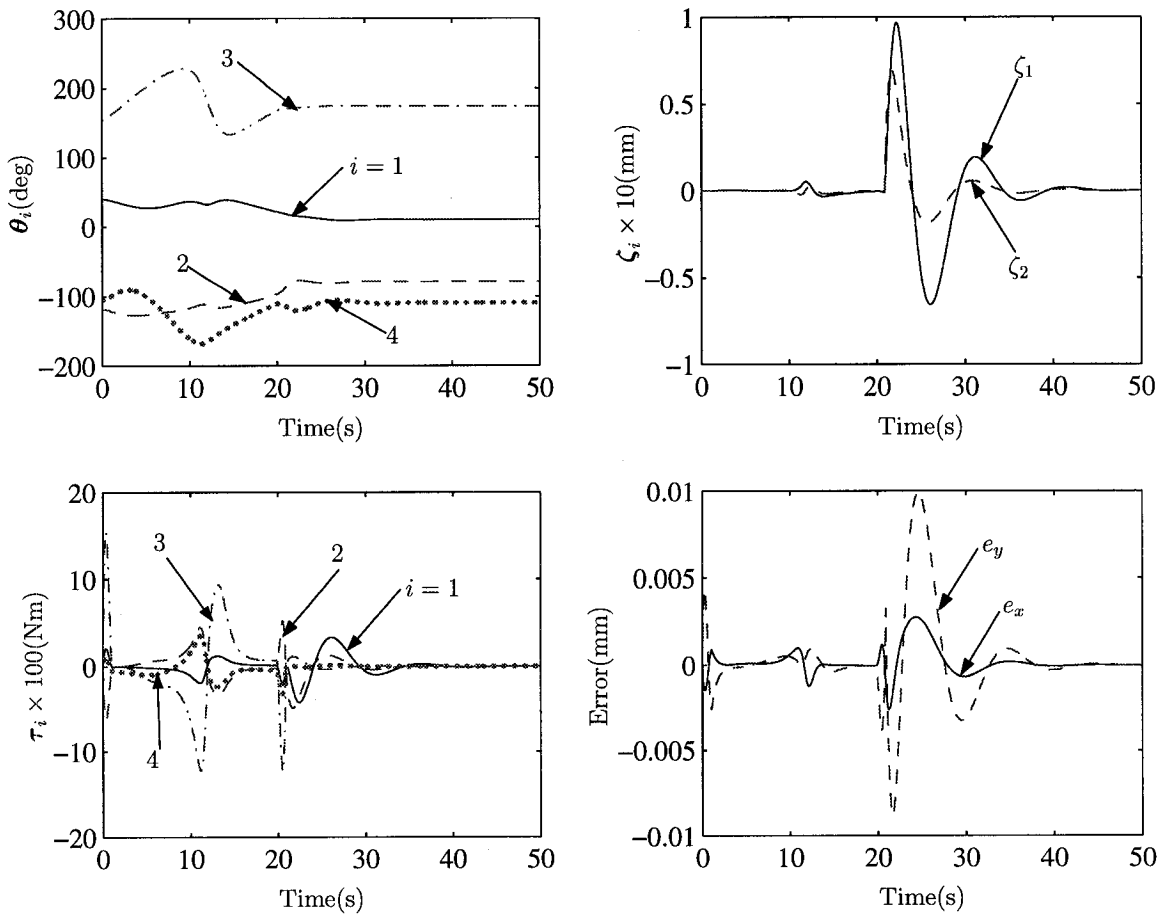

Figure 6.7: Results for $R = 0.5$ m

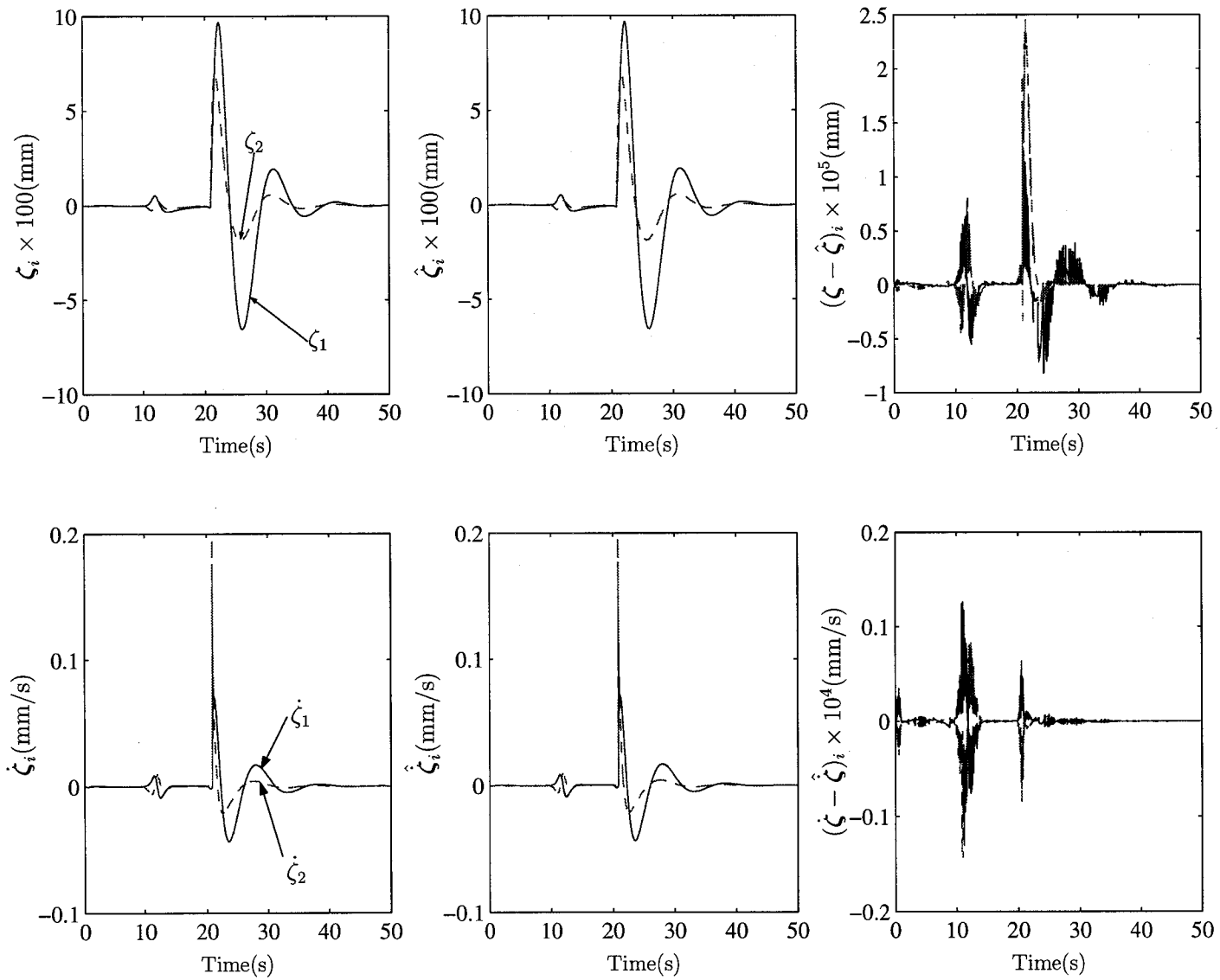

Figure 6.8: The state-estimation results for $R = 0.5$ m

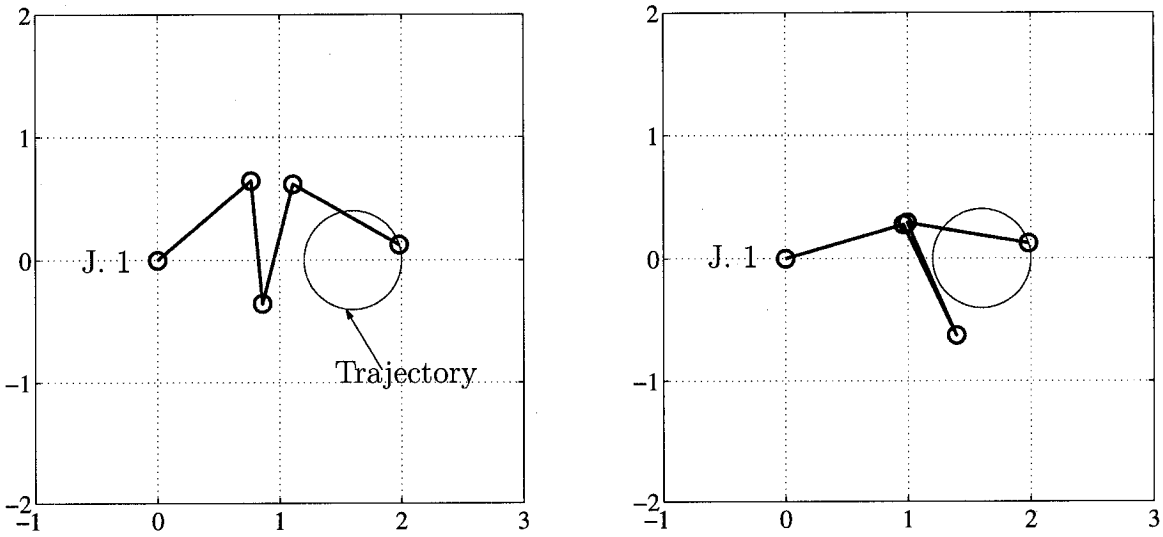

Figure 6.9: Initial (left) and final (right) postures of the manipulator for $R = 0.4$ m

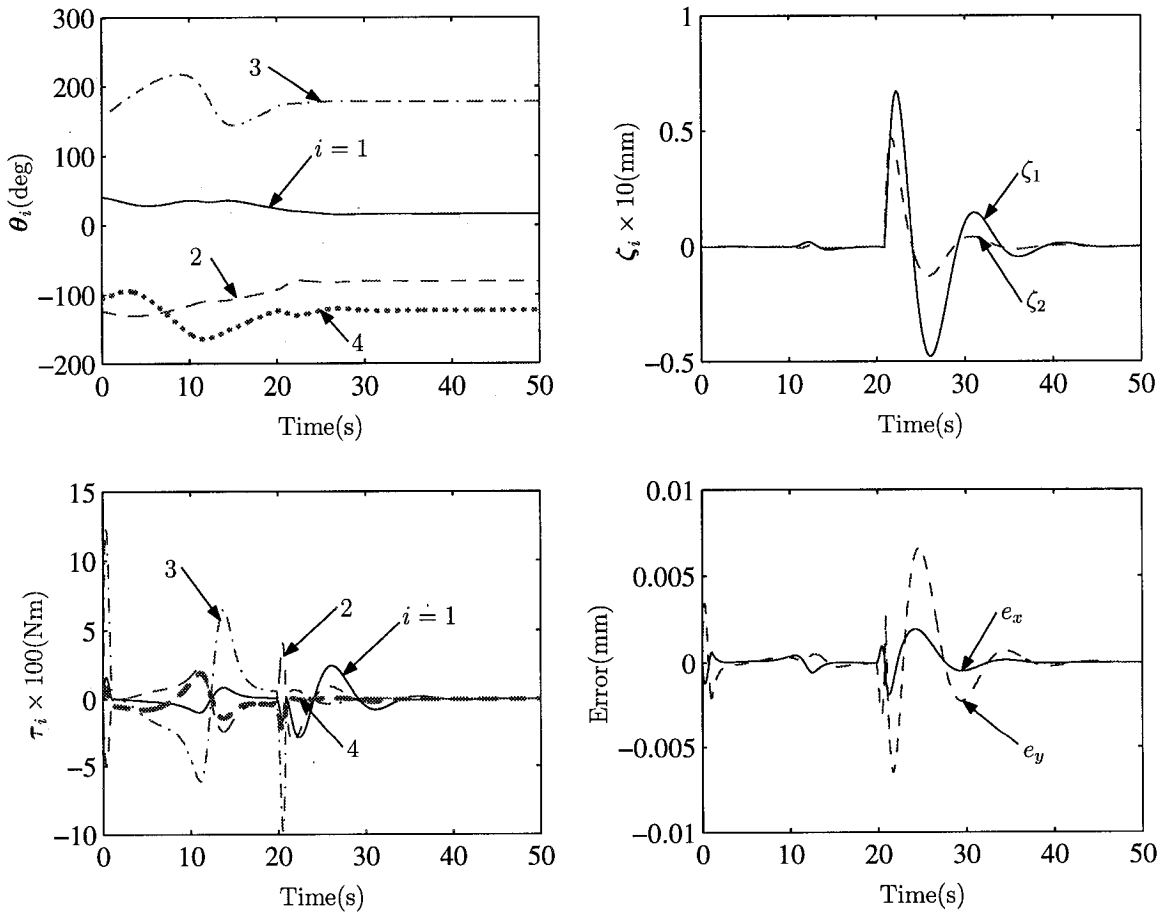

Figure 6.10: Results for $R = 0.4$ m

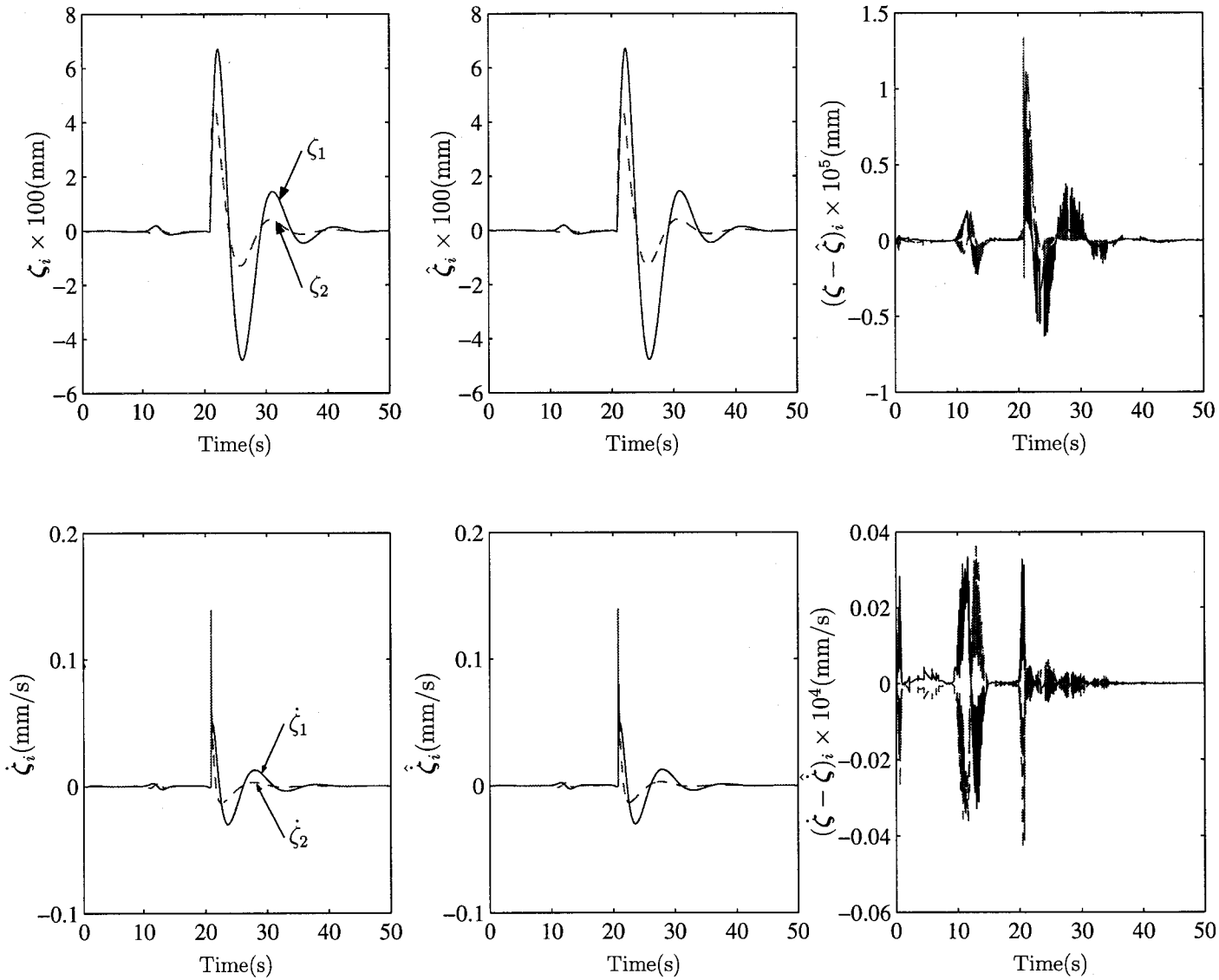

Figure 6.11: The state-estimation results for $R = 0.4$ m

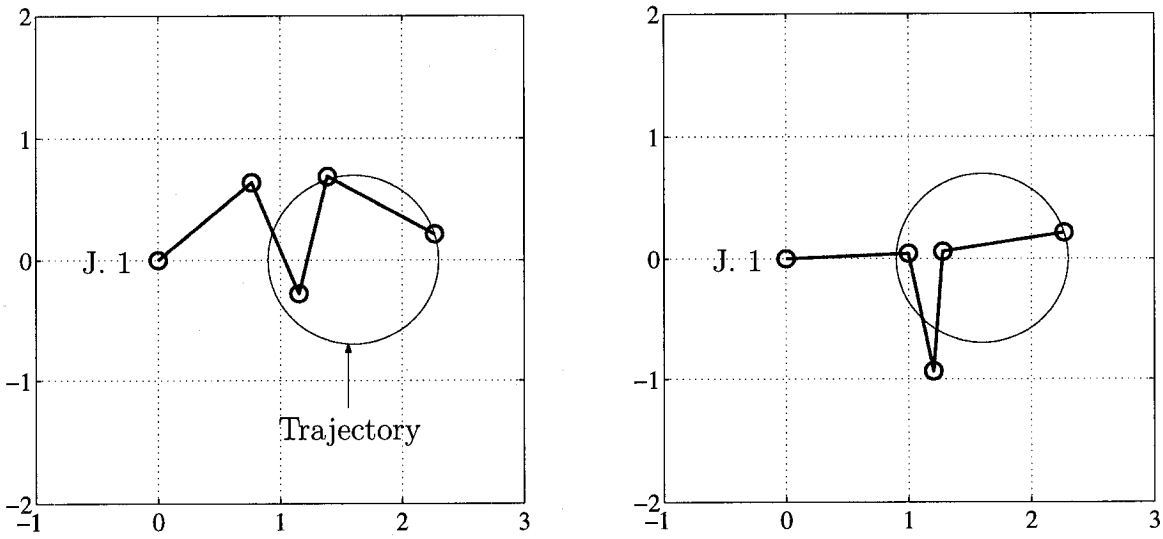

Figure 6.12: Initial (left) and final (right) postures of the manipulator for $R = 0.7$ m

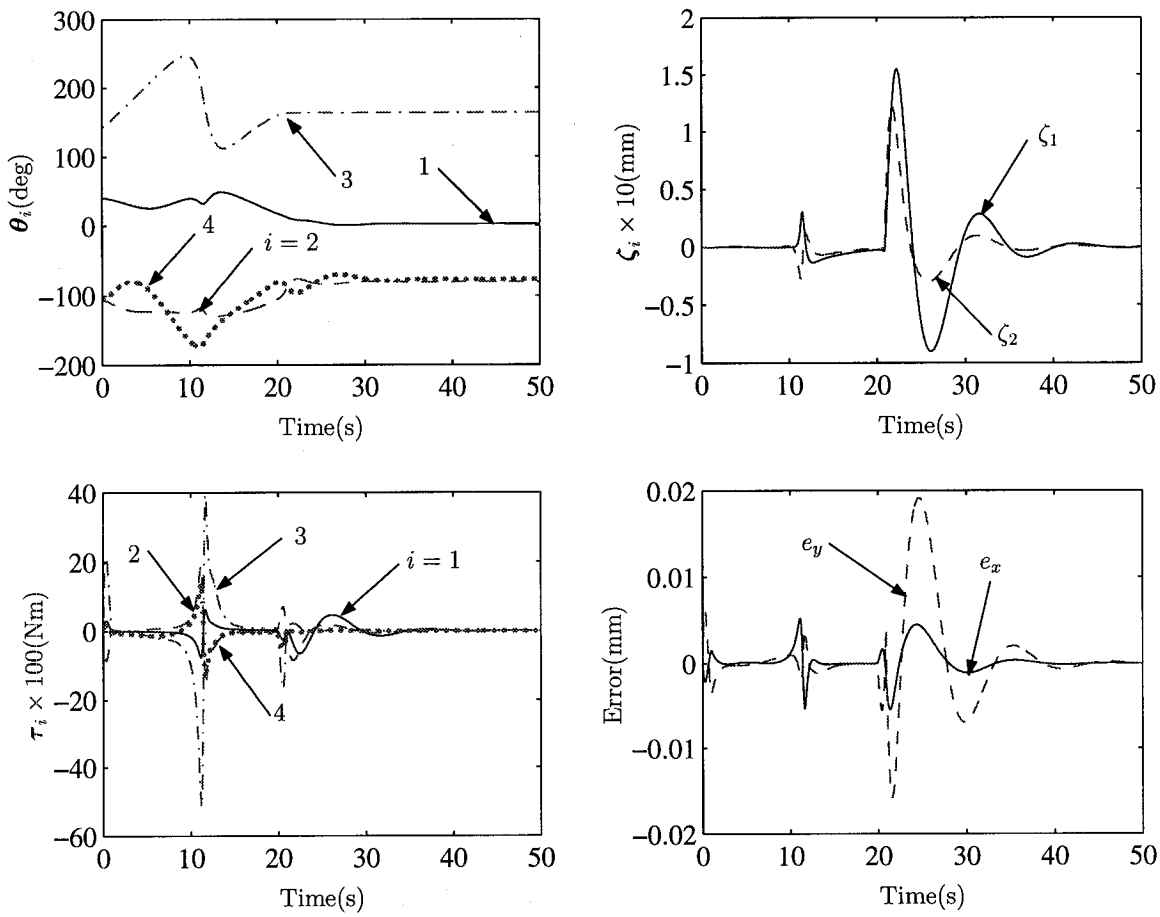

Figure 6.13: Results for $R = 0.7$ m

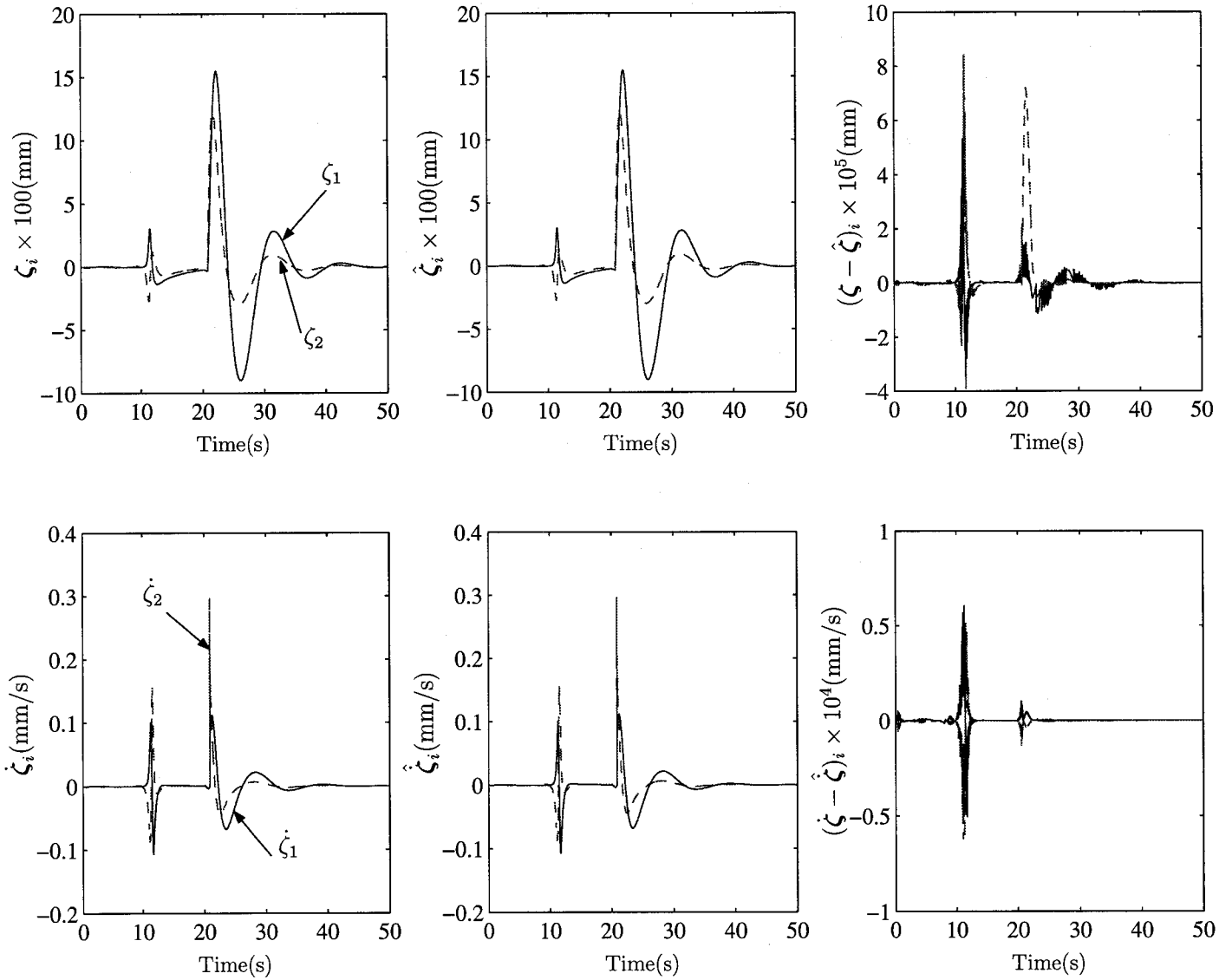

Figure 6.14: The state-estimation results for $R = 0.7$ m

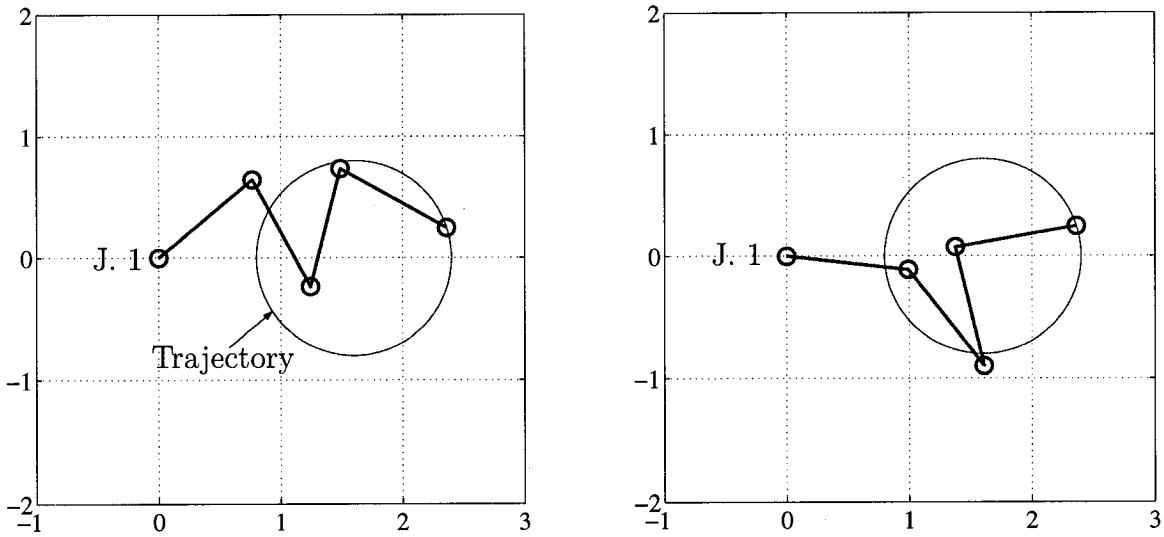

Figure 6.15: Initial (left) and final (right) postures of the manipulator for $R = 0.8$ m

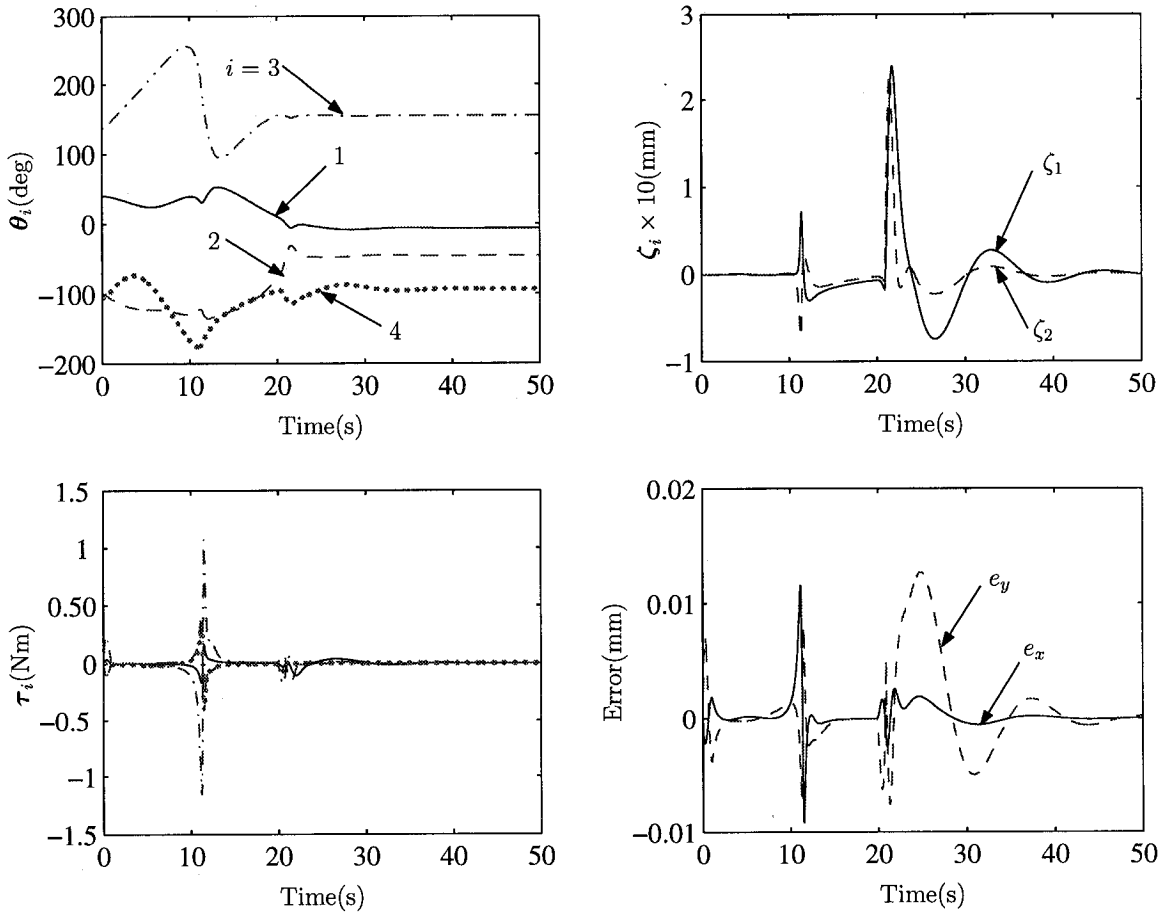

Figure 6.16: Results for $R = 0.8$ m

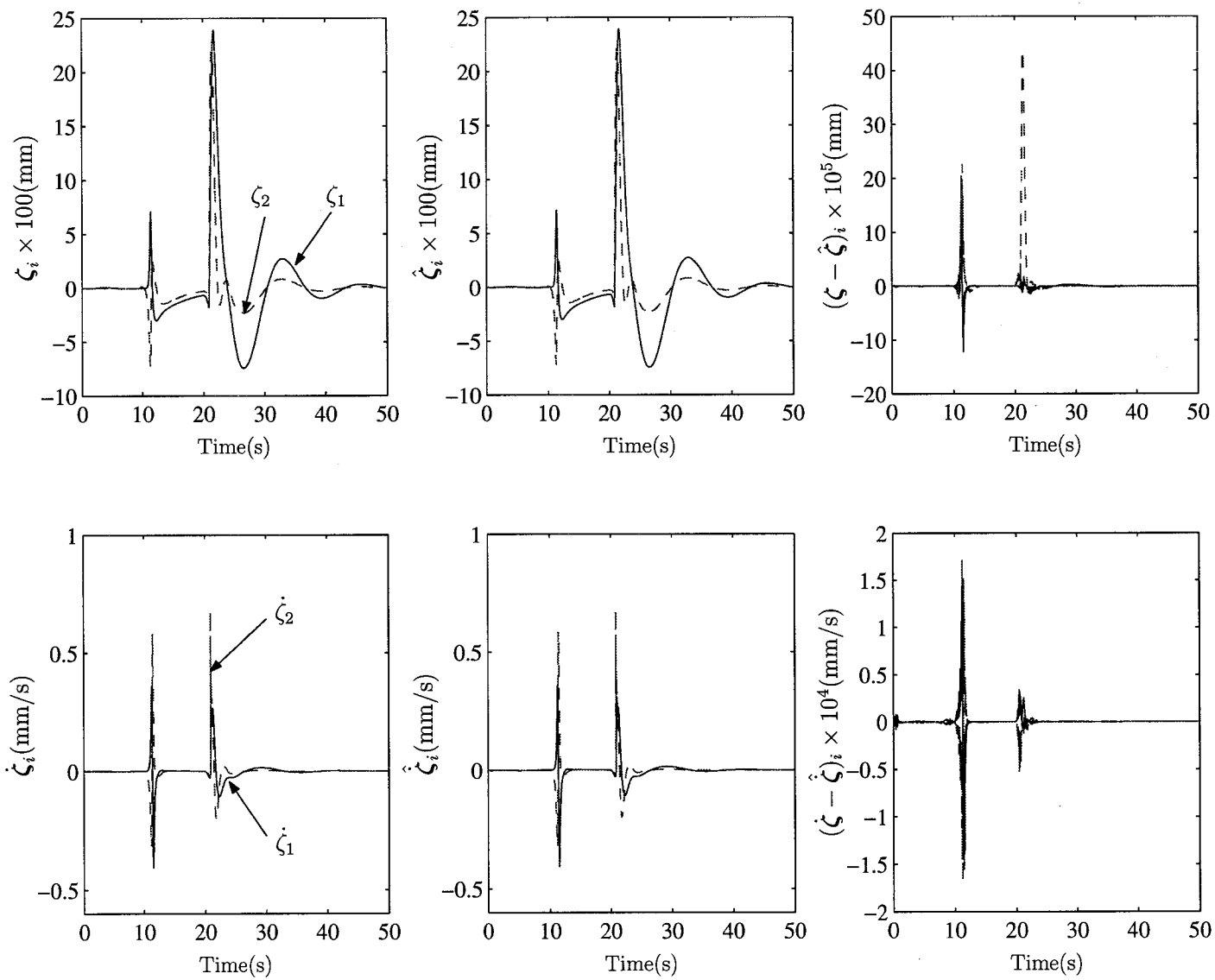

Figure 6.17: The state-estimation results for $R = 0.8$ m

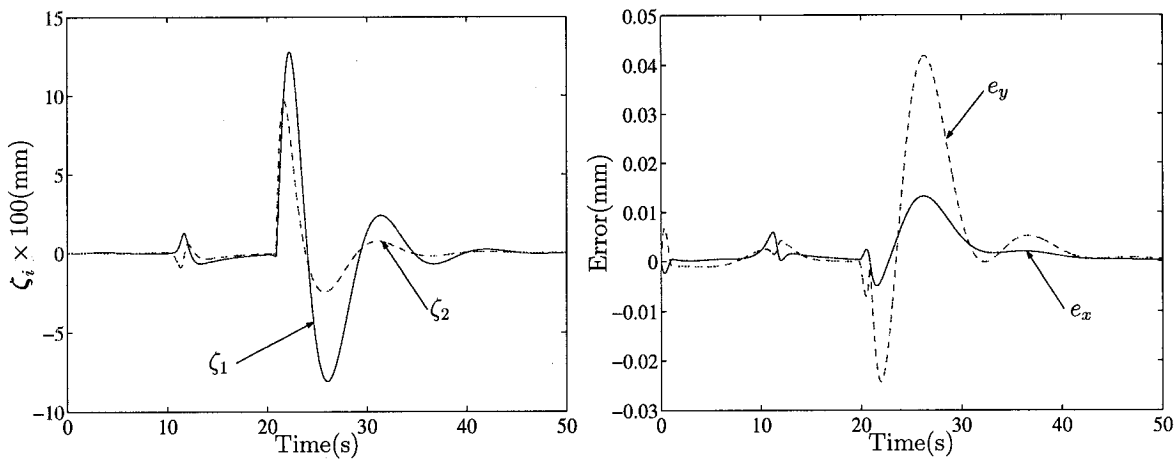

(a) (b)

Figure 6.18: The flexural coordinates (a) and the tracking error (b) for $K_p = 25$ and $K_t = 150$

exhibit no observable influence on the vibration-dampening behaviour of the system, whether during the task-execution or afterwards. This is indeed expected because the objective of the vibration-control scheme is to reduce the excitation force, no matter what happens within the control system. Now, the system is just doing that. The same behaviour is seen when the derivative-action gain is changed.

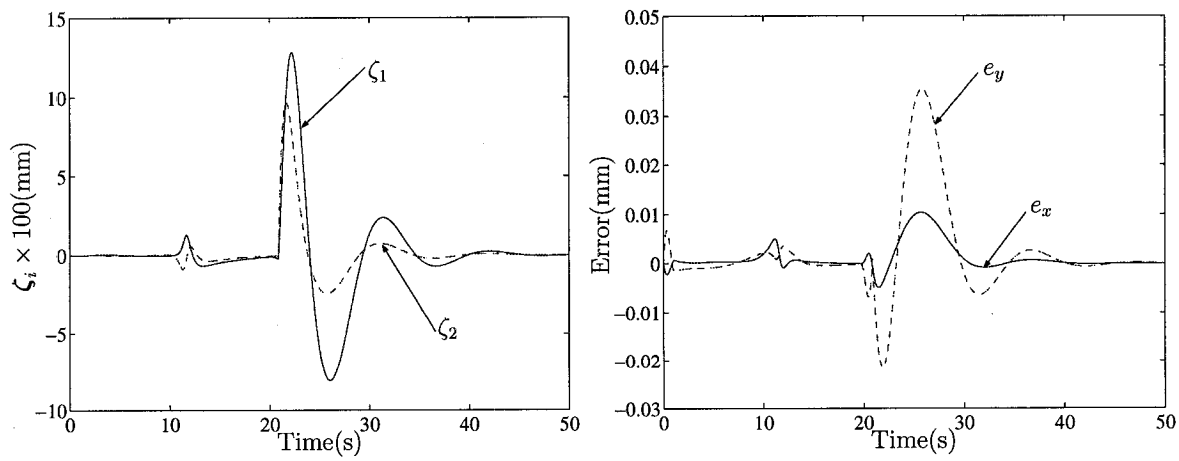

(a) (b)

Figure 6.19: The flexural coordinates (a) and the tracking error (b) for $K_p = 50$ and $K_t = 150$

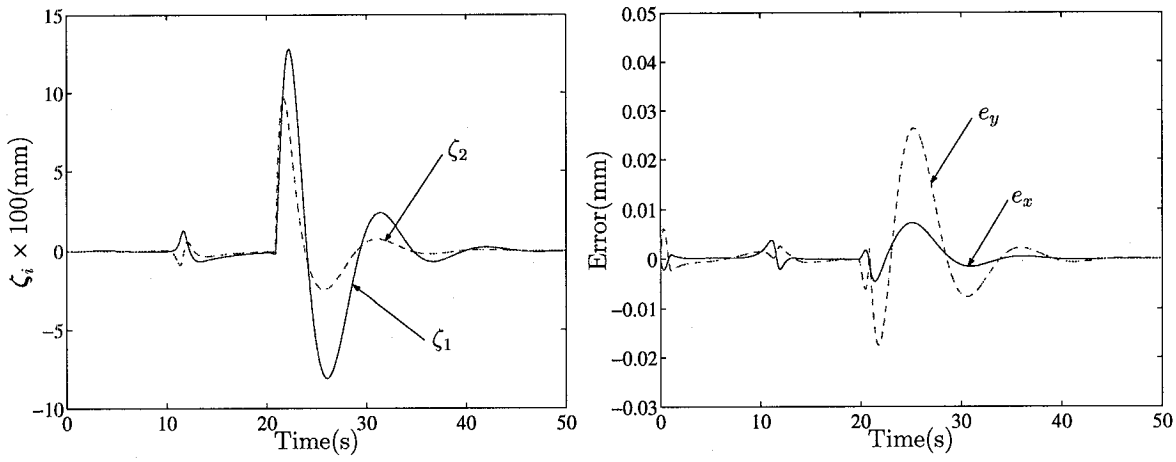

(a) (b)

Figure 6.20: The flexural coordinates and the tracking error for $K_p = 100$ and $K_t = 150$

For the error in the end-effector trajectory, however, the gain change does affect the response, and the effects are to a great extent typical: Increasing K_p brings about faster responses with smaller-amplitude errors. As a result, the settling time becomes smaller. This is particularly evident in the *post-manoeuvre* region of the responses, where the system behaves like a linear system due to the small variations in the joint

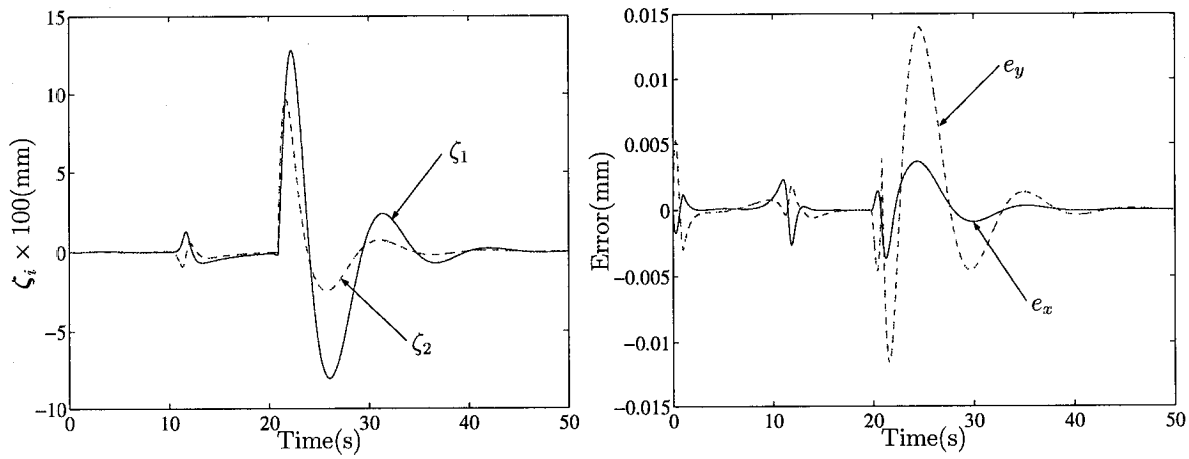

(a) (b)

Figure 6.21: The flexural coordinates (a) and the tracking error (b) for $K_p = 250$ and $K_t = 150$

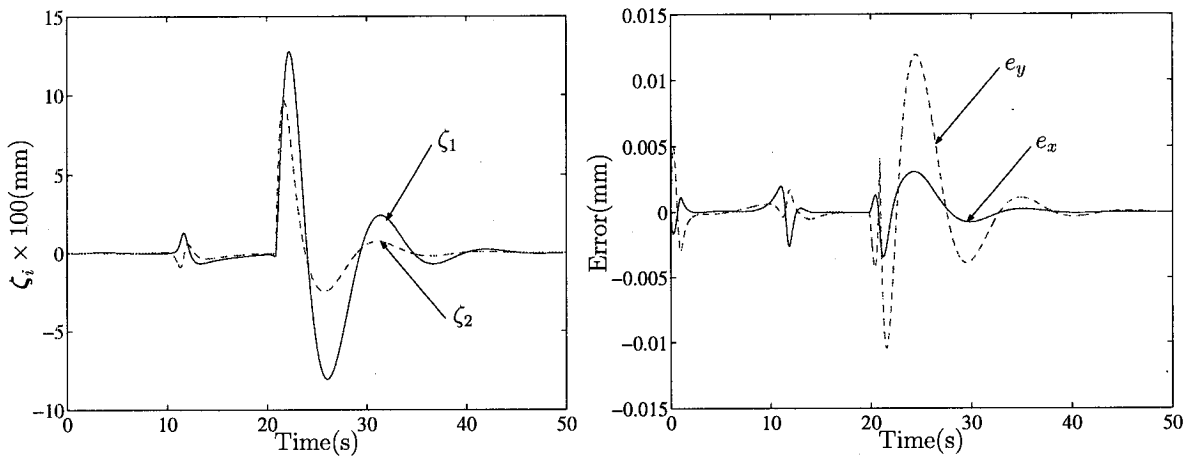

(a) (b)

Figure 6.22: The flexural coordinates (a) and the tracking error (b) for $K_p = 300$ and $K_t = 150$

angles and flexural coordinates.

To observe the effects of variations in the derivative-action gain on the behaviour of the control system, the gain K_p is kept fixed at 250 while K_t is given values 25, 100, and 200. Figures 6.23, 6.24, 6.25 show the simulation results for these control gains. As seen in the figures, increasing this gain from 25 to 150 constantly decreases

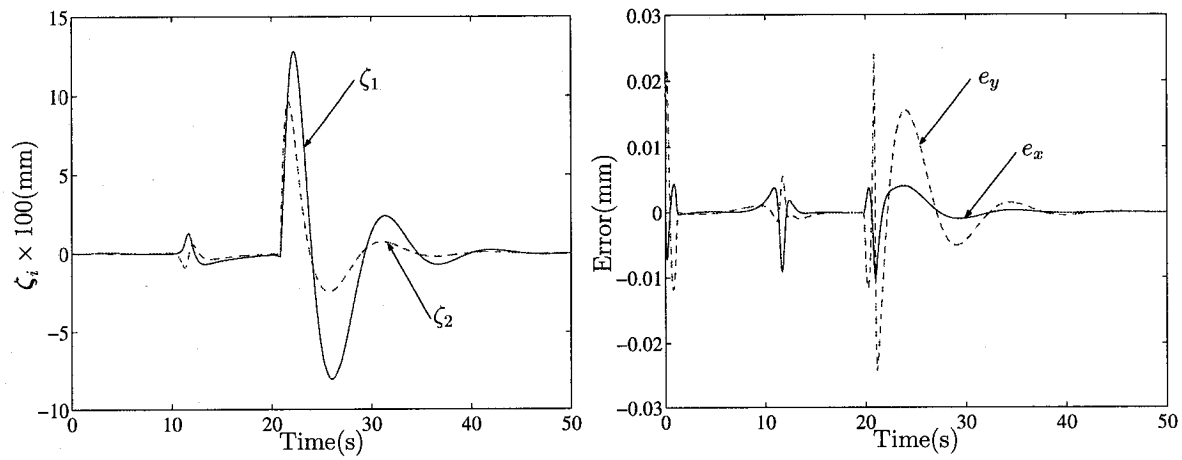

(a) (b)

Figure 6.23: The flexural coordinates (a) and the tracking error (b) for $K_p = 250$ and $K_t = 25$

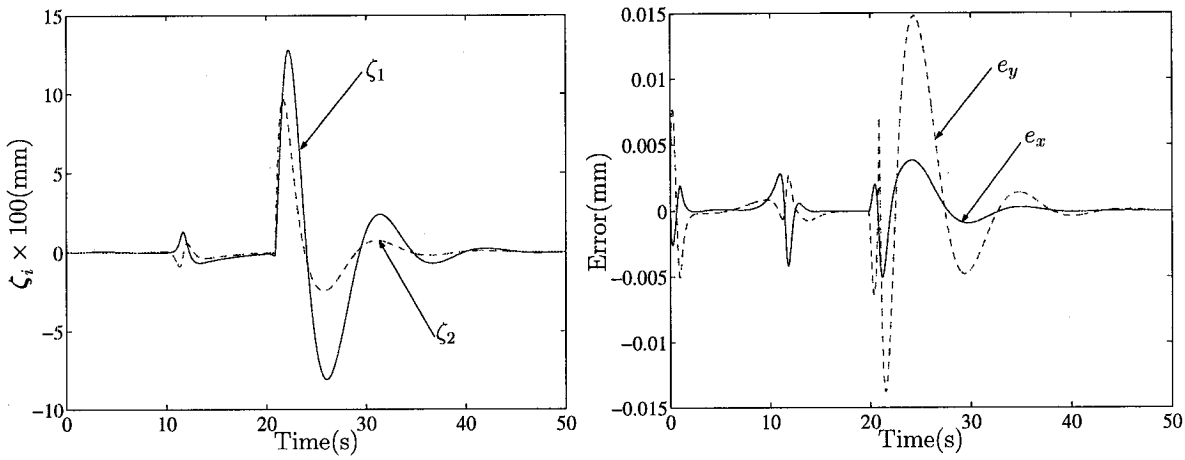

(a) (b)

Figure 6.24: The flexural coordinates (a) and the tracking error (b) for $K_p = 250$ and $K_t = 100$

the tracking error, but, if the gain is further increased to 200, the tracking error, while decreasing at the beginning, ends up with a drift. It seems that the reason should be numerical error because both the x and y components of the tracking error show added noise-like effects. The same effect is not present in the flexural-coordinate response. The reason could be that all generalized coordinates are obtained through

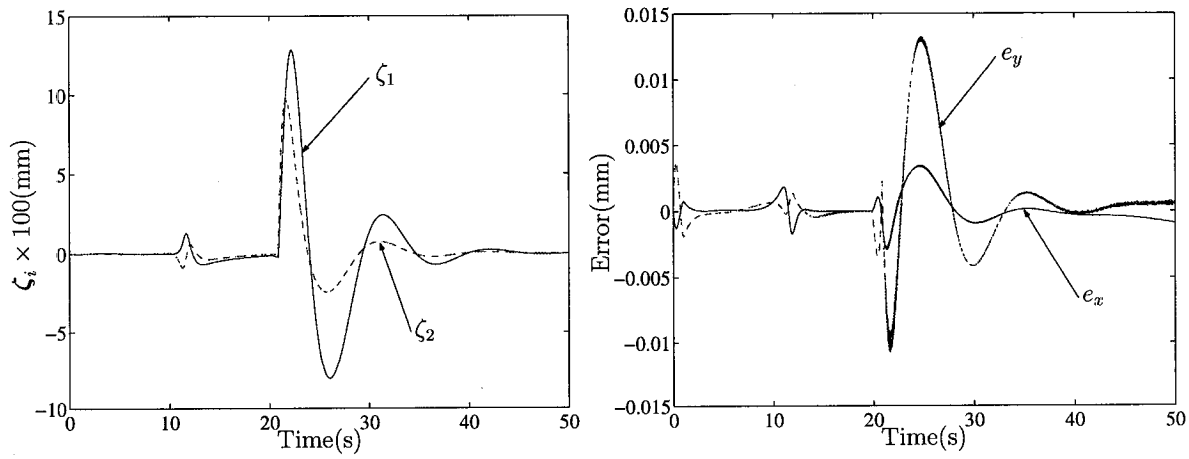

(a) (b)

Figure 6.25: The flexural coordinates (a) and the tracking error (b) for $K_p = 250$ and $K_t = 200$

the integration of the dynamics equations by the stiff integrator `ode15s` of MATLAB.

Chapter 7

Conclusions

7.1 Summary

The problems of dynamics modelling, flexural-state estimation, and the control of kinematically redundant manipulators with flexible and rigid subsystems were studied.

The dynamics of each submanipulator was obtained separately by means of assembling the dynamics equations derived for all links and then eliminating all extra equations using the Natural Orthogonal Complement (NOC). Then, the NOC was used once again to obtain the dynamics model of the entire system. The two separate sets of dynamics equations were also beneficial to the estimation of the flexural states of the flexible submanipulator; the flexural states are composed of the flexural generalized coordinates and the flexural generalized velocities. It was suggested that these states can be estimated if the twist and the twist-rate of the base of the rigid submanipulator, taken to be the outputs, are known. This was done by feeding the outputs, inferred from the measurement data, to an extended Kalman filter whereby the dynamics of the flexible manipulator is assumed to be the governing dynamics.

Therefore, a pose and twist estimation algorithm which uses redundant acceleration sensing was proposed. The acceleration measurements were considered to be made using an accelerometer array which was assumed to be rigidly attached to the base of the rigid submanipulator. All the kinematic relations were written in the body frame, thus having the advantage of pose-estimation errors not propagating to

the twist estimates. It was shown that, mainly due to the calibration errors and the double integration of the accelerometer data, the results could turn out to be unstable.

To overcome the above-mentioned instability problem, a novel iterative calibration procedure for accelerometer arrays was devised. The procedure was based on the compatibility of point accelerations of a rigid body undergoing a general motion. It was demonstrated that, using this procedure, one can estimate and thus account for fairly large installation errors, the direct calculation of the angular-velocity vector from acceleration data thus being possible. The calibration scheme is so powerful that, as long as the accelerometer orientations are roughly known, the scheme produces highly accurate results.

State estimation requires linear state-output relations. However, the flexural states are *nonlinearly* related to the output kinematic variables. Therefore, the state-output relations had to be linearized. That, in turn, required calculating the partial derivatives of the twist and the twist-rate with respect to the generalized coordinates, generalized velocities, and generalized accelerations. Among all the partial derivatives, that of the twist with respect to the generalized coordinates is the most important one. The reason is that the others are either directly related to the Jacobian matrix, or that it is this very partial derivative which can be utilized to derive the rest in closed form through algebraic manipulations.

To obtain compact, closed-form expressions for the above-mentioned partial derivatives, rather general definitions for the twist vector and the Jacobian matrix—in the context of kinematic chains—were given. Next, the partial derivatives sought were derived in terms of the Jacobian, its time rate, and other available kinematic variables. These relations make it possible to evaluate the partial derivatives without resorting to extra symbolic manipulations.

The control algorithm employed was based on the well-known computed-torque control method. However, due to the kinematic redundancy of the manipulator, trajectory planning was a part of the problem as well. In order to resolve the redun-

dancy, a joint-space trajectory with minimum-norm joint acceleration was obtained using the Moore-Penrose generalized inverse. In this regard, two ways of resolving the redundancy were considered: *Flexible-link resolution*, and *rigid-link resolution*. The latter corresponded to neglecting the flexibility of the manipulator, whereas the former meant accounting for all the flexibilities modelled in the dynamics of the system. Then, since moving the joints could excite vibrations in the flexible links, a self-motion that would minimize the excitation force in the modal space was computed. The degree of redundancy of the system dictated the number of the "natural modes" to be dampened. Furthermore, it was shown that, under certain conditions, this control algorithm would be stable.

Albeit the results reported in this thesis have been developed mainly for the particular purposes explained at each occasion, other applications also seem possible. For example, even though the pose-and-twist-estimation algorithm was originally intended for the pose and twist estimation of rigid bodies undergoing vibratory motions, it may also be applied for mobile-robot localization. Another example of such a multipurpose result is the closed-form expression we obtained for the partial-derivative of the twist with respect to the generalized coordinates. This expression was derived for the linearization of the state-output relations. However, it can as well be useful in the dynamics modelling of multibody systems at large, or in the derivation of optimal-control relations for such systems.

7.2 Recommendations for Further Research

To further examine the effectiveness of the methods developed here, the practical implementation of the proposed observer-controller system on a test manipulator with rigid and flexible submanipulators should certainly be helpful. As a follow-up to the feasibility study that motivated this work, Professors Jorge Angeles of McGill University and Rajni Patel of University of Western Ontario secured the NSERC

financing of such a system[1]; the system is expected to be operational in 2003.

The algorithm proposed in this thesis for pose and twist estimation is based on the assumption that each triaxial accelerometer measures all three components of the acceleration of a single point. However, this is actually not true: A triaxial accelerometer is, in fact, composed of three separate single-axis accelerometers located at small offsets with respect to each other. Consequently, what each of these three accelerometers measures is actually one single component of the acceleration of the point at which that particular accelerometer is located. Therefore, it would be desirable to account for these offsets in the procedure; this will reduce the errors incurred in an actual task of pose and twist estimation. Moreover, an experimental study of the proposed algorithm can shed more light on the issues involved and is, thus, recommended.

The partial-derivative expressions we have derived can only be used for the systems in which the generalized velocities are *not* dependent on the generalized coordinates. As such, the relations obtained are not directly applicable to a large class of systems; included are parallel manipulators and nonholonomic systems. This limitation was not a problem for this thesis, however, because the scope of the thesis only included serial manipulators, for which, by nature, the generalized velocities are independent of the generalized coordinates. To overcome this limitation, one can examine the steps taken to prove Theorem 1 and make the changes required to accommodate a wider range of systems.

One of the major problems that we were faced with, for the generation of the final results, was the instability of the control law. Even though it was shown that under certain conditions the control system would be stable, it was not possible to predict whether the conditions remained fully met during the entire course of the end-effector manoeuvre. Furthermore, the behaviour of the control was quite dependent on the selection of the initial posture of the manipulator, i.e., by a wrong choice of initial joint angles the control could turn out unstable, which is, of course, a known problem

[1]The project is registered under the title "A frame work for the design and control of a macro-micro manipulator system," and the reference number STGP215729-98.

of nonlinear systems. Hence, a more thorough investigation of the control problem is recommended.

Finally, in the dynamics modelling of the *RRRR* manipulator studied as an example in Chapter 6, the *dynamic-stiffening effect* was neglected in the interest of the model simplicity. It has been established in the literature that neglecting this effect may render the dynamics model unstable, whereas the actual system is stable. Thus, it could be anticipated that accounting for this effect, during the derivation of the mass and the stiffness matrices, may indeed help solve the instability problem.

Bibliography

Alder, L. J. and Rock, S. M., 1993, "Adaptive Control of a Flexible-Link Robotic Manipulator with Unknown Payload Dynamics," in *Proc. The American Control Conf.*, pp. 2088–2092, San Fransisco, CA.

Alder, L. J. and Rock, S. M., 1994, "Experiments in Control of a Flexible-Link Robotic Manipulator with Unknown Payload Dynamics: An Addaptive Approach," *The Int. J. Robotics Research*, **13**(6):481–495.

Angeles, J., 1986, "Automatic Computation of the Screw Parameters of Rigid-Body Motions, Part I: Infinitesimally Separated Positions," *ASME J. Dynamic Syst., Meas., and Control*, **108**(6):39–43.

Angeles, J., 1987, "Computation of Rigid-body Angular Acceleration from Point Acceleration Measurements," *ASME J. Dynamic Syst., Meas., and Control*, **109**:124–127.

Angeles, J., 1990, "Rigid-body Pose and Twist Estimation in the Presence of Noisy Redundant Measurements," in *Proc. Eighth CISM–IFToMM Symp. Theory and Practice of Robots and Manipulators*, pp. 69–78, Cracow.

Angeles, J., 1999, "The Angular-Acceleration Tensor of Rigid-Body Kinematics and Its Properties," *Archive of Applied Mechanics*, **69**(3):204–214.

Angeles, J., 2002, *Fundamentals of Robotic Mechanical Systems, Theory, Methods, and Algorithms*, 2nd ed., Springer Verlag, New York, NY.

Angeles, J. and Ostrovskaya, S., 2002, "The Proportional-Damping Matrix of

Arbitrarily-Damped Linear Mechanical Systems," *ASME J. Applied Mechanics*, **69**:649–656.

Arfken, G., 1985, *Mathematical Methods for Physicists*, 3rd ed., Academic Press, Orlando, FL.

Åström, K. J. and Wittenmark, B., 1997, *Computer-Controlled Systems: Theory and Design*, 3rd ed., Prentice-Hall, Upper Saddle River, NJ.

Baerveldt, A.-J. and Klang, R., 1997, "A Low-Cost and Low-Weight Attitude Estimation System for an Autonomous Helicopter," in *Proc. IEEE Int. Conf. Intelligent Engineering Systems*, pp. 391–395.

Ball, R. S., 1900, *A Treatise on the Theory of Screws*, Cambridge University Press.

Book, W. J., 1993, "Structural Flexibility of Motion Systems in the Space Environment," *IEEE Trans. Robotics and Automation*, **9**(5):524–530.

Book, W. J. and Loper, J. C., 1999, "Inverse Dynamics for Commanding Micromanipulator Inertial Forces to Damp Macromanipulator Vibration," in *Proc. IEEE/RSJ Int. Conf. Intelligent Robot and Systems*, vol. 2, pp. 707–714.

Brogan, W. L., 1991, *Modern Control Theory*, 3rd ed., Prentice-Hall, Englewood Cliffs, NJ.

Browder, A. M. and Alexander, R. M., 1988, "A General Approach to Modal Analysis for Time-Varying Systems," *AIAA paper 88-2356*, pp. 1162–1168.

Caines, P. E., 1999, *Lectures on Non-linear Systems*, Department of Electrical and Computer Engineering, McGill University, Montreal, Canada.

Cannon, R. H., Jr. and Schmitz, E., 1984, "Initial Experiments on the End-Point Control of a Flexible One-Link Robot," *The Int. J. of Robotics Research*, **3**(3):62–75.

Canudas de Witt, C. and Slotine, J.-J. E., 1991, "Sliding Observers for Robot Manipulators," *Automatica*, **27**(5):859–864.

Carusone, J., Buchan, K. S., and D'Eluterio, G. M. T., 1993, "Experiments in End-Effector Tracking Control for Structurally Flexible Space Manipulators," *IEEE Trans. Robotics and Automation*, **9**(5):553–560.

Carusone, J. and D'Eluterio, G. M. T., 1993, "Tracking Control for End-Effector Position and Orientation of Structurally Flexible Manipulators," *J. Robotic Systems*, **10**(6):847–870.

Chiang, W.-W., Kraft, R., and Cannon, R. H., Jr., 1991, "Design and Experimental Demonstration of Rapid, Precise End-Point Control of a Wrist Carried by a Very Flexible Manipulator," *The Int. J. Robotics Research*, **10**(1):30–40.

Cho, K.-S., 1995, *Feedback Control of Planar Mechanisms with Structurally-Flexible Links: Theory and Experiments*, Ph.D. Thesis, Department of Mechanical Engineering, McGill University, Montreal, Canada.

Chui, C. K. and Chen, G., 1991, *Kalman Filtering with Real-Time Applications*, Springer Series in Information Sciences, 2nd ed., Springer Verlag, New York.

Cleary, K., Nguyen, L., and Frisch, H., 1992, "A Demonstration of Vibration Reduction for a Flexible Beam Using Input Shaping," in *Proc. IEEE/RSJ Int. Conf. Intelligent Robot and Systems*, pp. 1711–1716, Raleigh, NC.

Craig, J. J., 1989, *Introduction to Robotics, Mechanics and Control*, 2nd ed., Addison Wesley.

Cyril, X., 1988, *Dynamics of Flexible-Link Manipulators*, Ph.D. Thesis, Department of Mechanical Engineering, McGill University, Montreal, Canada.

Danisch, L. A., 1998, "Topological and Motion Measuring Tool," PCT Patent Application PCT/CA98/00213, Measurand, Inc., Fredricton, Canada.

Danisch, L. A., 2000, "Smart Move Human Machine Interface, Volume 1A: Report for Phase II, Part II," CSA Report CSA-ST-CR-2000-0030, STEAR 10 Project, Canadian Space Agency, St. Hubert, QC.

Danisch, L. A., Englehart, K., and Trivett, A., 1999, "Spatially Continuous Six Degrees of Freedom Position and Orientation Sensor," *Sensor Review*, **19**(2):106–112.

Doyle, J. C., 1978, "Guaranteed Margins for LQG Regulators," *IEEE Trans. Automatic Control*, **23**:756–757.

Fattah, A., 1995, *Dynamics of Robotic Manipulators with Flexible Links and Kinematic Loops*, Ph.D. Thesis, Department of Mechanical Engineering, McGill University, Montreal, Canada.

Fukuda, T. and Arakawa, A., 1989, "Optimal Control and Sensitivity Analysis of Two Links Flexible Arm with Three Degrees of Freedom," in *Proc. IEEE Conf. Decision and Control*, pp. 2101–2106, Tampa, FL.

Giardina, C. R., Bronson, R., and Wallen, L., 1975, "An Optimal Normalization Scheme," *IEEE Trans. Aerospace and Electronic Systems*, **11**:443–446.

Goldstein, H., 1980, *Classical Mechanics*, 2nd ed., Addison-Wesley, Reading, MA.

Grubin, C., 1973, "Attitude Determination for a Strapdown Inertial System Using the Euler Axis/Angle and Quaternion Parameters," in *AIAA Paper 73-900*, Key Biscayne, FL.

Hanson, M. L. and Tolson, R. H., 1995, "Reducing Flexible Base Vibrations Through Local Redundancy Resolution," *Journal of Robotic Systems*, **12**(11):767–779.

Hillsley, K. L. and Yurkovich, S., 1991, "Vibration Control of a Two-Link Flexible Robot Arm," in *Proc. IEEE Int. Conf. Robotics and Automation*, pp. 2121–2126, Sacramento, CA.

Hughes, P. C., 1987, "Space Structure Vibration Modes: How Many Exist? Which Ones Are Important?" *IEEE Control Magazine*, **7**(1):22–28.

Hunt, K. H., 2000, "Don't Cross-Thread the Screw!" in *Proc. A Symp. Commemorating the Lagacy, Works, and Life of Sir Robert Stawell Ball*, A Keynote Address, pp. 1–35, University of Cambridge, Trinity College.

Jiang, Z. and Goldenberg, A. A., 1998, "Dynamic End-Effector Trajectory Control for Flexible Micro-Macro Manipulators Using an Ideal Manifold," *JSME Int. Journal, Series C*, **41**(2):269–277.

Kalman, R. E. and Bertram, J. E., 1960, "Control System Analysis and Design via the "Second Method" of Lyapunov I: Continuous-Time Systems," *ASME J. Basic Engineering, Series D*, **82**:371–393.

Kane, T. R., Ryan, R. R., and Banerjee, A. K., 1987, "Dynamics of a Cantilever Beam Attached to a Moving Base," *J. Guidance*, **10**(2):139–150.

Kim, S.-J. and Park, Y.-S., 1996, "Motion Resolution of Flexible, Redundant Robot Manipulators for Vibration Reduction," in *Proc. Third Int. Conf. Motion and Vibration Control*, pp. 251–256, Chiba, Japan.

Kim, S.-J. and Park, Y.-S., 1998, "Self-motion Utilization for Reducing Vibration of a Structurally Flexible Redundant Robot Manipulator System," *Robotica*, **16**:669–677.

Klein, C. A. and Huang, C. H., 1983, "Review of Pseudoinverse Control for Use with Kinematically Redundant Manipulators," *IEEE Trans. System, Man, and Cybernetics*, **13**(3):245–250.

Konno, A., Uchiyama, M., Kito, Y., *et al.*, 1997, "Configuration-Dependent Vibration Controllability of Flexible-Link Manipulators," *The Int. J. Robotics Research*, **16**(4):567–576.

Kotnik, P. T., Yurkovich, S., and Özgüner, Ü., 1988, "Acceleration Feedback Control for a Flexible Manipulator Arm," *J. Robotic Systems*, **5**(3):181–196.

Lee, K.-S. and Park, Y.-S., 1998, "Vibration Reduction of Time-Varying System[s] Using a Modified Input Shaping Concept," in *Proc. Int. Conf. Motion and Vibration Control*, vol. 4, pp. 553–558, Switzerland.

Lew, J. Y. and Moon, S.-M., 1999, "Active Damping Control of Compliant Base Manipulators," in *Proc. IEEE/RSJ Int. Conf. Intelligent Robots and Systems*, pp. 812–817.

Lew, J. Y. and Trudnowski, D. J., 1996, "Vibration Control of a Micro/Macro-Manipulator System," *IEEE Control Systems*, pp. 26–31.

Li, Y. F. and Chen, X. B., 1998, "Tip Deflection Measurement and State Observation of a Flexible Robot Arm," in *Proc. IEEE Instrumentation and Measurement Technology Conf.*, pp. 1174–1178, St. Paul, USA.

Liu, H. H. S. and Pang, G. K. H., 2001, "Accelerometer for Mobile Robot Positioning," *IEEE Trans. Industry Applications*, **37**(3):247–251.

Maciejewski, A. A. and Klein, C. A., 1985, "Obstacle Avoidance for Kinematically Redundant Manipulators in Dynamically Varying Environments," *Int. J. Robotics Research*, **4**(3):109–117.

Maciejowski, J. M., 1989, *Multivariable Feedback Design*, Addison-Wesley, Reading, MA.

Magee, D. P. and Book, W. J., 1995, "Filtering Micro-Manipulator Wrist Commands to Prevent Flexible Base Motion," in *Proc. American Control Conference*, pp. 924–928, Seatle, Washington.

Markley, F. L., Berman, N., and Shaked, U., 1994, "Deterministic EKF-like Estimator for Spacecraft Attitude Estimation," in *Proc. American Control Conference*, pp. 247–251.

Matsuno, F. and Sakawa, Y., 1990, "A Simple Model of flexible Manipulators with Six Axes and Vibration Control by Using Accelerometers," *J. Robotic Systems*, **7**(4):575–597.

Meckl, P. H. and Seering, W. P., 1988, "Controlling Velocity-Limited Systems to Reduce Residual Vibration," in *Proc. IEEE Int. Conf. Robotics and Automation*, vol. 3, pp. 1428–1433, Washington D.C., USA.

Meirovitch, L., 1997, *Principles and Techniques of Vibrations*, Prentice Hall, Upper Saddle River, NJ.

Misawa, E. A. and Hedrick, J. K., 1989, "Nonlinear Observers—A State-of-the-Art Survey," *J. Dynamic Systems, Measurement, and Control*, **111**:344–352.

Moallem, M., Patel, R. V., and Khorasani, K., 1996, "An Observer-Based Inverse Dynamics Control Strategy for Flexible Multi-Link Manipulators," in *Proc. IEEE Conf. Decision and Control*, pp. 4112–4117, Kobe, Japan.

Moallem, M., Patel, R. V., and Khorasani, K., 1997, "Experimental Results for Nonlinear Decoupling Control of Flexible Multi-Link Manipulators," in *Proc. IEEE Int. Conf. Robotics and Automation*, pp. 3142–3147, Albuquerque, NM.

Moallem, M., Patel, R. V., and Khorasani, K., 2000, *Flexible-Link Robot Manipulators: Control Techniques and Structural Design*, Springer, London.

Nakamura, Y., 1991, *Advanced Robotics, Redundancy and Optimization*, Addison Wesley.

Nenchev, D. N., Yoshida, K., Vichitkulsawat, P., *et al.*, 1997, "Experiments on Reaction Null-Space Based Decoupled Control of a Flexible Structure Mounted Manipulator System," in *Proc. IEEE Int. Conf. Robotics and Automation*, vol. 3, pp. 2528–2534, Albuquerque, New Mexico.

Nenchev, D. N., Yoshida, K., Vichitkulsawat, P., *et al.*, 1999, "Reaction Null-Space Control of Flexible Structure Mounted Manipulator Systems," *IEEE Trans. Robotics and Control*, **15**(6):1011–1023.

Nguyen, L. A., Walker, I. D., and Defigueiredo, R. J. P., 1992, "Dynamic Control of Flexible, Kinematically Redundant Robot Manipulators," *IEEE Trans. Robotics and Control*, **8**(6):759–767.

Nikravesh, P. E., Wehage, R. A., and Kwon, O. K., 1985, "Euler Parameters in Computational Kinematics and Dynamics, Part 1," *ASME J. of Mech. Trans. and Auto. in Design*, **107**:358–365.

Nobel, B. and Daniel, J. W., 1988, *Applied Linear Algebra*, 3rd ed., Prentice-Hall, Englewood Cliffs, NJ.

Panzieri, S. and Ulivi, G., 1993, "Design and Implementation of a Sate Observer for a Flexible Robot," in *Proc. IEEE Int. Conf. Robotics and Automation*, pp. 204–209, Atlanta, GA.

Parsa, K., Angeles, J., and Misra, A. K., 2001, "Pose and Twist Estimation of a Rigid Body Using Accelerometers," in *Proc. IEEE Int. Conf. Robotics and Automation*, pp. 2873–2878, Seoul, Korea.

Parsa, K., Angeles, J., and Misra, A. K., 2002a, "Attitude Calibration of an Accelerometer Array," in *Proc. IEEE Int. Conf. Robotics and Automation on CD Rom*, Washington D.C., USA.

Parsa, K., Angeles, J., and Misra, A. K., 2002b, "Linearized Kinematics for State Estimation in Robotics," in *Advances in Robot Kinematics: Theory and Applications*, J. Lenarčič and F. Thomas (eds.), pp. 39–48, Kluwer Academic Publishers, Dordrecht.

Qian, W. T. and Ma, C. C. H., 1992, "A New Controller Design for a Flexible One-Link Manipulator," *IEEE Trans. Automatic Control*, **37**(1):132–137.

Rehbinder, H. and Hu, X., 2001, "Drift-Free Attitude Estimation for Accelerated Rigid Bodies," in *Proc. IEEE Int. Conf. Robotics and Automation*, vol. 4, pp. 4244–4249, Seoul, Korea.

Resnick, R., 1968, *Introduction to Special Relativity*, Wiley, New York, NY.

Reynolds, R. G., 1998, "Quaternion Parameterization and a Simple Algorithm for Global Attitude Estimation," *Journal of Guidance, Control, and Dynamics*, **21**(4):669–671.

Robins, A. (Editor), 1997, "Space Station, Strategic Technologies in Automation and Robotics Program, Phase 1," Final Report UAV-ROB-97/60, Bombardier, Inc., Defence Systems Devision, Mirabel, QC.

Roumeliotis, S. I., Sukhatme, G. S., and Bekey, G. A., 1998, "Smoother Based 3-D Attitude Estimation for Mobile Robot Localization," Tech. Rep. IRIS-98-363, USC, `http://iris.usc.edu/~irislib/`.

Roumeliotis, S. I., Sukhatme, G. S., and Bekey, G. A., 1999a, "Circumventing Dynamic Modelling: Evaluation of the Error-State Kalman Fillter Applied to Mobile-Robot Localization," in *Proc. IEEE Int. Conf. Robotics and Automation*, pp. 1656–1663, Detroit, MI.

Roumeliotis, S. I., Sukhatme, G. S., and Bekey, G. A., 1999b, "Smoother-Based 3D Attitude Estimation for Mobile-Robot Localization," in *Proc. IEEE Int. Conf. Robotics and Automation*, pp. 1979–1986, Detroit, MI.

Sadigh, M. J. and Misra, A. K., 1995, "More on the So-Called Dynamic Stiffening Effect," *The J. of the Astronimical Sciences*, **43**(2):101–125.

Sanchis, R. and Nijmeijer, H., 1998, "Sliding Controller-Sliding Observer Design for Non-linear Systems," *European J. of Control*, **4**(3):208–234.

Schiehlen, W., 1997, "Multibody Systems Dynamics: Roots and Perspectives," *Multibody System Dynamics*, **1**:149–188.

Schwertassek, R., 1998, "Flexible Bodies in Multibody Systems," in *Computational Methods in Mechanical Systems: Mechanism Analysis, Synthesis, and Optimization*, J. Angeles and E. Zakhariev (eds.), NATO ASI Series, pp. 329–363, Springer Verlag, Berlin.

Shabana, A. A., 1997, "Flexible Multibody Dynamics: Review of the Past and Recent Developments," *Multibody System Dynamics*, **1**:189–222.

Sharf, I., 1996, "Active Damping of a Large Flexible Manipulator with a Short-Reach Robot," *ASME J. Dynamic Systems, Measurement, and Control*, **118**:704–713.

Sim, E. and Lee, S. W., 1993, "Active Vibration Control of Flexible Structures with Acceleration Feedback," *J. Guidance, Control, and Dynamics*, **16**(2):413–415.

Slotine, J.-J. E. and Li, W., 1991, *Applied Nonlinear Control*, Prentice-Hall, Englewood Cliffs, NJ.

Söffker, D., Yu, T.-J., and Müller, P. C., 1995, "State Estimation of Dynamical Systems with Nonlinearities by Using Proportional-Integral Observer," *Int. J. Systems Science*, **26**(9):1571–1852.

Sommer III, H. J., 1992, "Determination of First and Second Order Instant Screw Parameters from Landmark Trajectories," *ASME J. Mechanical Design*, **114**:274–282.

Staffetti, E., Bruyninckx, H., and de Schutter, J., 2002, "On the Invariance of Manipulability Indices," in *Advances in Robot Kinematics: Theory and Applications*, J. Lenarčič and F. Thomas (eds.), pp. 57–66, Kluwer Academic Publishers, Dordrecht.

Strang, G., 1988, *Linear Algebra and Its Applications*, 3rd ed., Harcourt Brace Jovanovich Publishers, San Diego.

Tiemin, Z., Youwu, L., Shaoze, Y., *et al.*, 1996, "Comparative Study on the Acceleration Feedback on the Strain Feedback of a Flexible Manipulator," in *IEEE Int. Conf. Systems, Man, and Cybernetics*, vol. 2, pp. 1031–1035, Beijing.

Tokhi, M. O. and Azad, A. K. M., 1997, "Design and Development of an Experimental Flexible Manipulator System," *Robotica*, **15**:283–292.

Tonsunoglu, S., Lin, S.-H., and Tesar, D., 1989, "Identification of Inaccessible Oscillations in N-Link Flexible Robotic Systems," in *Proc. IEEE Conf. Decision and Control*, pp. 2512–2518, Tampa, FL.

Tonsunoglu, S., Lin, S.-H., and Tesar, D., 1990, "Complete Accessibility of Oscillations in Robotic Systems by Orthogonal Projections," *J. Dynamic Systems, Measurement, and Control*, **112**:194–202.

Tonsunoglu, S., Lin, S.-H., and Tesar, D., 1992, "Accessibility and Controllability of Flexible Robotic Manipulators," *J. Dynamic Systems, Measurement, and Control*, **114**:50–58.

Torres, M. A. and Dubowsky, S., 1993, "Path-Planning for Elastically Constrained Space Manipulator Systems," in *Proc. IEEE Int. Conf. Robotics and Automation*, vol. 1, pp. 812–817.

Torres, M. A., Dubowsky, S., and Pisoni, A. C., 1994, "Path-Planning for Elastically Mounted Space Manipulators: Experimental Evaluation of the Coupling Map," in *Proc. IEEE Int. Conf. Robotics and Automation*, pp. 2227–2233, San Diego, CA.

Torres, M. A., Dubowsky, S., and Pisoni, A. C., 1996, "Vibration Control of Deployment Structures, Long Reach Manipulators: The P-PED method," in *Proc. IEEE Int. Conf. Robotics and Automation*, pp. 2498–2504, Minneapolis, MN.

Vaganay, J. and Aldon, M. J., 1994, "Attitude Estimation for a Vehicle Using Inertial Sensors," *Control Eng. Practice*, **2**(2):281–287.

Vaganay, J., Aldon, M. J., and Fournier, A., 1993, "Mobile Robot Attitude Estimation by Fusion of Inertial Data," in *Proc. IEEE Int. Conf. Robotics and Automation*, pp. 277–282, Atlanta, GA.

Wertz, J. R., 1978, *Spacecraft Attitude Determination and Control*, vol. 73 of *Astrophysics and Space Science Library*, D. Reidel Publishing Company, Dordrecht.

Wilson, D. G., Parker, G. G., Starr, G. P., *et al.*, 1998, "Output Feedback Sliding Mode Control for a Planar Flexible Manipulator," in *Robotics 98, Proc. The Third ASCE Speciality Conference on Robotics for Challenging Environments*, pp. 8–14, Albuquerque, NM.

Yoshikawa, T., Harada, K., and Matsumoto, A., 1996, "Hybrid Position/Force Control of Flexible-Macro/Rigid-Micro Manipulator Systems," *IEEE Trans. Robotics and Automation*, **12**(4):633–639.

Yoshikawa, T., Hosoda, K., Doi, T., *et al.*, 1993, "Quasi-Static Trajectory Tracking Control of Flexible Manipulator by Macro-Micro Manipulator System," in *Proc. IEEE Int. Conf. Robotics and Automation*, pp. 210–214, Atlanta, GA.

Zaki, A. S. and ElMaraghy, W. H., 1993, "Model Reference Adaptive Control for a Three-Degree of Freedom Manipulator with Flexible Links," in *Proc. the American Control Conf.*, pp. 1400–1405, San Fransisco, CA.

Zaki, A. S. and ElMaraghy, W. H., 1995, "A Robust Observer for Flexible-Link Manipulators Control," in *Proc. the American Control Conf.*, pp. 3334–3338, Seattle, WA.

Zaki, A. S., Mir, H., and ElMaraghy, W. H., 1998a, "Desing, Testing and Simulation of a Flexible Robot for the Study of Dynamics and Control," *Int. J. Robotics and Automation*, **13**(1):24–29.

Zaki, A. S., Mir, H., and ElMaraghy, W. H., 1998b, "Initial Experiments on UWO Flexible Manipulator," *Int. J. Robotics and Automation*, **13**(2):54–59.

Zhu, J. and Johnson, C. D., 1990, "A Unified Eigenvalue Theory for Time-Varying Linear Circuits and Systems," in *Proc. IEEE Int. Symp. Circuits and Systems*, vol. 2, pp. 1393–1397.

Appendix A

Time-Derivative of the Euler-Parameter Array in the Body-Frame

Lemma 4. *The time derivative* $\dot{\boldsymbol{\eta}}$ *of the Euler-parameter array* $\boldsymbol{\eta} = \begin{bmatrix}\mathbf{u}^T & u_0\end{bmatrix}^T$ *of a rigid body in its body-frame* $\mathcal{B}$ *is related to the body-frame representation of its angular velocity and that of its Euler parameters according to*

$$\dot{\boldsymbol{\eta}} = \mathbf{H}\boldsymbol{\omega} \tag{A.1}$$

$$\mathbf{H} \triangleq \frac{1}{2}\begin{bmatrix} u_0\mathbf{1} + \mathbf{U} \\ -\mathbf{u}^T \end{bmatrix}, \tag{A.2}$$

in which $\mathbf{U}$ *is the cross-product matrix of* $\mathbf{u}$.

Proof: If we denote the fixed coordinate frame with $\mathcal{R}$, and call it in short the *fixed-frame*, then, the relation between $\dot{\boldsymbol{\eta}}$ and $\boldsymbol{\omega}$ in this frame is given by (Angeles, 2002)

$${}^{\mathcal{R}}\dot{\boldsymbol{\eta}} = \frac{1}{2}\begin{bmatrix} u_0\mathbf{1} - {}^{\mathcal{R}}\mathbf{U} \\ -{}^{\mathcal{R}}\mathbf{u}^T \end{bmatrix} {}^{\mathcal{R}}\boldsymbol{\omega}. \tag{A.3}$$

Hence, it is apparent that

$$\begin{bmatrix} {}^{\mathcal{R}}\dot{\mathbf{u}} \\ \dot{u}_0 \end{bmatrix} = \frac{1}{2}\begin{bmatrix} u_0\mathbf{1} - {}^{\mathcal{R}}\mathbf{U} \\ -{}^{\mathcal{R}}\mathbf{u}^T \end{bmatrix} \mathbf{Q}\,{}^{\mathcal{B}}\boldsymbol{\omega} = \frac{1}{2}\begin{bmatrix} u_0\mathbf{Q} - {}^{\mathcal{R}}\mathbf{U}\mathbf{Q} \\ -{}^{\mathcal{R}}\mathbf{u}^T\mathbf{Q} \end{bmatrix} {}^{\mathcal{B}}\boldsymbol{\omega}, \tag{A.4}$$

in which $\mathbf{Q}$ is the rotation matrix from the body-frame to the fixed-frame.

On the other hand, ${}^{\mathcal{R}}\mathbf{u} = \mathbf{Q}\,{}^{\mathcal{B}}\mathbf{u}$; upon differentiating this relation and solving it for ${}^{\mathcal{B}}\dot{\mathbf{u}}$, we have

$$\begin{aligned} {}^{\mathcal{B}}\dot{\mathbf{u}} &= \mathbf{Q}^T\,{}^{\mathcal{R}}\dot{\mathbf{u}} - \mathbf{Q}^T\dot{\mathbf{Q}}\,{}^{\mathcal{B}}\mathbf{u} = \mathbf{Q}^T\,{}^{\mathcal{R}}\dot{\mathbf{u}} - {}^{\mathcal{B}}\boldsymbol{\Omega}\,{}^{\mathcal{B}}\mathbf{u} \\ &= \mathbf{Q}^T\,{}^{\mathcal{R}}\dot{\mathbf{u}} + {}^{\mathcal{B}}\mathbf{U}\,{}^{\mathcal{B}}\boldsymbol{\omega}. \end{aligned} \tag{A.5}$$

Consequently,

$$\begin{aligned} {}^{\mathcal{B}}\dot{\boldsymbol{\eta}} \equiv \begin{bmatrix} {}^{\mathcal{B}}\dot{\mathbf{u}} \\ \dot{u}_0 \end{bmatrix} &= \begin{bmatrix} \frac{1}{2}\mathbf{Q}^T\left(u_0\mathbf{Q} - {}^{\mathcal{R}}\mathbf{U}\mathbf{Q}\right) + {}^{\mathcal{B}}\mathbf{U} \\ -\frac{1}{2}\,{}^{\mathcal{B}}\mathbf{u}^T \end{bmatrix} {}^{\mathcal{B}}\boldsymbol{\omega} \\ &= \frac{1}{2}\begin{bmatrix} u_0\mathbf{1} + {}^{\mathcal{B}}\mathbf{U} \\ -\,{}^{\mathcal{B}}\mathbf{u}^T \end{bmatrix} {}^{\mathcal{B}}\boldsymbol{\omega} \end{aligned} \tag{A.6}$$

because ${}^{\mathcal{R}}\mathbf{U}$ can be taken from the inertial reference frame to the body-frame using the similarity transformation ${}^{\mathcal{B}}\mathbf{U} \equiv \mathbf{Q}^T\,{}^{\mathcal{R}}\mathbf{U}\,\mathbf{Q}$.

Thus, in the body-frame, we have

$$\mathbf{H} \triangleq \frac{\partial\dot{\boldsymbol{\eta}}}{\partial\boldsymbol{\omega}} = \frac{1}{2}\begin{bmatrix} u_0\mathbf{1} + \mathbf{U} \\ -\mathbf{u}^T \end{bmatrix}.$$

□

Appendix B

Simplifications of the Link Dynamics Equations

For the simplification of the link dynamics equations, three relations were used:

$$\frac{\partial \mathbf{t}}{\partial \mathbf{q}} \equiv -\frac{d}{dt}\Big(\frac{\partial \mathbf{t}}{\partial \dot{\mathbf{q}}}\Big), \tag{B.1}$$

$$\Big(\frac{\partial \dot{\mathbf{q}}}{\partial \mathbf{t}}\Big)^T \frac{d}{dt}\Big(\frac{\partial \mathbf{t}}{\partial \dot{\mathbf{q}}}\Big)^T \equiv \frac{1}{2}\,\mathrm{diag}(\mathbf{O}_{3\times 3}, \boldsymbol{\Omega}, \mathbf{O}_{n_f \times n_f}), \tag{B.2}$$

$$\Big(\frac{\partial \dot{\mathbf{q}}}{\partial \mathbf{t}}\Big)^T \mathbf{t}^T \frac{\partial \mathbf{M}}{\partial \mathbf{q}}\mathbf{t} \equiv \mathbf{t}^T \frac{\partial \dot{\mathbf{M}}}{\partial \mathbf{t}}\mathbf{t}, \tag{B.3}$$

in which the subscripts have been dropped for brevity.

These identities are proven here for the flexible-manipulator links:

(i) $\partial \mathbf{t}/\partial \mathbf{q}$ reduces to

$$\frac{\partial \mathbf{t}}{\partial \mathbf{q}} = \begin{bmatrix} \mathbf{O}_{3\times 3} & \mathbf{O}_{3\times 4} & \mathbf{O}_{3\times n_{fi}}, \\ \mathbf{O}_{4\times 3} & \partial \boldsymbol{\omega}/\partial \boldsymbol{\eta} & \mathbf{O}_{4\times n_{fi}}, \\ \mathbf{O}_{n_{fi}\times 3} & \mathbf{O}_{n_{fi}\times 4} & \mathbf{O}_{n_{fi}\times n_{fi}} \end{bmatrix}. \tag{B.4}$$

As seen from the above relation, the only non-zero block of this matrix is $\partial \boldsymbol{\omega}/\partial \boldsymbol{\eta}$. From eqs. (2.5a, 2.5b, 2.6b, & 2.6d), however, it is apparent that

$$\frac{\partial \boldsymbol{\omega}}{\partial \boldsymbol{\eta}} = \overline{\mathbf{K}}(\dot{\boldsymbol{\eta}}) = -\dot{\overline{\mathbf{H}}} = -\frac{d}{dt}\Big(\frac{\partial \boldsymbol{\omega}}{\partial \dot{\boldsymbol{\eta}}}\Big). \tag{B.5}$$

On the other hand, from the definitions of $\mathbf{t}$ and $\mathbf{q}$, it can readily be seen that

$$\frac{\partial \mathbf{t}}{\partial \dot{\mathbf{q}}} = \mathrm{diag}(\mathbf{1}_3, \frac{\partial \boldsymbol{\omega}}{\partial \dot{\boldsymbol{\eta}}}, \mathbf{1}_{n_{fi}}). \tag{B.6}$$

Hence, differentiating eq. (B.6) and using the relations given by eqs. (B.4 & B.5), one obtains eq. (B.1).

(*ii*) To prove eq. (B.2), notice that the partial derivative of $\dot{\mathbf{q}}$ with respect to $\mathbf{t}$, and that of $\mathbf{t}$ with respect to $\dot{\mathbf{q}}$ can be readily derived as

$$\frac{\partial \dot{\mathbf{q}}}{\partial \mathbf{t}} = \mathrm{diag}(\mathbf{1}_3, \mathbf{H}, \mathbf{1}_{n_f}), \tag{B.7a}$$

$$\frac{\partial \mathbf{t}}{\partial \dot{\mathbf{q}}} = \mathrm{diag}(\mathbf{1}_3, 4\,\mathbf{H}^T, \mathbf{1}_{n_f}). \tag{B.7b}$$

Hence,

$$\left(\frac{\partial \dot{\mathbf{q}}}{\partial \mathbf{t}}\right)^T \frac{d}{dt}\left(\frac{\partial \mathbf{t}}{\partial \dot{\mathbf{q}}}\right)^T = \mathrm{diag}(\mathbf{1}_3, \mathbf{H}^T, \mathbf{1}_{n_f}) \cdot \mathrm{diag}(\mathbf{O}_{3\times 3}, 4\,\dot{\mathbf{H}}, \mathbf{O}_{n_f \times n_f}) \tag{B.8}$$

$$= \mathrm{diag}(\mathbf{O}_{3\times 3}, 4\mathbf{H}^T\dot{\mathbf{H}}, \mathbf{O}_{n_f \times n_f}). \tag{B.9}$$

However, according to Lemma 2 of Chapter 2 and using eq. (2.5b),

$$\overline{\mathbf{H}}\,\dot{\mathbf{H}} \equiv 4\mathbf{H}^T\dot{\mathbf{H}} \equiv \frac{1}{2}\boldsymbol{\Omega}. \tag{B.10}$$

Therefore,

$$\left(\frac{\partial \dot{\mathbf{q}}}{\partial \mathbf{t}}\right)^T \frac{d}{dt}\left(\frac{\partial \mathbf{t}}{\partial \dot{\mathbf{q}}}\right)^T = \frac{1}{2}\overline{\boldsymbol{\Omega}} \tag{B.11}$$

where

$$\overline{\boldsymbol{\Omega}} \triangleq \mathrm{diag}(\mathbf{O}_{3\times 3}, \boldsymbol{\Omega}, \mathbf{O}_{n_f \times n_f}). \tag{B.12}$$

(*iii*) It is apparent that $\mathbf{t}^T(\partial \mathbf{M}/\partial \mathbf{q})\mathbf{t}$ can be evaluated as

$$\mathbf{t}^T \frac{\partial \mathbf{M}}{\partial \mathbf{q}}\mathbf{t} = \frac{\partial}{\partial \mathbf{q}}(\mathbf{a}^T\mathbf{M}\mathbf{a})\bigg|_{\mathbf{a}=\mathbf{t}} \tag{B.13}$$

in which $\mathbf{a}$ is a dummy variable. From this relation, we can see that

$$\left(\frac{\partial \dot{\mathbf{q}}}{\partial \mathbf{t}}\right)^T \mathbf{t}^T \frac{\partial \mathbf{M}}{\partial \mathbf{q}}\mathbf{t} = \left(\frac{\partial \dot{\mathbf{q}}}{\partial \mathbf{t}}\right)^T \frac{\partial}{\partial \mathbf{q}}(\mathbf{a}^T\mathbf{M}\mathbf{a})\bigg|_{\mathbf{a}=\mathbf{t}} = \left(\frac{\partial \dot{\mathbf{q}}}{\partial \mathbf{t}}\right)^T \frac{\partial}{\partial \dot{\mathbf{q}}}(\mathbf{a}^T\dot{\mathbf{M}}\mathbf{a})\bigg|_{\mathbf{a}=\mathbf{t}}$$

$$= \frac{\partial}{\partial \mathbf{t}}(\mathbf{a}^T\dot{\mathbf{M}}\mathbf{a})\bigg|_{\mathbf{a}=\mathbf{t}} = \mathbf{t}^T \frac{\partial \dot{\mathbf{M}}}{\partial \mathbf{t}}\mathbf{t}.$$

Appendix C

Calculating the Link Mass Matrix

C.1 Deriving the Link Kinetic Energy

Subject to the assumptions mentioned in Section 2.4, the kinetic energy of a flexible link can be expressed as

$$T = \frac{1}{2}\int_0^l \rho \|\mathbf{v}(x,t)\|^2 \mathrm{d}x + \frac{1}{2}\int_0^l \rho \frac{J}{A}\left(\frac{\partial \gamma}{\partial t}\right)^2 \mathrm{d}x + \frac{1}{2} M \|\mathbf{v}(l,t)\|^2 \qquad \text{(C.1)}$$

in which $\rho, J, A, \gamma,$ and M are the mass per unit length, the polar moment of inertia, the cross-sectional area, the angle of torsion of the link, and the concentrated mass at the end of the link, respectively, all of them assumed constant. For brevity, we have dropped the subscript i from all our equations in this Appendix.

We will derive the kinetic energy in four steps: First, the square of the norm of the absolute velocity is obtained; then, over the next two steps, the first and the second integrals of eq. (C.1) are evaluated in terms of the generalized velocities and the shape-functions; as the fourth step, we put all the results together and obtain the link kinetic-energy.

Deriving $\|\mathbf{v}(x,t)\|^2$

To calculate $\|\mathbf{v}(x,t)\|^2$, let the position vector $\mathbf{p}$ of the origin of the ith frame be expressed in the body-frame. Then, the velocity $\mathbf{v}(x,t)$ is obtained from

$$\mathbf{v}(x,t) = \frac{d}{dt}\mathbf{p} + \boldsymbol{\omega} \times \boldsymbol{\rho}(x,t) + \dot{\boldsymbol{\rho}}(x,t) \qquad \text{(C.2)}$$

where, from eqs. (2.51 & 2.62), we have

$$\boldsymbol{\rho}(x,t) = x\mathbf{x} + \mathbf{u}(x,t) \tag{C.3}$$

$$\mathbf{u}(x,t) = \mathbf{B}(x)\boldsymbol{\xi}(t), \tag{C.4}$$

in which $\mathbf{x}$ is a unit vector parallel to the X axis.

However,

$$\frac{d}{dt}\mathbf{p} = \dot{\mathbf{p}} + \boldsymbol{\omega} \times \mathbf{p}, \tag{C.5}$$

which, upon substituting into eq. (C.2), we obtain

$$\mathbf{v}(x,t) = \dot{\mathbf{p}} + \boldsymbol{\omega} \times \mathbf{p} + \boldsymbol{\omega} \times \boldsymbol{\rho}(x,t) + \dot{\mathbf{u}}(x,t). \tag{C.6}$$

It can be shown (Cyril, 1988) that the square of the Euclidean norm of $\mathbf{v}(x,t)$ is given by

$$\begin{aligned} \|\mathbf{v}(x,t)\|^2 = \|\frac{d}{dt}\mathbf{p}\|^2 &- \Big(\frac{d}{dt}\mathbf{p}\Big)^T \big(2x\mathbf{X} + 2\mathbf{U}(x,t)\big)\boldsymbol{\omega} + 2\Big(\frac{d}{dt}\mathbf{p}\Big)^T \dot{\mathbf{u}}(x,t) \\ &+ \boldsymbol{\omega}^T \Big[x^2(\mathbf{1} - \mathbf{x}\mathbf{x}^T) - x\big(\mathbf{x}\mathbf{u}^T(x,t) + \mathbf{u}(x,t)\mathbf{x}^T\big) \\ &\qquad + \big(\|\mathbf{u}(x,t)\|^2 - \mathbf{u}(x,t)\mathbf{u}^T(x,t)\big)\Big] \\ &+ \boldsymbol{\omega}^T(2x\mathbf{X} + 2\mathbf{U}(x,t))\dot{\mathbf{u}} + \|\dot{\mathbf{u}}(x,t)\|^2 \end{aligned} \tag{C.7}$$

where

$$\mathbf{U}(x,t) \triangleq \mathrm{CPM}\big(\mathbf{u}(x,t)\big), \qquad \text{and} \qquad \mathbf{X} \triangleq \mathrm{CPM}(\mathbf{x}). \tag{C.8}$$

However, the first three terms of eq. (C.7) are obtained from (C.5) as

$$\begin{aligned} \|\frac{d}{dt}\mathbf{p}\|^2 &= (\dot{\mathbf{p}} + \boldsymbol{\omega} \times \mathbf{p})^T(\dot{\mathbf{p}} + \boldsymbol{\omega} \times \mathbf{p}) \\ &= \|\dot{\mathbf{p}}\|^2 + 2\dot{\mathbf{p}}^T(\boldsymbol{\omega} \times \mathbf{p}) + (\boldsymbol{\omega} \times \mathbf{p})^T\boldsymbol{\omega} \times \mathbf{p}) \\ &= \|\dot{\mathbf{p}}\|^2 - 2\dot{\mathbf{p}}^T\mathbf{P}\,\boldsymbol{\omega} + \boldsymbol{\omega}^T(\|\mathbf{p}\|^2\mathbf{1} - \mathbf{p}\mathbf{p}^T)\boldsymbol{\omega}, \end{aligned} \tag{C.9}$$

$$\begin{aligned} \Big(\frac{d}{dt}\mathbf{p}\Big)^T \big(2x\mathbf{X} + 2\mathbf{U}(x,t)\big)\boldsymbol{\omega} &= \dot{\mathbf{p}}^T\big(2x\mathbf{X} + 2\mathbf{U}(x,t)\big)\boldsymbol{\omega} \\ &\quad + \boldsymbol{\omega}^T\mathbf{P}\big(2x\mathbf{X} + 2\mathbf{U}(x,t)\big)\boldsymbol{\omega}, \end{aligned} \tag{C.10}$$

and

$$\Big(\frac{d}{dt}\mathbf{p}\Big)^T\dot{\mathbf{u}}(x,t) = \dot{\mathbf{p}}^T\dot{\mathbf{u}}(x,t) + \boldsymbol{\omega}^T\mathbf{P}\,\dot{\mathbf{u}}(x,t), \tag{C.11}$$

in which $\mathbf{P} \triangleq \mathrm{CPM}(\mathbf{p})$.

Thus, $\|\mathbf{v}(x,t)\|^2$ can be calculated as

$$\begin{aligned}\|\mathbf{v}(x,t)\|^2 = \|\dot{\mathbf{p}}\|^2 &- \dot{\mathbf{p}}^T\big(2x\mathbf{X} + 2\mathbf{U}(x,t) + 2\mathbf{P}\big)\boldsymbol{\omega} + 2\dot{\mathbf{p}}^T\dot{\mathbf{u}}(x,t)\\ &+ \boldsymbol{\omega}^T\Big[x^2(\mathbf{1} - \mathbf{x}\mathbf{x}^T) - x\big(\mathbf{x}\mathbf{u}^T(x,t) + \mathbf{u}(x,t)\mathbf{x}^T\big) - (\|\mathbf{p}\|^2\mathbf{1} - \mathbf{p}\mathbf{p}^T)\\ &\qquad + \big(\|\mathbf{u}(x,t)\|^2 - \mathbf{u}(x,t)\mathbf{u}^T(x,t)\big) - \mathbf{P}\big(2x\mathbf{X} + 2\mathbf{U}(x,t)\big)\Big]\boldsymbol{\omega}\\ &+ \boldsymbol{\omega}^T\big(2x\mathbf{X} + 2\mathbf{U}(x,t) + 2\mathbf{P}\big)\dot{\mathbf{u}}(x,t) + \|\dot{\mathbf{u}}(x,t)\|^2.\end{aligned} \tag{C.12}$$

However, for any vector $\mathbf{a}$, we have

$$\mathbf{A}^2 \equiv -(\|\mathbf{a}\|^2\mathbf{1} - \mathbf{a}\mathbf{a}^T), \qquad \text{for} \quad \mathbf{A} \triangleq \mathrm{CPM}(\mathbf{a}). \tag{C.13}$$

Therefore, eq. (C.12) is simplified to

$$\begin{aligned}\|\mathbf{v}(x,t)\|^2 = \|\dot{\mathbf{p}}\|^2 &- 2\dot{\mathbf{p}}^T\big(x\mathbf{X} + \mathbf{U}(x,t) + \mathbf{P}\big)\boldsymbol{\omega} + 2\dot{\mathbf{p}}^T\dot{\mathbf{u}}(x,t)\\ &+ \boldsymbol{\omega}^T\Big[-x^2\mathbf{X}^2 - x\big(\mathbf{x}\,\mathbf{u}^T(x,t) + \mathbf{u}(x,t)\mathbf{x}^T\big) - \mathbf{U}^2(x,t) - \mathbf{P}^2\\ &\qquad - 2\mathbf{P}\big(x\mathbf{X} + \mathbf{U}(x,t)\big)\Big]\boldsymbol{\omega}\\ &+ 2\boldsymbol{\omega}^T\big(x\mathbf{X} + \mathbf{U}(x,t) + \mathbf{P}\big)\dot{\mathbf{u}}(x,t) + \|\dot{\mathbf{u}}(x,t)\|^2.\end{aligned} \tag{C.14}$$

Consequently, the square of the norm of the link-endpoint velocity is calculated as

$$\begin{aligned}\|\mathbf{v}(l,t)\|^2 = \|\dot{\mathbf{p}}\|^2 &- 2\dot{\mathbf{p}}^T\Big(l\mathbf{X} + \mathbf{U}(l,t) + \mathbf{P}\Big)\boldsymbol{\omega} + 2\dot{\mathbf{p}}^T\dot{\mathbf{u}}(l,t)\\ &+ \boldsymbol{\omega}^T\Big[-l^2\mathbf{X}^2 - l\big(\mathbf{x}\mathbf{u}^T(l,t) + \mathbf{u}(l,t)\mathbf{x}^T\big) - \mathbf{U}^2(l,t) - \mathbf{P}^2\\ &\qquad - 2\mathbf{P}\big(l\mathbf{X} + \mathbf{U}(l,t)\big)\Big]\boldsymbol{\omega}\\ &+ 2\boldsymbol{\omega}^T\big(l\mathbf{X} + \mathbf{U}(l,t) + \mathbf{P}\big)\dot{\mathbf{u}}(l,t) + \|\dot{\mathbf{u}}(l,t)\|^2.\end{aligned} \tag{C.15}$$

Simplifying the First Integral

Using eq. (C.14), the first integral of eq. (C.1) can be written as

$$\begin{aligned} T_1 &\triangleq \frac{1}{2}\int_0^l \rho\|\mathbf{v}(x,t)\|^2 dx \\ &= \frac{1}{2}\rho\Big[l\|\dot{\mathbf{p}}\|^2 - 2\dot{\mathbf{p}}^T\int_0^l \big(x\mathbf{X}+\mathbf{U}(x,t)+\mathbf{P}\big)dx\boldsymbol{\omega} + 2\dot{\mathbf{p}}^T\int_0^l \dot{\mathbf{u}}(x,t)dx \\ &\quad + \boldsymbol{\omega}^T\int_0^l \Big(-2\mathbf{P}\big(x\mathbf{X}+\mathbf{U}(x,t)\big) - x^2\mathbf{X}^2 \\ &\qquad - x\big(\mathbf{x}\,\mathbf{u}^T(x,t)+\mathbf{u}(x,t)\mathbf{x}^T\big) - \mathbf{U}^2(x,t) - \mathbf{P}^2\Big)dx\,\boldsymbol{\omega} \\ &\quad + 2\boldsymbol{\omega}^T\int_0^l \big(x\mathbf{X}+\mathbf{U}(x,t)+\mathbf{P}\big)\dot{\mathbf{u}}(x,t)dx + \int_0^l \|\dot{\mathbf{u}}(x,t)\|^2 dx\Big]. \end{aligned} \tag{C.16}$$

However, upon differentiating eq. (C.4), one can write

$$\dot{\mathbf{u}}(x,t) = \mathbf{B}(x)\dot{\boldsymbol{\xi}}(t). \tag{C.17}$$

Hence, some of the integrals on the right-hand side of eq. (C.16) can be evaluated as given below:

$$\int_0^l \big(x\mathbf{X}+\mathbf{U}(x,t)+\mathbf{P}\big)dx = \frac{l^2}{2}\mathbf{X} + \int_0^l \mathbf{U}(x,t)\mathrm{d}x + \mathbf{P}l, \tag{C.18}$$

$$\int_0^l \dot{\mathbf{u}}(x,t)dx = \int_0^l \mathbf{B}(x)dx\dot{\boldsymbol{\xi}}, \tag{C.19}$$

$$\int_0^l -2\mathbf{P}\big(x\mathbf{X}+\mathbf{U}(x,t)\big)dx = -\Big(l^2\mathbf{P}\mathbf{X} + 2\mathbf{P}\int_0^l \mathbf{U}(x,t)dx\Big), \tag{C.20}$$

$$\int_0^l -x^2\mathbf{X}^2 dx = -\frac{l^3}{2}\mathbf{X}^2, \tag{C.21}$$

$$\int_0^l -x\big(\mathbf{x}\,\mathbf{u}^T(x,t)+\mathbf{u}(x,t)\mathbf{x}^T\big)dx = -\Big(\mathbf{x}\boldsymbol{\xi}^T\int_0^l \mathbf{x}\mathbf{B}^T(x)dx + \int_0^l \mathbf{x}\mathbf{B}(x)dx\boldsymbol{\xi}\mathbf{x}^T\Big), \tag{C.22}$$

$$\int_0^l -\mathbf{P}^2 dx = -\mathbf{P}^2 l, \tag{C.23}$$

$$\int_0^l \|\dot{\mathbf{u}}(x,t)\|^2 dx = \dot{\boldsymbol{\xi}}^T\left(\int_0^l \mathbf{B}^T(x)\mathbf{B}(x)\mathrm{d}x\right)\dot{\boldsymbol{\xi}}, \tag{C.24}$$

$$\begin{aligned} \int_0^l \big(x\mathbf{X}+\mathbf{U}(x,t)+\mathbf{P}\big)\dot{\mathbf{u}}dx = \Big(&\mathbf{X}\int_0^l x\mathbf{B}(x)dx + \int_0^l \mathbf{U}(x,t)\mathbf{B}(x)dx \\ &+ \mathbf{P}\int_0^l \mathbf{B}(x)dx\Big)\dot{\boldsymbol{\xi}}. \end{aligned} \tag{C.25}$$

Furthermore, one can readily derive $\mathbf{U}^2(x,t)$ as explained below: From eq. (C.4), we know that

$$\mathbf{u}(x,t) = \mathbf{B}(x)\boldsymbol{\xi}(t) = \begin{bmatrix} \mathbf{0}^T & \mathbf{0}^T \\ \boldsymbol{\varphi}^T & \mathbf{0}^T \\ \mathbf{0}^T & \boldsymbol{\varphi}^T \end{bmatrix} \begin{bmatrix} \boldsymbol{\xi}_{(1)} \\ \boldsymbol{\xi}_{(2)} \end{bmatrix} = \begin{bmatrix} 0 \\ \boldsymbol{\varphi}^T\boldsymbol{\xi}_{(1)} \\ \boldsymbol{\varphi}^T\boldsymbol{\xi}_{(2)} \end{bmatrix}. \tag{C.26}$$

The cross-product-matrix of $\mathbf{u}$ is therefore given by

$$\mathbf{U} = \begin{bmatrix} 0 & -\boldsymbol{\varphi}^T\boldsymbol{\xi}_{(2)} & \boldsymbol{\varphi}^T\boldsymbol{\xi}_{(1)} \\ \boldsymbol{\varphi}^T\boldsymbol{\xi}_{(2)} & 0 & 0 \\ -\boldsymbol{\varphi}^T\boldsymbol{\xi}_{(1)} & 0 & 0 \end{bmatrix}. \tag{C.27}$$

Then,

$$\mathbf{U}^2 = \begin{bmatrix} (\boldsymbol{\varphi}^T\boldsymbol{\xi}_{(2)})^2 + (\boldsymbol{\varphi}^T\boldsymbol{\xi}_{(1)})^2 & 0 & 0 \\ 0 & (\boldsymbol{\varphi}^T\boldsymbol{\xi}_{(2)})^2 & -(\boldsymbol{\varphi}^T\boldsymbol{\xi}_{(2)}\boldsymbol{\varphi}^T\boldsymbol{\xi}_{(1)}) \\ 0 & -(\boldsymbol{\varphi}^T\boldsymbol{\xi}_{(2)}\boldsymbol{\varphi}^T\boldsymbol{\xi}_{(1)}) & (\boldsymbol{\varphi}^T\boldsymbol{\xi}_{(1)})^2 \end{bmatrix}. \tag{C.28}$$

Hence, using eqs. (C.27 & C.28), one can conclude that

$$\int_0^l \mathbf{U}dx = \begin{bmatrix} 0 & -\int_0^l \boldsymbol{\varphi}^T dx\boldsymbol{\xi}_{(2)} & \int_0^l \boldsymbol{\varphi}^T dx\boldsymbol{\xi}_{(1)} \\ \int_0^l \boldsymbol{\varphi}^T dx\boldsymbol{\xi}_{(2)} & 0 & 0 \\ -\int_0^l \boldsymbol{\varphi}^T dx\boldsymbol{\xi}_{(1)} & 0 & 0 \end{bmatrix}, \tag{C.29}$$

and

$$-\int_0^l \mathbf{U}^2 dx = \begin{bmatrix} \boldsymbol{\xi}_{(2)}^T \int_0^l \boldsymbol{\varphi}\boldsymbol{\varphi}^T dx\boldsymbol{\xi}_{(2)} + \boldsymbol{\xi}_{(1)}^T \int_0^l \boldsymbol{\varphi}\boldsymbol{\varphi}^T dx\boldsymbol{\xi}_{(1)} & 0 & 0 \\ 0 & \boldsymbol{\xi}_{(2)}^T \int_0^l \boldsymbol{\varphi}\boldsymbol{\varphi}^T dx\boldsymbol{\xi}_{(2)} & -\boldsymbol{\xi}_{(2)}^T \int_0^l \boldsymbol{\varphi}\boldsymbol{\varphi}^T dx\boldsymbol{\xi}_{(1)} \\ 0 & -\boldsymbol{\xi}_{(2)}^T \int_0^l \boldsymbol{\varphi}\boldsymbol{\varphi}^T \mathrm{d}x\boldsymbol{\xi}_{(1)} & \boldsymbol{\xi}_{(1)}^T \int_0^l \boldsymbol{\varphi}\boldsymbol{\varphi}^T dx\boldsymbol{\xi}_{(1)} \end{bmatrix},$$

which, if the clamped-free eigenfunctions are chosen as shape-functions, becomes

$$-\int_0^l \mathbf{U}^2 dx = \begin{bmatrix} l(\|\boldsymbol{\xi}_{(2)}\|^2 + \|\boldsymbol{\xi}_{(1)}\|^2) & 0 & 0 \\ 0 & l\|\boldsymbol{\xi}_{(2)}\|^2 & -l\boldsymbol{\xi}_{(2)}^T\boldsymbol{\xi}_{(1)} \\ 0 & -l\boldsymbol{\xi}_{(2)}^T\boldsymbol{\xi}_{(1)} & l\|\boldsymbol{\xi}_{(1)}\|^2 \end{bmatrix}. \tag{C.30}$$

Moreover, in body-frame coordinates,

$$\mathbf{X} \equiv \mathrm{CPM}(\mathbf{x}) = \begin{bmatrix} 0 & 0 & 0 \\ 0 & 0 & -1 \\ 0 & 1 & 0 \end{bmatrix}, \tag{C.31}$$

and therefore,

$$\mathbf{X}^2 = \begin{bmatrix} 0 & 0 & 0 \\ 0 & -1 & 0 \\ 0 & 0 & -1 \end{bmatrix}, \tag{C.32}$$

and

$$\mathbf{PX} = \begin{bmatrix} 0 & -p_z & p_y \\ p_z & 0 & -p_x \\ -p_y & p_x & 0 \end{bmatrix} \begin{bmatrix} 0 & 0 & 0 \\ 0 & 0 & -1 \\ 0 & 1 & 0 \end{bmatrix} = \begin{bmatrix} 0 & p_y & p_z \\ 0 & -p_x & 0 \\ 0 & 0 & -p_x \end{bmatrix}. \tag{C.33}$$

Also, one can show that

$$\int_0^l \mathbf{UB}dx = \begin{bmatrix} -\boldsymbol{\xi}_{(2)}^T \int_0^l \boldsymbol{\varphi}\boldsymbol{\varphi}^T dx & \boldsymbol{\xi}_{(1)}^T \int_0^l \boldsymbol{\varphi}\boldsymbol{\varphi}^T dx \\ \mathbf{0}^T & \mathbf{0}^T \\ \mathbf{0}^T & \mathbf{0}^T \end{bmatrix} = \begin{bmatrix} -l\,\boldsymbol{\xi}_{(2)}^T & l\,\boldsymbol{\xi}_{(1)}^T \\ \mathbf{0}^T & \mathbf{0}^T \\ \mathbf{0}^T & \mathbf{0}^T \end{bmatrix}.$$

Here, let us use some of the definitions given by Cyril (1988) to simplify the results:

$$\mathbf{T}_1 \triangleq \int_0^l \mathbf{B}(x)dx, \tag{C.34}$$

$$\mathbf{T}_2 \triangleq \int_0^l x\mathbf{B}(x)dx, \tag{C.35}$$

$$\mathbf{T}_3 \triangleq \int_0^l \mathbf{B}^T(x)\mathbf{B}(x)dx, \tag{C.36}$$

$$\mathbf{T}_4 \triangleq \int_0^l \mathbf{h}(x)\,\mathbf{h}^T(x)dx, \tag{C.37}$$

$$\mathbf{T}_7 \triangleq \int_0^l \mathbf{U}(x,t)dx. \tag{C.38}$$

Furthermore, we would like to define some other dummy variables, which are different from the ones defined in Cyril (1988).

$$\mathbf{T}_9 \triangleq \int_0^l \mathbf{U}^2(x,t)dx, \tag{C.39}$$

$$\mathbf{T}_{10} \triangleq \int_0^l x(\mathbf{x}\,\mathbf{u}^T(x,t) + \mathbf{u}(x,t)\,\mathbf{x}^T)dx = \mathbf{x}\boldsymbol{\xi}^T \int_0^l x\mathbf{B}^T(x)dx + \int_0^l x\mathbf{B}(x)dx\boldsymbol{\xi}\mathbf{x}^T, \tag{C.40}$$

$$\mathbf{T}_{11} \triangleq \int_0^l \mathbf{U}(x,t)\mathbf{B}(x)dx. \tag{C.41}$$

Hence, in light of eqs. (C.18–C.25) and definitions (C.34–C.41), one can simplify eq. (C.16) as

$$\begin{aligned} \frac{1}{2}\int_0^l \rho\|\mathbf{v}(x,t)\|^2 dx = \frac{1}{2}\Big[& \rho l\|\dot{\mathbf{p}}\|^2 - 2\rho\dot{\mathbf{p}}^T(\frac{l^2}{2}\mathbf{X} + \mathbf{T}_7 + \mathbf{P}l)\boldsymbol{\omega} + 2\rho\dot{\mathbf{p}}^T\mathbf{T}_1\dot{\boldsymbol{\xi}} \\ & + \rho\boldsymbol{\omega}^T(-l^2\mathbf{PX} - 2\mathbf{PT}_7 - \frac{l^3}{3}\mathbf{X}^2 - \mathbf{T}_9 - \mathbf{T}_{10} - l\mathbf{P}^2)\boldsymbol{\omega} \\ & + 2\rho\boldsymbol{\omega}^T(\mathbf{XT}_2 + \mathbf{T}_{11} + \mathbf{PT}_1)\dot{\boldsymbol{\xi}} + \rho\dot{\boldsymbol{\xi}}^T\mathbf{T}_3\dot{\boldsymbol{\xi}}\Big]. \end{aligned} \tag{C.42}$$

Simplifying the Second Integral

Using eq. (C.15), the second integral of eq. (C.1) is written

$$\begin{aligned}\frac{1}{2}\int_0^l \rho\frac{J}{A}\Big(\frac{\partial\gamma}{\partial t}\Big)^2 dx &= \frac{1}{2}\int_0^l \rho\frac{J}{A}\dot{\boldsymbol{\mu}}^T\mathbf{h}(x)\mathbf{h}(x)^T\dot{\boldsymbol{\mu}}\mathrm{d}x \\ &= \frac{1}{2}\dot{\boldsymbol{\mu}}^T\left(\int_0^l \rho\frac{J}{A}\mathbf{h}(x)\mathbf{h}^T(x)dx\right)\dot{\boldsymbol{\mu}}. \end{aligned} \tag{C.43}$$

Obtaining the Kinetic-Energy Expression

Finally, the kinetic-energy expression for the link takes the form

$$\begin{aligned} T = \frac{1}{2}\Bigg[&(\rho l + M)\|\dot{\mathbf{p}}\|^2 - 2\dot{\mathbf{p}}^T\Big(\rho(\frac{l^2}{2}\mathbf{X} + \mathbf{T}_7 + \mathbf{P}l) + M\big(l\mathbf{X} + \mathbf{U}(l,t) + \mathbf{P}\big)\Big)\boldsymbol{\omega} \\ &+ 2\dot{\mathbf{p}}^T\big(\rho\mathbf{T}_1 + M\mathbf{B}(l)\big)\dot{\boldsymbol{\xi}} \\ &- \boldsymbol{\omega}^T\Bigg(\rho\big(l^2\mathbf{P}\mathbf{X} + 2\mathbf{P}\mathbf{T}_7 + \frac{l^3}{3}\mathbf{X}^2 + \mathbf{T}_9 + \mathbf{T}_{10} + l\mathbf{P}^2\big) \\ &\quad + M\Big(2\mathbf{P}\big(l\mathbf{X} + \mathbf{U}(l,t)\big) + l^2\mathbf{X}^2 \\ &\quad\quad + l\big(\mathbf{x}\mathbf{u}^T(l,t) + \mathbf{u}(l,t)\mathbf{x}^T\big) + \mathbf{U}^2(l,t) + \mathbf{P}^2\Big)\Bigg)\boldsymbol{\omega} \\ &+ 2\boldsymbol{\omega}^T\Big(\rho(\mathbf{X}\mathbf{T}_2 + \mathbf{T}_{11} + \mathbf{P}\mathbf{T}_1) + M\big(l\mathbf{X} + \mathbf{U}(l,t) + \mathbf{P}\big)\mathbf{B}(l)\Big)\dot{\boldsymbol{\xi}} \\ &+ \dot{\boldsymbol{\xi}}^T\big(\rho\mathbf{T}_3 + M\mathbf{B}^T(l)\mathbf{B}(l)\big)\dot{\boldsymbol{\xi}} + \frac{\rho J}{A}\dot{\boldsymbol{\mu}}^T\mathbf{T}_4\dot{\boldsymbol{\mu}}\Bigg]. \end{aligned} \tag{C.44}$$

C.2 The Mass Matrix

The expression obtained for the kinetic energy, in the foregoing section, can be cast in the form

$$T = \frac{1}{2}\mathbf{t}^T\mathbf{M}\mathbf{t}$$

where $\mathbf{t}$ is the link twist defined as

$$\mathbf{t} \triangleq \begin{bmatrix}\dot{\mathbf{p}}^T & \boldsymbol{\omega}^T & \dot{\boldsymbol{\xi}}^T & \dot{\boldsymbol{\mu}}^T\end{bmatrix}^T. \tag{C.45}$$

Thus, the mass matrix $\mathbf{M}$ has the structure given below

$$\mathbf{M} = \begin{bmatrix}\mathbf{M}_{\mathrm{dd}} & \mathbf{M}_{\mathrm{dr}} & \mathbf{M}_{\mathrm{db}} & \mathbf{O} \\ \mathbf{M}_{\mathrm{dr}}^T & \mathbf{M}_{\mathrm{rr}} & \mathbf{M}_{\mathrm{rb}} & \mathbf{O} \\ \mathbf{M}_{\mathrm{db}}^T & \mathbf{M}_{\mathrm{rb}}^T & \mathbf{M}_{\mathrm{bb}} & \mathbf{O} \\ \mathbf{O} & \mathbf{O} & \mathbf{O} & \mathbf{M}_{\mathrm{tt}}\end{bmatrix} \tag{C.46}$$

in which

$$\mathbf{M}_{\mathrm{dd}} \triangleq (\rho l + M)\mathbf{1}_{3\times 3}, \tag{C.47a}$$

$$\mathbf{M}_{\mathrm{dr}} \triangleq -\rho(\frac{l^2}{2}\mathbf{X} + \mathbf{T}_7 + \mathbf{P}l) - M(l\mathbf{X} + \mathbf{U}(l,t) + \mathbf{P}), \tag{C.47b}$$

$$\mathbf{M}_{\mathrm{db}} \triangleq \rho\mathbf{T}_1 + M\mathbf{B}(l) \tag{C.47c}$$

$$\begin{aligned}\mathbf{M}_{\mathrm{rr}} \triangleq & -\rho(l^2\mathbf{P}\mathbf{X} + 2\mathbf{P}\mathbf{T}_7 + \frac{l^3}{3}\mathbf{X}^2 + \mathbf{T}_9 + \mathbf{T}_{10} + l\mathbf{P}^2), \\ & - M\big(2\mathbf{P}(l\mathbf{X} + \mathbf{U}(l,t)) + l^2\mathbf{X}^2 + l(\mathbf{x}\mathbf{u}^T(l) + \mathbf{u}(l)\mathbf{x}^T) + \mathbf{U}^2(l,t) + \mathbf{P}^2\big),\end{aligned} \tag{C.47d}$$

$$\mathbf{M}_{\mathrm{rb}} \triangleq \rho(\mathbf{X}\mathbf{T}_2 + \mathbf{T}_{11} + \mathbf{P}\mathbf{T}_1) + M\big(l\mathbf{X} + \mathbf{U}(l,t) + \mathbf{P}\big)\mathbf{B}(l), \tag{C.47e}$$

$$\mathbf{M}_{\mathrm{bb}} \triangleq \rho\mathbf{T}_3 + M\mathbf{B}^T(l)\mathbf{B}(l), \tag{C.47f}$$

$$\mathbf{M}_{\mathrm{tt}} \triangleq \frac{\rho J}{A}\mathbf{T}_4. \tag{C.47g}$$

As seen in Chapter 4, in addition to the link mass matrix, the time-derivative of the mass matrix is also needed. Therefore, eqs. (C.47) are differentiated with respect to time. The results are given below:

$$\dot{\mathbf{M}}_{\mathrm{dd}} = \mathbf{O}_{3\times 3}, \tag{C.48a}$$

$$\dot{\mathbf{M}}_{\mathrm{dr}} = -\rho(\dot{\mathbf{T}}_7 + \dot{\mathbf{P}}l) - M\big(\dot{\mathbf{U}}(l,t) + \dot{\mathbf{P}}\big), \tag{C.48b}$$

$$\dot{\mathbf{M}}_{\mathrm{db}} = \mathbf{O}_{6\times n_f^b}, \tag{C.48c}$$

and

$$\begin{aligned}\dot{\mathbf{M}}_{\mathrm{rr}} = & -\rho\big(l^2\dot{\mathbf{P}}\mathbf{X} + 2\dot{\mathbf{P}}\mathbf{T}_7 + 2\mathbf{P}\dot{\mathbf{T}}_7 + \dot{\mathbf{T}}_9 + \dot{\mathbf{T}}_{10} + l(\dot{\mathbf{P}}\mathbf{P} + \mathbf{P}\dot{\mathbf{P}})\big) \\ & - M\Big(2\dot{\mathbf{P}}\big(l\mathbf{X} + \mathbf{U}(l,t)\big) + 2\mathbf{P}\dot{\mathbf{U}}(l,t) + l\big(\mathbf{x}\dot{\mathbf{u}}^T(l,t) + \dot{\mathbf{u}}(l,t)\mathbf{x}^T\big) \\ & \qquad + \dot{\mathbf{U}}(l,t)\mathbf{U}(l,t) + \mathbf{U}(l,t)\dot{\mathbf{U}}(l,t) + \dot{\mathbf{P}}\mathbf{P} + \mathbf{P}\dot{\mathbf{P}}\Big),\end{aligned} \tag{C.48d}$$

$$\dot{\mathbf{M}}_{\mathrm{rb}} = \rho(\dot{\mathbf{T}}_{11} + \dot{\mathbf{P}}\mathbf{T}_1) + M\big(\dot{\mathbf{U}}(l,t) + \dot{\mathbf{P}}\big)\mathbf{B}(l), \tag{C.48e}$$

$$\dot{\mathbf{M}}_{\mathrm{bb}} = \mathbf{O}_{n_f^b\times n_f^b}, \tag{C.48f}$$

$$\dot{\mathbf{M}}_{\mathrm{tt}} = \mathbf{O}_{n_f^t\times n_f^t}, \tag{C.48g}$$

where

$$\dot{\mathbf{T}}_7 = \begin{bmatrix} 0 & -\int_0^l \boldsymbol{\varphi}^T dx \dot{\boldsymbol{\xi}}_{(2)} & \int_0^l \boldsymbol{\varphi}^T dx \dot{\boldsymbol{\xi}}_{(1)} \\ \int_0^l \boldsymbol{\varphi}^T dx \dot{\boldsymbol{\xi}}_{(2)} & 0 & 0 \\ -\int_0^l \boldsymbol{\varphi}^T dx \dot{\boldsymbol{\xi}}_{(1)} & 0 & 0 \end{bmatrix}, \tag{C.49}$$

$$\dot{\mathbf{T}}_9 = -l \begin{bmatrix} 2\left(\dot{\boldsymbol{\xi}}_{(2)}^T \boldsymbol{\xi}_{(2)} + \dot{\boldsymbol{\xi}}_{(1)}^T \boldsymbol{\xi}_{(1)}\right) & 0 & 0 \\ 0 & 2\dot{\boldsymbol{\xi}}_{(2)}^T \boldsymbol{\xi}_{(2)} & -\left(\dot{\boldsymbol{\xi}}_{(2)}^T \boldsymbol{\xi}_{(1)} + \boldsymbol{\xi}_{(2)}^T \dot{\boldsymbol{\xi}}_{(1)}\right) \\ 0 & -\left(\dot{\boldsymbol{\xi}}_{(2)}^T \boldsymbol{\xi}_{(1)} + \boldsymbol{\xi}_{(2)}^T \dot{\boldsymbol{\xi}}_{(1)}\right) & 2\dot{\boldsymbol{\xi}}_{(1)}^T \boldsymbol{\xi}_{(1)} \end{bmatrix}, \tag{C.50}$$

$$\dot{\mathbf{T}}_{10} = \left(\mathbf{x}\dot{\boldsymbol{\xi}}^T \int_0^l x\mathbf{B}^T dx + \int_0^l x\mathbf{B} dx \dot{\boldsymbol{\xi}} \mathbf{x}^T\right) \tag{C.51}$$

$$\dot{\mathbf{T}}_{11} = \begin{bmatrix} -l\,\dot{\boldsymbol{\xi}}_{(2)}^T & l\,\dot{\boldsymbol{\xi}}_{(1)}^T \\ \mathbf{0}^T & \mathbf{0}^T \\ \mathbf{0}^T & \mathbf{0}^T \end{bmatrix}. \tag{C.52}$$

Appendix D

Deriving the NOC

D.1 The NOC of the Rigid Submanipulator

Dropping the terms related to link flexibility from eqs. (2.60 & 2.61), we obtain

$$\dot{\mathbf{p}}_j = \mathbf{R}_j^T(\dot{\mathbf{p}}_{j-1} + \boldsymbol{\Upsilon}_{j-1}\dot{\theta}_j\mathbf{R}_j\mathbf{z}_j) \tag{D.1}$$

with

$$\boldsymbol{\Upsilon}_j \triangleq \mathrm{CPM}(\mathbf{p}_j + l_j\mathbf{x}_j) \equiv \mathbf{P}_j + l_j\mathbf{X}_j. \tag{D.2}$$

Upon substitution of eq. (D.1) into itself recursively, for $j = 1, \ldots, i$, one obtains

$$\dot{\mathbf{p}}_i = \mathbf{Q}_i^T\dot{\mathbf{p}}_0 + \sum_{k=1}^{i}\Big(\prod_{j=k+1}^{i}\mathbf{R}_j\Big)^{T\,k}\boldsymbol{\Upsilon}_{k-1}\,\dot{\theta}_k\mathbf{z}_k \tag{D.3}$$

in which $\mathbf{p}_0$ is the position vector of the base of the rigid submanipulator, and $\mathbf{Q}_j$ for $j = 1, \ldots, n_{\mathrm{R}}$ is the rotation matrix that takes $\mathcal{F}_j$ to $\mathcal{F}_0$, which is attached to the base. The product operator in the above equation is defined such that the matrix-multiplication order shown below is conserved:

$$\prod_{j=k+1}^{i}\mathbf{R}_j \triangleq \mathbf{R}_{k+1}\mathbf{R}_{k+2}\cdots\mathbf{R}_i = \mathbf{Q}_k^T\mathbf{Q}_i. \tag{D.4}$$

Hence, eq. (D.3) is simplified to

$$\dot{\mathbf{p}}_i = \mathbf{Q}_i^T\dot{\mathbf{p}}_0 + \sum_{k=1}^{i}\mathbf{Q}_i^T\mathbf{Q}_k{}^{k}\boldsymbol{\Upsilon}_{k-1}\,\dot{\theta}_k\mathbf{z}_k, \tag{D.5}$$

which can be rewritten as

$$\dot{\mathbf{p}}_i = \begin{bmatrix} \mathbf{Q}_i^T & \mathbf{Q}_i^T\mathbf{Q}_1{}^1\boldsymbol{\Upsilon}_0\,\mathbf{z}_1 & \cdots & \mathbf{Q}_i^T\mathbf{Q}_{i-1}{}^{i-1}\boldsymbol{\Upsilon}_{i-2}\,\mathbf{z}_{i-1} & {}^i\boldsymbol{\Upsilon}_{i-1}\,\mathbf{z}_i \end{bmatrix} \begin{bmatrix} \dot{\mathbf{p}}_0 \\ \dot{\theta}_1 \\ \vdots \\ \dot{\theta}_i \end{bmatrix}. \tag{D.6}$$

Regarding the angular velocity of the ith link, on the other hand, we recall eq. (2.46), which, upon and dropping the terms related to link deformation, results in

$$\boldsymbol{\omega}_i = \mathbf{R}_i^T\boldsymbol{\omega}_{i-1} + \dot{\theta}_i\mathbf{z}_i = \mathbf{Q}_i^T\boldsymbol{\omega}_0 + \sum_{j=1}^{i}\dot{\theta}_j\mathbf{z}_j, \tag{D.7}$$

or

$$\boldsymbol{\omega}_i = \begin{bmatrix} \mathbf{Q}_i^T & {}^i\mathbf{z}_1 & {}^i\mathbf{z}_2 & \cdots & \mathbf{z}_i \end{bmatrix} \begin{bmatrix} \boldsymbol{\omega}_0 \\ \dot{\theta}_1 \\ \vdots \\ \dot{\theta}_i \end{bmatrix}, \tag{D.8}$$

where $\boldsymbol{\omega}_0$ is the base angular velocity.

Now, using eqs. (D.6 & D.7) and the definition of $\mathbf{N}_\mathrm{R}$, given by eq. (4.53), we can obtain the blocks of $\mathbf{N}_\mathrm{R}$. Given the large number of the blocks of this array, we display $\mathbf{N}_\mathrm{R}$ using a tabular format in Table D.1.

The time-derivative of $\mathbf{N}_\mathrm{R}$, which is also needed for our calculations, can readily be computed through differentiating its elements one by one. We start with the elements corresponding to $\dot{\mathbf{p}}_i$:

$$\frac{d}{dt}\mathbf{Q}_i^T = \dot{\mathbf{Q}}_i^T = -\boldsymbol{\Omega}_i\mathbf{Q}_i^T \tag{D.9}$$

where $\boldsymbol{\Omega}_i$ is the cross-product-matrix of $(\boldsymbol{\omega}_i - \boldsymbol{\omega}_0)$ expressed in $\mathcal{F}_i$. Also, we notice that

$$\begin{aligned} \frac{d}{dt}{}^k\boldsymbol{\Upsilon}_{k-1} &= \frac{d}{dt}(\mathbf{R}_k^T\boldsymbol{\Upsilon}_{k-1}\mathbf{R}_k) = \dot{\mathbf{R}}_k^T\boldsymbol{\Upsilon}_{k-1}\mathbf{R}_k + \mathbf{R}_k^T\dot{\boldsymbol{\Upsilon}}_{k-1}\mathbf{R}_k + \mathbf{R}_k^T\boldsymbol{\Upsilon}_{k-1}\dot{\mathbf{R}}_k \\ &= -{}^k\boldsymbol{\Omega}_k^r\,{}^k\boldsymbol{\Upsilon}_{k-1} + {}^k\dot{\mathbf{P}}_{k-1} + {}^k\boldsymbol{\Upsilon}_{k-1}\,\boldsymbol{\Omega}_k^r \\ &= -\dot{\theta}_k\mathbf{Z}_k\,{}^k\boldsymbol{\Upsilon}_{k-1} + {}^k\mathbf{P}_{k-1} + \dot{\theta}_k\,{}^k\boldsymbol{\Upsilon}_{k-1}\,\mathbf{Z}_k \end{aligned} \tag{D.10}$$

because, as defined by eq. (2.49), ${}^k\boldsymbol{\Omega}_k^r$ is given by

$${}^k\boldsymbol{\Omega}_k^r = \mathrm{CPM}(\dot{\theta}_k\mathbf{z}_k) = \dot{\theta}_k\mathbf{Z}_k. \tag{D.11}$$

$$
\mathbf{N_R} = \begin{bmatrix}
\mathbf{1}_{3\times3} & \mathbf{O}_{3\times3} & \mathbf{0}_3 & \cdots & & & & & \\
\mathbf{O}_{3\times3} & \mathbf{1}_{3\times3} & \mathbf{0}_3 & \cdots & & & & & \\
\mathbf{Q}_1^T & \mathbf{O}_{3\times3} & {}^1\boldsymbol{\Upsilon}_0\,\mathbf{z}_1 & \mathbf{0}_3 & \cdots & & & & \\
\mathbf{O}_{3\times3} & \mathbf{Q}_1^T & \mathbf{z}_1 & \mathbf{0}_3 & \cdots & & & & \\
\mathbf{Q}_2^T & \mathbf{O}_{3\times3} & \mathbf{R}_2^T\,{}^1\boldsymbol{\Upsilon}_0\,\mathbf{z}_1 & {}^2\boldsymbol{\Upsilon}_1\,\mathbf{z}_2 & \mathbf{0}_3 & \cdots & & & \\
\mathbf{O}_{3\times3} & \mathbf{Q}_2^T & {}^2\mathbf{z}_1 & \mathbf{z}_2 & \mathbf{0}_3 & \cdots & & & \\
\cdots & \cdots & \cdots & \cdots & \cdots & \cdots & \cdots & \cdots & \cdots \\
\mathbf{Q}_i^T & \mathbf{O}_{3\times3} & \mathbf{Q}_i^T\mathbf{Q}_1{}^1\boldsymbol{\Upsilon}_0\,\mathbf{z}_1 & \mathbf{Q}_i^T\mathbf{Q}_2{}^2\boldsymbol{\Upsilon}_1\,\mathbf{z}_2 & \cdots & \mathbf{R}_i^T\,{}^{i-1}\boldsymbol{\Upsilon}_{i-2}\,\mathbf{z}_{i-1} & {}^i\boldsymbol{\Upsilon}_{i-1}\,\mathbf{z}_i & \mathbf{0}_3 & \cdots \\
\mathbf{O}_{3\times3} & \mathbf{Q}_i^T & {}^i\mathbf{z}_1 & {}^i\mathbf{z}_2 & \cdots & {}^i\mathbf{z}_{i-1} & \mathbf{z}_i & \mathbf{0}_3 & \cdots \\
\cdots & \cdots & \cdots & \cdots & \cdots & \cdots & \cdots & \cdots & \cdots \\
\mathbf{Q}_n^T & \mathbf{O}_{3\times3} & \mathbf{Q}_n^T\mathbf{Q}_1{}^1\boldsymbol{\Upsilon}_0\,\mathbf{z}_1 & \mathbf{Q}_n^T\mathbf{Q}_2{}^2\boldsymbol{\Upsilon}_1\,\mathbf{z}_2 & \cdots & \mathbf{R}_n^T\,{}^{n-1}\boldsymbol{\Upsilon}_{n-2}\,\mathbf{z}_{n-1} & {}^n\boldsymbol{\Upsilon}_{n-1}\,\mathbf{z}_n & & \\
\mathbf{O}_{3\times3} & \mathbf{Q}_n^T & {}^n\mathbf{z}_1 & {}^n\mathbf{z}_2 & \cdots & {}^n\mathbf{z}_{n-1} & \mathbf{z}_n & &
\end{bmatrix}
$$

Table D.1: The NOC of the rigid submanipulator

Therefore,

$$\begin{aligned}\frac{d}{dt}(\mathbf{Q}_i^T\mathbf{Q}_k\,{}^k\boldsymbol{\Upsilon}_{k-1}\,\mathbf{z}_k) &= -\boldsymbol{\Omega}_i\mathbf{Q}_i^T\mathbf{Q}_k\,{}^k\boldsymbol{\Upsilon}_{k-1}\,\mathbf{z}_k + \mathbf{Q}_i^T\mathbf{Q}_k\boldsymbol{\Omega}_k\,{}^k\boldsymbol{\Upsilon}_{k-1}\,\mathbf{z}_k \\ &\quad + \mathbf{Q}_i^T\mathbf{Q}_k(-\dot{\theta}_k\mathbf{Z}_k\,{}^k\boldsymbol{\Upsilon}_{k-1} + {}^k\dot{\mathbf{P}}_{k-1} + \dot{\theta}_k\,{}^k\boldsymbol{\Upsilon}_{k-1}\,\mathbf{Z}_k)\mathbf{z}_k \\ &= -\boldsymbol{\Omega}_i\mathbf{Q}_i^T\mathbf{Q}_k\,{}^k\boldsymbol{\Upsilon}_{k-1}\,\mathbf{z}_k + \mathbf{Q}_i^T\mathbf{Q}_k({}^k\boldsymbol{\Omega}_{k-1}\,{}^k\boldsymbol{\Upsilon}_{k-1} + {}^k\dot{\mathbf{P}}_{k-1})\mathbf{z}_k \quad \text{(D.12)}\end{aligned}$$

because

$$\mathbf{Z}_k\mathbf{z}_k \equiv \mathbf{0},$$

and

$$\boldsymbol{\Omega}_k = {}^k\boldsymbol{\Omega}_{k-1} + \dot{\theta}_k\mathbf{Z}_k \quad \text{(D.13)}$$

in which

$${}^k\boldsymbol{\Omega}_{k-1} = \mathrm{CPM}\big(\mathbf{R}_k^T(\boldsymbol{\omega}_{k-1} - \mathbf{Q}_{k-1}^T\boldsymbol{\omega}_0)\big). \quad \text{(D.14)}$$

For the elements of $\mathbf{N}_\mathrm{R}$ pertaining to $\boldsymbol{\omega}_i$, however, we have

$$\frac{d\,{}^i\mathbf{z}_k}{dt} = \frac{d}{dt}(\mathbf{Q}_i^T\mathbf{Q}_k\mathbf{z}_k) = -\boldsymbol{\Omega}_i\,\mathbf{Q}_i^T\mathbf{Q}_k\mathbf{z}_k + \mathbf{Q}_i^T\mathbf{Q}_k\,\boldsymbol{\Omega}_k\,\mathbf{z}_k. \quad \text{(D.15)}$$

D.2 The NOC of the Flexible Submanipulator

Using eq. (2.60), in a manner similar to the derivation of eq. (D.3), one can readily show that

$$\begin{aligned}\dot{\mathbf{p}}_i &= \mathbf{R}_i^T\big[\dot{\mathbf{p}}_{i-1} + \dot{\mathbf{u}}_{i-1}(l_{i-1},t) + \boldsymbol{\Upsilon}_{i-1}\dot{\boldsymbol{\delta}}_{i-1} + \boldsymbol{\Upsilon}_{i-1}\mathbf{R}_i\mathbf{z}_i\dot{\theta}_i\big] \\ &= \mathbf{Q}_i^T\dot{\mathbf{p}}_0 + \sum_{k=1}^{i}\mathbf{Q}_i^T\mathbf{Q}_k\,{}^k\boldsymbol{\Upsilon}_{k-1}\,\mathbf{z}_k\dot{\theta}_k + \sum_{k=1}^{i-1}\mathbf{Q}_i^T\mathbf{Q}_k\mathbf{B}_k\dot{\boldsymbol{\xi}}_k \\ &\quad + \sum_{k=1}^{i-1}\mathbf{Q}_i^T\mathbf{Q}_k\boldsymbol{\Upsilon}_k\big(\mathbf{C}_k(l_k)\dot{\boldsymbol{\mu}}_k + \mathbf{D}_k(l_k)\dot{\boldsymbol{\xi}}_k\big) \\ &= \mathbf{Q}_i^T\dot{\mathbf{p}}_0 + \sum_{k=1}^{i}\mathbf{Q}_i^T\mathbf{Q}_k\,{}^k\boldsymbol{\Upsilon}_{k-1}\,\mathbf{z}_k\dot{\theta}_k + \sum_{k=1}^{i-1}\mathbf{Q}_i^T\mathbf{Q}_k\big(\mathbf{B}_k(l_k) + \boldsymbol{\Upsilon}_k\mathbf{D}_k(l_k)\big)\dot{\boldsymbol{\xi}}_k \\ &\quad + \sum_{k=1}^{i-1}\mathbf{Q}_i^T\mathbf{Q}_k\boldsymbol{\Upsilon}_k\mathbf{C}_k(l_k)\dot{\boldsymbol{\mu}}_k.\end{aligned} \quad \text{(D.16)}$$

To calculate the angular velocity of $\mathcal{F}_i$, recalling eq. (2.46), we write

$$\begin{aligned}\boldsymbol{\omega}_i &= \mathbf{R}_i^T(\boldsymbol{\omega}_{i-1} + \dot{\boldsymbol{\delta}}_{i-1}) + \dot{\theta}_i \mathbf{z}_i = \sum_{k=1}^{i} {}^i\mathbf{z}_k\, \dot{\theta}_k + \sum_{k=1}^{i-1} {}^i\dot{\boldsymbol{\delta}}_k \\ &= \sum_{k=1}^{i} \mathbf{Q}_i^T\mathbf{Q}_k\mathbf{z}_k\dot{\theta}_k + \sum_{k=1}^{i-1} \mathbf{Q}_i^T\mathbf{Q}_k\mathbf{D}_k(l_k)\dot{\boldsymbol{\xi}}_k + \sum_{k=1}^{i-1} \mathbf{Q}_i^T\mathbf{Q}_k\mathbf{C}_k(l_k)\dot{\boldsymbol{\mu}}_k. \end{aligned} \tag{D.17}$$

The coefficients of the generalized velocities in relations (D.16 & D.17) are the blocks of $\mathbf{N}_\mathrm{F}$, which can be obtained by assembling the blocks obtained for $i = 1, \ldots, n_\mathrm{F}$, as done for $\mathbf{N}_\mathrm{R}$ in the previous section.

To derive $\dot{\mathbf{N}}_\mathrm{F}$, one should differentiate the coefficients of the generalized velocities in relations (D.16 & D.17) with respect to time. Then, for the coefficients of $\dot{\mathbf{p}}_i$, we have

$$\frac{d}{dt}\mathbf{Q}_i^T = -\boldsymbol{\Omega}_i\mathbf{Q}_i^T \tag{D.18}$$

where $\boldsymbol{\Omega}_i = \mathrm{CPM}(\boldsymbol{\omega}_i)$.

The next term to be differentiated is $\mathbf{Q}_i^T\mathbf{Q}_k\,{}^k\boldsymbol{\Upsilon}_{k-1}\,\mathbf{z}_k$:

$$\begin{aligned}\frac{d}{dt}(\mathbf{Q}_i^T\mathbf{Q}_k\,{}^k\boldsymbol{\Upsilon}_{k-1}\,\mathbf{z}_k) = &-\boldsymbol{\Omega}_i\mathbf{Q}_i^T\mathbf{Q}_k\,{}^k\boldsymbol{\Upsilon}_{k-1}\,\mathbf{z}_k + \mathbf{Q}_i^T\mathbf{Q}_k\boldsymbol{\Omega}_k\,{}^k\boldsymbol{\Upsilon}_{k-1}\,\mathbf{z}_k \\ &+ \mathbf{Q}_i^T\mathbf{Q}_k\frac{d}{dt}({}^k\boldsymbol{\Upsilon}_{k-1})\mathbf{z}_k.\end{aligned} \tag{D.19}$$

However, noticing that $d\big({}^k\boldsymbol{\Upsilon}_{k-1}\big)/dt = d(\mathbf{R}_k^T\boldsymbol{\Upsilon}_{k-1}\mathbf{R}_k)/dt$, we obtain

$$\begin{aligned}\frac{d}{dt}({}^k\boldsymbol{\Upsilon}_{k-1}) &= -\boldsymbol{\Omega}_k^r\mathbf{R}_k^T\boldsymbol{\Upsilon}_{k-1}\mathbf{R}_k + \mathbf{R}_k^T\boldsymbol{\Upsilon}_{k-1}\mathbf{R}_k\boldsymbol{\Omega}_k^r + \mathbf{R}_k^T\dot{\boldsymbol{\Upsilon}}_{k-1}\mathbf{R}_k \\ &= -\boldsymbol{\Omega}_k^r\,{}^k\boldsymbol{\Upsilon}_{k-1} + {}^k\boldsymbol{\Upsilon}_{k-1}\,\boldsymbol{\Omega}_k^r + \mathbf{R}_k^T\dot{\boldsymbol{\Upsilon}}_{k-1}\mathbf{R}_k\end{aligned} \tag{D.20}$$

in which $\dot{\boldsymbol{\Upsilon}}_{k-1}$ can be calculated from

$$\dot{\boldsymbol{\Upsilon}}_{k-1} = \mathrm{CPM}\big(\dot{\mathbf{p}}_{k-1} + \dot{\mathbf{u}}_{k-1}(l_{k-1}, t)\big) \equiv \dot{\mathbf{P}}_{k-1} + \dot{\mathbf{U}}_{k-1}(l_{k-1}, t). \tag{D.21}$$

Hence, eq. (D.19) can be simplified as

$$\begin{aligned}\frac{d}{dt}(\mathbf{Q}_i^T\mathbf{Q}_k\,{}^k\boldsymbol{\Upsilon}_{k-1}\,\mathbf{z}_k) = &-\boldsymbol{\Omega}_i\mathbf{Q}_i^T\mathbf{Q}_k\,{}^k\boldsymbol{\Upsilon}_{k-1}\,\mathbf{z}_k + \mathbf{Q}_i^T\mathbf{Q}_k\boldsymbol{\Omega}_k\,{}^k\boldsymbol{\Upsilon}_{k-1}\,\mathbf{z}_k \\ &+ \mathbf{Q}_i^T\mathbf{Q}_k\Big[-\boldsymbol{\Omega}_k^r\,{}^k\boldsymbol{\Upsilon}_{k-1} + {}^k_{k-1}\boldsymbol{\Upsilon}\,\boldsymbol{\Omega}_k^r + \mathbf{R}_k^T\big(\dot{\mathbf{P}}_{k-1} + \dot{\mathbf{U}}_{k-1}(l_{k-1}, t)\big)\mathbf{R}_k\Big],\end{aligned}$$

or

$$\frac{d}{dt}(\mathbf{Q}_i^T\mathbf{Q}_k\,{}^k\boldsymbol{\Upsilon}_{k-1}\,\mathbf{z}_k) = -\boldsymbol{\Omega}_i\mathbf{Q}_i^T\mathbf{Q}_k\,{}^k\boldsymbol{\Upsilon}_{k-1}\,\mathbf{z}_k + \mathbf{Q}_i^T\mathbf{Q}_k\big({}^k\boldsymbol{\Omega}_{k-1}\,{}^k\boldsymbol{\Upsilon}_{k-1} + {}^k\dot{\mathbf{P}}_{k-1} + {}^k\dot{\mathbf{U}}_{k-1}(l_{k-1},t)\big)\mathbf{z}_k. \tag{D.22}$$

The rest of the time-derivatives related to $\dot{\mathbf{p}}_i$ can be readily computed as

$$\begin{aligned}\frac{d}{dt}\Big(\mathbf{Q}_i^T\mathbf{Q}_k\big(\mathbf{B}_k(l_k)+\boldsymbol{\Upsilon}_k\mathbf{D}_l(l_k)\big)\Big) &= -\boldsymbol{\Omega}_i\mathbf{Q}_i^T\mathbf{Q}_k\big(\mathbf{B}_k(l_k)+\boldsymbol{\Upsilon}_k\mathbf{D}_l(l_k)\big)\\ &\quad+\mathbf{Q}_i^T\mathbf{Q}_k\boldsymbol{\Omega}_k\big(\mathbf{B}_k(l_k)+\boldsymbol{\Upsilon}_k\mathbf{D}_l(l_k)\big)\\ &\quad+\mathbf{Q}_i^T\mathbf{Q}_k\big(\dot{\mathbf{P}}_k+\dot{\mathbf{U}}_k(l_k,t)\big),\end{aligned} \tag{D.23}$$

$$\begin{aligned}\frac{d}{dt}\big(\mathbf{Q}_i^T\mathbf{Q}_{j-1}\mathbf{B}_{j-1}(d_{j-1})\big) &= -\boldsymbol{\Omega}_i\mathbf{Q}_i^T\mathbf{Q}_{j-1}\mathbf{B}_{j-1}(d_{j-1})\\ &\quad+\mathbf{Q}_i^T\mathbf{Q}_{j-1}\boldsymbol{\Omega}_{j-1}\mathbf{B}_{j-1}(d_{j-1}),\end{aligned} \tag{D.24}$$

and

$$\begin{aligned}\frac{d}{dt}\big(\mathbf{Q}_i^T\mathbf{Q}_k\boldsymbol{\Upsilon}_k\mathbf{C}_k(l_k)\big) &= -\boldsymbol{\Omega}_i\mathbf{Q}_i^T\mathbf{Q}_k\boldsymbol{\Upsilon}_k\mathbf{C}_k(l_k)\\ &\quad+\mathbf{Q}_i^T\mathbf{Q}_k\boldsymbol{\Omega}_k\boldsymbol{\Upsilon}_k\mathbf{C}_k(l_k)\\ &\quad+\mathbf{Q}_i^T\mathbf{Q}_k\big(\dot{\mathbf{P}}_k+\dot{\mathbf{U}}_k(l_k,t)\big)\mathbf{C}_k(l_k).\end{aligned} \tag{D.25}$$

The derivation of the time-derivative of the elements of $\dot{\mathbf{N}}_{\mathrm{F}}$ pertaining to $\boldsymbol{\omega}_i$ is also straightforward, the results being

$$\frac{d}{dt}(\mathbf{Q}_i^T\mathbf{Q}_k\mathbf{z}_k) = -\boldsymbol{\Omega}_i\mathbf{Q}_i^T\mathbf{Q}_k\mathbf{z}_k + \mathbf{Q}_i^T\mathbf{Q}_k\boldsymbol{\Omega}_k\mathbf{z}_k, \tag{D.26}$$

$$\frac{d}{dt}(\mathbf{Q}_i^T\mathbf{Q}_k\mathbf{D}_k(l_k)) = -\boldsymbol{\Omega}_i\mathbf{Q}_i^T\mathbf{Q}_k\mathbf{D}_k(l_k) + \mathbf{Q}_i^T\mathbf{Q}_k\boldsymbol{\Omega}_k\mathbf{D}_k(l_k), \tag{D.27}$$

$$\frac{d}{dt}(\mathbf{Q}_i^T\mathbf{Q}_k\mathbf{C}_k(l_k)) = -\boldsymbol{\Omega}_i\mathbf{Q}_i^T\mathbf{Q}_k\mathbf{C}_k(l_k) + \mathbf{Q}_i^T\mathbf{Q}_k\boldsymbol{\Omega}_k\mathbf{C}_k(l_k). \tag{D.28}$$

Appendix E

Simplifications for a Planar RRR Manipulator

Here the dynamics equations of a planar RRR manipulator are derived using the procedure laid out in Chapter 4. The first link of the manipulator being flexible, it is taken to be the flexible submanipulator. The two other links are rigid and constitute the rigid submanipulator.

E.1 Link Mass Matrices and System Wrenches

E.1.1 Link 1

Simplifying the mass-matrix relations (C.46 & C.47) for a flexible link moving in plane, we obtain

$$\mathbf{M}_1 = \begin{bmatrix} M^1_{\text{rr}} & \mathbf{m}^1_{\text{rb}} \\ (\mathbf{m}^1_{\text{rb}})^T & \mathbf{M}^1_{\text{bb}} \end{bmatrix} \tag{E.1}$$

where

$$M^1_{\text{rr}} \triangleq -\rho(-\frac{l_1^3}{3} + l_1\|\boldsymbol{\xi}\|^2) = -m_1(-\frac{l_1^2}{3} + \boldsymbol{\xi}^T\boldsymbol{\xi}), \tag{E.2a}$$

$$\mathbf{m}^1_{\text{rb}} \triangleq \rho\int_0^{l_1} x\boldsymbol{\phi}_1^T(x)\,dx, \tag{E.2b}$$

$$\mathbf{M}^1_{\text{bb}} \triangleq m_1\mathbf{1}_{n_1\times n_1} \tag{E.2c}$$

in which n_1 is the number of mode shapes used to discretize this link.

The system wrench for this link is obtained by simplifying eq. (4.18d):

$$\mathbf{w}_1^{\mathrm{s}} = \begin{bmatrix} 2m_1\omega_1\dot{\boldsymbol{\xi}}_1^T\boldsymbol{\xi}_1 \\ -m_1\omega_1^2\boldsymbol{\xi}_1 - \mathbf{K}_1(\beta_1\dot{\boldsymbol{\xi}}_1 + \boldsymbol{\xi}_1) \end{bmatrix} \tag{E.3}$$

where

$$\mathbf{K}_1 \triangleq \int_0^{l_1} E_1 I_1 \boldsymbol{\phi}_1''(x)\big(\boldsymbol{\phi}_1''(x)\big)^T dx. \tag{E.4}$$

E.1.2 Link 2

Similarly, the mass matrix of the second link is obtained as

$$\mathbf{M}_2 = \begin{bmatrix} \mathbf{M}_{\mathrm{dd}}^2 & \mathbf{m}_{\mathrm{dr}}^2 \\ (\mathbf{m}_{\mathrm{dr}}^2)^T & M_{\mathrm{rr}}^2 \end{bmatrix} \tag{E.5}$$

where

$$\mathbf{M}_{\mathrm{dd}}^2 \triangleq m_2\mathbf{1}_{2\times 2}, \tag{E.6a}$$

$$\mathbf{m}_{\mathrm{dr}}^2 \triangleq -m_2(\frac{l_2}{2}\mathbf{X} + \mathbf{P}_2)_{(1:2,3)} = -m2\begin{bmatrix} \mathbf{p}_2^T\mathbf{y} \\ -l_2/2 - \mathbf{p}_2^T\mathbf{x} \end{bmatrix}, \tag{E.6b}$$

$$M_{\mathrm{rr}}^2 \triangleq m_2(l_2\mathbf{P}_2\mathbf{X} + \frac{l_2^2}{3}\mathbf{X}^2 + \mathbf{P}_2^2)_{(3,3)} = m_2\big(l_2(\mathbf{p}_2^T\mathbf{x} + \frac{l_2}{3}) + \mathbf{p}_2^T\mathbf{p}_2\big), \tag{E.6c}$$

and the system wrench for this link is calculated from

$$\mathbf{w}_2^{\mathrm{s}} = m_2\omega_2\begin{bmatrix} -2\mathbf{E}\dot{\mathbf{p}}_2 + \omega_2(l_2\mathbf{x}/2 + \mathbf{p}_2) \\ -(l_2\dot{\mathbf{p}}_2\mathbf{x} + 2\dot{\mathbf{p}}_2\mathbf{p}_2) \end{bmatrix} \tag{E.7}$$

where

$$\mathbf{E} \triangleq \begin{bmatrix} 0 & -1 \\ 1 & 0 \end{bmatrix}. \tag{E.8}$$

E.1.3 Link 3

The mass matrix and the system wrench of the third link is similar to those of the second link

$$\mathbf{M}_3 = \begin{bmatrix} \mathbf{M}_{\mathrm{dd}}^3 & \mathbf{m}_{\mathrm{dr}}^3 \\ (\mathbf{m}_{\mathrm{dr}}^3)^T & M_{\mathrm{rr}}^3 \end{bmatrix} \tag{E.9}$$

in which

$$\mathbf{M}_{\mathrm{dd}}^{3} \triangleq m_3 \mathbf{1}_{2\times 2}, \tag{E.10a}$$

$$\mathbf{m}_{\mathrm{dr}}^{3} \triangleq -m_3(l_3\mathbf{X}/2 + \mathbf{P}_3)_{(1:2,3)} = -m3 \begin{bmatrix} \mathbf{p}_3^T\mathbf{y} \\ -l_3/2 - \mathbf{p}_3^T\mathbf{x} \end{bmatrix}, \tag{E.10b}$$

$$M_{\mathrm{rr}}^{3} \triangleq m_3\big(l_3(\mathbf{p}_3^T\mathbf{x} + \frac{l_3}{3}) + \mathbf{p}_3^T\mathbf{p}_3\big), \tag{E.10c}$$

and

$$\mathbf{w}_3^{\mathrm{s}} = m_3\omega_3 \begin{bmatrix} -2\mathbf{E}\dot{\mathbf{p}}_3 + \omega_3(l_3\mathbf{x}/2 + \mathbf{p}_3) \\ -(l_3\dot{\mathbf{p}}_3\mathbf{x} + 2\dot{\mathbf{p}}_3\mathbf{p}_3) \end{bmatrix}. \tag{E.11}$$

E.2 Dynamics Equations

Now, the equations can be assembled to obtain the mathematical model of the system:

$$\mathbf{M}\ddot{\boldsymbol{\psi}} = \mathbf{w}^{\mathrm{s}} + \mathbf{B}\,\mathbf{u}(t) \tag{E.12}$$

where

$$\mathbf{M} \triangleq \mathbf{N}^T\,\widehat{\mathbf{M}}\,\mathbf{N}, \tag{E.13}$$

and

$$\mathbf{w}^{\mathrm{s}} \triangleq \mathbf{N}^T(\hat{\mathbf{w}}^{\mathrm{s}} - \widehat{\mathbf{M}}\,\dot{\mathbf{N}}\,\dot{\boldsymbol{\psi}}), \tag{E.14}$$

in which

$$\widehat{\mathbf{M}} \triangleq \begin{bmatrix} \mathbf{M}_1 & \mathbf{O} & \mathbf{O} \\ \mathbf{O} & \mathbf{M}_2 & \mathbf{O} \\ \mathbf{O} & \mathbf{O} & \mathbf{M}_3 \end{bmatrix}, \tag{E.15}$$

and

$$\hat{\mathbf{w}}^{\mathrm{s}} \triangleq \begin{bmatrix} (\mathbf{w}_1^{\mathrm{s}})^T & (\mathbf{w}_2^{\mathrm{s}})^T & (\mathbf{w}_3^{\mathrm{s}})^T \end{bmatrix}^T. \tag{E.16}$$